DYNAMIC AND SEISMIC CHARACTERISTICS OF CABLE-STAYED BRIDGES

by

Osama A. Hodhod

A Thesis

Submitted to the School of Graduate Studies

in Partial Fulfilment of the Requirements

for the Degree

Doctor of Philosophy

McMaster University

DYNAMIC AND SEISMIC CHARACTERISTICS OF CABLE-STAYED BRIDGES

DOCTOR OF PHILOSOPHY (1993)
(Civil Engineering)

McMASTER UNIVERSITY
Hamilton, Ontario

TITLE: Dynamic and Seismic Characteristics of Cable-Stayed Bridges

AUTHOR: Osama A. Hodhod, B.Sc. (Cairo University)
M.Sc. (Cairo University)

SUPERVISOR: Professor John C. Wilson

NUMBER OF PAGES: xxiii, 271

ABSTRACT

Cable-stayed bridges have been gaining popularity in the last few decades as a viable, efficient, economical and aesthetically appealing design for spanning medium to long crossings. The construction of these bridges in seismic regions has created a need to more fully understand their dynamic behaviour and seismic response.

The objectives of this research work are to: (1) define a dynamic modal analysis procedure suitable for cable-stayed bridges, and (2) use the developed procedure to study seismic response characteristics of cable-stayed bridges.

The research program was divided into four main stages: (1) development of analytic models for estimating frequencies of two of the main structural systems of cable-stayed bridges (i.e. deck and tower); (2) a 3-D model of Quincy Bayview Bridge was used as a prototype structure to study the modal characteristics of cable-stayed bridges and investigate the effect of major geometric parameters on the modal characteristics of cable-stayed bridges; (3) eigenvectors and load dependent Ritz vectors were examined to compare their appropriateness as bases for modal transformation of the equation of motion of cable-stayed bridges. A seismic response study was conducted of the Quincy Bayview Bridge in each vector basis to judge which is more appropriate for dynamic and seismic analysis of cable-stayed bridges. Frequency cut-off criteria were proposed that would ensure the inclusion of all important modes in a dynamic analysis; and (4) the

proposed criteria were applied in a seismic response study that used a 3-D finite element model of the Quincy Bayview Bridge. The study investigated the effect of frequency content of ground motion on the seismic response of cable-stayed bridges with different deck supports.

The results of the study showed that modal characteristics of cable-stayed bridges are most affected by the cable arrangement, the tower shapes, and deck supports. Almost the same number of eigenvectors or Ritz vectors are required to ensure the inclusion of all important modes in a modal analysis. To ensure the inclusion of all important modes, it is proposed to calculate an upper limit frequency using the developed analytic models, generate modal vectors up to the set limit and then check the effective modal mass of these vectors to meet a pre-set percentage of the total mass. The study showed that seismic response of a cable-stayed bridge is strongly dependent upon the deck support condition, and the frequency content of input motion. It also showed that towers are less sensitive to changes in frequency content of the ground motion than the deck.

ACKNOWLEDGEMENT

I wish to express my gratitude and appreciation to Professor John C. Wilson, my research supervisor, for his guidance, invaluable contributions, and criticism throughout the course of this research work. It has been a privilege to have Dr. Wilson as my supervisor. His dedication to academic excellence is quite inspiring.

I wish to extend my appreciation to Dr. A. Ghobarah and Dr. D. S. Weaver, members of my supervisory committee, for their constant encouragement and valuable suggestions.

I gratefully acknowledge the financial support of the Canadian International Development Agency (CIDA), in the form of tuition bursary, and McMaster University, in the form of scholarships and teaching assistantships offered through the department.

Finally, I thank God who bestowed his blessings on me and helped me to accomplish my research program.

To my Late Mother, my Father, my Wife and Daughter

TABLE OF CONTENTS

Table of Contents (cont'd)

Table of Contents (cont'd)

LIST OF TABLES

LIST OF TABLES (cont'd)

LIST OF FIGURES

List of Figures (cont'd)

List of Figures (cont'd)

List of Figures (cont'd)

List of Figures (cont'd)

List of Figures (cont'd)

List of Figures (cont'd)

List of Figures (cont'd)

LIST OF SYMBOLS

A	= Maximum ground acceleration in (g)
A_{ci}	= Cross sectional area of the i^{th} cable
a,b	= Distances into which a span of a cable-stayed bridge is divided by cable "r"
C	= Main span length of a cable-stayed bridge
[C]	= Damping matrix
d	= Bridge deck width
E	= Modulus of elasticity
E_c	= Modulus of elasticity of cables
E_D	= Modulus of elasticity of deck
E_T	= Modulus of elasticity of towers
e	= Eccentricity between deck cross section centre of mass and centre of stiffness
{F(x,t)}	= Dynamic load vector
F_x	= Normal force
f_i	= i^{th} frequency of a structure
g	= Acceleration due to gravity
GJ	= Torsional rigidity
H	= Total height of tower
h_i	= Height of the anchorage of the i^{th} cable above the deck level
I	= Moment of inertia

List of Symbols (cont'd)

I_D (= I_{Tr}) = Moment of inertia of deck for vertical bending

I_p = Polar moment of inertia

I_T = Moment of inertia of tower for longitudinal bending

I_v = Moment of inertia of the deck around its vertical axis

I_{yy} = Moment of inertia about local y-axis

I_{zz} = Moment of inertia about local z-axis

[K] = Stiffness matrix

K = Vertical spring stiffness per unit length of deck

K^* = Spring stiffness at the tower top for the analytic model

K_{ci}, K_{cj} = Axial stiffness of cables i and j

K_D = Bending stiffness of deck

K_T = Bending stiffness of tower

K_ϕ = Equivalent torsional stiffness per unit length of deck, provided by cables, towers and adjacent deck span

L = Span length of a beam

M_x = Torsional moment

M_y = Bending moment about local y-axis of a structural member

M_z = Bending moment about local z-axis of a structural member

m = Mass/unit length for a beam

[M] = Mass matrix

N = Total number of degrees of freedom

n = Total number of requested modes

List of Symbols (cont'd)

Q_y = Shear force in the local y-axis direction

Q_z = Shear force in the local z-axis direction

$\{r_m\}$ = Influence factors vector for the m^{th} direction

S = Average spacing between any two adjacent cables on the deck

T = Period (sec.)

{u} = Nx1 relative displacement vector

$\ddot{U}_g$ = Ground acceleration

V = Maximum ground velocity in (m/sec.)

v = Deflection Function for the Tower

W_i = Mode shape for the i^{th} span of the deck

X_i = Distance along the i^{th} span measured from the left end of the i^{th} span

[X(x)] = Modal matrix

{Y(t)} = Vector of time functions

Z_a = Acceleration-related zone

Z_v = Velocity-related zone

z = Distance along the tower measured from its base

β = Main span/side span ratio of a cable-stayed bridge

Γ = Tower stiffness parameter

$\Gamma_{n,m}$ = Modal participation factor of the n^{th} mode in the global m^{th} direction

γ_D = Deck mass per unit length

γ_T = Tower mass per unit height

List of Symbols (cont'd)

Δt = Time step (sec.)

ζ_i = i^{th} modal damping (% of critical)

θ_i, θ_j = Acute angle that cables i and j make with the deck

λ_T = Bending frequency parameter for the tower analytic model

λ^2_i = Bending frequency parameter (normalized frequency)

λ^2_ϕ = Torsional frequency parameter

ϕ_i = Twist function for the i^{th} span

$\{\phi_n\}$ = n^{th} mode shape

ϕ_{imj} = Translational component at the i^{th} node in the global m^{th} direction of the j^{th} mode shape

Ψ_i = i^{th} modal force

ω_i = i^{th} circular frequency (rad./sec.)

% EM_{mj} = Percentage of effective modal mass of the j^{th} mode in the global m^{th} direction

CHAPTER 1

INTRODUCTION

1.1 BACKGROUND AND MOTIVATION

Cable-stayed bridges have acquired popularity around the world as a viable bridge design for medium to long span crossings. Their aesthetic form, competitive cost, and the efficient and fast mode of construction are some of the reasons behind their increasing popularity. In Canada cable-stayed bridges in service include the Skytrain and Alex Fraser bridges near Vancouver, B.C., and Longs Creek Bridge in New Brunswick. In the United States, Europe and Japan there are numerous other examples of the use of this type of bridge construction. Table 1.1 summarizes structural details of a few selected cable-stayed bridges.

A cable-stayed bridge consists of three principal sub-systems (deck, towers, cables) each differing in inertial and stiffness properties. These three sub-systems are designed to interact to produce an efficient system of load transfer within the bridge. This thesis focuses on the dynamic characteristics of these sub-systems, and on the loads imposed on the structural elements by earthquakes.

Static design procedures have evolved during the last half century so that literature on the subject (Podolny and Scalzi, 1986; Troitsky, 1988; Gimsing, 1983; Leonhardt and Zellner, 1980) give guidelines for optimum design against traditional loads such as dead,

live and impact. Simple approximate analysis methods as well as elaborate stiffness or flexibility based analysis methods are illustrated by Podolny and Scalzi (1986) and Troitsky (1988). Smith (1967) suggested a mixed flexibility-stiffness method suitable for use on micro computers to be used in the analysis of different kinds of cable-stayed bridges. Rajaraman et al (1980) studied the effects of cable-sag, large deformations and beam-column effect in the deck and towers on a 2-D discrete model of a cable-stayed bridge. They reported differences of 10% between linear and non-linear analyses. Bruno and Leonardi (1986) developed a continuous analytical model for a single plane cable-stayed bridge and analyzed it under eccentric load taking the cable-sag effect into consideration.

1.1.1 Modelling of Cable-Stayed Bridges for Dynamic Analysis

Many researchers have investigated dynamic characteristics and modelling of cable-stayed bridges. Goshy (1961) derived frequency equations for a pipe cable-stayed bridge by applying the approximate Rayleigh-Ritz technique, however the derived expressions were valid only for the one bridge. Fleming and Egesli (1980) studied the dynamic behaviour of a 2-D model of the Norbrüke Bridge at Düsseldorf, Germany and concluded that linear dynamic analysis was sufficiently accurate for design purposes. Nazmy and Abdel-Ghaffar (1990a) formulated the equations of motion for 3-D hypothetical models of cable-stayed bridges taking into account several sources of non-linearities. They also gave a solution technique in the modal coordinates. Wilson and Gravelle (1991) modelled the Quincy Bayview Bridge, Quincy, Illinois, using linear 3-D

finite elements to simulate its dynamic characteristics. Abdel-Ghaffar and Khalifa (1991) studied the effect of cable vibration on the dynamic characteristics of cable-stayed bridges. Scanlan (1987) and Scanlan and Jones (1990) have used dynamic models in aeroelastic analysis of cable-stayed bridges.

The work on the modelling of cable-stayed bridges for dynamic analysis shows that:

1- Linear modelling of the bridge elements is adequate and it provides a good representation of the frequencies and mode shapes of the bridge. This conclusion is supported by the comparison between ambient vibration survey (AVS) results (section 1.1.2) and model results for Quincy Bayview and Sunshine Skyway bridges.

2- Cable vibrations, although having an importance in their own right, do not seem to significantly affect the global dynamic behaviour of the deck or towers. A single finite element representation of each cable appears to be sufficient for dynamic modelling of the deck and towers.

1.1.2 Ambient Vibration Surveys (AVS)

Stiemer et al (1988) conducted an AVS study on Alex Fraser bridge near Vancouver, B.C. to study the dynamic characteristics of the bridge and measure wind-induced cable vibrations. Muria Villa et al (1991) conducted an AVS and pull back test on Tampico bridge, Mexico. They identified mode shapes, frequencies and estimated damping ratios of various modes. Garevski et al (1991, 1992) built a small scale model of the Jindo Bridge in Korea and used it to identify mode shapes, measure frequencies, and estimate damping coefficients corresponding to each mode. Wilson and Liu (1991)

conducted an AVS on the Quincy Bayview Bridge, Quincy, Illinois. They identified 25 modes below 2.0 Hz. This work was used later (Wilson and Gravelle 1991) to validate a linear 3-D finite element model of the same bridge. Jones and Thompson (1992) conducted an AVS on the Sunshine Skyway Bridge in Tampa, Florida and identified many modes with frequencies up to 5.0 Hz. They were able, using linear 3-D finite element modelling, to produce most of the identified modes numerically.

The research work on AVS reveals that:

1- Most modes of cable-stayed bridges exhibit some degree of spatial coupling because of the interaction of the three subsystems of the bridge (deck, towers, cables).

2- Cable-stayed bridges are generally very flexible structures with low, closely spaced frequencies.

3- Modal damping ratios measured during AVS are typically very small (less than 1%) and they appear to be amplitude dependent.

4- Cables are the most light sub system and they can be excited at low wind speeds. In some cases special dampers are required to control their vibration (Alex Fraser Bridge).

1.1.3 Seismic Behaviour of Cable-Stayed Bridges

Although research on the dynamics of cable-stayed bridges has been conducted for several decades publications on investigations of their seismic behaviour have appeared only more recently. Parvez et al (1988) studied the earthquake effects on Jamuna Bridge across Jamuna River in Bangladesh using a design spectrum with peak

acceleration of 0.216g and concluded that the bridge could cope with earthquakes very well. Yokoyama et al (1988) studied the non-linear response of a cable-stayed concrete bridge, considering the only source of non linearity to be the degradation of tower stiffness under severe earthquake motions. They took into account the effect of cable vibrations. Vaz et al (1988) studied the soil-bridge interaction problem for Arade River bridge using 80 modes of vibration to cover the frequencies from 0.14 Hz- 5.5 Hz. They used linear analysis and concluded that there is a need to improve the characterization of the influence of site conditions in earthquake vibrations. Abdel-Ghaffar, (1991) reviewed the general characteristics of cable-stayed bridges' seismic behaviour but did not investigate the effect of ground motion frequency content on them. Abdel-Ghaffar and Nazmy, (1991) studied the effect of different non-linearities on the seismic behaviour of cable-stayed bridges. Nazmy and Abdel-Ghaffar (1990b, 1992) studied the seismic behaviour of two hypothetical cable-stayed bridges under synchronous and non-synchronous ground motion inputs. They reported that for long bridges, depending on the soil condition, the effect of non-synchronous input motions could be significant. They concluded that the simultaneous application of the three components of ground motion is essential for realistic response calculations.

The literature shows that:

1- Modal analysis is the most commonly used dynamic analysis because it gives information about frequencies, mode shapes, modal participation factors, and spatial coupling. It is preferred over direct integration because of savings in time and storage

for subsequent runs, and because both response spectrum and time history analysis can be used.

2- Spatial coupling within the structure requires careful seismic analysis. This fact urged some researchers to recommend the simultaneous application of the three ground motion components in 3-D analysis.

3- There were tries to include the effect of ground motion variability on the seismic response of cable-stayed bridges but these were not related to definite ground motion characteristics.

1.1.4 Aseismic Design Procedures for Cable-Stayed Bridges

Taylor et al (1985) showed the aseismic design steps followed for the design of the, then-longest cable-stayed bridge in the world (Alex Fraser Bridge, Vancouver, B.C.) with 465m span. The seismic design criterion was to build a bridge that was not governed in its design by the earthquake load. To accomplish this the deck was supported on lead-rubber bearings. Special reinforcement detailing was used in the towers to carry the earthquake loading. Khalil and Bush (1987a,b) discussed the analysis and design considerations of the Skytrain Bridge, Vancouver, which is located in a highly seismic area with different soil conditions on the two banks of the river. They used a linear 3-D model of the bridge but applied ground motions in two separate loading cases, transverse ground motion component alone and then longitudinal component alone. The combination procedure suggested by AASHTO (1983) was used to account for simultaneous occurrence of earthquake motions in the two directions. Masaki et al (1987) demonstrated

the seismic design procedure used for the first S-curved cable-stayed bridge in the world, in Tokyo. Both 2-D and 3-D linear analyses were used, however they did not show how many modes were considered or what earthquakes used in the design. Stroh (1987) discussed the dynamic considerations for the design of three U.S. bridges: Sunshine Skyway Bridge, Tampa, Florida; Eugene Talmadge Memorial Bridge, Savannah, Georgia; and Houston Ship Channel Bridge, Baytown, Texas. Yamada et al (1991) and Kitazawa et al (1992) demonstrated the design procedure adopted to design the Higashi-Kobe Bridge, Osaka, Japan. This bridge has a completely movable deck. The designer did this to lower the bridge's fundamental frequency and consequently reduce the seismic forces on the bridge substructure.

1.1.5 Research Problem

The previous discussions provide an overview of the current state of knowledge about cable-stayed bridges. From these discussions, several points arise that indicate that the dynamic and seismic behaviour of cable-stayed bridges is still not fully understood:

1- Spatial coupling has been identified within the mode shapes of cable-stayed bridges but the parameters affecting it have not been examined in a detailed manner.

2- Most researchers suggest that linear dynamic analysis is generally sufficiently accurate for design purposes. This opens the way to using modal analysis, but no reference was made in any of the work to a criterion for selecting the number of modes that could be sufficient for an accurate dynamic analysis. The general recommendation was to use many modes.

3- Cable-stayed bridges are flexible structures with many low, closely-spaced frequencies. This characteristic supports the suggestion in 2 above that many modes are required in seismic modal analysis, but it also raises the issue of whether eigenvectors are the best modal transformation basis.

4- The analysis of cable-stayed bridges for aseismic design requires the use of input ground motions to study the bridge response. This kind of study is usually site specific to reflect the particular frequency characteristics of ground motions at the site. However, there is also a need to investigate the behaviour of cable-stayed bridges under ground motions having different frequency characteristics in order to get a complete picture of the seismic sensitivity of each sub-system of the bridge.

5- Several ways have been tried to isolate the bridge deck from seismic forces in an attempt to reduce the seismic forces on the tower. Achieving a favourable level of reduced seismic response in these structures is of considerable importance for future aseismic design of cable-stayed bridges.

The research program will address these issues.

1.2 RESEARCH OBJECTIVES AND SCOPE

The research objectives are to:

1- Define a dynamic modal analysis procedure that is suitable for cable-stayed bridges. The procedure will contain criteria, that will ensure the inclusion of all important modes in dynamic response calculations. These criteria will be based on a parametric study of the dynamic characteristics of cable-stayed bridges with different geometric properties.

2- Study the seismic response characteristics of cable-stayed bridges and the effects of ground motion frequency content. This investigation identifies locations on the bridge vulnerable to seismic forces. It is also the aim of this study to determine the sensitivity of the bridge response to changes in the frequency characteristics of ground motions, and including the effect of bridge support condition.

The research program studies symmetric three-span cable-stayed bridges, having symmetric deck cross sections and double-plane multi-cable arrangements. This study assumes linear bridge behaviour and synchronous seismic support excitations. The effect of these two assumptions has been discussed in studies by Nazmy and Abdel-Ghaffar (1987). Geometric non-linear behaviour may result from cable sag effect, large amplitude displacements and P-Δ effects in the towers. Non-synchronous support excitations may result from different soil conditions at each tower, orientation of the bridge with respect to the direction of the seismic wave propagation and travelling seismic wave effects. Nazmy and Abdel-Ghaffar (1987) reported that linear dynamic analysis is sufficiently accurate for cable-stayed bridges with main spans up to approximately 1500 ft. This main span length includes almost all existing cable-stayed bridges. The assumption of synchronous base excitation is used in the present study because it has been shown by Nazmy and Abdel-Ghaffar (1987) that the effects of non-synchronous support excitations in cable-stayed bridges with main spans up to approximately 1500 ft are relatively small.

The research program uses the Quincy Bayview Bridge as a prototype structure because it represents this class of cable-stayed bridges and there is an extensive amount of experimental and analytic data available on this bridge (Modjeski and Masters, 1985;

Wilson and Liu, 1991; and Wilson and Gravelle, 1991). Although the research is oriented toward earthquake engineering aspects, much of the dynamic aspects of the work may also be of relevance to wind engineering for cable-stayed bridges.

1.3 ORGANIZATION OF THE THESIS

The research program is documented in the following five chapters. Chapter 2 describes the development of analytic models that provide frequency estimates of the deck and tower. These models can be useful in preliminary stages of bridge design, and they are an important development for the seismic modal analysis criteria in Chapter 4.

The third chapter presents a study on the dynamic characteristics of cable stayed bridges and the effect of various bridge geometries on the modal behaviour[1]. This provides a clearer understanding of the spatial coupling within the different modes, and identifies important deck and tower modes. It also forms the basis of criteria for determining the number of modes required for seismic analysis.

The fourth chapter compares eigenvectors to load dependent Ritz vectors as two prospective modal transformation bases for seismic analysis of cable-stayed bridges. Criteria are proposed for modal analysis of cable-stayed bridges.

The fifth chapter contains a comprehensive seismic response study of alternative designs of a cable-stayed bridge, and includes the effect of variations of ground motions on the response of a bridge with pinned deck and a bridge with longitudinally movable deck. The sixth chapter contains the summary and conclusions of the study.

---

[1] Units of ft and lb are used throughout this thesis, as all structural information was directly available in this form.

Table 1.1 Data for Some Modern Cable-Stayed Bridges

Bridge	Reference	Location	Main Span (ft)	Cable Arrangement	Deck	Tower	Fundamental Freq. (Hz)
Quincy	Wilson and Gravelle, 1991	Quincy, Illinois	900	Fan	Comp.	R.C.	0.371
NGBI	Abdel-Ghaffar and Nazmy, 1987	____	1100	Fan	Comp.	R.C.	0.320
NGBII	Abdel-Ghaffar and Nazmy, 1987	____	2200	Fan	Comp.	R.C.	0.190
Jindo	Garevski et al, 1991	Korea	1128	Radiating	Steel	Steel	0.467
Higashi Kobe	Kitazawa et al, 1992	Kobe, Japan	1590	Harp	Steel	Steel	0.115
Sunshine Skyway	Jones and Thompson, 1992	Tampa, Florida	1200	Fan	Comp.	R.C.	0.287
Skytrain	Khalil and Bush, 1987a	Vancouver, B.C.	1115	Fan	P.C.	R.C.	0.270
Alex Fraser	Taylor et al, 1985	Vancouver, B.C.	1525	Fan	Comp.	R.C.	0.275
Talmadge	Stroh, 1987	Savannah, Georgia	1100	Fan	Comp.	R.C.	0.271
Baytown	Stroh, 1987	Baytown, Texas	1250	Fan	Comp.	R.C.	0.273

Comp. = composite reinforced concrete and steel.

R.C. = reinforced concrete.

P.C. = pre-stressed concrete.

CHAPTER 2

ANALYTIC MODELS FOR DYNAMIC ANALYSIS

2.1 INTRODUCTION

A cable-stayed bridge is a highly statically indeterminate structure demonstrating complex behaviour under static and dynamic loads. Modelling and analysis of these bridges poses a challenging problem to engineers. Approximate analyses were developed as the original method to analyze and design such a structure. Goshy (1961) proposed the use of approximate Ritz analysis to calculate the fundamental frequencies in each direction (vertical, lateral, and torsional) for a pipe cable-stayed bridge. At the time, this type of analysis was the only manual means to calculate acceptable frequency estimations. The proposed procedure required an estimate of the mode shape before calculating the frequency, and the derived expressions were suitable only for the bridge under consideration. Troitsky (1988), Podolny and Scalzi (1986) and Gimsing (1983) summarize some approximate static analysis methods suitable for hand calculations.

Recently, with the growing popularity of cable-stayed bridges and developments in computing, the use of more established methods of stiffness analysis have become the standard approach. Troitsky (1988) and Podolny and Scalzi (1986) describe in detail such procedures. Smith (1967) proposed a mixed analysis approach (stiffness-flexibility) suitable for static analysis of cable-stayed bridges using micro computers. However, these methods have been generally applied only to 2-D models of cable-stayed bridges. More

recently, engineers such as Abdel-Ghaffar and Nazmy (1987), Khalil and Bush (1987a,b), and Kitazawa et al (1992) have used 3-D analysis.

In this chapter, a brief reference is first made to the 3-D mathematical model of Quincy Bayview Bridge (Gravelle, 1990) that will be used as the reference for the developments of this chapter. Analytic models for the bridge deck and tower are then developed using the well-established differential equation approach to give estimates of the bridge frequencies. These analytic models, together with the observations and results on dynamic characteristics in Chapter 3, are used in Chapter 4 to propose a procedure for efficient and accurate seismic analysis of cable-stayed bridges.

2.2 REFERENCE FINITE ELEMENT MODEL

During this research work a 3-D linear elastic finite element model of the Quincy Bayview Bridge has been used for the dynamic and seismic studies. Complete modelling details are given in Gravelle (1990) and Wilson and Gravelle (1991). The validity of this model has been verified by comparisons with results of full-scale vibration measurements on the Quincy Bayview Bridge (Liu, 1989; and Wilson and Liu, 1991). The model is illustrated in Figures 2.1-2.3. The deck is modeled as a single spine having equivalent bending and torsional stiffnesses as the full bridge deck.

2.3 ANALYTIC MODELS OF CABLE-STAYED BRIDGES

Despite the apparent structural complexity of cable-stayed bridges, it is possible to develop analytic models for free vibration frequency calculations. Such models are

useful in both the preliminary and detailed design stages by providing frequency estimates of the main bridge components (deck and tower). The frequency estimates can be used to determine the frequency range to be covered in a detailed dynamic analysis for seismic or wind engineering.

The subsequent sections present a development of the deck and tower analytic model formulations. The models are applied to several cable-stayed bridges to evaluate their accuracy as compared to published results from more elaborate finite element models.

2.3.1 Bridge Deck

The bridge deck will be considered in two separate cases, for bending vibration and for torsional vibration.

2.3.1.1 Vertical and Transverse Bending Vibrations

In the vertical plane, the cable-stayed bridge in Figure 2.4 is modeled as a continuous beam pin-connected at the abutments and towers and elastically supported at cable anchorage points. The main span length is denoted as C, and the two side spans are of equal length βC. In the transverse direction, the stiffness effect of the cables is negligible because the cable planes are vertical or nearly vertical. In this direction the bridge deck is modelled as a continuous beam pin-connected at the abutments and tower locations.

Mode shapes and frequencies of this simple idealization for bending vibration are

governed by the following differential equations, written for the i^{th} span as:

$$\frac{d^4 W_i}{dX^4_i} - \alpha W_i = 0 \qquad i=1,2,3 \qquad (2.1)$$

where,

$W_i = W_i(X_i)$ = displacement shape of the i^{th} span

X_i = distance along the i^{th} span

$$\alpha = \gamma_D \omega^2 / EI_V \qquad \textit{for Transverse Bending} \qquad (2.2)$$

$$\alpha = (\gamma_D \omega^2 - K) / EI_{Tr} \qquad \textit{for Vertical Bending} \qquad (2.3)$$

In equations 2.2 and 2.3

γ_D = deck mass per unit length.

ω = circular frequency.

K = vertical spring stiffness per unit length of the deck.

E = modulus of elasticity of the bridge deck.

I_{Tr} = moment of inertia of the bridge deck around its transverse axis.

I_V = moment of inertia of the bridge deck around its vertical axis.

Evaluation of "K" will be discussed in section 2.3.1.3.

Referring to Figure 2.4, the mode shapes W_1, W_2, W_3 must satisfy the following boundary conditions:

$$W_i(0)=0 \qquad i=1,2,3 \tag{2.4a}$$

$$\frac{d^2W_1(0)}{dX^2_1} = 0 \tag{2.4b}$$

$$W_i(\beta C)=0 \qquad i=1,3 \tag{2.4c}$$

$$\frac{dW_1(\beta C)}{dX_1}=\frac{dW_2(0)}{dX_2} \tag{2.4d}$$

$$\frac{d^2W_1(\beta C)}{dX^2_1}=\frac{d^2W_2(0)}{dX^2_2} \tag{2.4e}$$

$$W_2(C)=0 \tag{2.4f}$$

$$\frac{dW_2(C)}{dX_2}=\frac{dW_3(0)}{dX_3} \tag{2.4g}$$

$$\frac{d^2W_2(C)}{dX^2_2}=\frac{d^2W_3(0)}{dX^2_3} \tag{2.4h}$$

$$\frac{d^2W_3(\beta C)}{dX^2_3} = 0 \tag{2.4i}$$

The solution of equation 2.1 will take the form:

$$W_1 = A_1 \sin\frac{\lambda X_1}{C} + A_2 \sinh\frac{\lambda X_1}{C} + A_3 \cos\frac{\lambda X_1}{C} + A_4 \cosh\frac{\lambda X_1}{C} \tag{2.5}$$

$$W_2 = B_1 \sin\frac{\lambda X_2}{C} + B_2 \sinh\frac{\lambda X_2}{C} + B_3 \cos\frac{\lambda X_2}{C} + B_4 \cosh\frac{\lambda X_2}{C} \tag{2.6}$$

$$W_3 = C_1 \sin\frac{\lambda X_3}{C} + C_2 \sinh\frac{\lambda X_3}{C} + C_3 \cos\frac{\lambda X_3}{C} + C_4 \cosh\frac{\lambda X_3}{C} \tag{2.7}$$

where,

$$\lambda^4 = \alpha C^4 \tag{2.8}$$

Substituting equations 2.5, 2.6, 2.7 into the boundary conditions 2.4, and eliminating constants gives a set of 3 homogeneous equations.

$$B_4[\coth(\beta\lambda) - \cot(\beta\lambda)] - B_1 - B_2 = 0 \tag{2.9a}$$

$$B_4[\cosh(\lambda) - \cos(\lambda)] + B_1 \sin(\lambda) + B_2 \sinh(\lambda) = 0 \tag{2.9b}$$

$$B_4[2[\sinh(\lambda) + \sin(\lambda)] - [\cosh(\lambda) + \cos(\lambda)][\cot(\beta\lambda) - \coth(\beta\lambda)]]$$

$$+ B_1[2\cos(\lambda) + \sin(\lambda)[\cot(\beta\lambda) - \coth(\beta\lambda)]]$$

$$+ B_2[2\cosh(\lambda) - \sinh(\lambda)[\cot(\beta\lambda) - \coth(\beta\lambda)]] = 0 \tag{2.9c}$$

This may be further reduced to a single frequency equation. The first root of the frequency equation corresponds to the required fundamental frequency of the system.

This is a function only of β. The frequency parameter "λ^2" for the first bending frequency of a 3-span beam, calculated for side span/main span ratios (β) of 0.2-0.65, is shown in Figure 2.5a.

2.3.1.2 Torsional Vibration

The torsional vibration of the bridge deck may be described by:

$$\frac{d^2\phi_i}{dX^2_i}+b^2\phi_i=0 \qquad i=1,2,3 \tag{2.10}$$

where,

$\phi_i = \phi_i(X_i)$ = torsional mode shape of i^{th} span.

$$b^2=\frac{\omega^2 I_p}{GJ}-\frac{K_\phi}{GJ} \tag{2.11}$$

I_P = mass polar moment of inertia of the bridge deck.

K_ϕ = equivalent torsional stiffness per unit length of deck, provided by cables, towers and adjacent deck span.

GJ = torsional rigidity of the bridge deck.

The general solution of equation 2.10 is:

$$\phi_1=A_1\sin(bX_1)+A_2\cos(bX_1) \tag{2.12}$$

$$\phi_2=B_1\sin(bX_2)+B_2\cos(bX_2) \tag{2.13}$$

$$\phi_3 = C_1 \sin(bX_3) + C_2 \cos(bX_3) \tag{2.14}$$

Equation 2.10 is subject to the boundary conditions:

$$\phi_1(0) = 0 \tag{2.15a}$$

$$\phi_3(\beta c) = 0 \tag{2.15b}$$

$$\phi_1(\beta C) = \phi_2(0) \tag{2.15c}$$

$$\frac{d\phi_1(\beta C)}{dX_1} = \frac{d\phi_2(0)}{dX_2} \tag{2.15d}$$

$$\phi_2(C) = \phi_3(0) \tag{2.15e}$$

$$\frac{d\phi_2(C)}{dX_2} = \frac{d\phi_3(0)}{dX_3} \tag{2.15f}$$

Substituting the expressions for ϕ_1, ϕ_2, ϕ_3 and their derivatives into equations 2.15a-f, condensing and re-arranging, gives the frequency equation:

$$\cos(\lambda_\phi)[\sin(2\beta\lambda_\phi)] + \sin(\lambda_\phi)[\cos^2(\beta\lambda_\phi) - \sin^2(\beta\lambda_\phi)] = 0 \tag{2.16}$$

where,

$$\lambda^2_{\phi} = b^2 C^2 \tag{2.17}$$

Figure 2.5b shows λ^2_{ϕ} as a function of β. These results may be used with equations 2.11 and 2.17 to approximate the first torsional deck frequency.

2.3.1.3 Calculation of Spring Stiffness (K)

In the case of vertical vibration, the spring stiffness K must include the vertical stiffness effect of the stay cables, towers, and adjacent deck span. In this analysis, reference is made to a segment of a cable-stayed bridge as shown in Figure 2.6. The vertical motion of point "r" is restrained by the resistance of cables "i" and "j", the tower bending stiffness, and the bending stiffness of the adjacent deck span. Cable "i" is anchored at point "r"; cable "j" is the cable on the adjacent span that is anchored at the same location on the tower as cable "i". The equivalent stiffness of the spring support at "r" per unit length is calculated as follows:

$$\frac{1}{K} = \left(\frac{1}{k_{ci}} + \frac{1}{K_{cj}} + \frac{1}{k_T} + \frac{1}{K_D}\right) * S \tag{2.18}$$

where;

$$K_{ci}=\frac{E_{ci}A_{ci}\sin^2(\theta_i)}{h_i} \tag{2.19}$$

$$K_{cj}=\frac{E_{cj}A_{cj}\sin^2(\theta_j)}{h_j} \tag{2.20}$$

are the vertical components of stiffness of cables "i" and "j". The bending stiffness of a prismatic tower is

$$K_T=\frac{3E_TI_T}{H^3} \tag{2.21}$$

and

$$K_D=\frac{3E_DI_DL}{a^2b^2} \tag{2.22}$$

is the bending stiffness of the adjacent span.

In these equations

θ_i, θ_j = acute angles that cables i and j make with the deck, as defined on Figure 2.6.

E_{ci}, E_{cj} = modulus of elasticity of cables i, j.

A_{ci}, A_{cj} = cross sectional area of cables i, j.

h_i, h_j = height above deck level for tower anchor points for cables i, j.

K_T = stiffness of tower acting as a cantilever. The expression assumes prismatic, or near prismatic, towers.

E_T = modulus of elasticity of the tower.

I_T = moment of inertia of the tower for bending in the longitudinal direction.

H = total height of the tower.

E_D = modulus of elasticity of the deck.

I_D = moment of inertia of the deck.

L = adjacent span length; if "r" is on the main span then L is the side span length, and vice versa.

a,b = distances on adjacent span as defined on Figure 2.6.

S = average spacing along the deck between 2 adjacent cable anchor points.

To calculate the stiffness, it is assumed that point "j" does not move when point "i" is in motion and that the effect of stiffness of other cables on the motion of point "i" is negligible. These two assumptions have been made to simplify the procedure. Their effect on frequency estimations was found to be negligible as will be shown in examples in the next section. A set of K's is calculated for all cable anchorage points. The average value of all K's is recommended to be used to calculate the vertical deck frequency.

The elastic spring coefficient K_ϕ for the torsional frequency calculation is related to the vertical elastic spring (K_v) by the following relation:

$$K_\phi = \frac{K_v d^2}{4} \tag{2.23}$$

where,

d= width of the bridge deck.

and

$$\frac{1}{K_v}=(\frac{1}{K_{ci}}+\frac{1}{K_{cj}}+\frac{1}{K_T}+\frac{1}{K_D})*S \qquad (2.24)$$

with K_{ci} and K_{cj} as before, and

$$K_D=\frac{LGJ}{2abd} \qquad (2.25)$$

is the torsional stiffness of the adjacent deck span.

K_T describes the torsional stiffness of the tower. It is dependent on the tower shape and the distance between the two tower legs at the top. To estimate this stiffness component it is required to find the value of the pair of equal and opposite longitudinal forces (F) that are applied at the tower top to make the points e,f of Figure 2.7 move a unit distance (D) apart in the longitudinal direction of the bridge. In the case of the H-shaped towers this stiffness is $K_T = 1.5E_TI_T/H^3$ (I_T is the moment of inertia of both tower legs).

2.3.1.4 Numerical Examples and Accuracy of Models

Two existing cable-stayed bridges were studied using the proposed analytic models, the Quincy Bayview Bridge that crosses the Mississippi River at Quincy, Illinois, and the Jindo Bridge in Korea. Two hypothetical cable-stayed bridges from Nazmy and Abdel-Ghaffar (1987) (NGBI & NGBII) were also included in this study. General lay outs of the bridges are shown in Figure 2.8. All bridges have been analyzed using 3-D finite element models in previous studies, Wilson and Gravelle (1991), Garevski et al

(1991), and Nazmy and Abdel-Ghaffar (1987), and estimations of their frequencies are available from the references. The required structural data of the four bridges are summarized in Tables 2.1 and 2.2, as well as results of calculations of K and estimations of fundamental frequencies using the proposed analytic models. Table 2.3 compares 3-D finite element frequencies to the frequencies obtained from the analytic models.

The first proposed bridge deck analytic model predicts pure transverse deck frequency for bridges with vertical double cable planes with 100% accuracy because the cables do not contribute to the deck stiffness in the lateral direction. In the case of plate girder bridge or any other type of open cross section bridge decks, transverse-torsional coupling occurs due to the eccentricity between mass and stiffness centres and the pure transverse modes no longer exist.

Research conducted by Kosko (1968), shows that the coupling that occurs will affect the frequency values and mode shapes. However, he concluded that the effect on frequency values was found to be very slight (less than 10% in most cases). This result is clearly demonstrated by comparing the analytic predicted transverse frequency of Quincy Bayview Bridge; which is of the plate girder type; to the corresponding value predicted by the finite element method as shown in Table 2.3.

The proposed model predicts the fundamental vertical deck frequency with good accuracy (less than 10% error in most cases). The error may be attributed to neglecting the coupling among the motion of the different deck points, and the approximation in calculating the tower stiffness. There are two approximations made in calculating the tower stiffness, the first is assuming it as a cantilever, the second is in assuming the

cable anchor point is at the top. To evaluate the effect of these two approximations, the stiffness computed from the analytic models of the Quincy Bayview, and the two Nazmy and Abdel-Ghaffar bridges were compared to the stiffness calculated using finite elements. Table 2.4 provides a comparison between the two methods which shows that the error is negligible. When the side span/main span ratio (β) is less than 0.35 (case of Jindo Bridge) there is likely to be fewer cables on the short span side of the tower. In such case, a different approach is required to calculate a representative average value of (K). It is suggested to consider the longest and the shortest cables of the main span with the longest and the shortest cables of the side span.

2.3.2 Bridge Tower

Field measured mode shapes of cable-stayed bridges show that the first few modes involve coupled deck-tower motions. However, at somewhat higher frequencies, it is possible to identify local tower modes that are characterized by bending of towers in the longitudinal direction of the deck without appreciable deck motion. In the following sections this behaviour is modeled analytically using a differential equation approach.

2.3.2.1 Theoretical Formulation

The tower is modeled as a vertical beam fixed at its base and elastically supported at the top as shown in Figure 2.9. The behaviour of the tower is modeled by the differential equation:

$$\frac{d^4v}{dz^4} - \alpha_T z = 0 \qquad (2.26)$$

where,

v = v(z) = deflection of tower in X direction,

z = distance along the tower height, and

$$\alpha_T = \gamma_T \omega^2 / E_T I_T \qquad (2.27)$$

where,

γ_T = tower mass per unit height.

and E_T and I_T are as defined in 2.3.1.3.

The deflection function (v) will take the general form:

$$v = A_1 \sin(\lambda_T \frac{z}{H}) + A_2 \sinh(\lambda_T \frac{z}{H}) + A_3 \cos(\lambda_T \frac{z}{H}) + A_4 \cosh(\lambda_T \frac{z}{H}) \qquad (2.28)$$

with,

$$\lambda^4_T = \alpha_T H^4$$

The geometric boundary conditions are:

$$v(0) = 0 \qquad (2.29)$$

$$\frac{dv(0)}{dz} = 0 \qquad (2.30)$$

$$\frac{d^2v(H)}{dz^2} = 0 \qquad (2.31)$$

and the natural boundary condition at v(H) is:

$$K^{*}v(H)=E_T I_T \frac{d^3 v(H)}{dz^3} \qquad (2.32)$$

where K^{*} = the stiffness of the spring at the tower top.

Equation 2.32 is obtained by equating the shear force just below point "m" in Figure 2.9 to the force in spring K^{*}.

Substituting "v" and its derivatives in equations 2.29-2.32 yields a set of two homogeneous equations:

$$A_2[\sin(\lambda_T)+\sinh(\lambda_T)]+A_4[\cos(\lambda_T)+\cosh(\lambda_T)]=0 \qquad (2.33)$$

$$A_2[K^{*}(\sinh(\lambda_T)-\sin(\lambda_T))-\frac{E_T I_T \lambda_T^{\,3}}{H^3}(\cosh(\lambda_T)+\cos(\lambda_T))]$$

$$+\ A_4[K^{*}(\cosh(\lambda_T)-\cos(\lambda_T))-\frac{E_T I_T \lambda_T^{\,3}}{H^3}(\sinh(\lambda_T)-\sin(\lambda_T))]=0 \qquad (2.34)$$

These can be reduced to a single characteristic equation for the frequency of the tower.

An appropriate value for (K^{*}) may be calculated for fan or radiating cable arrangement, where cables are anchored near the top of the tower:

Calculate the horizontal component of axial stiffness of each cable attached to the tower ($E_c A_c \sin\theta \cos\theta/h$) Figure 2.9. The required K^{*} may be found from the relation:

$$\frac{1}{K^*}=\frac{1}{\Sigma K_{cli}}+\frac{1}{\Sigma K_{cri}} \qquad (2.35)$$

where,

K_{cli}, K_{crj} = horizontal components of the axial stiffness of cables i (on the tower's left side) and cable j (on the right side of the tower).

The value of K^* may be used to calculate the required local tower frequency.

This tower model is applicable to most tower shapes and cable configurations. However, in the case of a harp arrangement of cables changes may be necessary in the evaluation of K^* because the cable anchor points are spread along a substantial portion of the tower height.

The quantity $\Gamma=E_T I_T/H^3K^*$ is used to represent the stiffness properties of the tower with reference to the stiffness K^* of the top elastic spring. A numerical study on the effect of Γ on the values of λ_T was performed and the result is summarized in Figure 2.10. This graph may be used to obtain λ_T provided that Γ is known to predict the fundamental local tower frequency in the longitudinal direction.

2.3.2.2 Numerical Example and Accuracy of the Model

The first longitudinal local tower mode of Quincy bridge was identified using 3-D finite element analysis to have frequency of 2.33 Hz, and the second longitudinal local tower mode was found to have a frequency of 4.4 Hz. The tower height (above the pier) is 220 ft and its moment of inertia about the Y-axis is 3300 ft^4. K^* was found to be 5,300,000 lb/ft and the stiffness parameter (Γ) was evaluated as 0.024. From Figure 2.10

λ_{T1} =3.19 and λ_{T2} = 5.15. These give frequencies of 2.4 Hz for the first local tower mode and 4.8 Hz for the second local tower mode. The agreement between the finite element value of the local tower frequencies and the analytic model frequencies is good.

Although the tower analytic model is very simple, it predicts the fundamental frequency of the tower structure with an error of less than 10%. There is insufficient published data on frequencies of the local tower modes to test the tower model for the Jindo Bridge.

2.3.3 Applicability to Other Bridge Configurations

The frequency equations and parameters given in Figures 2.5a and 2.5b are suitable for computing bridge deck frequencies for 3-span cable-stayed bridges with radiating or fan cable arrangements. This approach may be extended to 2-span cable-stayed bridges as shown in Figure 2.11. In this case the longer span length is "C" and the shorter span length is "βC". There will be 2 differential equations and a process similar to that used in 2.3.1 gives:

$$B_1\sin(\beta\lambda)+B_2\sinh(\beta\lambda)+B_4[\cosh(\beta\lambda)-\cos(\beta\lambda)]=0 \qquad (2.36a)$$

$$-B_1\sin(\beta\lambda)+B_2\sinh(\beta\lambda)+B_4[\cosh(\beta\lambda)+\cos(\beta\lambda)]=0 \qquad (2.36b)$$

$$B_1+B_2+B_4[\cot(\lambda)-\coth(\lambda)]=0 \qquad (2.36c)$$

By eliminating constants this can be reduced to a single characteristic equation.

A plot of λ^2 vs β, computed from the resulted characteristic equation is shown in Figure 2.12.

Two cable-stayed bridges were used to test this model. The first, shown in Figure 2.13a, is basically the right half of the Quincy Bayview Bridge. The second, shown in Figure 2.13b, is the Suigo Bridge in Japan, slightly modified to redistribute the cable anchorage points over the entire left span. The required structural data and average values of K for each structure are shown in Table 2.5. In the same table, the finite element bridge deck frequencies are compared to the analytic frequencies. It is evident that the analytic models are capable of predicting the frequencies quite closely.

2.4 SUMMARY AND CONCLUSIONS

This chapter presents the development of analytic models that can be used to predict the first vertical, transverse and torsional frequencies of the deck, and the first two frequencies of the local tower modes. The proposed analytic models for the deck are based on a differential equation formulation for a multiple span beam and account for the stiffness of the deck, towers and cables. They are applicable to most 3-span and 2-span cable-stayed bridges having radiating or fan shaped cable systems. The analytic models for the towers are based on a cantilever restrained by a spring at the top.

The models were shown to give reasonably accurate frequency estimations compared to values obtained from detailed finite element analysis. Although the finite element approach provides much greater versatility and can produce more detailed responses than the analytic models, the analytic approach is helpful in the early stages of design when frequency estimations may be required for wind engineering, or in determining the frequency range that should be considered in subsequent modal seismic

analysis. These situations may occur before structural details are complete enough to permit development of a detailed finite element model.

Table 2.1 Structural Data and Frequency Calculations of Quincy Bayview Bridge, and Nazmy and Abdel-Ghaffar Bridges (NGB)

	Quincy	Nazmy and Abdel-Ghaffar	
		NGBI	NGBII
Deck:			
Main Span (C) ft	900	1100	2200
Side span/Main span Ratio (β)	0.5	0.44	0.44
E_D lb/ft^2	4.32×10^9	4.18×10^9	4.18×10^9
I_{Tr} ft^4	39.5	15.0	30.0
I_v ft^4	2289	2500	12500
γ_D lb.sec^2/ft^2	250	188	230
Tower:			
E_T lb/ft^2	6.43×10^8	5.80×10^8	5.80×10^8
H ft	220	300	560
I_T ft^4	3300	6700	32000
Cables[1]:			
A_{c1}, A_{c14} ft^2	0.193, 0.164	0.39,0.40	0.86,0.9
A_{c7}, A_{c8} ft^2	0.075	0.12	0.26
h_1, h_{14} ft	165	200	400
h_7, h_8 ft	111	155	315
θ_1, θ_{14} degrees	21.5	22.6	22.6
θ_7, θ_8 degrees	61.6	62.1	62.1
S ft	60	80	160
Spring Stiffness Elements[1]:			
K_{c1}, K_{c14} lb/ft	620000,510000	1200000	1300000
K_{c7}, K_{c8} lb/ft	2200000	2600000	2900000
K_T lb/ft	600000	430000	320000
K lb/ft^2	1320	681	250
K_ϕ lb/ft^2	2200	—	—
Frequency Parameters:			
λ	3.87	3.93	3.93
λ_ϕ	1.55	—	—
Computed Frequencies:			
f_{1v} (vertical) Hz	0.382	0.300	0.170
f_{1Tr} (transverse) Hz	0.604	—	—
$f_{1\phi}$ (torsion) Hz	0.62	—	—

[1] a single entry means that both parameters have the same value.

Table 2.2 Structural Data and Frequency Calculations of Jindo Bridge

Deck:	
Main Span (C) ft	1128
Side span/Main span Ratio (β)	0.2
E_D lb/ft^2	4.32×10^9
I_{Tr} ft^4	62.56
γ_D lb.sec^2/ft^2	74
Tower:	
E_T lb/ft^2	4.32×10^9
H ft	226
I_T ft^4	63.96
Cables[2]:	
A_{c1}, A_{c12} ft^2	0.128
A_{c9}, A_{c10} ft^2	0.053, 0.128
h_1, h_{12} ft	226
h_9, h_{10} ft	226
θ_1, θ_{12} degrees	22.95, 44.6
θ_9, θ_{10} degrees	75.3, 71.6
S ft	65
Spring Stiffness Elements[2]:	
K_{c1}, K_{c12} lb/ft	370000, 1200000
K_{c9}, K_{c10} lb/ft	947500, 2200000
K_T lb/ft	71800
K lb/ft^2	716
Frequency Parameter:	
λ	4.272
Computed Frequencies:	
f_{1v} Hz	0.500

[2] a single entry means both parameters have the same value.

Table 2.3 Comparison of Analytic and Finite Element Frequencies (Hz) of Quincy, Jindo, and NGB I,II Bridges.

Bridge		Quincy	Jindo	NG B I	NG B II
Reference		Wilson and Gravelle 1991	Garevski et al 1991	Nazmy and Ghaffar 1987	Nazmy and Ghaffar 1987
Finite Element Frequency	Vl	0.371	0.467	0.311	0.192
	Hl	0.633	___	0.699	0.301
	To	0.577	___	0.515	0.333
Analytic Frequency Estimation	Vl	0.382	0.500	0.300	0.170
	Hl	0.604	___	___	___
	To	0.620	___	___	___
Error with respect to Finite Element	Vl	3.0%	7%	3.5%	11%
	Hl	4.6%	___	___	___
	To	7.4%	___	___	___

Vl: Vertical
Hl: Transverse
To: Torsional

Table 2.4 Comparison of Analytic and Finite Element Bridge Tower Stiffness

Bridge	Quincy	NGBI	NGBII
Finite Element	620000 lb/ft	431667 lb/ft	317048 lb/ft
Analytic	598800 lb/ft	431050 lb/ft	316832 lb/ft

Table 2.5 Structural Data and Frequencies of Two-Span Cable-Stayed Bridges

	Modified Quincy	Modified Suigo
Deck:		
Main Span (C) ft	450	587.3
Side span/Main span Ratio (β)	1.0	0.6
E_D lb/ft^2	4.32×10^9	4.32×10^9
I_{T_r} ft^4	39.5	4259
γ_D lb.sec^2/ft^2	250	143
Tower:		
E_T lb/ft^2	6.43×10^8	4.32×10^9
H ft	220	144.4
I_T ft^4	3300	52.14
Cables:		
A_{c1}, A_{c14}, (A_{c1}, A_{c6}) ft^2	0.193	(0.678)
A_{c7}, A_{c8}, (A_{c3}, A_{c4}) ft^2	0.75	(0.409)
h_1, h_{14}, (h_1, h_6) ft	165	(141.7)
h_7, h_8, (h_3, h_4) ft	120	(53.2)
θ_1, θ_{14}, (θ_1, θ_6) degrees	21.5	(13.5 , 15.1)
θ_7, θ_8, (θ_3, θ_4) degrees	63.6	(15.1 , 22)
S ft	60	164
Spring Stiffness Elements:		
K_{c1}, K_{c14}, (K_{c1}, K_{c3}) lb/ft	680000	(114.4,269.1)
K_{c7}, K_{c8}, (K_{c3}, K_{c4}) lb/ft	1600000	(226.1,464.3)
K_T lb/ft	300000	22.5
K lb/ft^2	1320	0.12
Frequency Parameter:		
λ	3.145	3.505
Computed Frequencies:		
f_1 (analytic) Hz	0.44	0.31
f_1 (finite element) Hz	0.50	0.33
Error with respect to finite Element	11 %	5.6 %

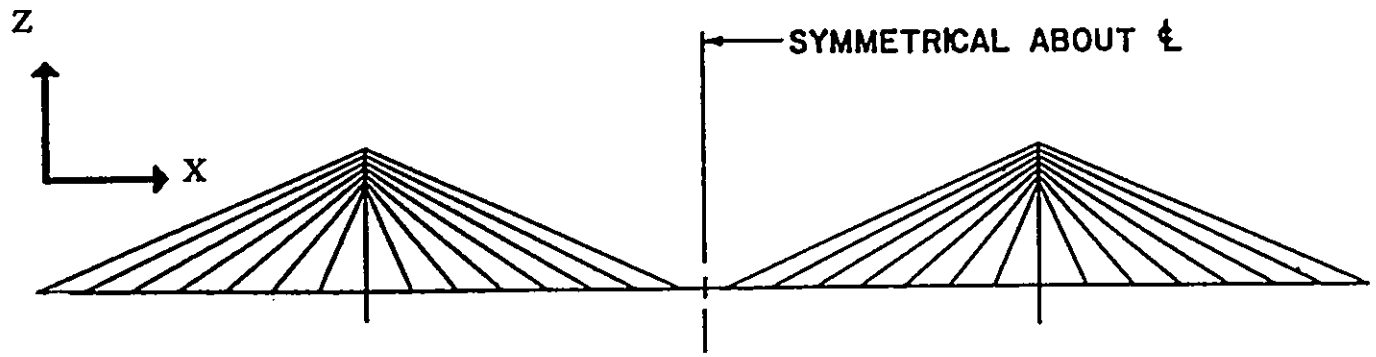

Figure 2.1 Front Elevation of Quincy Bayview Bridge (Wilson and Gravelle, 1991)

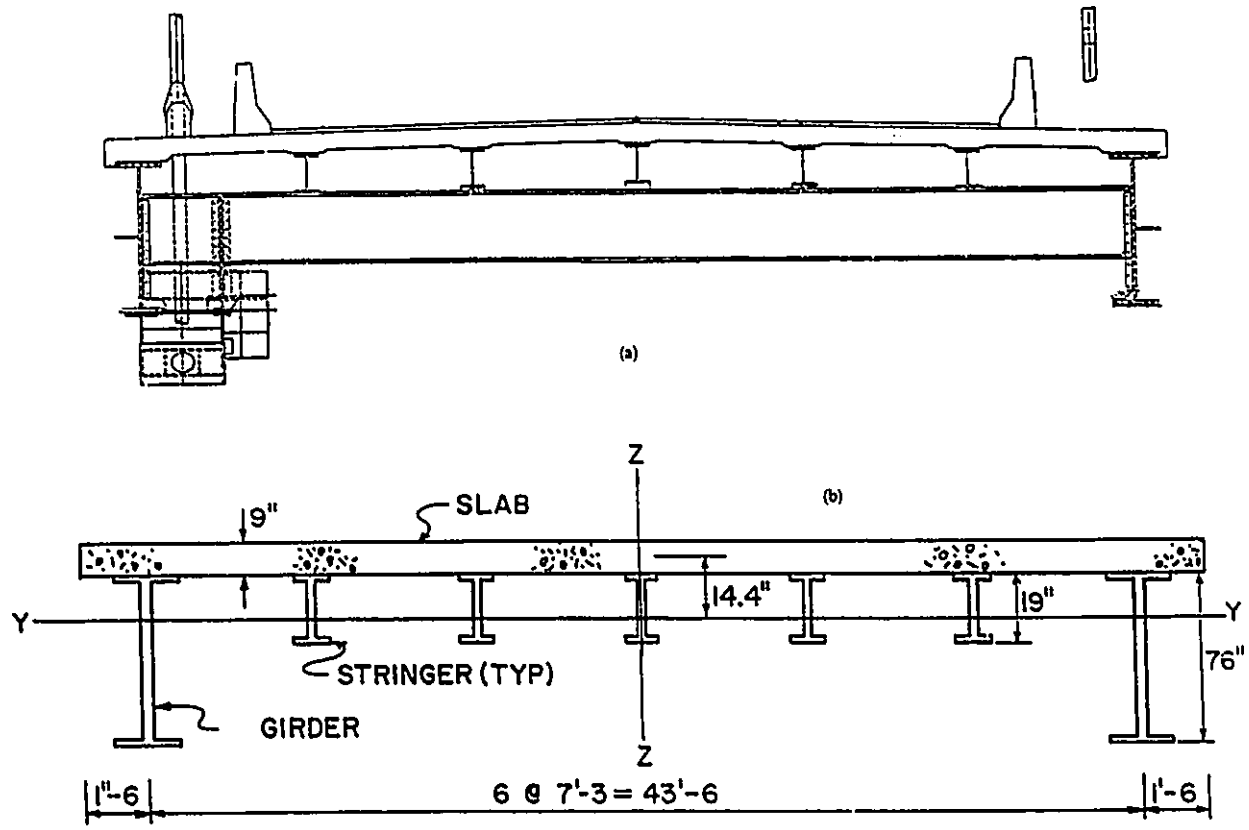

Figure 2.2 Idealized Deck Cross Section of Quincy Bayview Bridge (Wilson and Gravelle, 1991)

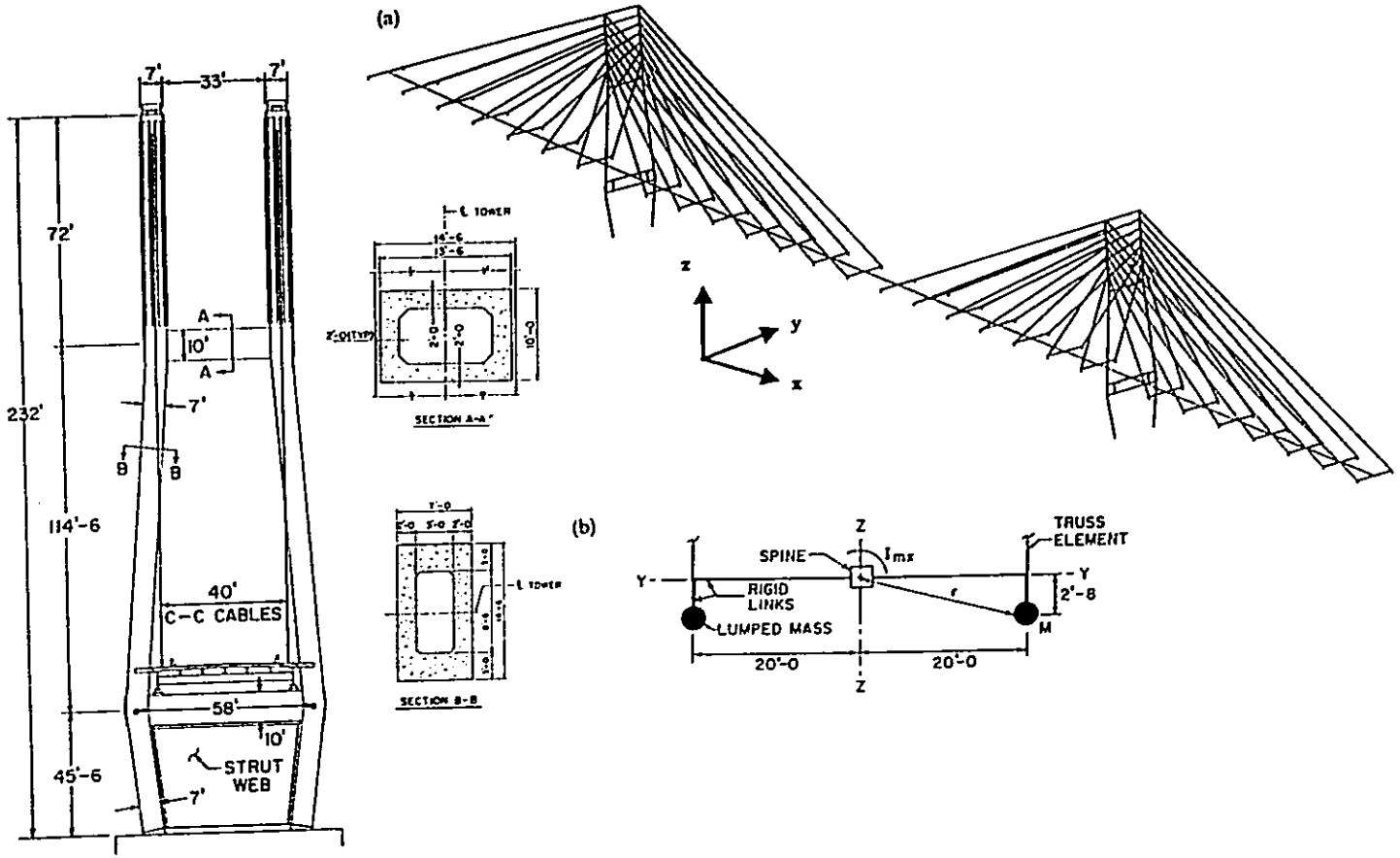

Figure 2.3 Schematic Diagram of 3-D Quincy Bridge Model (Wilson and Gravelle, 1991)

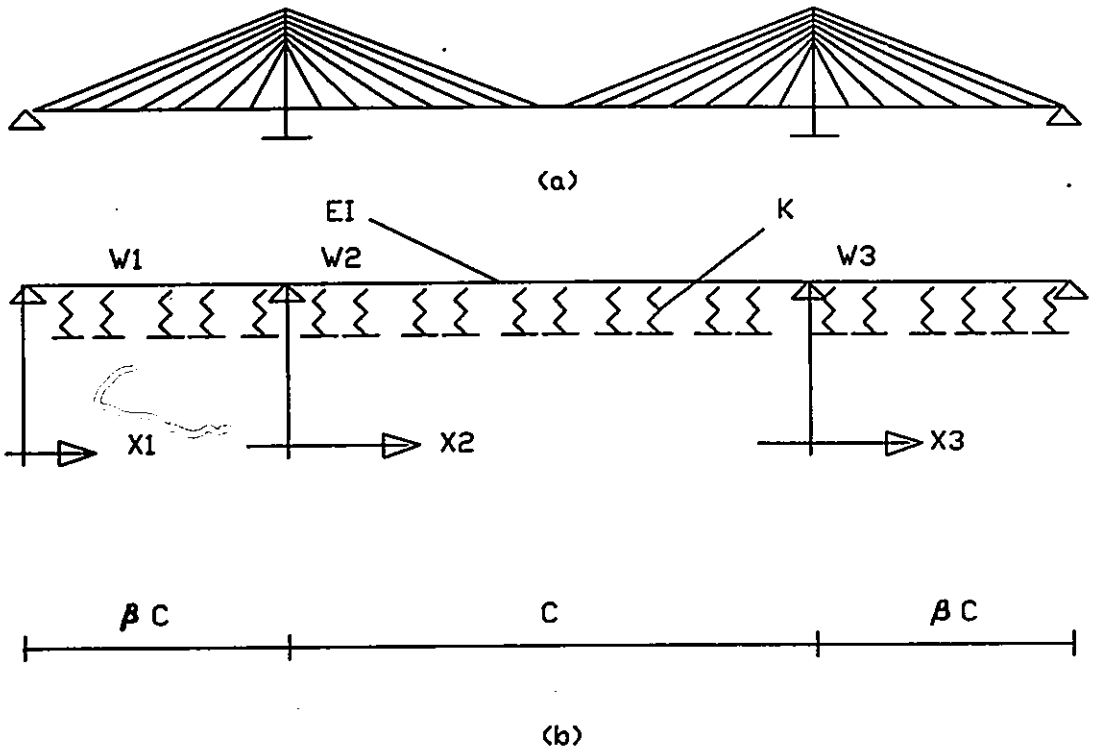

Figure 2.4 a) General Lay out of a Typical Cable-Stayed Bridge with Three Spans and Multi-Cable Arrangement b) Idealization of a Cable-Stayed Bridge as a Beam on Elastic Supports.

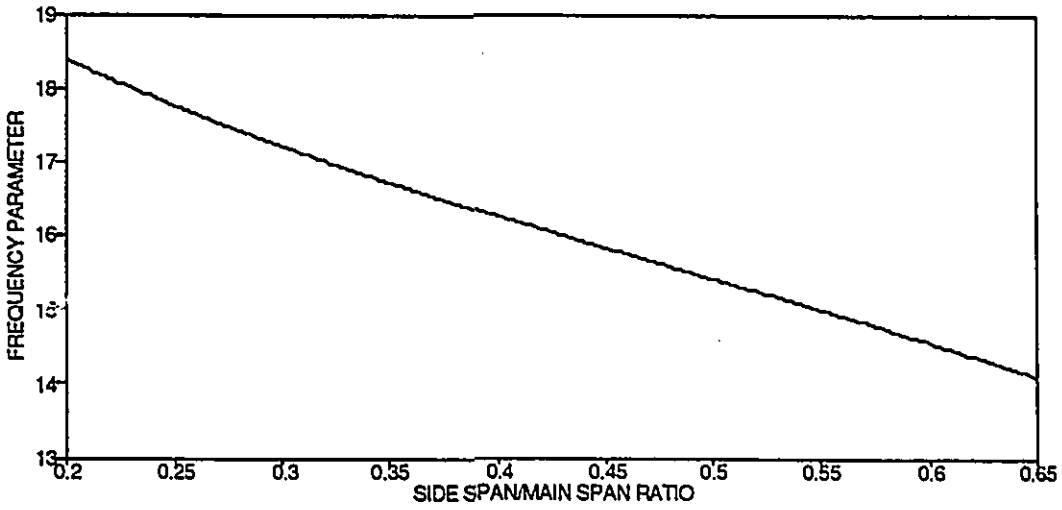

Figure 2.5a Relation Between the Frequency Parameter of the First Bending Frequency of a 3-Span Cable-Stayed Bridge (λ^2_1) and its Side Span/Main Span Ratio (β).

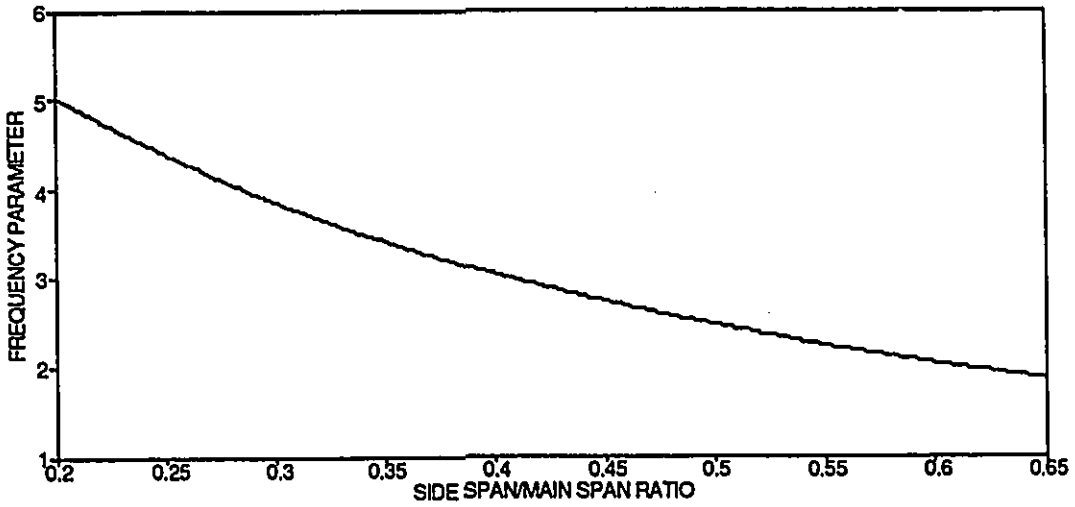

Figure 2.5b Relation Between the Frequency Parameter of the First Torsional Frequency of a 3-Span Cable-Stayed Bridge ($\lambda^2_{\phi 1}$) and its Side Span/Main Span Ratio (β).

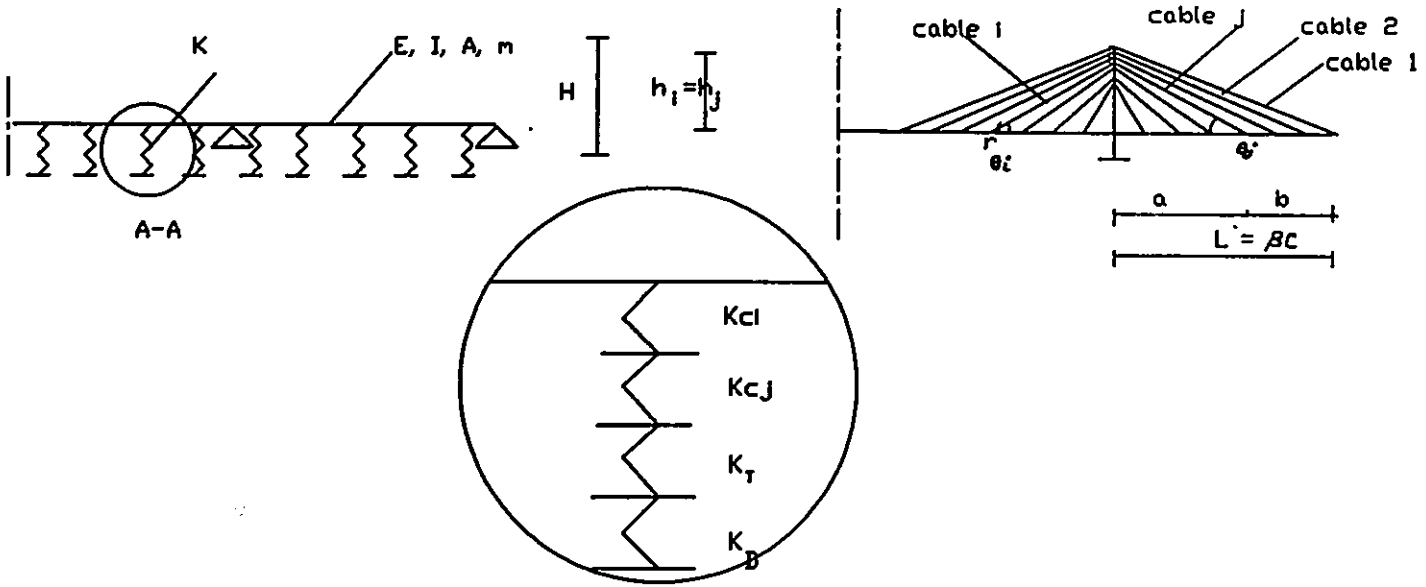

Figure 2.6 Elements of Elastic Spring at Point "r" of a Cable-Stayed Bridge Deck.

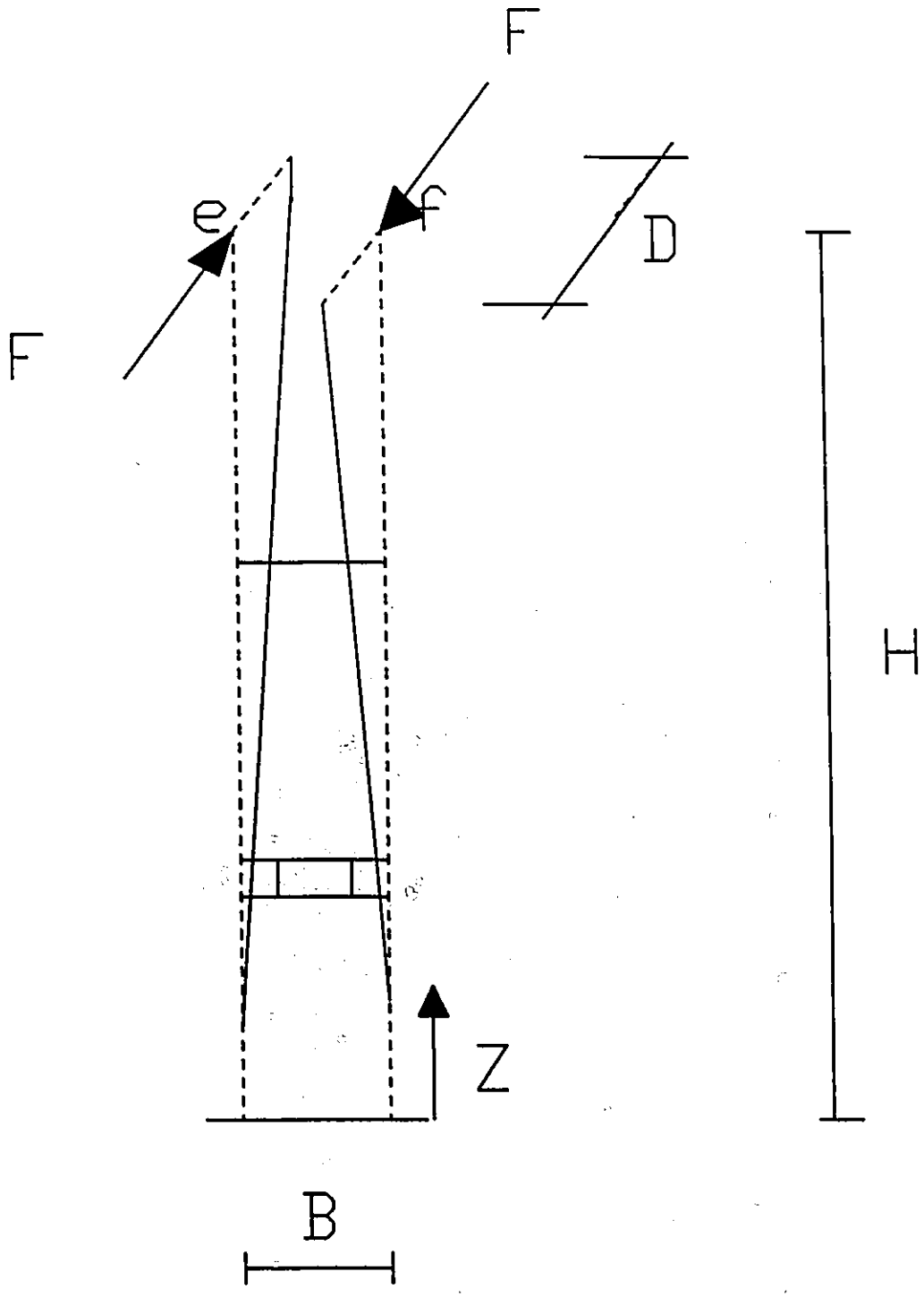

Figure 2.7 Torsional Stiffness of the Tower Structure

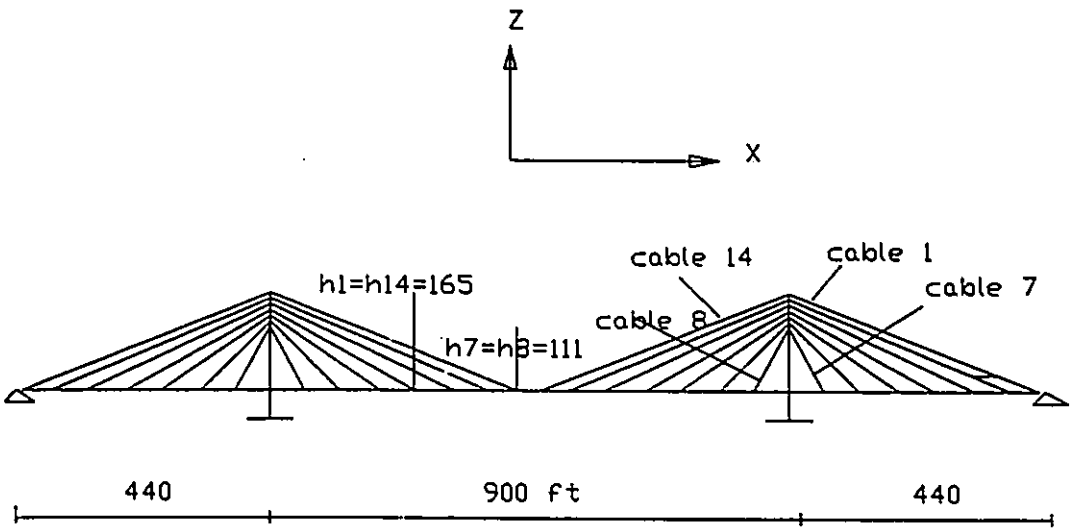

(a) Quincy Bayview Bridge

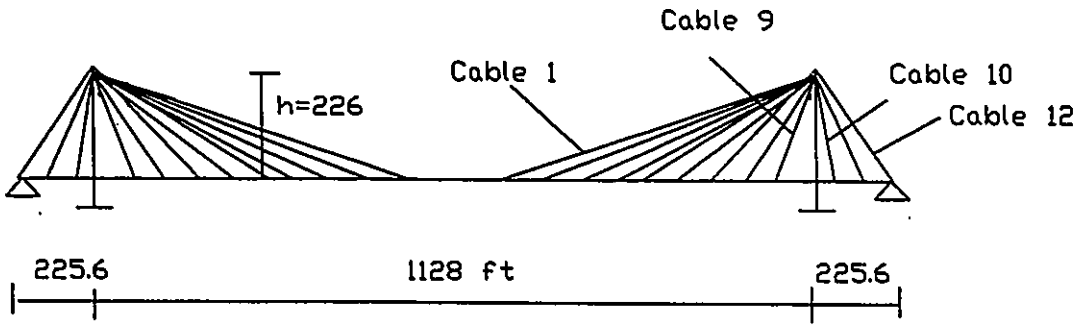

(b) Jindo Bridge (Garevski et al, 1991)

Figure 2.8 Schematic Diagrams of Four 3-Span Cable-Stayed Bridges

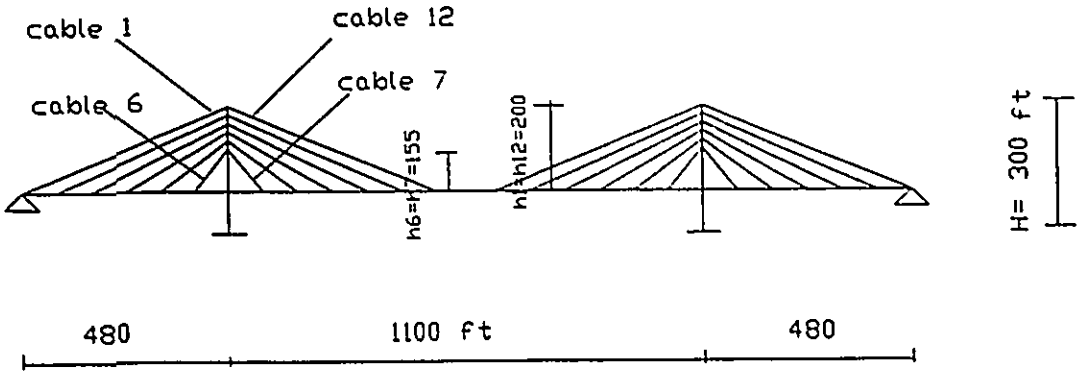

(c) NGBI (Nazmy and Abdel-Ghaffar, 1987)

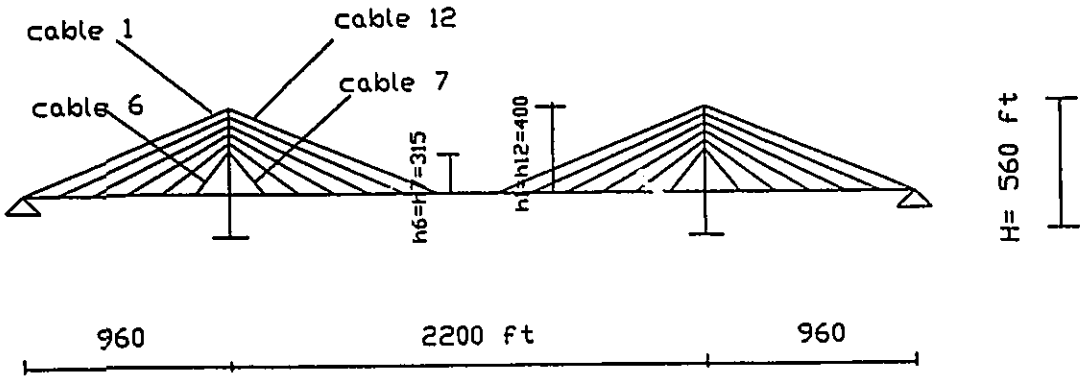

(d) NGBII (Nazmy and Abdel-Ghaffar, 1987)

Figure 2.8 Cont'd

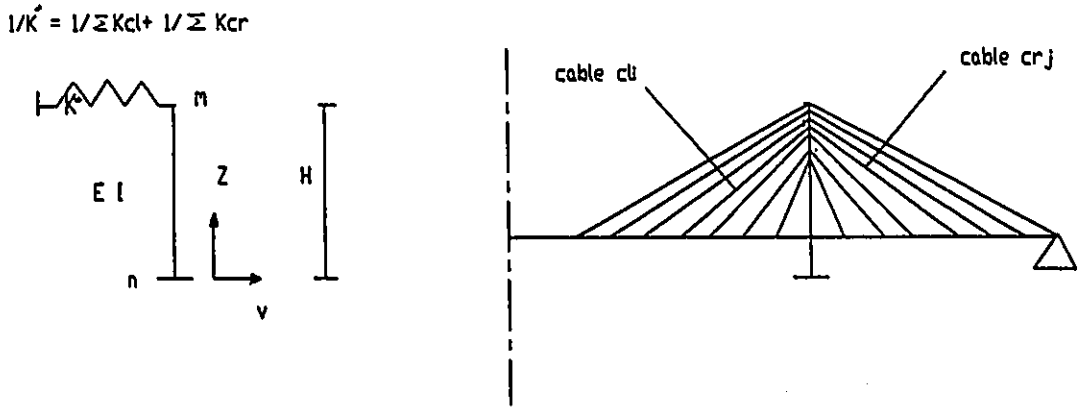

Figure 2.9 Idealization and Elements of Elastic Top Spring for the Tower Model.

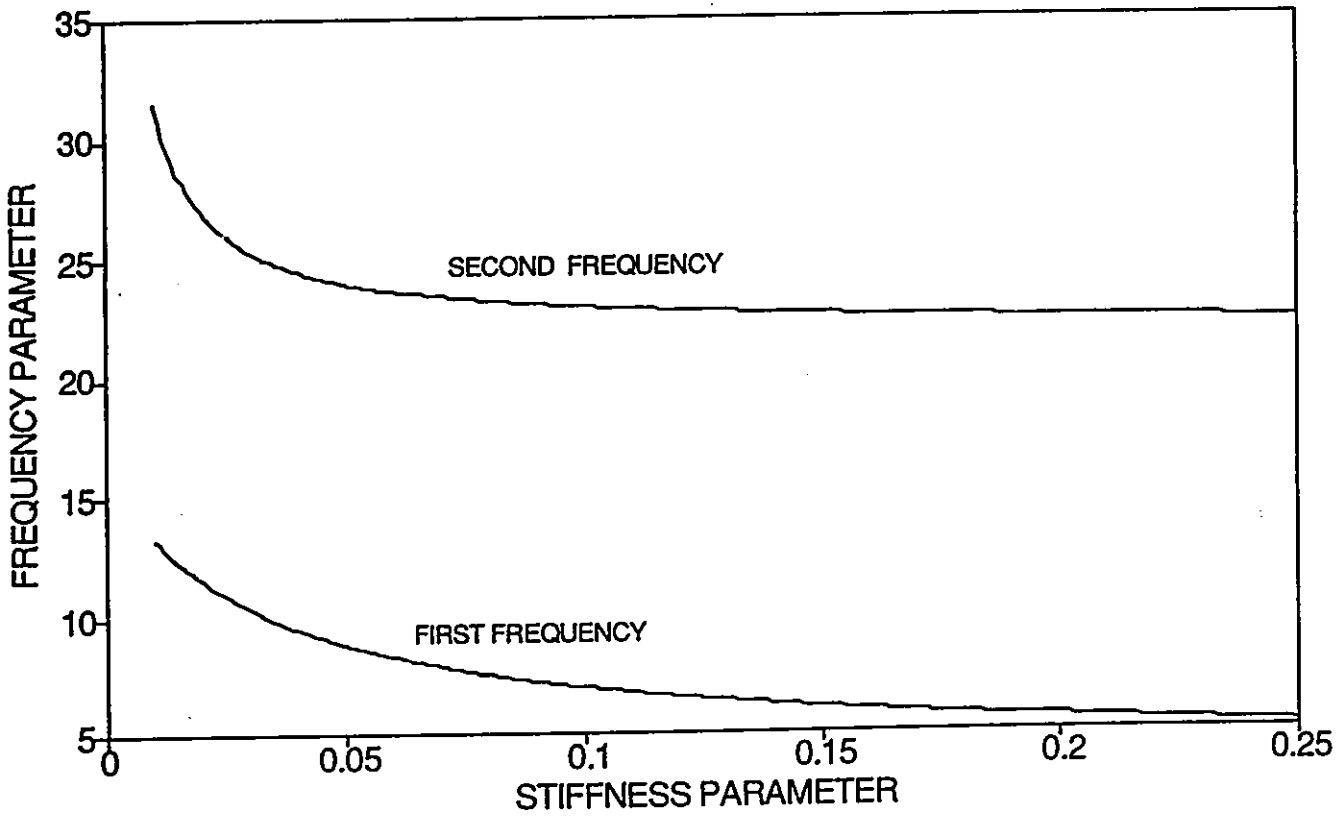

Figure 2.10 Relation Between Frequency Parameter of the Tower's Lowest 2 Local Modes (λ^2_T) and its Stiffness Parameter (Γ)

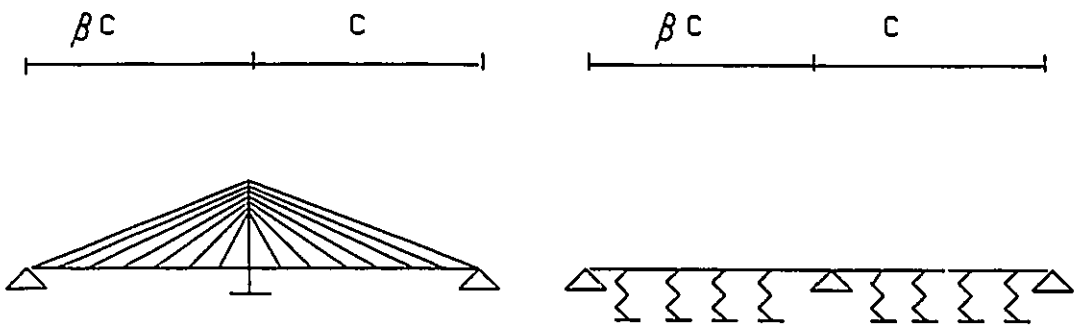

Figure 2.11 General Lay out and Analytic Idealization of a 2-Span Cable-Stayed Bridge.

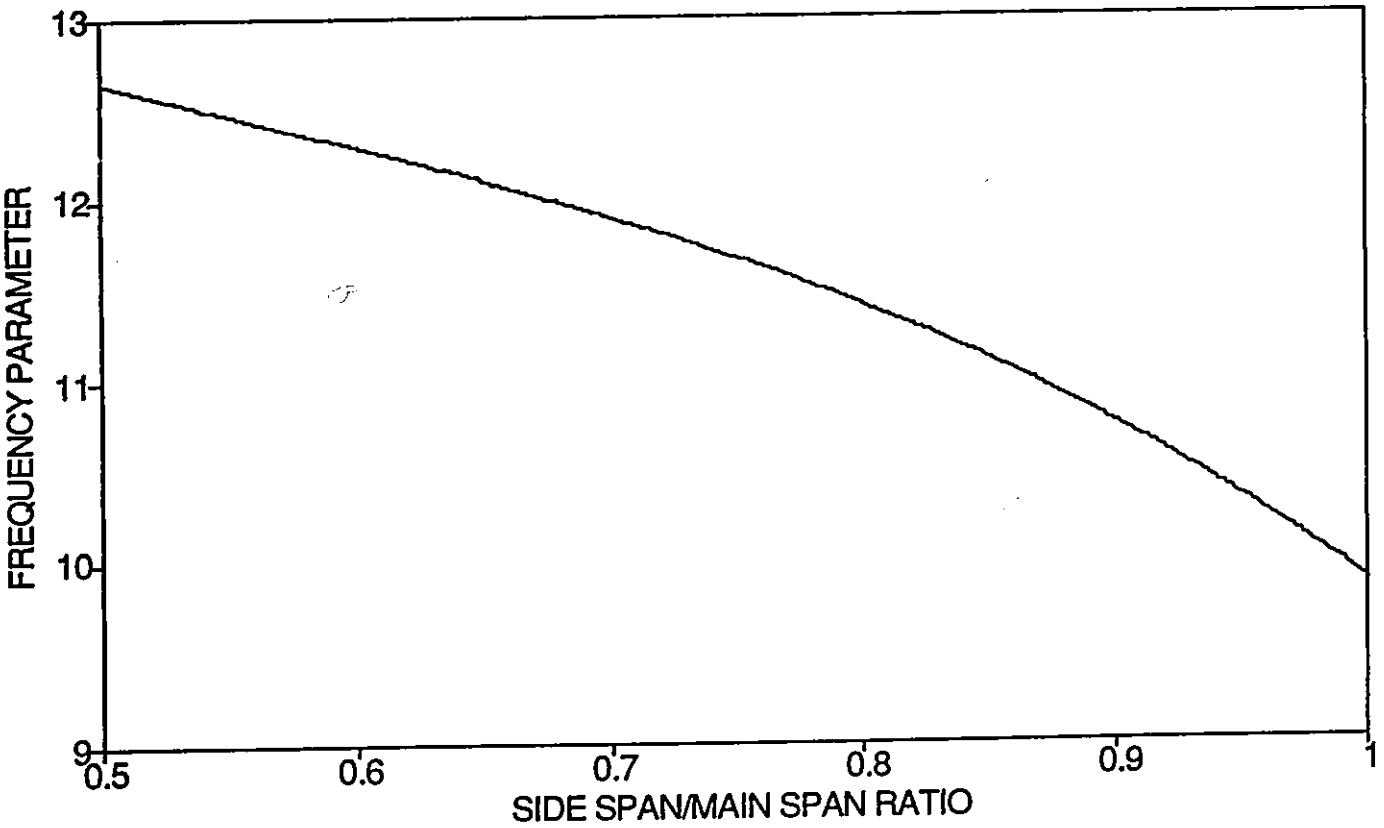

Figure 2.12 Relation Between the Frequency Parameter of the First Bending Frequency of a 2-Span Cable-Stayed Bridge (λ^2_1) and its Span Ratio (β).

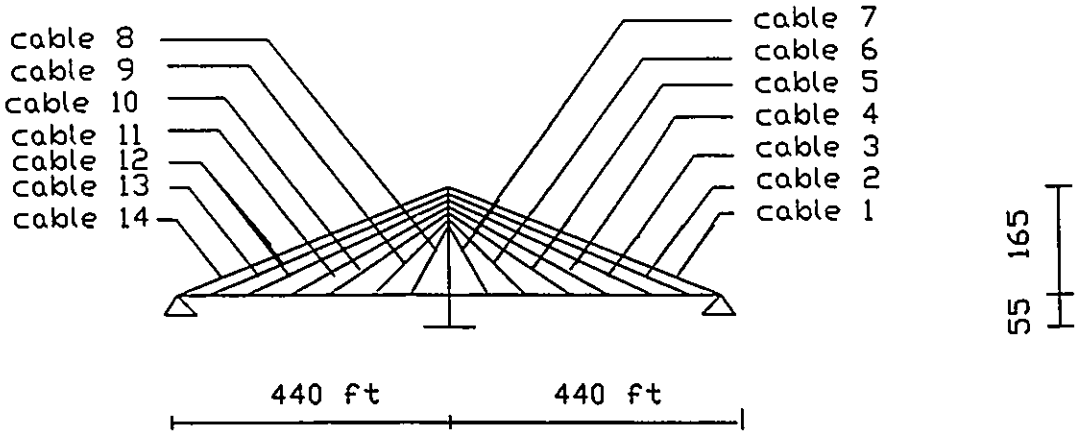

Figure 2.13a Half of Quincy Bayview Bridge.

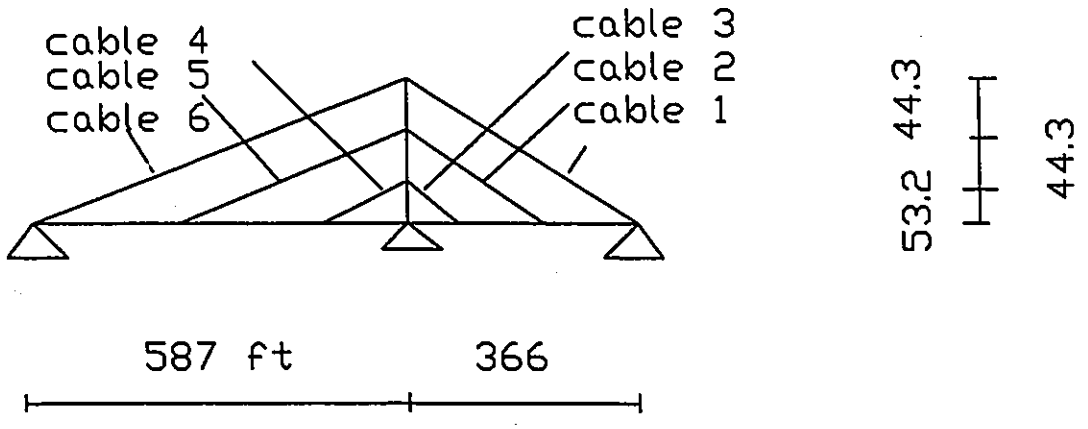

Figure 2.13b Modified Suigo bridge.

CHAPTER 3

DYNAMIC CHARACTERISTICS OF CABLE-STAYED BRIDGES

3.1 INTRODUCTION

In this chapter, a detailed study of the dynamic characteristics of 3-span cable-stayed bridges is conducted using the validated finite element model of the Quincy Bayview Bridge, from section 2.2 as the prototype model. The dynamic characteristics of interest are: frequencies, mode shapes, modal participation factors and effective modal masses. The study investigates frequency-mode number relation, mode classification, modal participation factor-mode number relation, and effective modal mass-mode number relation. The bridge's vertical plane characteristics were studied separately from the torsional/transverse (T/T) characteristics.

The effect of changing major geometric parameters namely, deck eccentricity, tower shape, cable arrangement, cable stiffness and deck support conditions, on the dynamic characteristics of the bridge are investigated. The objective of the study is to develop an understanding of the effect of each parameter on the dynamic characteristics of cable-stayed bridges. The results of this study (and results from Chapter 2) are used in Chapter 4 to define a frequency cut-off criterion for dynamic seismic analysis of cable-stayed bridges.

3.2 MODAL CHARACTERISTICS

A free vibration study was conducted using finite element models to investigate the dynamic characteristics of 3-span cable-stayed bridges, using the 543 m Quincy Bayview Bridge as the prototype. This bridge is representative of a large class of cable-stayed bridges having three spans with double plane symmetric cable-stays. Furthermore, there exists extensive analytic and experimental information on structural and dynamic aspects of this bridge (Modjeski and Masters, 1983; Wilson and Liu, 1991; and Wilson and Gravelle, 1991). The results of an AVS conducted by Wilson and Liu (1991), showed that noticeable spatial coupling occurred in many mode shapes. In almost all modes the longitudinal motion of the towers was found to be coupled to the vertical motion of the deck through the action of the cables. There was also coupling between transverse and torsional motions of the deck because of the vertical eccentricity between the centre of mass and the centre of stiffness of the deck. These observations provide a convenient means to classify the modal behaviour of the bridge into two main groups: (1) modes involving vertical (Z-direction) planar response of the deck and associated longitudinal (X-direction) motion of the towers, and (2) modes involving coupled torsional and transverse (Y-direction) motion of the deck and associated motion of the towers. These two groupings are used in subsequent discussions of the dynamic characteristics.

3.2.1 Frequencies and Mode Shapes

Figures 3.1 through 3.10 show the lowest 10 modes for the full bridge structure, as computed from the 3-D model by Wilson and Gravelle, (1991). This study extends Wilson and Gravelle's interpretation of these mode shapes. Each figure is divided into six parts: (a) and (b) show the mode shape components in the vertical plane (X-Z), and (c) through (f) show the transverse and torsional components of the mode. Line representations of the towers are indicated in (a) and (e), and their locations in the plan view of (c) are shown by solid blocks. In the end elevation views of (b), (d), and (f), the deck is at elevation zero. The frequency of each mode is given on the figure. Within the broad categorization of modes as vertical and torsional/transverse (T/T), a more detailed classification is required to relate the different forms of the mode shapes to basic deformation mechanisms. In the vertical plane category, mode shapes may have one of the following basic deformation mechanisms:

. pure vertical motion of the deck (VL),

. pure longitudinal motion of the deck (LO),

. pure longitudinal motion of the towers (TL),

. vertical motion of the deck coupled with longitudinal motion of the towers (VT).

In the T/T category, mode shapes may have one of the following basic deformation mechanisms:

. pure transverse motion of the deck (TR),

. pure torsional motion of the deck (TS),

. pure transverse motion of the tower (TY),

. coupled transverse-torsional motion of the deck (TT),

. coupled torsional deck-tower motion (ST),

. coupled torsional deck-transverse tower motion (TS-TY),

. coupled torsional motion of deck with torsional-transverse tower motion (ST-TY).

A two-letter symbol is used to a mode shape that has a predominantly single mechanism and where other deformation mechanisms have less than 10% of the maximum eigenvector ordinate of the main mechanism. A four-letter symbol is used to indicate that more than 10% of the maximum scaled eigenvector ordinate is also observed in a second basic mechanism. The 10% limit was selected somewhat arbitrary, but this classification has the basic advantage of providing a means to identify the separate contributions of uncoupled and coupled modes to various response quantities such as forces and displacements.

Table 3.1 provides the classification of the lowest 75 modes of the Quincy Bayview Bridge as computed from the 3-D finite element model. Examination of Figures 3.1-3.10 and Table 3.1 reveals several important features of the modal behaviour of cable-stayed bridges. The results clearly show that Quincy Bayview Bridge has a low fundamental frequency and modes with closely-spaced frequencies. Another prominent feature is that, over one-half of the 75 modes are either vertical (VL) or torsional (TS) deck modes. Relatively few modes exist in each of the other seven mode shape classes. Table 3.1 also shows that only three longitudinal local tower mode exist in the first 75 3-D modes of the bridge. The first local tower mode occurs at a frequency of 2.325 Hz at mode number 42. The second longitudinal tower mode is detected at a frequency of

4.43 Hz which corresponds to mode number 61. Mode number 62 is the same as number 61 but the towers move out of phase. The first transverse tower mode occurs at 1.233 Hz; the second occurs at 2.201 Hz. These frequencies correspond to modes numbers 12, and 39 respectively. Modes 12, 39 involve in-phase transverse motion of the towers. Modes 13, 40 involve out-of-phase transverse motion of the towers. Although some of the coupled deck-tower modes appear at low frequencies and are expected to contribute toward the bridge's dynamic response, contribution toward the total dynamic response of the bridge is also expected from the local tower modes that occur at higher frequencies.

Figure 3.11 shows the frequency-mode number relation for the full 3-D structure. This is a simple and convenient way to display the frequency characteristics of a structure. Frequencies of the vertical plane modes and the T/T modes are separated in Figures 3.12a and 3.12b. Most mode shapes in the vertical plane are vertical bending of the deck. The distribution of vertical frequencies in Figure 3.12a can be explained by comparison to the frequencies of single and multiple span beams. The bending frequencies of a beam are related to the mode number by the relation, Blevins (1984):

$$f_i=\frac{\lambda_i^2}{2\pi L^2}\left(\frac{EI}{m}\right)^{1/2} \qquad i=1, 2, 3, \ldots \tag{3.1}$$

where,

i = mode number.

$\lambda_i = i\pi$ (for single beam).

L = span length.

m = mass per unit length.

I = moment of inertia.

E = modulus of elasticity.

The form of this relation remains the same for single and multi-span continuous beams except for changes in the numerical value of λ_i. Values of the frequency parameter (λ_i^2) for beams with 2 and 3 equal spans are given in Figure 3.13 (Blevins, 1984). The values of λ_i^2 for a single span beam are also given to provide a quantitative comparison. It is noticed that increasing the number of spans reduces the values of λ_i^2 and consequently flattens the relation between the frequency and mode number. This is the reason for the nearly linear relation between the frequency and mode number for the vertical plane of the cable-stayed bridges shown in Figure 3.12a.

Frequencies of the T/T modes, as described by Figure 3.12b, appear to be a bi-linear function of the mode number. A sharp change in the slope of the line in Figure 3.12b at T/T mode 35 is observed, indicating a change in the mode type. The lowest 35 T/T modes are mainly torsional deck modes (only five are transverse deck and tower modes) that have low, closely-spaced frequencies because of the low torsional rigidity of the deck. Frequencies of the transverse modes of the deck and tower are well separated and hence most of them appear at high frequencies after all torsional deck modes have appeared.

3.2.2 Modal Participation Factors

A modal participation factor "$\Gamma_{j,m}$" is defined (Clough and Penzien 1975) as:

$$\Gamma_{j,m} = \{\phi_j^T\}\,[M]\,\{r_m\} \tag{3.2}$$

where,

j = mode number.

m = X, Y, or Z global directions.

$\{\phi_j\}$ = j^{th} mode shape, normalized here so that $\{\phi_j^T\}[M]\{\phi_j\}=1$.

$\{r_m\}$ = influence factors vector for the m^{th} direction.

[M] = mass matrix of the structure.

The modal participation factor $\Gamma_{j,m}$ indicates the extent to which the response in mode "j" will be excited by the earthquake component in direction "m". For framed structures, modal participation factors are often used as a criterion to determine the number of modes to include in a dynamic modal superposition analysis because of their obvious trend of decay for higher modes. Figure 3.14 shows the modal participation factors of the previously generated 75 mode shapes of the cable-stayed bridge in the three spatial directions. It is difficult to identify a clear trend in the behaviour of $\Gamma_{j,m}$ as the mode number increases, although there does appear to be a gradual decay in $\Gamma_{j,Z}$ for higher modes (Figure 3.14c).

Figure 3.15 shows the same data after separating the vertical plane modes from the T/T modes. Although decay trends are not entirely obvious in these figures either,

they do indicate that there is a different behaviour of $\Gamma_{j,m}$ for each class of mode (i.e. VL, TR, TL, ...). It may be deduced from Figures 3.14 and 3.15 that, most response quantities will be affected by only a few number of modes. Collectively, however, the full 3-D bridge response depends on many modes. Hence, an arbitrary choice of the number of modes to be used in a dynamic modal superposition analysis may result in important higher modes being omitted. In order to ensure the inclusion of these important higher modes, criteria are required that specify an appropriate upper frequency limit for the analysis. This upper frequency limit should be based on the dynamics of the structure as well as the expected frequency content of the input motion. In this thesis it is referred to it as a cut-off frequency.

The foregoing discussion showed that modal participation factors do not seem to be suitable for defining the required frequency cut-off criteria for modal analysis because they do not show a clear decay trend for the 3-D finite element model of the cable-stayed bridge. Hence, it is difficult to determine, a priori, an upper frequency limit for ensuring that all important modes are included in modal analysis of cable-stayed bridges.

Another candidate that has been considered as a basis for the required criteria is effective modal mass. The suitability of this quantity is investigated in the following section.

3.2.3 Effective Modal Masses

Effective modal mass, for mode j and global direction m, is defined as (Habibullah and Wilson, 1989):

$$\%EM_{jm} = \frac{(\sum_i M_{im}\phi_{imj})^2}{\sum_i M_{im}\phi_{imj}^2} * \frac{100}{\sum_i M_{im}} \qquad (3.3)$$

where,

m = X, Y, or Z global directions.

i = structural node number.

j = mode number.

M_{im} = translational mass associated with the i^{th} node in the global m direction.

ϕ_{imj} = translational component at the i^{th} node in the global m direction of the j^{th} mode shape.

The effective modal mass ($\%EM_{jm}$) measures the percentage of the total mass that is excited by the j^{th} mode shape in the m^{th} global direction. This interpretation implies that its value represents the percentage of the total response that is expected to come from the j^{th} mode shape in the m^{th} direction.

Figure 3.16 shows the effective modal mass in the three spatial directions as a function of the number of modes (eigenvectors) included in a 3-D analysis of Quincy Bayview Bridge. The horizontal intervals on the curves indicate modes that do not contribute in the specified direction. Increasing the number of modes included in the response will increase the percentage of effective modal mass, up to a maximum of 100% when all possible modes are included. The obvious growth trend and the 100%

ceiling value of $\%EM_{jm}$ make modal mass a more suitable basis for frequency cut-off criteria. Its use in setting the frequency cut-off criteria is described in section 4.5.

3.2.4 Modal Damping

It has been reported by Wilson and Liu (1991), Wilson and Gravelle (1991) and Kawashima et al (1992) that frequencies and mode shapes of cable-stayed bridges can be reasonably predicted using finite element modelling. On the other hand, little information is available about damping characteristics of cable-stayed bridges. Kawashima et al (1988, 1989), presented experimental and analytical study on the damping caused by friction at movable supports of three hypothetical cable-stayed bridges. The results of the study gave an indication that this kind of damping is very low (calculated damping ratios were less than 0.5%). Kawashima et al (1990) analyzed the recorded response of Suigo Bridge in Japan under 20 strong ground motions. They correlated the response calculated using finite element dynamic analysis to the recorded response by examining different damping ratios. They found that damping ratios between 1%-2% gave good response predictions for the towers, and damping ratios between 2%-5% gave good response predictions for the deck. Kawashima et al (1993), showed experimentally (on 5 different lab models of cable-stayed bridges with different cable arrangements) that damping ratios are strongly dependent on mode shapes, cable arrangement and oscillation amplitudes. They presented an analytic method to calculate the energy dissipation within each sub-system of the bridge (deck, towers) and correlated the calculated energy dissipation values with the damping ratio of the considered sub-system. They reported damping

ratios of 0.5%-5% for the different sub-systems in the models.

In the present study, a damping ratio of 2% was used for all modes. This is a generally conservative value for use in seismic design of cable-stayed bridges, and it also avoids the complexity of using different damping ratios for different parts of the bridge. This approach is judged to be appropriate for this study, as the main objectives of the work are to address issues other than damping in the dynamic and seismic response of cable-stayed bridges. Choice of other values of damping will not appreciably alter the results of this study because according to Newmark and Hall (1982) the acceleration spectral values increase by about 15% when the damping is reduced from 2% to 1%, and decrease by about 10% when the damping value is increased from 2% to 5%.

3.3 GEOMETRIC PARAMETERS AFFECTING THE DYNAMIC CHARACTERISTICS OF CABLE-STAYED BRIDGES

In this section a parametric study is described that investigates the effect of changes of deck eccentricity, tower shape, cable arrangement, cable stiffness, and deck support conditions on the dynamic characteristics of cable-stayed bridges. These parameters were chosen because they represent the most significant geometric changes that can be made to the three main structural systems (deck, tower, cables). Changes in span length are not included here because they were studied through the examples provided in Chapter 2.

Five modifications were made to the 3-D reference finite element model. Each modification was applied separately as follows to study the influence of each parameter:

1- The effect of deck eccentricity (e), as shown in Figure 3.17a, was studied using a low and high eccentricity based on one-tenth and twice the original Quincy Bridge eccentricity (0.27 ft and 5.4 ft, respectively) .

2- The tower shape was changed from the original H-shape to an A-shape, and a diamond-shape, as shown in Figure 3.17b.

3- The original fan cable arrangement was modified to examine radiating and harp cable arrangements as shown in Figure 3.17c.

4- Cable stiffness effects were examined using two extreme stiffnesses based on one-half and twice the cross sectional cable areas of the original Quincy Bridge cables.

5- The effect of deck support on the dynamic characteristics of cable-stayed bridges was investigated by comparing the frequencies and mode shapes of the original 3-D model of the Quincy Bridge which has a deck with pinned ends and roller supports at the towers, to those of the same model with roller ends and pinned to the towers, and to those of a model with completely movable deck in the longitudinal direction as shown in Figure 3.17d.

Table 3.2 summarizes the different geometric parameters and their assigned values.

Tables 3.3 and 3.4 present a summary of the frequencies and mode shape classifications for the first 30 modes as a representative sample of the modes generated for items 1 to 4 above. Item 5 is discussed separately in section 3.3.5. The following general observations are made on the results shown in Tables 3.3 and 3.4; specific observations related to each parametric variation are discussed in sections 3.3.1 to 3.3.5:

- The fundamental bridge mode shape is a coupled vertical deck-longitudinal tower mode (VT). The only exception to this is the case of the longitudinally movable

bridge deck where the fundamental mode becomes a longitudinal deck-tower mode.

- The majority of mode shapes (21 out of 30) are T/T modes because the bridge deck has low torsional stiffness. Only nine modes were detected in the vertical plane.
- In the vertical plane category most mode shapes are predominantly vertical deck modes.

The following sections provide further analyses and discussions of each parameter.

3.3.1 Deck Eccentricity

Cable-stayed bridges may have various deck shapes such as plate girders, single, twin, or multiple box girders, or thin prestressed concrete sections. Figure 3.18, from Podolny and Scalzi (1986), shows sample shapes of existing cable-stayed bridge cross-sections. These geometric bridge deck shapes have different values of the vertical offset (deck eccentricity "e") between the shear centre and the centre of mass of the deck cross-section, and this is the principal reason for considering a range of possible eccentricities. Plate girder bridge decks with open cross-section such as the Quincy Bridge may have considerable deck eccentricity while prestressed concrete bridge decks, such as the Dame Point Bridge (Figure 3.18), having shallow edge beams will have a very small deck eccentricity. Figure 3.19 shows frequencies computed for the three cases, separated into the vertical and T/T frequency classifications. It is noticeable that large changes in deck eccentricity have little effect on the frequency values. On examining Table 3.4, it is also

noticeable that the number of coupled T/T deck modes increases with an increase in the value of (e). These observations are in good agreement with the work conducted by Kosko (1968), on simple beams with stiffness eccentricities.

The case of (e = 0) was not considered because it is known that this value of (e) will simply cause the T/T coupling in the deck modes to disappear, and that the effect of the deck eccentricity on the frequency values is slight as shown earlier.

3.3.2 Tower Shape

Three tower shapes were studied: H-shape (such as original Quincy Bridge, Quincy, Illinois, and Alex Fraser Bridge, Vancouver), A-shape (similar to the tower shape of the Skytrain Bridge, Vancouver and Severin Bridge, Germany), and diamond-shape (such as the Kohlbrand Bridge, Germany and the Saint Nazaire Bridge, France). The 3-D model of Quincy Bridge is the reference model with an H-shape tower. The geometry of the tower was altered to give the A-shape and diamond-shape cases. The cables were anchored in the top 55 ft of each tower. Other parameters were kept at the values specified for the original H-shape tower. The frequencies of the lowest 30 modes for each of these configurations were calculated and separated into vertical and T/T frequencies. The frequencies of each category are shown in Figure 3.20. In the vertical plane, the different tower shapes do not affect the frequency values because the influence of the change in the tower shape is restricted to response in the transverse direction only. For the torsional/transverse response, it is noticeable that both the A-shape and diamond-shape towers stiffen the bridge structure for torsional vibrations because they have greater

torsional stiffness (about the vertical axis of the towers) than the H-shape towers. They also add stiffness to the bridge deck in the transverse direction because the cable planes are oblique and hence cable forces have transverse components that resist the transverse deflection of the deck. The A-shape produces the greatest torsional stiffness.

The mode classification presented in Table 3.4 shows that the shape of the tower does not substantially affect the mode shapes or the degree of spatial coupling in the case of the A-shape tower. However, in the case of a diamond-shape tower more coupling is introduced between the deck and tower transverse/torsional motions (evident from the increase in coupled torsional deck-transverse tower modes). The reason is that the A-shape tower is stiffer than diamond-shape tower in the transverse direction and hence has higher transverse frequencies than diamond-shape tower. These high transverse frequencies for the A-shape tower are separated from the deck torsional frequencies. However, the diamond-shape tower has transverse frequencies that are close to some of the deck torsional frequencies.

3.3.3 Cable Arrangement

The three cable arrangements studied were harp (such as the Higashi-Kobe and Suigo Bridges, Japan), radiating (such as the Papineau Bridge, Montreal) and fan (such as the Quincy Bayview Bridge, Illinois, and the Alex Fraser Bridge, Vancouver) arrangements. These arrangements are shown in Figure 3.17c. In the harp cable arrangement, cables are connected to the tower at different heights and are placed parallel to each other. This makes the cables appear not to be visually crossing each other when

viewed at an oblique angle. For this reason, this arrangement may be preferred to the others from an aesthetic point of view. In the radiating cable arrangement, all cables are attached near the top of the tower. This arrangement causes congestion at the tower top and requires special design consideration to carry the vertical force at the tower top. The fan cable arrangement (original Quincy Bayview Bridge) is a modification of the harp arrangement where the cables anchorages are spread over a considerable portion of the tower's height but the cables are not parallel. This cable arrangement enables the removal of one cable, for maintenance or replacement, without endangering the structural safety of the whole bridge and so, it is preferred in most modern designs of cable-stayed bridges.

Figure 3.21 shows the frequencies as a function of mode number for the three cable arrangements. The harp cable arrangement provides the most flexible deck supporting system because its cables are parallel at the least inclination angle with the deck so that the vertical stiffness component of a cable "i" in this arrangement is (Figure 3.17c):

$$K_{Hi} = \frac{E_{ci}\, A_{ci}\, \sin^2\theta_H}{h_i} \qquad (3.4)$$

where,

θ_H = The acute angle between cables and deck.

The other parameters were defined previously in Equation 2.19. This results in relatively

low frequencies in the vertical and torsional vibrations of the bridge. Using a harp cable arrangement rather than a fan cable arrangement has led to a reduction of 10% in the fundamental vertical frequency and a maximum reduction of 23% in vertical frequencies. The effect on the torsional frequencies was less pronounced. Only a 1% reduction in the fundamental T/T frequency and a maximum reduction of 13% were observed in the torsional/transverse frequencies.

The radiating cable configuration provides the stiffest deck supporting system because cables are not parallel and the least angle a cable makes with the deck equals θ_H. The result is relatively higher frequencies than the harp or fan cable arrangements in both the vertical and T/T directions. The increase in the frequency values is very slight. Approximately 1% increase was observed for the fundamental frequencies.

It is also noticeable that the shapes of vibration modes are slightly affected by the type of cable arrangement as shown in Table 3.4.

3.3.4 Cable Stiffness

A change in the cable areas can produce a significant change in the frequencies, as shown in Figure 3.22. Doubling the cable stiffness (to 2EA) results in an increase in bridge frequencies of about 25%-30%. A decrease of similar magnitude in frequencies occurs when the cable stiffnesses are reduced to 0.5EA. The change in the fundamental bridge frequency (Table 3.3a; mode 1) for these two conditions is the largest change observed for all the parametric variations in this study. The cable stiffness influences the coupling between the deck and the tower torsional motions. Less coupling is observed

between the deck and the tower torsional motions when the cable stiffnesses are decreased and greater coupling occurs when the cable stiffnesses are increased. This may be attributed to the fact that increasing the cable stiffness causes the torsional deck frequencies to increase to the point where they approach the torsional frequencies of the tower modes. The influence of cable stiffnesses on this coupling is shown in Table 3.4 where a greater number of coupled deck-tower torsional modes occur, and these appear earlier in the mode sequence than for the cables with decreased stiffness.

The loss of function of a cable during the lifetime of the bridge is a possible situation, though its probability is very low. To examine this aspect, the influence of removal of a single cable, a pair of cables, and multiple-paired cables on the overall dynamic characteristics of the Quincy Bridge was investigated. The results were examined to evaluate the practicality of assessing seismic damage to cable-stayed bridges by monitoring changes in the bridge frequencies. The 3-D finite element model of Quincy Bridge was used in the analysis after applying each of the following changes separately:

1- removal of a single backstay (single cable 1 at the left end of the deck as shown in Figure 2.8a)

2- removal of the outer most pair of backstays (pair of cable 1 at the left end of the deck as shown in Figure 2.8a)

3- removal of the two outer most pairs of backstays (both pairs of cable 1 at both left and right ends of the deck)

The effect of these changes on the frequencies was found to be very limited. In the first case the fundamental frequency decreased to 0.3588 Hz (3% difference from the original

Quincy Bridge fundamental frequency) and the first torsional/transverse frequency changed to 0.4766 Hz (4% decrease from the first TT frequency of the original Quincy Bridge). The second case gave a fundamental frequency of 0.3470 Hz (a decrease of 6% from the original). The third case gave fundamental frequency 0.3219 Hz (a decrease of 13% from the original) . The change in frequency decreases with higher modes. In all cases, the effect was limited to the first five modes. Deck mode shapes lose their symmetry as a result of removal of one backstay or a pair of backstays.

The percentage changes in frequency noted above are detectable using spectral analysis of bridge vibration measurements. However, the above study tends to be an extreme case scenario where the loss of stiffness is significant. One of the great benefits of detection of structural damage using vibration monitoring is to detect damage that is not readily visible to the eye. In this case, less pronounced change to the stiffness caused by structural damage may well result in changes in frequencies of much less than a few percent. Using this type of approach, a combination of frequency and mode shape monitoring may be a superior procedure, rather than relying solely on changes in frequency.

3.3.5 Deck Support Condition

The connection of a cable-stayed bridge deck to the abutments in the longitudinal direction may take various forms ranging from a free connection (such as used on the Higashi-Kobe Bridge, Japan) to a fully restrained (pin) connection. Under static loading, a free cable-stayed bridge (self anchored) has an inefficient normal force distribution

along the deck because the whole deck length is under axial compression as shown in Figure 3.23a (Ohtsuka and Sonoda, 1987). On the other hand, a cable-stayed bridge deck with pinned abutments usually has, due to its long span, an expansion joint in the side span (partially anchored bridge). This situation is more desirable because it gives a more efficient axial force distribution along the deck as some portions of the deck are under tension and others are under compression as shown in Figure 3.23b, (Ohtsuka et al, 1984; and Gilsanz and Biggs, 1983). This contributes to a reduction in cost of the bridge because the deck section will be smaller as a result of having shorter lengths under compression. At the towers, the deck may be designed to be free to move longitudinally with respect to the towers (original Quincy Bridge) or it may be pin-connected to the towers.

Frequencies and mode shapes of the original Quincy Bridge 3-D finite element model (deck is pin-connected to the abutments and free in the longitudinal direction at the towers) were compared to the frequencies and mode shapes of: (1) the original model with the deck having movable ends and pins at the towers and (2) the original model when the deck is completely free to move longitudinally with respect to abutments and towers. In the first case fundamental mode shape is the same and the frequency increases from 0.371 Hz to 0.389 Hz. When the bridge deck is free to move longitudinally, a new fundamental low frequency longitudinal deck-tower mode appears at a frequency of 0.230 Hz. This first mode is a coupled longitudinal deck-tower mode. The vertical, transverse and torsional deck modes are not affected by the change in the support condition at the deck ends. The local tower modes, previously identified for the original Quincy Bridge

remain at the same frequencies. The result is that (with the completely free deck) the tower becomes more susceptible to both low and high frequency excitations because the bridge has a fundamental coupled longitudinal deck-tower mode with a very low frequency, coupled vertical deck-longitudinal tower modes with moderate frequencies, and local longitudinal tower modes with high frequencies.

3.4 SUMMARY AND CONCLUSIONS

This chapter presents results on parametric studies of cable-stayed bridges. These studies were based on using the Quincy Bayview Bridge as a prototype bridge. Frequencies, mode shapes, modal participation factors, and effective modal masses were examined to determine modal coupling and directions of modal response. The important modes for each response quantity were of interest too. This part of the study is one of the initial steps toward establishing a frequency cut-off criterion (to be described in section 4.5) suitable for dynamic modal analysis of cable-stayed bridges. A parametric investigation into the effect of deck eccentricity, tower shape, cable arrangement, cable stiffness and deck support condition was carried out to examine the effect of these parameters on the dynamic characteristics of the prototype bridge.

The study showed that:

1- The modes of cable-stayed bridges, which have low, closely spaced frequencies, can be broadly categorized as vertical plane modes and torsional/transverse (T/T) modes. The vertical plane mode category contains vertical deck modes (VL), Longitudinal tower modes (TL), and coupled vertical deck-longitudinal tower modes (VT). The

torsional/transverse mode category contains numerous mode shapes: transverse deck modes (TR), torsional deck modes (TS), coupled torsional transverse deck modes (TT), transverse tower modes (TY), torsional tower modes (ST), coupled torsional deck-transverse tower modes (TS-TY). This categorization is an effective method to simplify the visualization of the rather complex modal behaviour of cable-stayed bridges.

2- The frequencies of the first basic mode category (V) demonstrated a nearly linear relationship with the V mode numbers. Frequencies of the second mode category (T/T) appear to be a bi-linear function of the T/T mode number with the torsional frequencies generally appearing first, followed by transverse modes at higher frequencies on the second branch of the bilinear relationship.

3- The modal participation factors do not demonstrate a clear decay trend with an increase in mode number when 3-D modes are studied.

4- The effective modal mass is a more suitable parameter for checking the accuracy of modal superposition. It is also easier to implement in a frequency cut-off criterion than modal participation factors because it has a ceiling value of 100% in each of the three global directions.

5- Eccentricity between the centre of mass and the shear centre of the deck has little effect on the bridge frequencies but it governs the degree of torsional/transverse coupling in the bridge deck.

6- Closed tower shapes such as A-shape and diamond-shape are torsionally stiffer than an open H-shape and provide increased torsional stiffness to the deck system.

7- A harp cable arrangement provides the most flexible support for the bridge deck and consequently produces the lowest frequencies. A radiating cable arrangement provides a stiffer support for the bridge deck and results in higher frequencies.

8- Cable stiffness has a significant effect on the bridge frequencies. Its influence was the most pronounced of the five parameters studied. Its effect on the spatial coupling is less pronounced than its effect on the frequencies.

9- Free longitudinal support of the deck adds a new very low frequency longitudinal mode. For the models studied here there was a change in the fundamental mode from vertical to longitudinal motion of the deck. This was accompanied by a decrease in the bridge's fundamental frequency of approximately 40%.

Table 3.1 Classification of Quincy Bayview Bridge Mode Shapes

Mode No.	Frequency (Hz)	Mode Classification								
		VL	TS	TL	TY	VT	TT	ST	TS-TY	ST-TY
1	0.3708					■				
2	0.4996					■				
3	0.5773						■			
4	0.6331						■			
5	0.7328		■							
6	0.7698	■								
7	0.8542	■								
8	0.9493		■							
9	1.0230		■							
10	1.0232	■								
11	1.1150		■							
12	1.2330				■					
13	1.2380				■					
14	1.2530								■	
15	1.2790	■								
16	1.2820								■	
17	1.2900								■	
18	1.3450	■								
19	1.3620		■							
20	1.3830	■								
21	1.4440		■							
22	1.4830		■							
23	1.4850		■							
24	1.5610		■							
25	1.5640						■			
26	1.6280		■							
27	1.6650	■								
28	1.6960		■							
29	1.6970		■							
30	1.7470		■							
31	1.7500		■							
32	1.8600		■							
33	1.8610		■							
34	1.9710		■							
35	1.9720		■							
36	1.9880					■				
37	2.0060						■			
38	2.1410					■				
39	2.2010				■					
40	2.2011				■					

■ identifies the mode shape occurring at that frequency

Table 3.1 Cont'd

Mode No.	Frequency (Hz)	Mode Classification								
		VL	TS	TL	TY	VT	TT	ST	TS-TY	ST-TY
41	2.2610					■				
42	2.3250			■						
43	2.4100						■			
44	2.4190					■				
45	2.4570		■							
46	2.4580		■							
47	2.5720		■							
48	2.5724		■							
49	2.6410					■				
50	3.0130				■					
51	3.0180				■					
52	3.0760									■
53	3.0780								■	
54	3.0820	■								
55	3.2970	■								
56	3.4250	■								
57	3.6840					■				
58	3.8380	■								
59	3.9050						■			
60	4.3550					■				
61	4.4330			■						
62	4.5270			■						
63	4.6240	■								
64	4.7790	■								
65	5.2000	■								
66	5.2610							■		
67	5.2614							■		
68	5.7350	■								
69	5.9460						■			
70	6.0450	■								
71	6.2280	■								
72	6.6130						■			
73	6.6210	■								
74	6.8150						■			
75	7.0120	■								
	Totals	19	22	3	6	9	9	2	4	1

■ identifies the mode shape occurring at that frequency

VL: Vertical Deck
TS: Torsional Deck
TT: Transverse-Torsional Deck
TL: Longitudinal Tower
TY: Transverse Tower
VT: Vertical Deck-Longitudinal Tower
ST: Coupled Torsional Deck-Tower
TS-TY: Torsional Deck-Transverse Tower
ST-TY: Coupled Torsional Motion of Deck with Torsional-Transverse Tower Motion

Table 3.2 Summary of Geometric Parameters Considered in the Study

Structural Component	Parameter	Original Configuration*	Parametric Variations
Deck	Eccentricity	e=2.7 ft	0.1e
			2.0e
	End Support Conditions	fixed in X,Y,Z,@X,@Z free @Y	fixed in Y,Z,@X,@Z free in X,@Y
	Deck Support at Towers	fixed in: Z, @X free in: X,Y,@Y,@Z	fixed in: X,Z,@X free in: Y,@Y,@Z
Tower	Shape	H-shape	A-shape
			Diamond-shape
Cables	Arrangement	Fan	Radiating
			Harp
	Stiffness	EA	0.5EA (Flexible)
			2EA (Stiff)

* Quincy Bayview Bridge

X: Longitudinal Direction
Y: Transverse Direction
Z: Vertical Direction

Table 3.3 (a) Vertical Plane Frequencies (Hz) for the Different Geometric Designs

Frequency Order	Original Bridge	High Eccentricity	Low Eccentricity	Diamond Tower	A-shape Tower	Flexible Cables	Stiff Cables	Harp Arrangement	Radiating Arrangement
1	0.3708	0.3707	.3708	0.3689	0.2937	0.2985	0.4695	0.3372	0.3756
2	0.4996	0.4994	0.4997	0.4955	0.4526	0.4167	0.6068	0.4080	0.5145
3	0.7698	0.7694	0.7700	0.7644	0.6999	0.5920	1.0080	0.6211	0.6098
4	0.8542	0.8537	0.8543	0.8509	0.8731	0.6598	1.1140	0.6846	0.9082
5	1.0230	0.9761	1.0420	1.0160	0.9451	0.8305	1.2940	0.7963	1.0770
6	1.2790	1.2450	1.3050	1.2630	1.2690	1.0850	1.5330	0.9833	1.3230
7	1.3450	1.3080	1.3460	1.3760	1.3410	1.1600	1.6110	1.1010	1.3820
8	1.3830	1.3800	1.3820	1.4510	1.3920	1.2130	1.6250	1.1880	1.4150
9	1.6650	1.6280	1.7220	1.6540	1.6960	1.5020	1.9230	1.4750	1.6830

Table 3.3 (b) Torsional Transverse Frequencies (Hz) for the Different Geometric Designs

Frequency Order	Original Bridge	High Eccentricity	Low Eccentricity	Diamond Tower	A-shape Tower	Flexible Cables	Stiff Cables	Harp Arrangement	Radiating Arrangement
1	0.5773	0.5359	0.5875	0.5804	0.5326	0.5022	0.5956	0.5707	0.5716
2	0.6331	0.6789	0.6210	0.8339	0.8249	0.6089	0.7265	0.6145	0.6286
3	0.7328	0.7009	0.7445	0.9761	0.8822	0.6432	0.8364	0.6653	0.7219
4	0.9493	0.9078	0.9657	1.0380	1.0030	0.7526	1.2080	0.8095	0.9731
5	1.0230	1.0220	1.0240	1.0460	1.0380	0.7966	1.2270	0.8569	1.0690
6	1.1150	1.0700	1.1340	1.1300	1.0520	0.8985	1.2490	0.9219	1.1580
7	1.2330	1.1950	1.2370	1.2480	1.1830	1.0320	1.3430	0.9978	1.1910
8	1.2380	1.2190	1.2400	1.2670	1.2390	1.0460	1.4220	1.0230	1.1980
9	1.2530	1.2193	1.2660	1.270.	1.2840	1.0470	1.5420	1.0420	1.3070
10	1.2820	1.2530	1.2800	1.3030	1.2880	1.1450	1.5640	1.1430	1.3480
11	1.2900	1.2760	1.2970	1.3100	1.3200	1.2360	1.6120	1.2450	1.3550
12	1.3620	1.3430	1.3820	1.3760	1.3760	1.2390	1.6250	1.2490	1.4200

Table 3.3 (b) Cont'd

Frequency Order	Original Bridge	High Eccentricity	Low Eccentricity	Diamond Tower	A-shape Tower	Flexible Cables	Stiff Cables	Harp Arrangement	Radiating Arrangement
13	1.4440	1.3860	1.4620	1.4510	1.4840	1.2610	1.6870	1.2510	1.4890
14	1.4830	1.4240	1.5040	1.4850	1.4850	1.2910	1.7280	1.2710	1.5300
15	1.4850	1.4260	1.5050	1.4852	1.5170	1.2920	1.7660	1.2790	1.5320
16	1.5610	1.4990	1.5480	1.5640	1.5460	1.3800	1.7740	1.3640	1.5620
17	1.5640	1.5630	1.5840	1.6210	1.5790	1.4680	1.8350	1.4220	1.6000
18	1.6280	1.6270	1.6520	1.6360	1.5870	1.4730	1.8530	1.4300	1.6520
19	1.6960	1.6340	1.6670	1.6940	1.6970	1.4732	2.0080	1.4420	1.7050
20	1.6970	1.6600	1.7200	1.6942	1.7440	1.5440	2.0300	1.5240	1.7053
21	1.7470	1.6760	1.7720	1.7460	1.7480	1.5640	2.0380	1.5600	1.7610

Table 3.4 Classification of Modes of Different Geometric Designs

No.	Original Bridge	High Eccentricity	Low Eccentricity	Diamond shape	A-shape	Flex. Cables	Stiff Cables	Harp Arrangement	Radiating Arrangement
1	VT	VT	VT	VT	VT	VT	VT	VT	VT
2	VT	VT	VT	VT	VT	VT	TR	VT	VT
3	TT	TR	TT	TT	TT	TT	VT	TT	TT
4	TT	TR	TT	VL	VL	VL	TR	TT	TT
5	TS	TS	TS	TS	TS	TT	TS	VL	TS
6	VL	VT	VT	VL	VL	TS	VT	TS	VL
7	VL	VL	VL	TS	TS	VL	VL	VL	VL
8	TS	TS	TS	VL	VL	TS	TS-TY	VL	TS
9	TS	TS	VL	TS	TS	TS	TS-TY	TS	TS
10	VL	VL	TS	TS	TS	VL	TS-TY	TS	VL
11	TS	TS	TS	TS	TS	TS	VL	TS	TS-TY
12	TY	TS-TY	TY	TS-TY	TS	TS	TS-TY	VL	TY
13	TY	TS-TY	TY	VL	TS	TS	TS-TY	TS	TY
14	TS-TY	TS-TY	ST	TS-TY	VL	TS	VT	TS	TS
15	VL	TY	VL	TS-TY	TS	VL	TS	TS	VL
16	TS-TY	TY	TS	TS-TY	TY	TS	TS	VL	TS
17	TS-TY	VT	TS-TY	TS-TY	TY	VL	VT	TS	TS
18	VL	TS	VL	VL	VL	VL	TS	VL	VL
19	TS	VL	TS	TS	TS	ST-TY	TS	TS-TY	VL
20	VL	VL	VL	VL	VL	TS-TY	VL	TS-TY	TS
21	TS	TS	TS	TS	TS	TS-TY	TS	TS-TY	TS
22	TS	TS	TS	TS	TS	TS	TS	TS	TS
23	TS	TS	TS	TS	TS	TS	TS	TS-TY	TS
24	TS	TS	TR	TS	TS	TS	TS	TS	TT
25	TT	TS	TS	TT	TT	TS	TS	TS	TS
26	TS	TT	TS	TT	TS	TS	TS	TS	TS
27	VL	TS	VT	VL	VL	TS	VT	TS	VL
28	TS	TR	TS	TS	TS	VL	TR	VL	TY
29	TS	VL	TS	TS	TS	TS	TS	TS	TY
30	TS	TS	TS	TS	TS	TT	TR	TT	TS

VL: VERTICAL DECK
TR: TRANSVERSE DECK
TS: TORSIONAL DECK
TT: TORSIONAL-TRANSVERSE DECK
TL: LONGITUDINAL TOWER
TY: TRANSVERSE TOWER
VT: VERTICAL DECK LONG. TOWER
ST: TORSIONAL DECK-TOWER
TS-TY: TORSIONAL DECK-TRANS. TOWER
ST-TY: COUPLED TORSIONAL MOTION OF DECK WITH TORSIONAL-TRANSVERSE TOWER MOTION

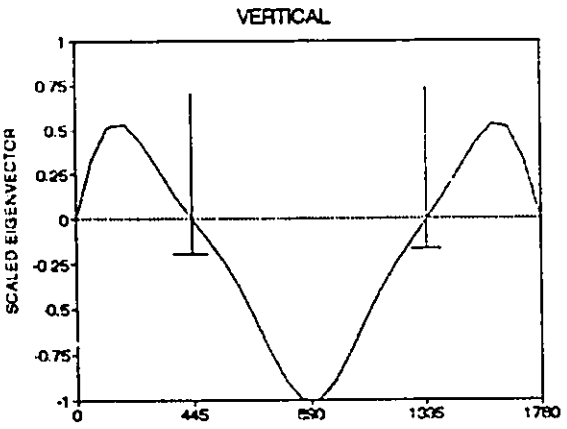

(a) Side Elevation of Deck: X-Z Plane

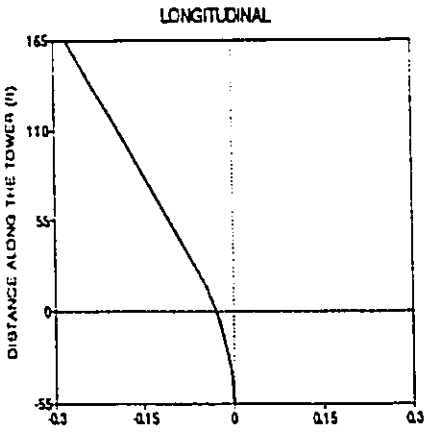

(b) Side Elevation of Tower: X-Z Plane

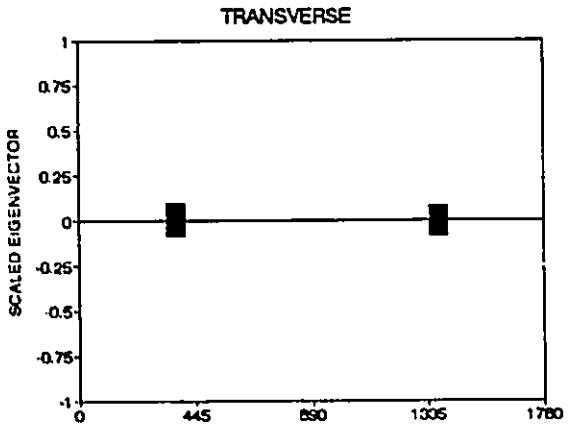

(c) Plan: X-Y Plane

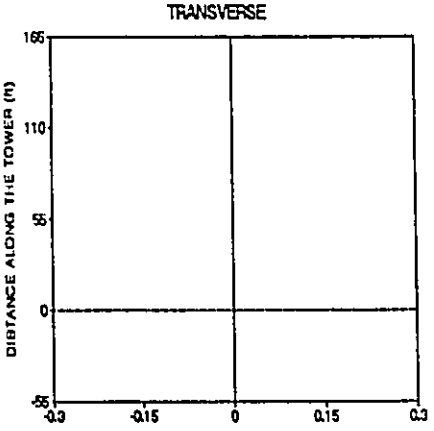

(d) End Elevation of Tower: Y-Z Plane

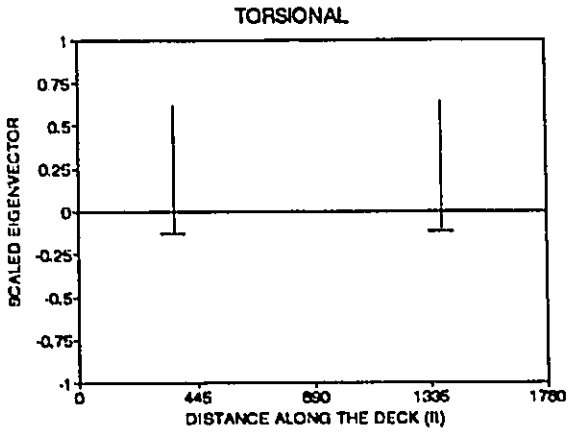

(e) Side Elevation: X-Z Plane

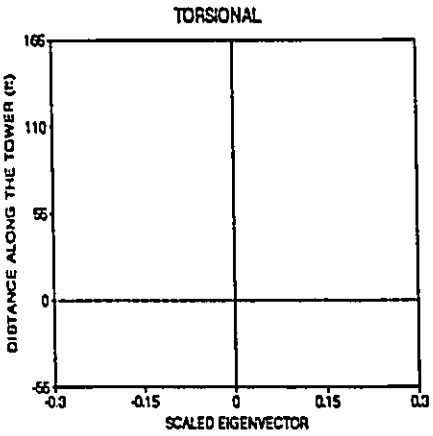

(f) Side Elevation of Tower: X-Z Plane

Figure 3.1 First Mode Shape of Quincy Bayview Bridge (f=0.3708 Hz)

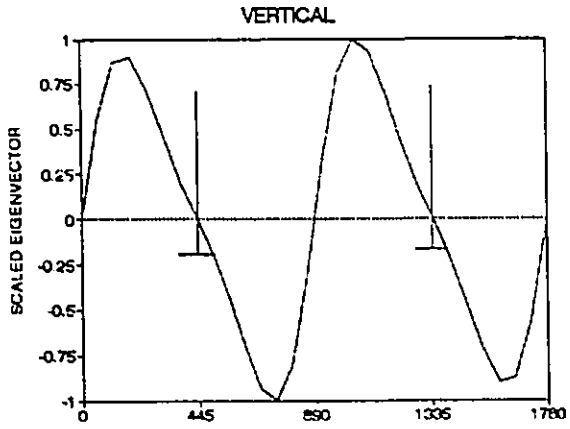

(a) Side Elevation of deck: X-Z Plane

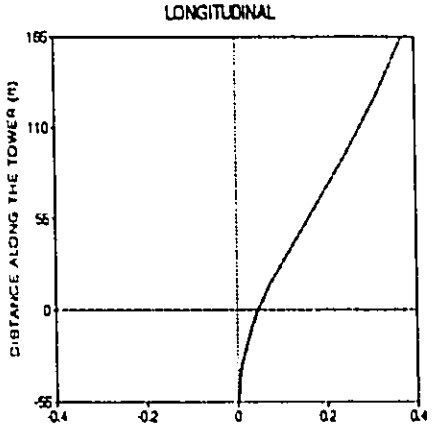

(b) Side Elevation of Tower: X-Z Plane

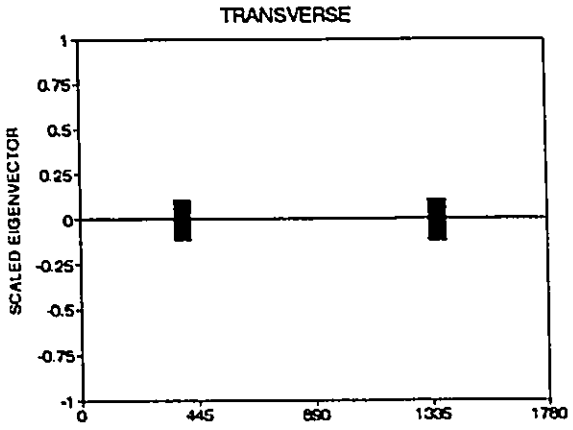

(c) Plan: X-Y Plane

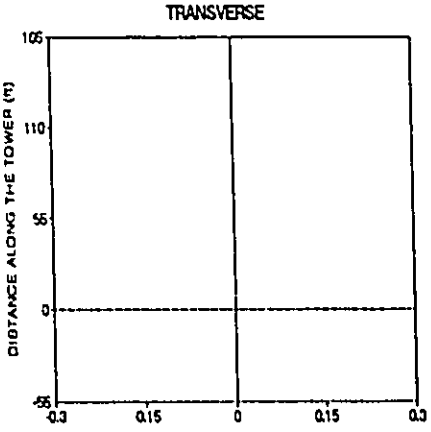

(d) End Elevation Of Tower: Y-Z Plane

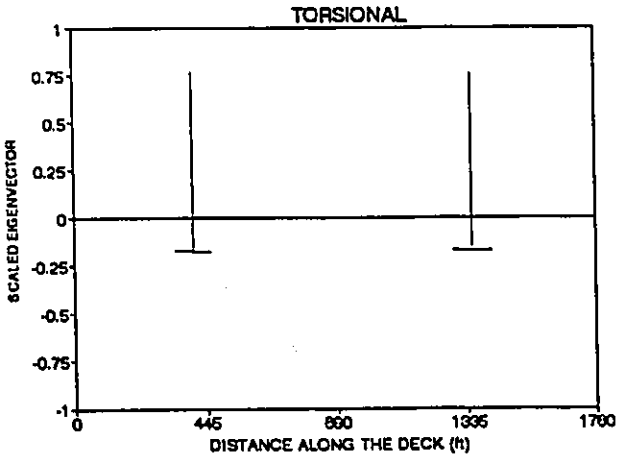

(e) Side Elevation: X-Z Plane

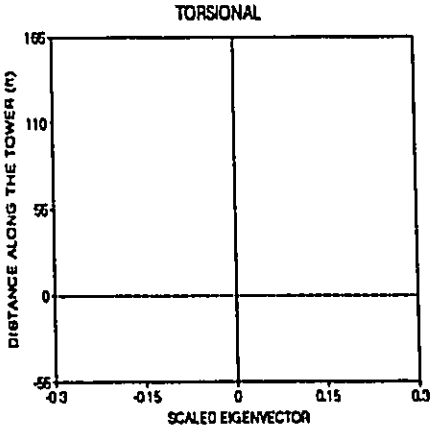

(f) Side Elevation of Tower: X-Z Plane

Figure 3.2 Second Mode Shape of Quincy Bayview Bridge (f=0.4996 Hz)

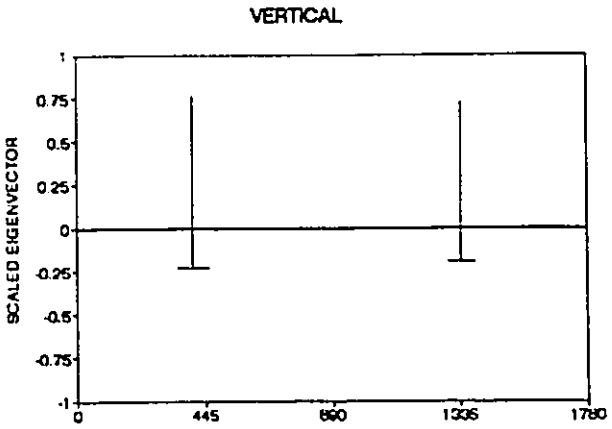

(a) Side Elevation of Deck: X-Z Plane

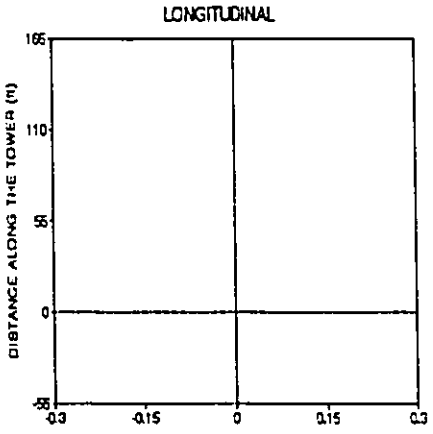

(b) Side Elevation of Tower: X-Z Plane

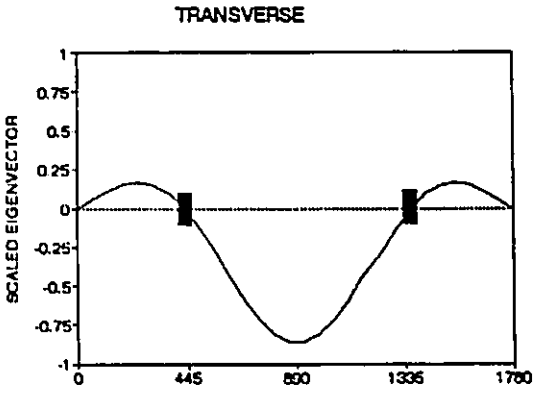

(c) Plan: X-Y Plane

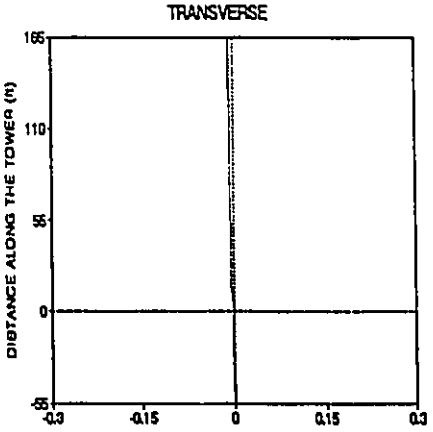

(d) End Elevation of Tower: Y-Z Plane

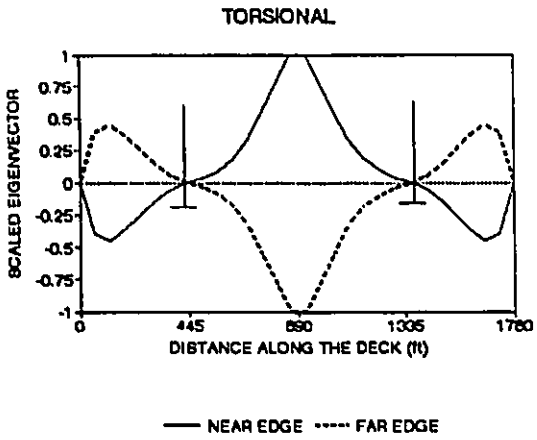

(e) Side Elevation: X-Z Plane

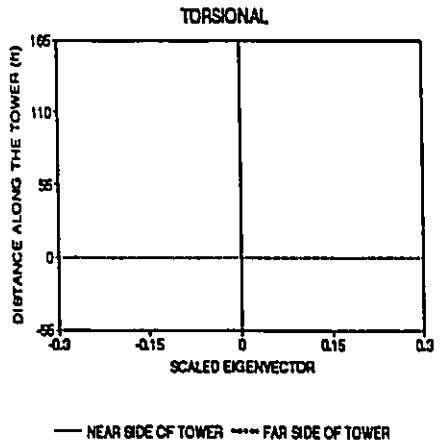

(f) Side Elevation ofTower: X-Z Plane

Figure 3.3 Third Mode Shape of Quincy Bayview Bridge (f=0.5773 Hz)

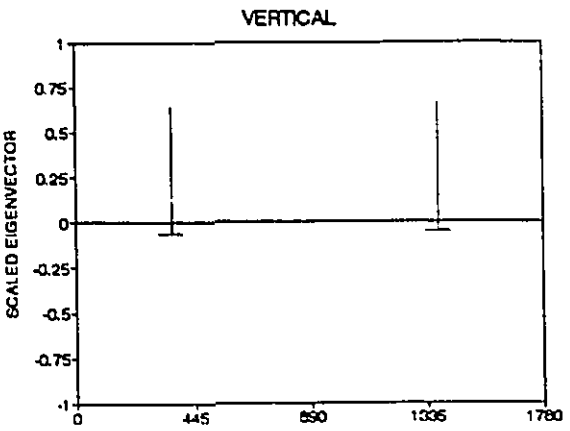

(a) Side Elevation of Deck: X-Z Plane

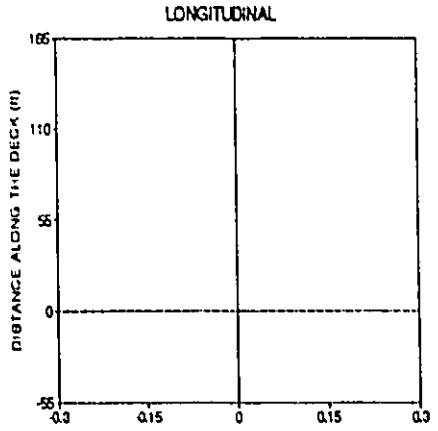

(b) Side Elevation of Tower: X-Z Plane

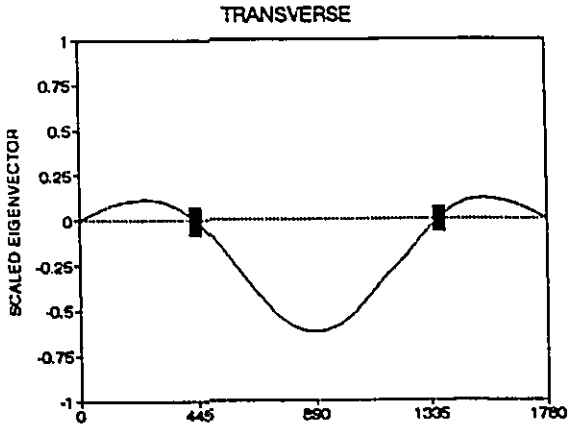

(c) Plan: X-Y Plane

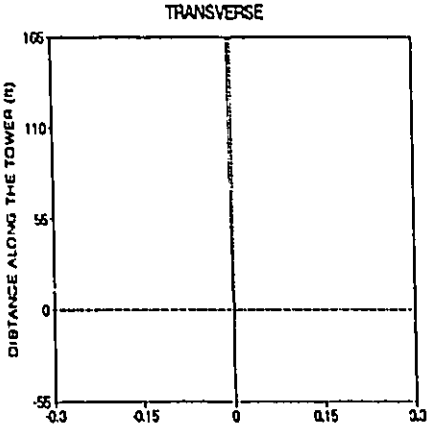

(d) End Elevation of Tower: Y-Z Plane

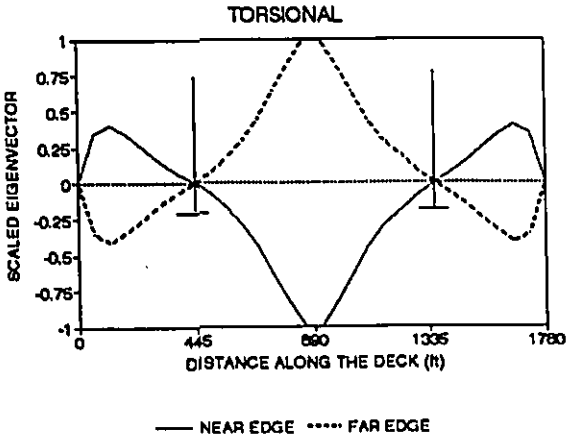

(e) Side Elevation: X-Z Plane

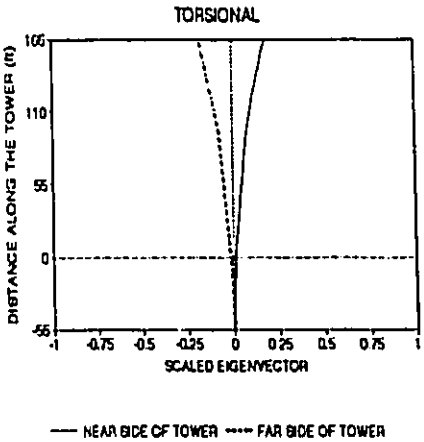

(f) Side Elevation of Tower: X-Z Plane

Figure 3.4 Fourth Mode Shape of Quincy Bayview Bridge (f=0.6331 Hz)

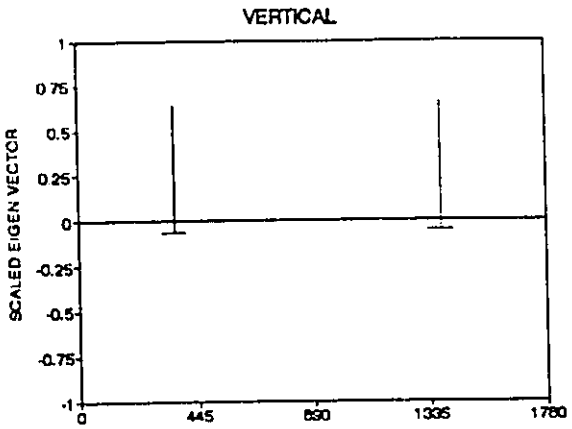

(a) Side Elevation of Deck: X-Z Plane

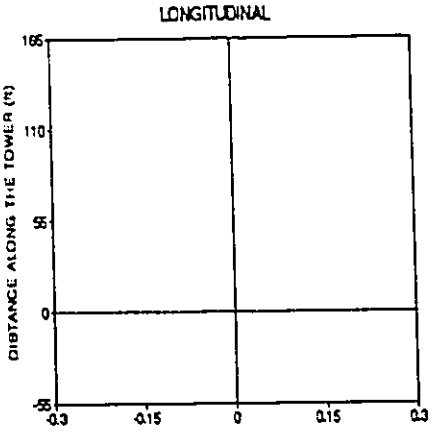

(b) Side Elevation of Tower: X-Z Plane

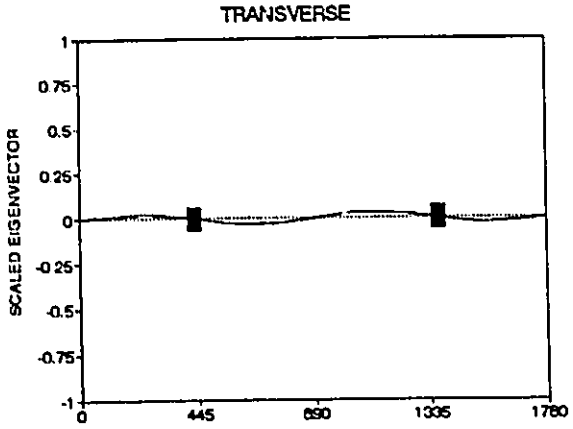

(c) Plan: X-Y Plane

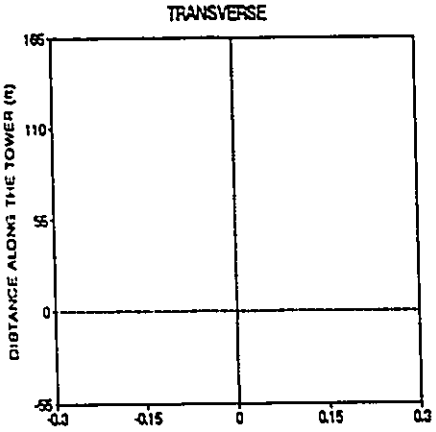

(d) End Elevation of Tower: Y-Z Plane

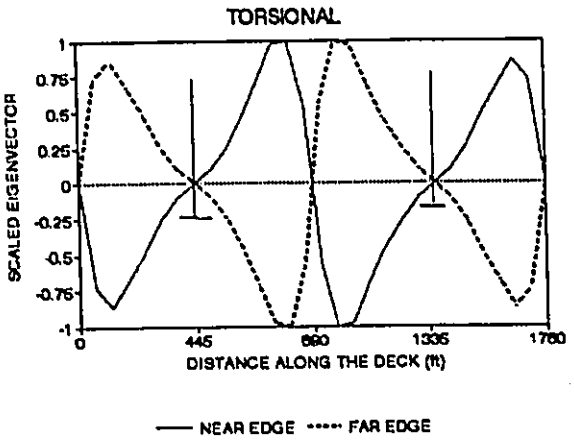

(e) Side Elevation: X-Z Plane

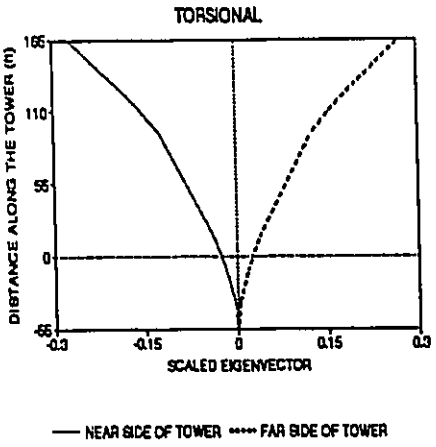

(f) Side Elevation of Tower: X-Z Plane

Figure 3.5 Fifth Mode Shape of Quincy Bayview Bridge (f=0.7328 Hz)

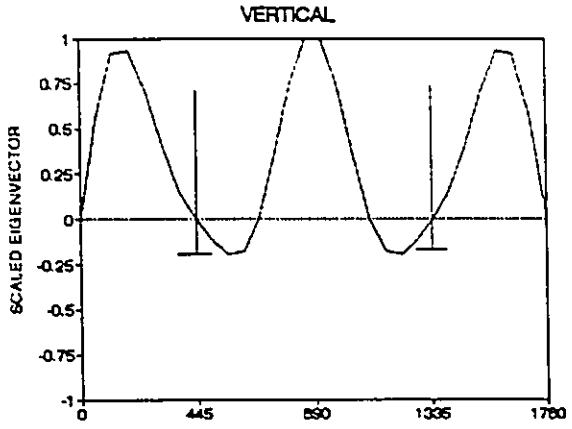

(a) Side Elevation of deck: X-Z Plane

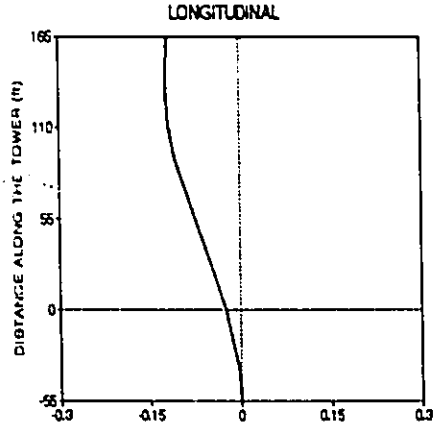

(b) Side Elevation of Tower: X-Z Plane

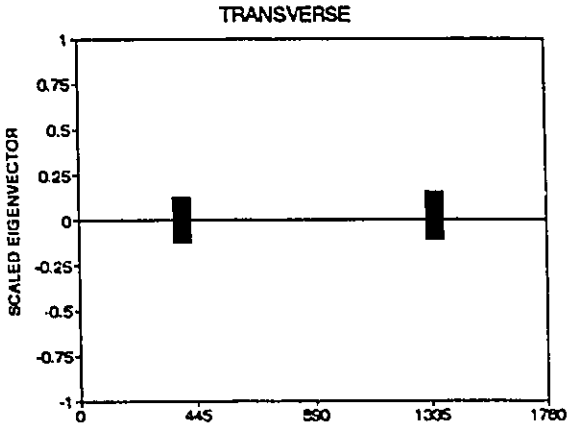

(c) Plan: X-Y Plane

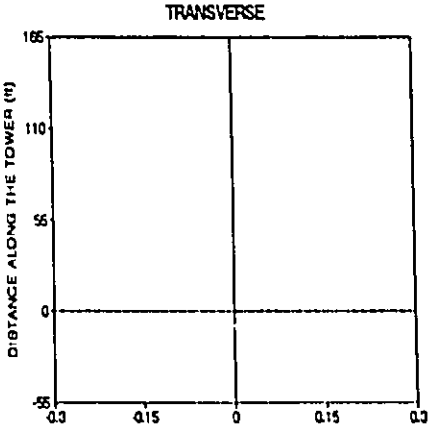

(d) End Elevation of Tower: Y-Z Plane

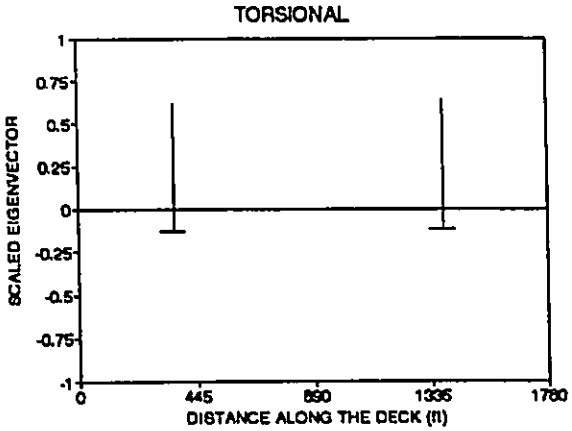

(e) Side Elevation: X-Z Plane

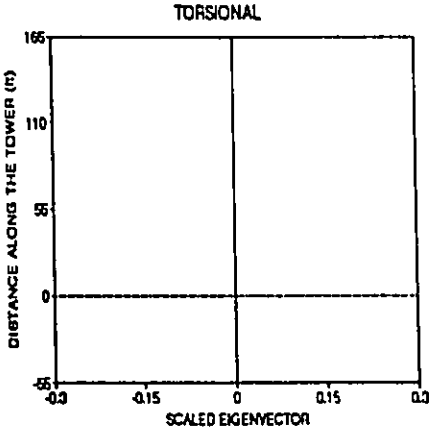

(f) Side Elevation of Tower: X-Z Plane

Figure 3.6 Sixth Mode Shape of Quincy Bayview Bridge (f=0.7698 Hz)

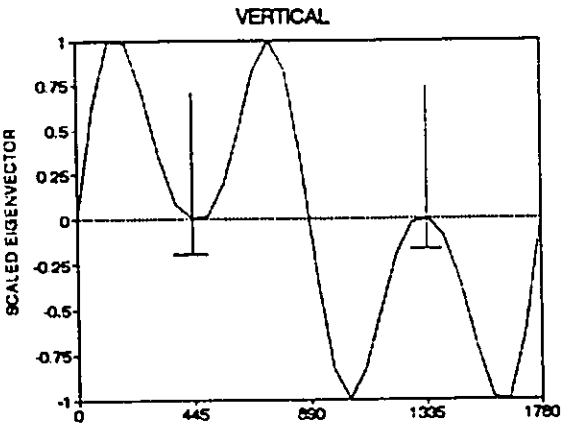

(a) Side Elevation of Deck: X-Z Plane

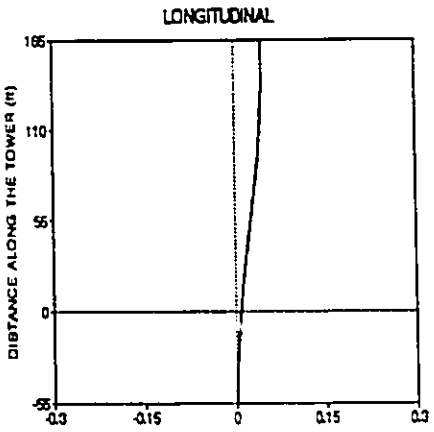

(b) Side Elevation of Tower: X-Z Plane

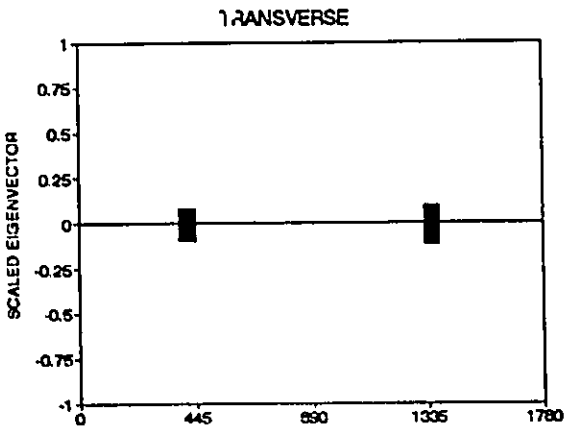

(c) Plan: X-Y Plane

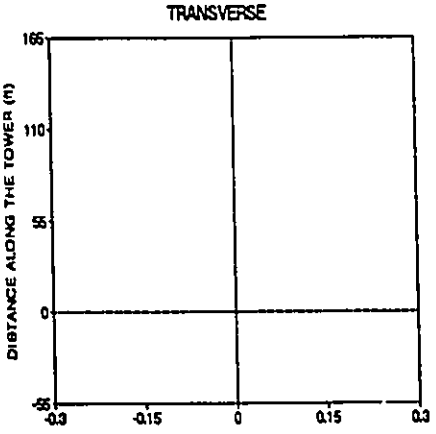

(d) End Elevation of Tower: Y-Z Plane

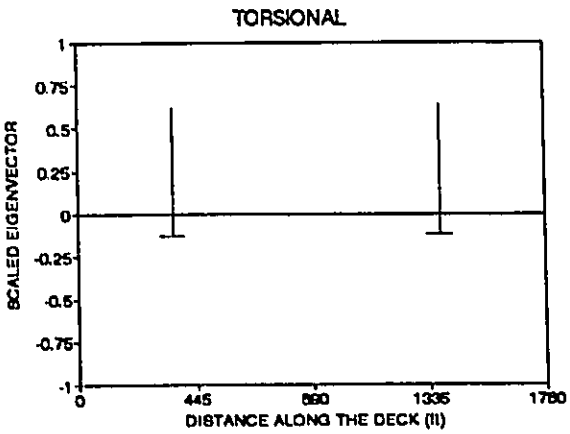

(e) Side Elevation: X-Z Plane

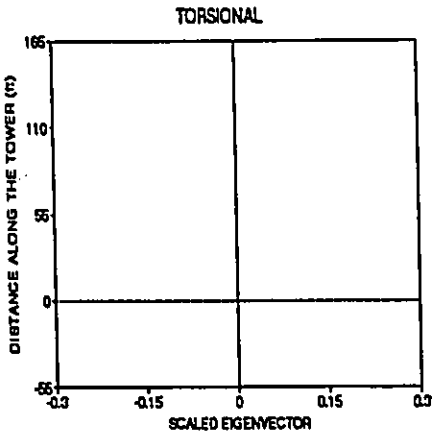

(f) Side Elevation of Tower: X-Z Plane

Figure 3.7 Seventh Modes Shape of Quincy Bayview Bridge (f=0.8542 Hz)

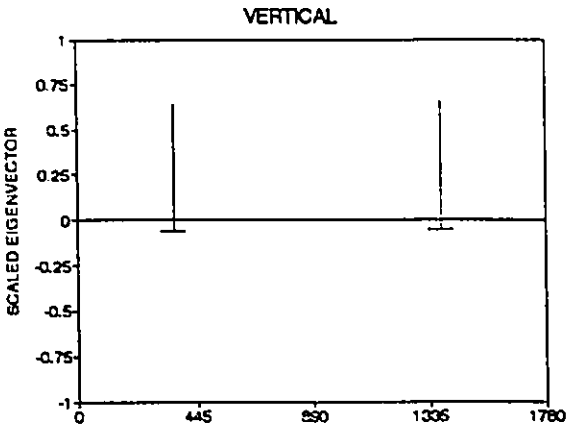

(a) Side Elevation of Deck: X-Z Plane

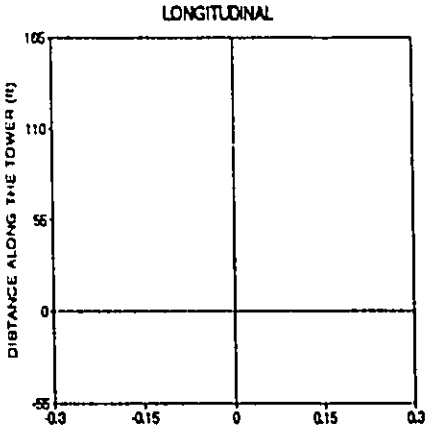

(b) Side Elevation of Tower: X-Z Plane

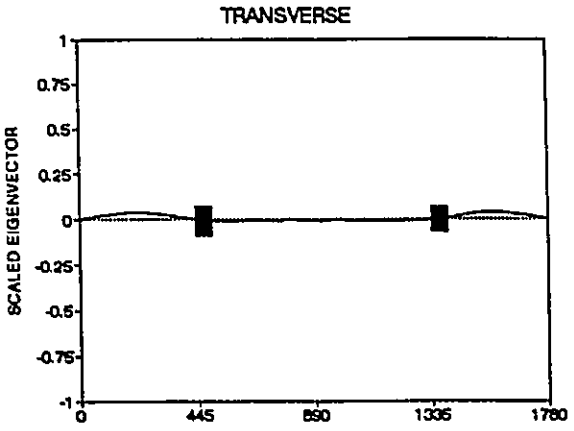

(c) Plan: X-Y Plane

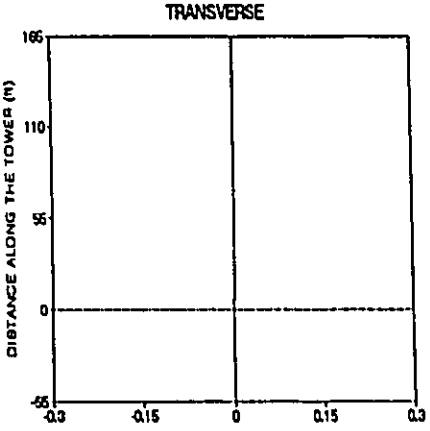

(d) End Elevation of Tower: Y-Z Plane

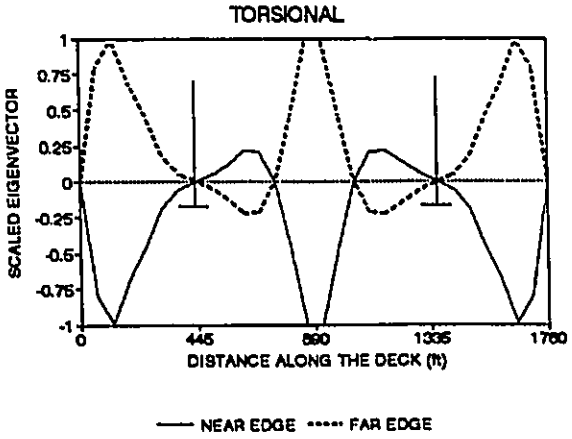

(e) Side Elevation: X-Z Plane

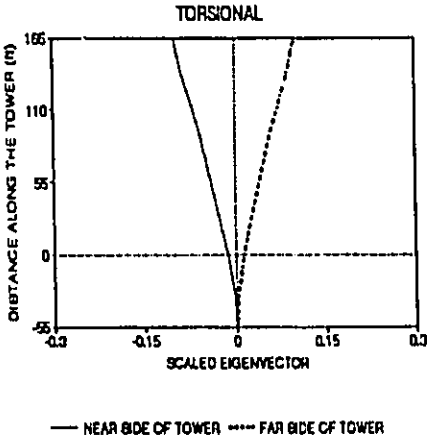

(f) Side Elevation of Tower: X-Z Plane

Figure 3.8 Eighth Mode Shape of Quincy Bayview Bridge (f=0.9493 Hz)

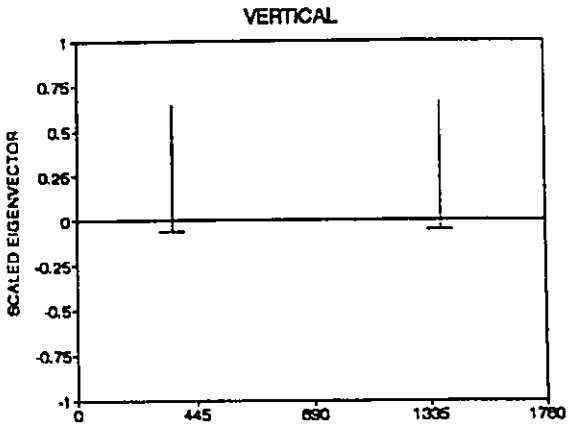

(a) Side Elevation of Deck: X-Z Plane

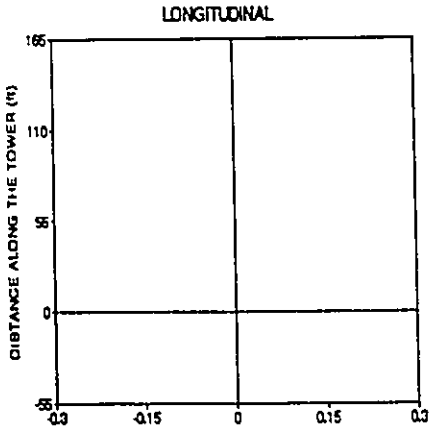

(b) Side Elevation of Tower: X-Z Plane

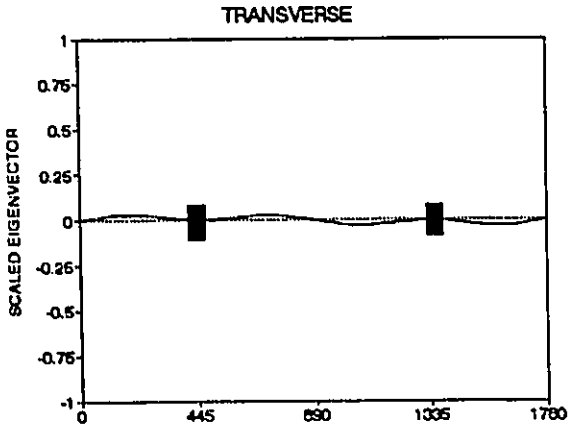

(c) Plan: X-Y Plane

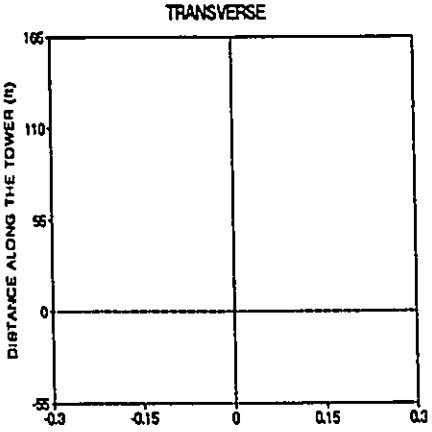

(d) End Elevation of Tower: Y-Z Plane

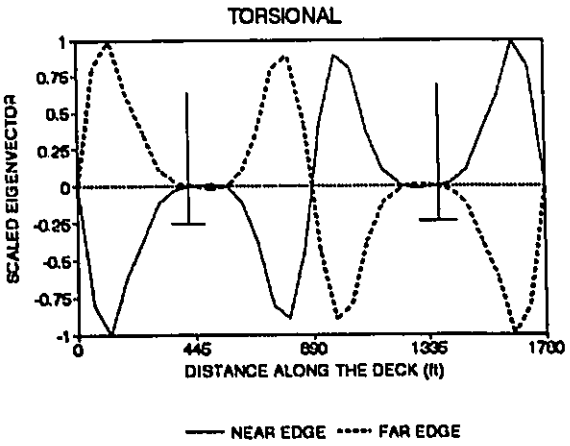

(e) Side Elevation: X-Z Plane

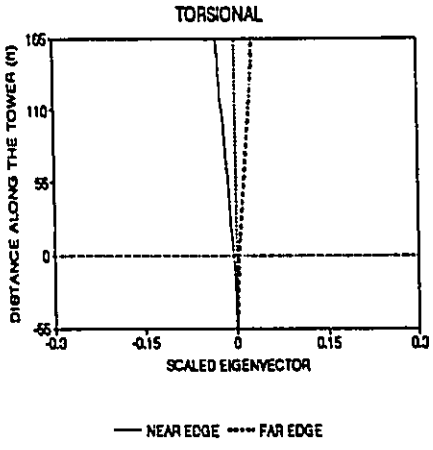

(f) Side Elevation of Tower: X-Z Plane

Figure 3.9 Ninth Mode Shape of Quincy Bayview Bridge (f=1.0230 Hz)

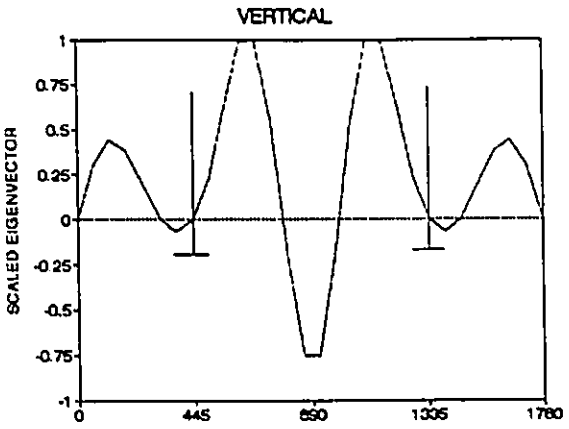

(a) Side Elevation of Deck: X-Z Plane

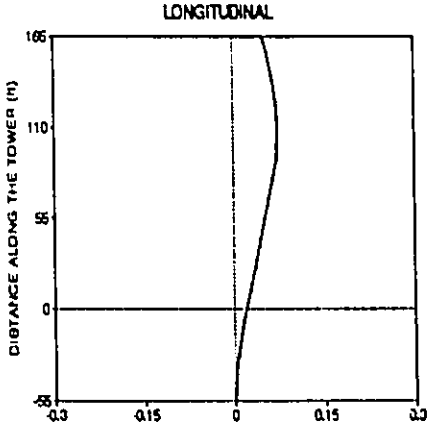

(b) Side Elevation of Tower: X-Z Plane

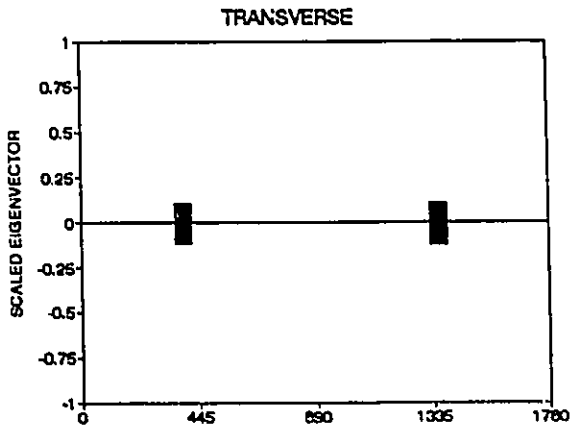

(c) Plan: X-Y Plane

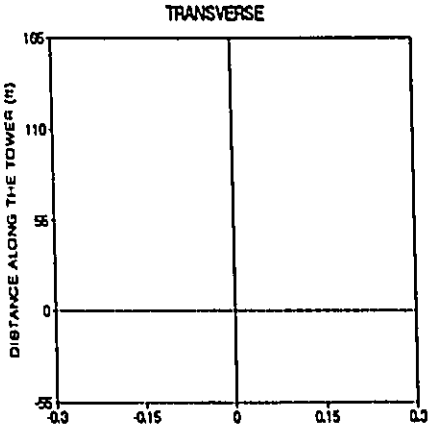

(d) End Elevation of Tower: Y-Z Plane

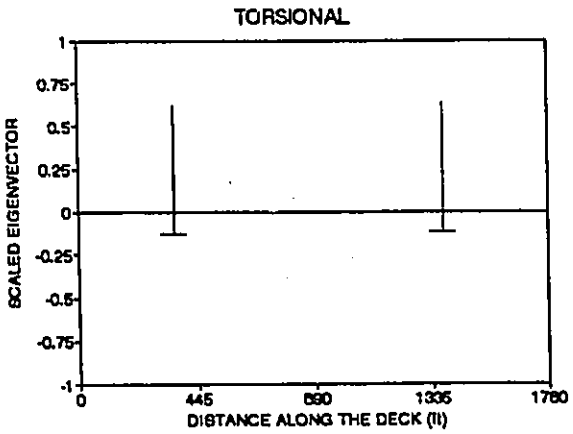

(e) Side Elevation: X-Z Plane

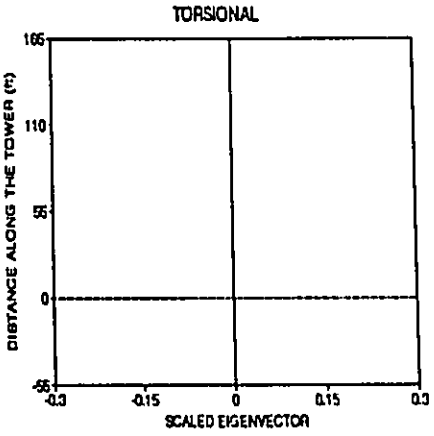

(f) Side Elevation of Tower: X-Z Plane

Figure 3.10 Tenth Modes Shape of Quincy Bayview Bridge (f=1.0232 Hz)

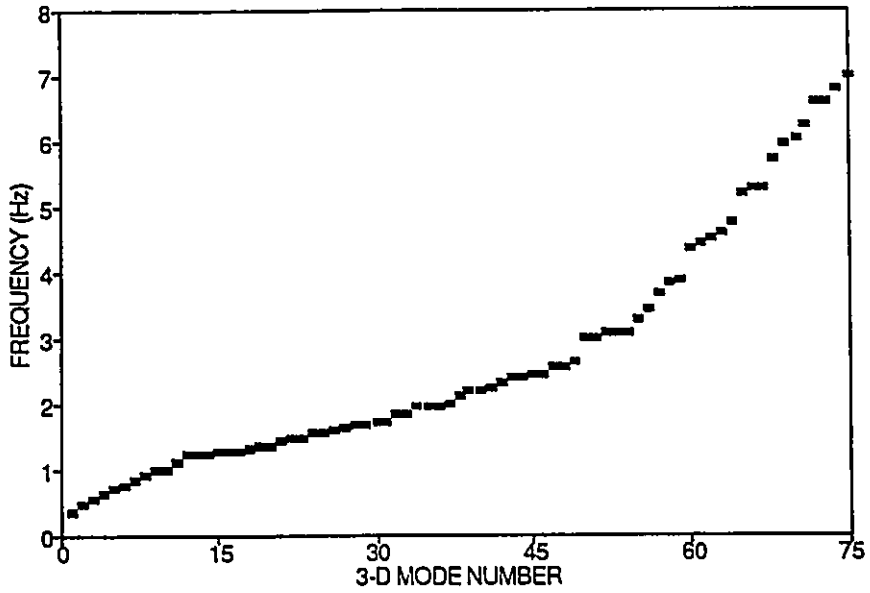

Figure 3.11 Frequencies of the 3-D Model of Quincy Bayview Bridge.

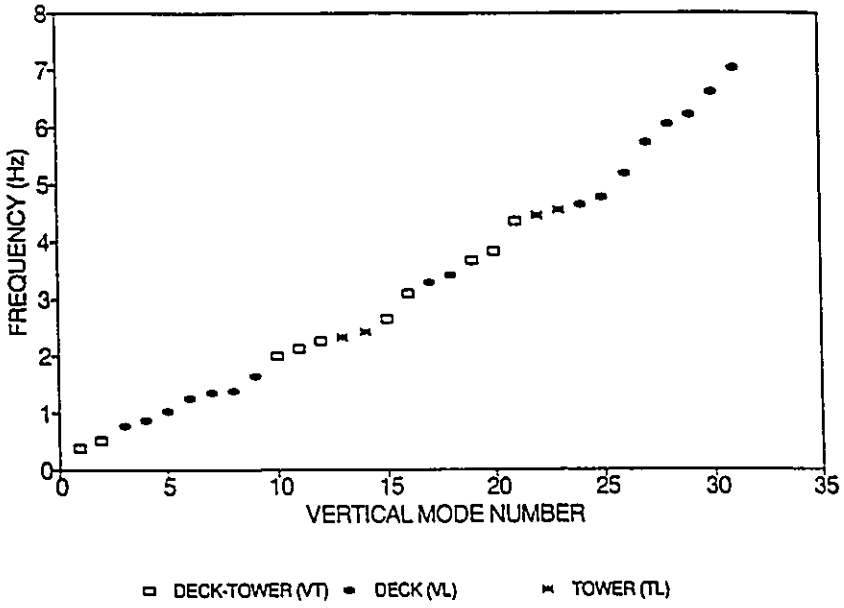

a)Vertical Plane Frequencies

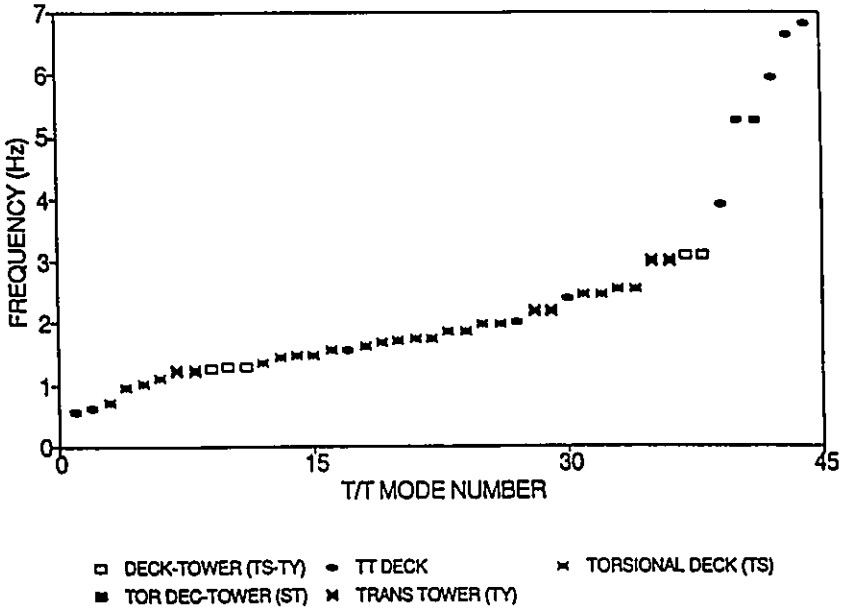

b) Torsional/Transverse Frequencies

Figure 3.12 Frequencies of Quincy Bridge as Separated into Vertical and Torsional/Transverse.

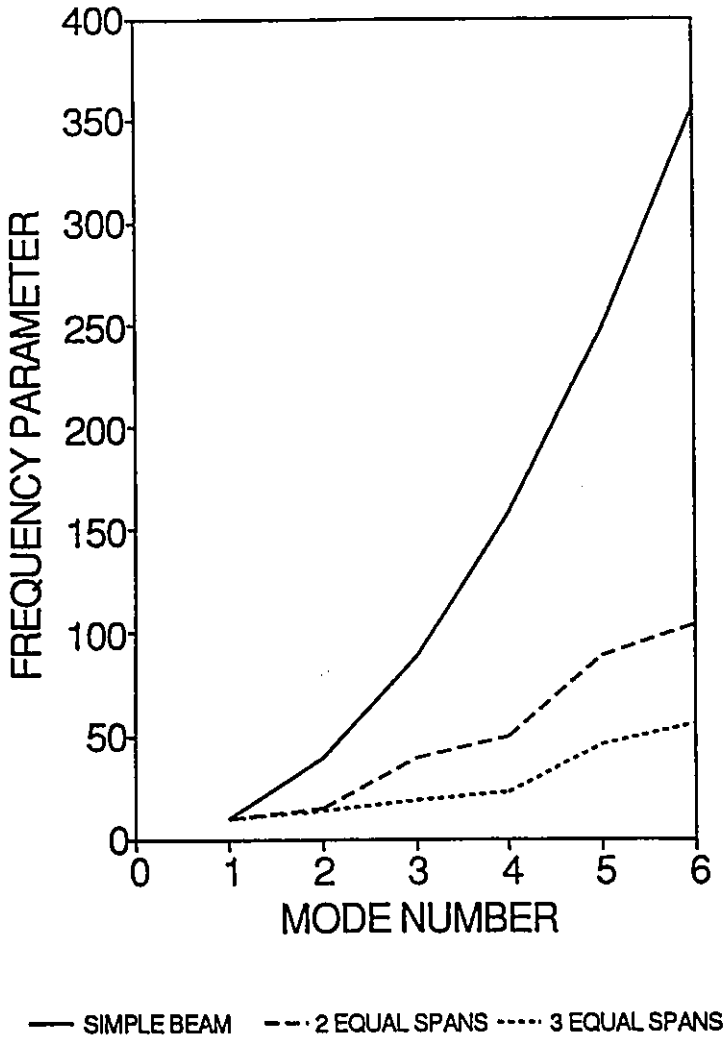

Figure 3.13 Frequency Parameter (λ^2_i) for Beams with Equal Spans.

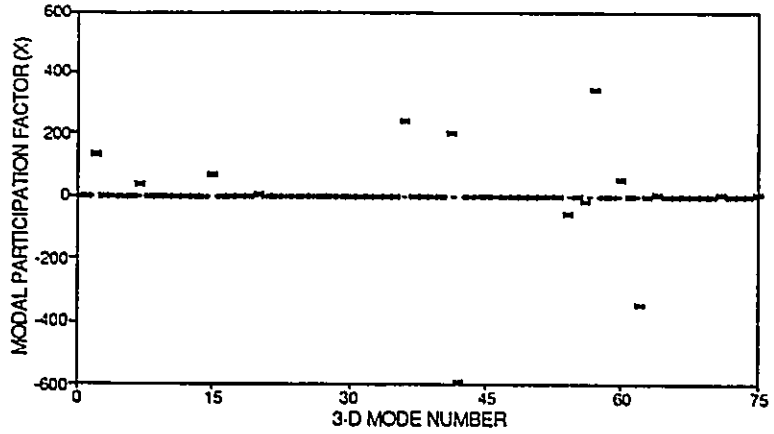

a)Modal Participation Factors in the X-Direction

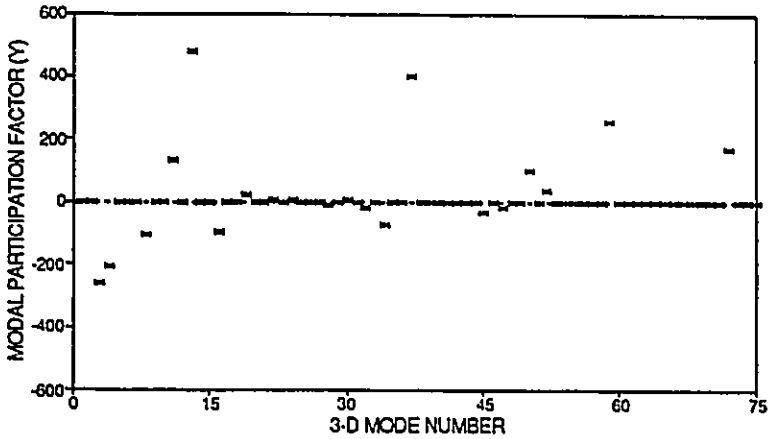

b) Modal Participation Factors in the Y-Direction

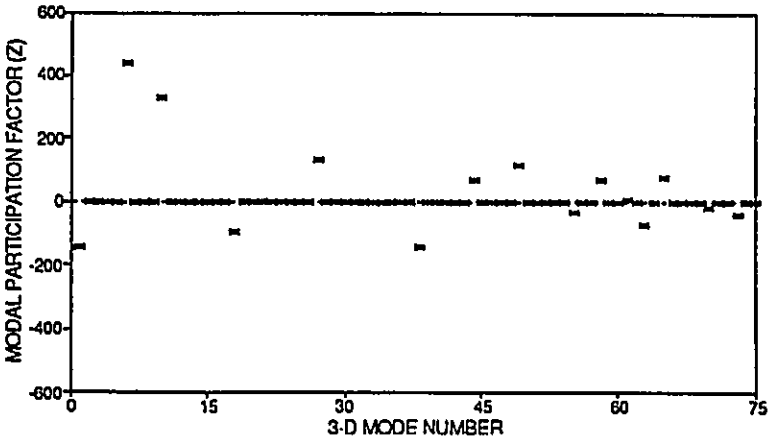

c) Modal Participation Factors in the Z-Direction

Figure 3.14 Modal Participation Factors for the 3-D Model.

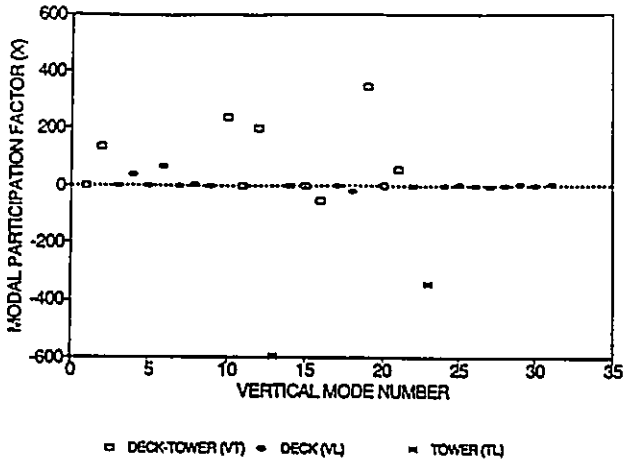

a) Modal Participation Factors in the X-Direction for the Vertical Plane Modes

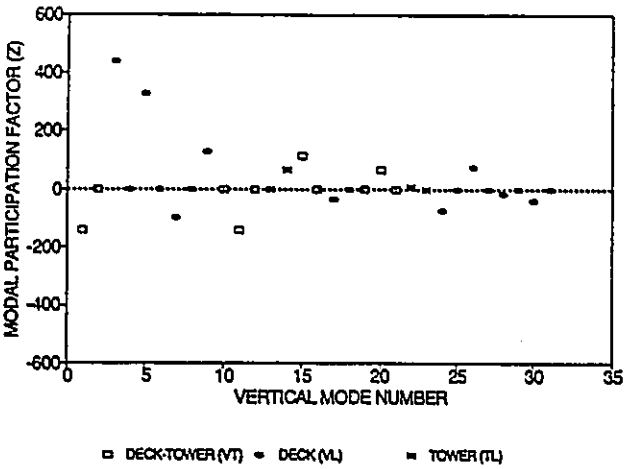

b) Modal Participation Factors in the Z-Direction for the Vertical Plane Modes

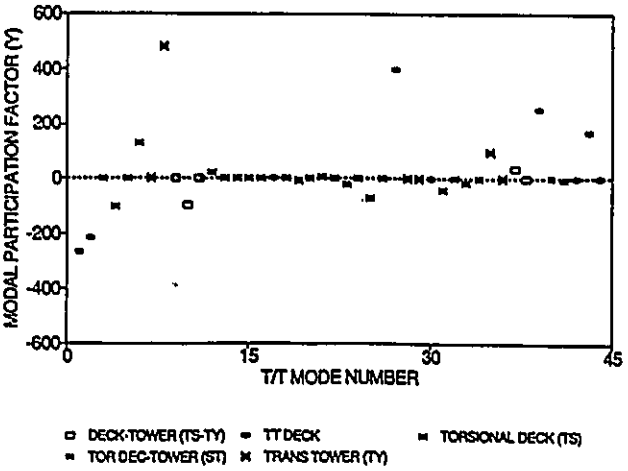

c) Modal Participation Factors in the Y-Direction for the T/T Modes

Figure 3.15 Modal Participation Factors Separated for the Two Mode Categories.

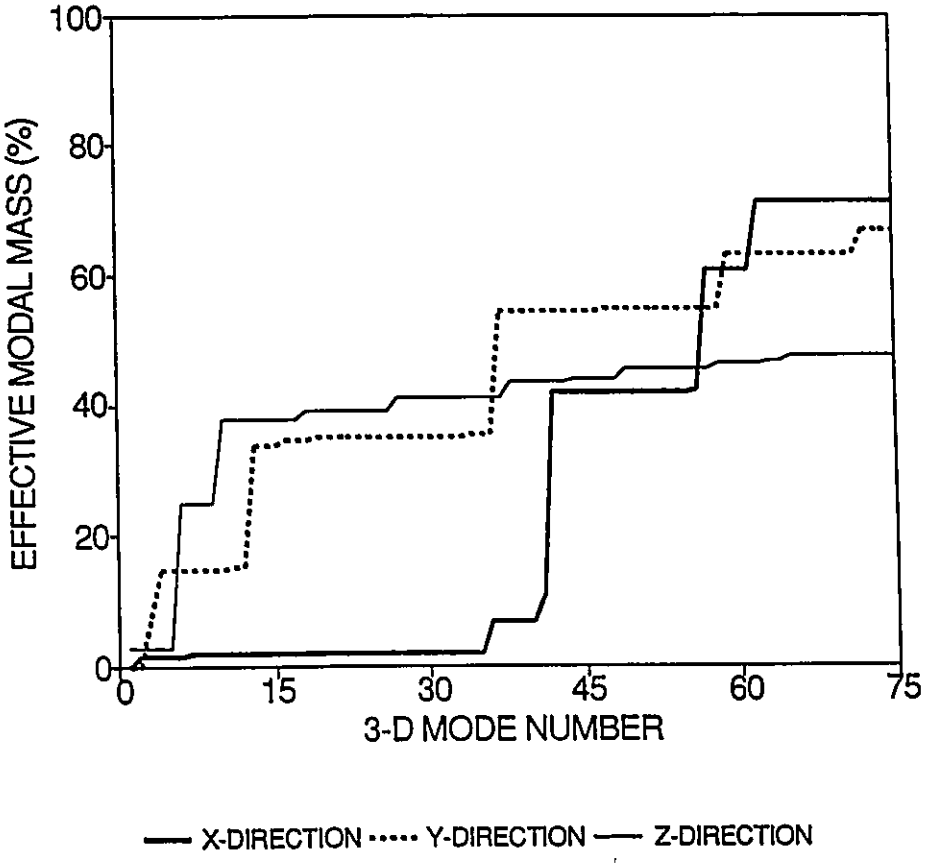

Figure 3.16 Effective Modal Mass in the Three Spatial Directions.

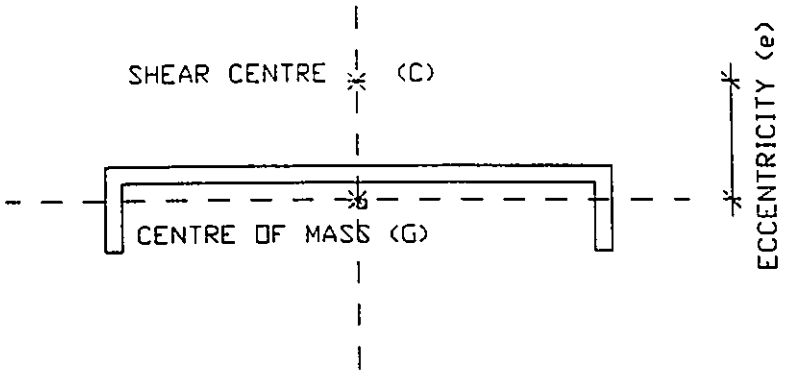

e1 = 2.7 ft (original bridge)

e2 = 0.27 ft (Low Eccentricity)

e3 = 5.4 ft (High Eccenetricity)

a) Deck Eccentricity

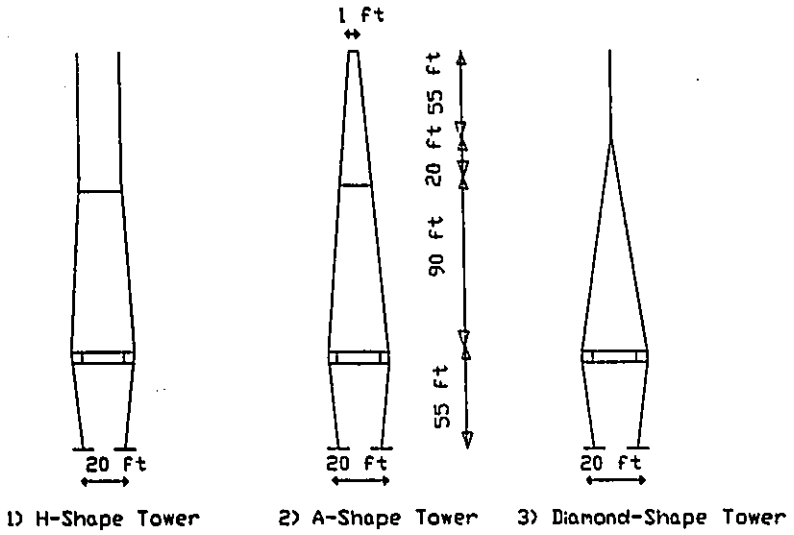

b) Different Studied Tower Shapes

Figure 3.17 Values of Different Studied Geometric Parameters.

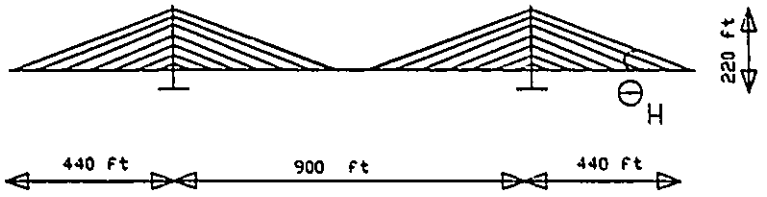

1) Quincy Bayview Bridge with Harp Cable Arrangement

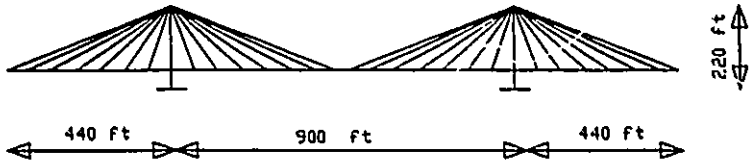

2) Quincy Bayview Bridge with Radiating Cable Arrangement

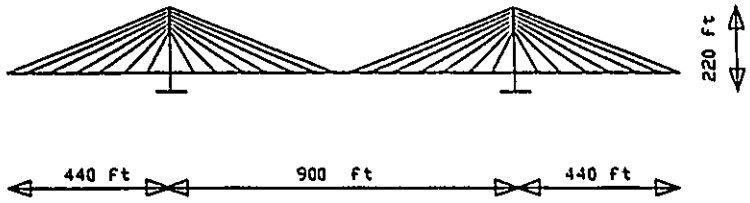

3) Original Quincy Bayview Bridge with Fan Cable Arrangement

c) Different Studied Cable Arrangements

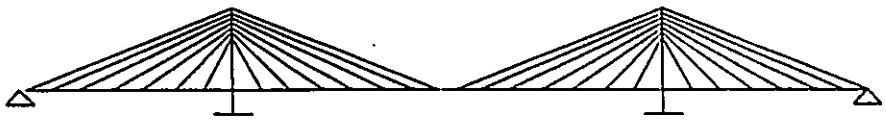

F	M	M	F	(Case FMMF)
M	F	F	M	(Case MFFM)
M	M	M	M	(case MMMM)

d) Different Studied Deck Support Cases

Figure 3.17 Cont'd

	Type of Girder	Typical Deck Cross Section
1	Twin I Girder (such as Quincy Bayview Bridge, Quincy, Illinois)	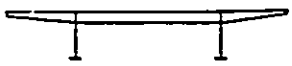
2	Single Box Girder (such as Wadi Kuf Bridge, Libya)	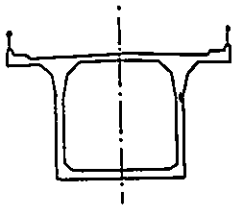
3	Central Box Girder and Side Single Web Girders (such as North Elbe Bridge, Germany)	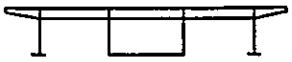
4	Twin Box Girders (such as River Waal Bridge, Holland)	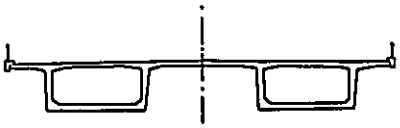
5	Highway and Railroad (such as Design by Sverdrup and Parcel and Associates, U.S.A. for the great belt project, Denmark)	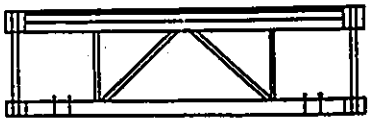
6	Prestressed Concrete Deck (such as Dame Point Bridge,)	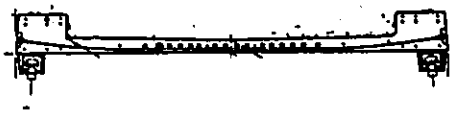

Figure 3.18 Sample of Geometric Shapes of Cable-Stayed Bridge Deck Cross Sections (Podolny and Scalzi 1986)

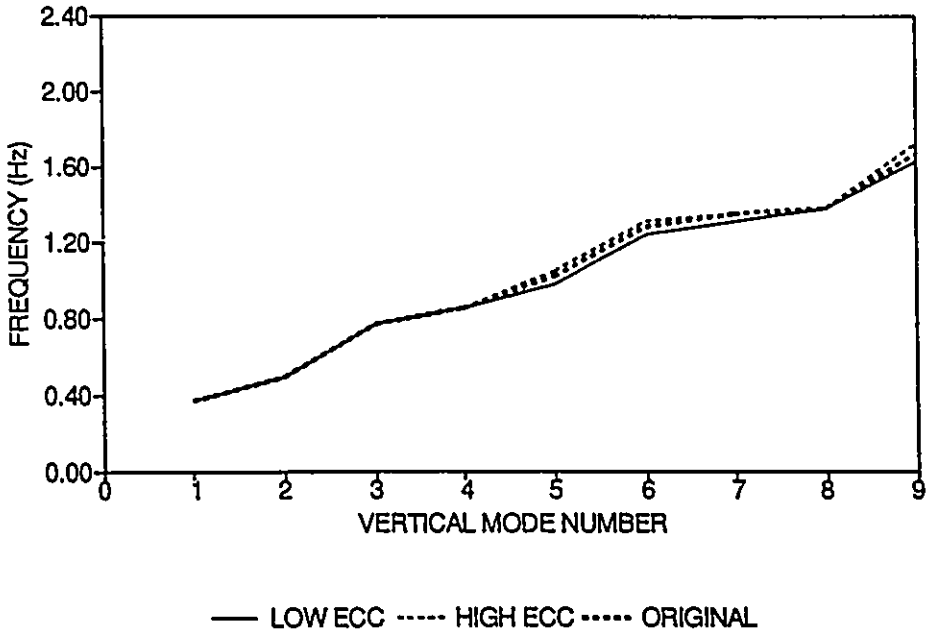

a) Vertical Plane Frequencies

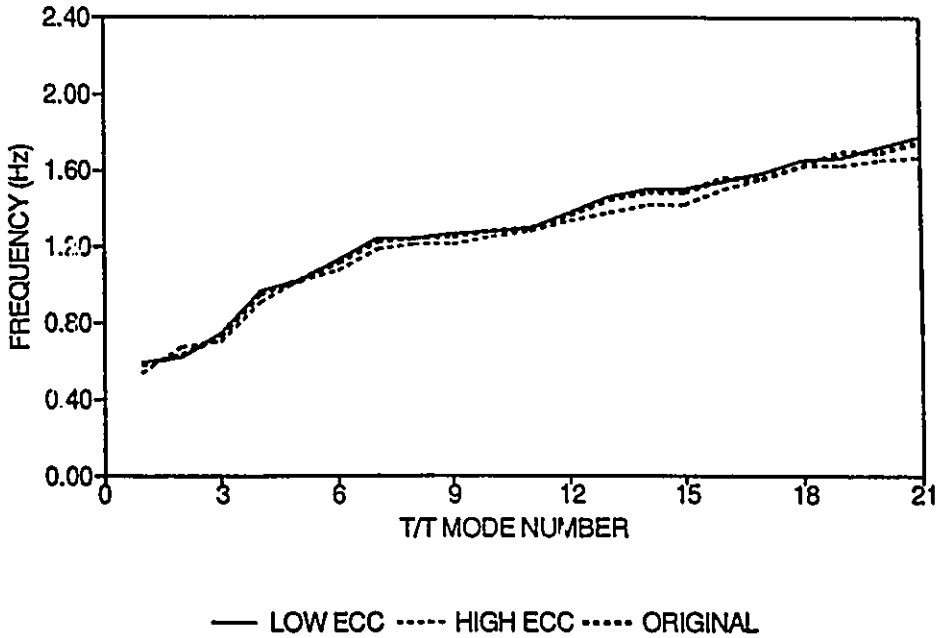

b) Torsional/Transverse Frequencies

Figure 3.19 Effect of Deck Eccentricity on Bridge Frequencies

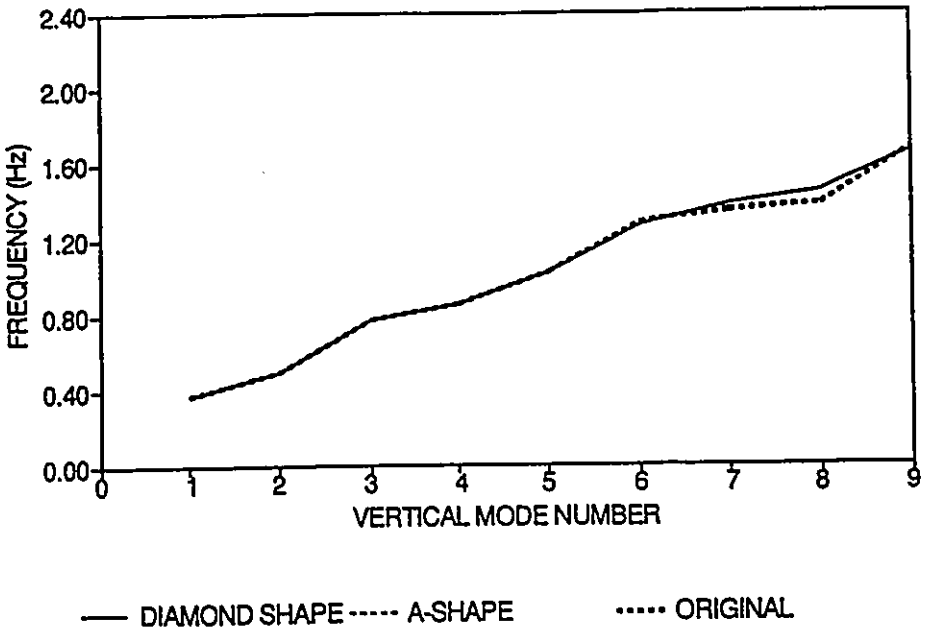

a) Vertical Plane Frequencies

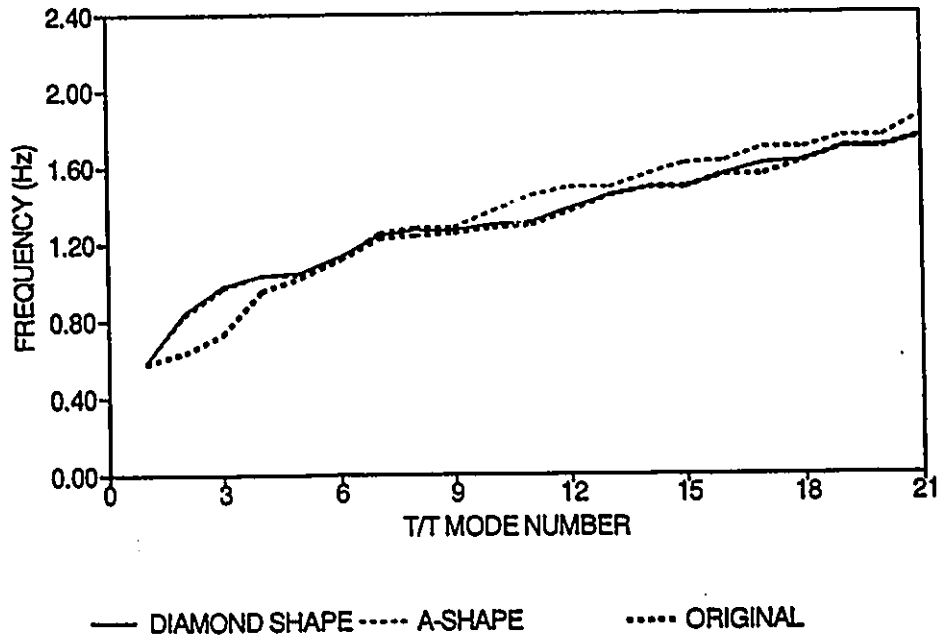

b) Torsional/Transverse Frequencies

Figure 3.20 Effect of Tower Shape on Bridge Frequencies

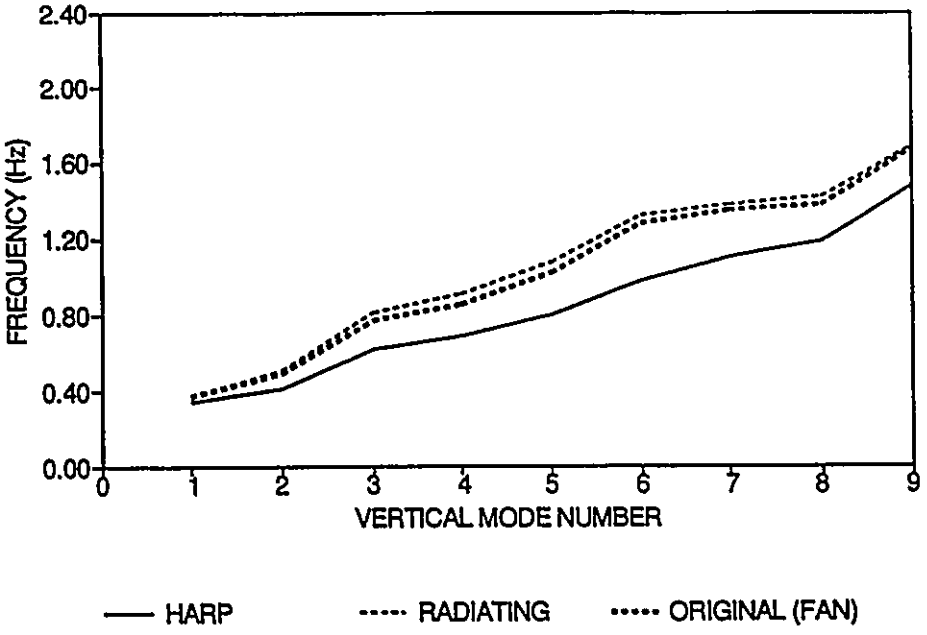

a) Vertical Plane Frequencies

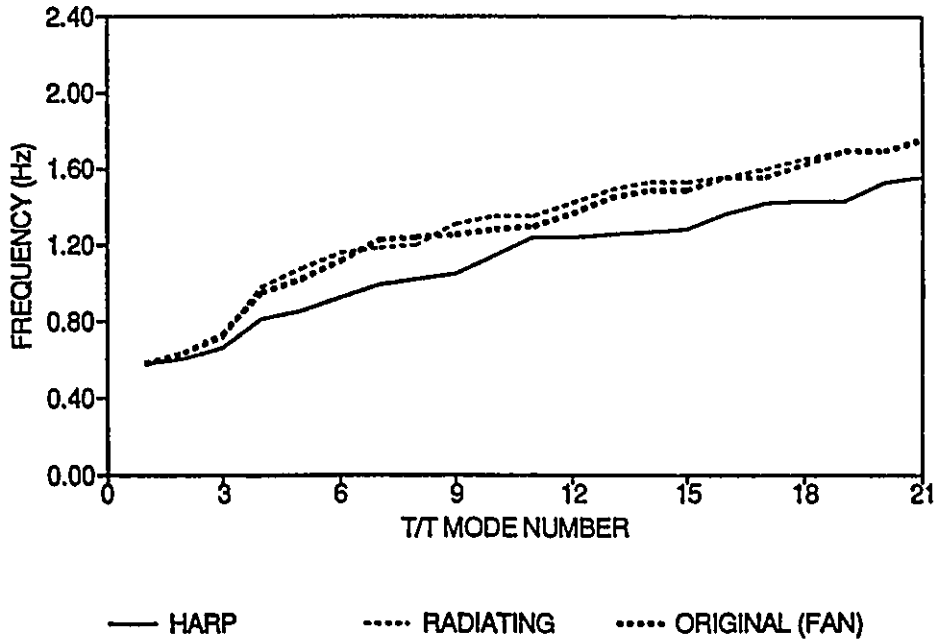

b) Torsional/Transverse Frequencies

Figure 3.21 Effect of Cable Arrangement on Bridge Frequencies

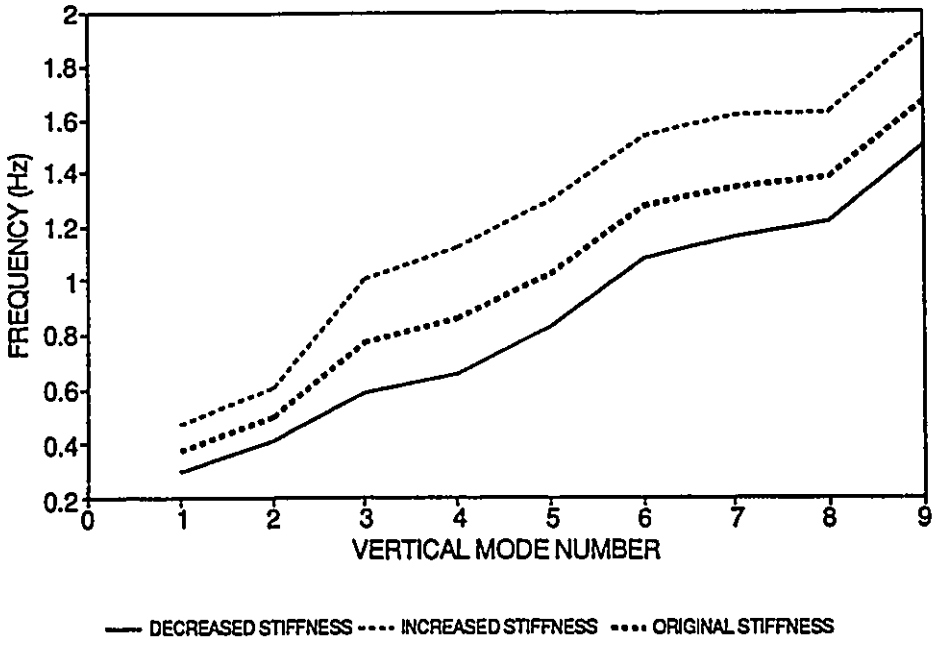

a) Vertical Plane Frequencies

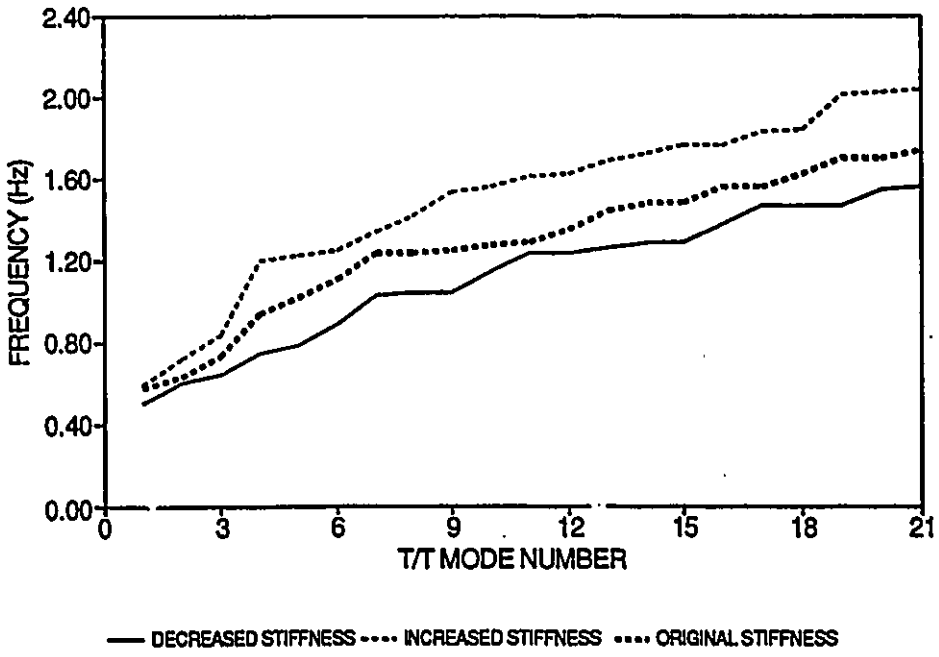

b) Torsional/Transverse Frequencies

Figure 3.22 Effect of Cable Stiffness on Bridge Frequencies

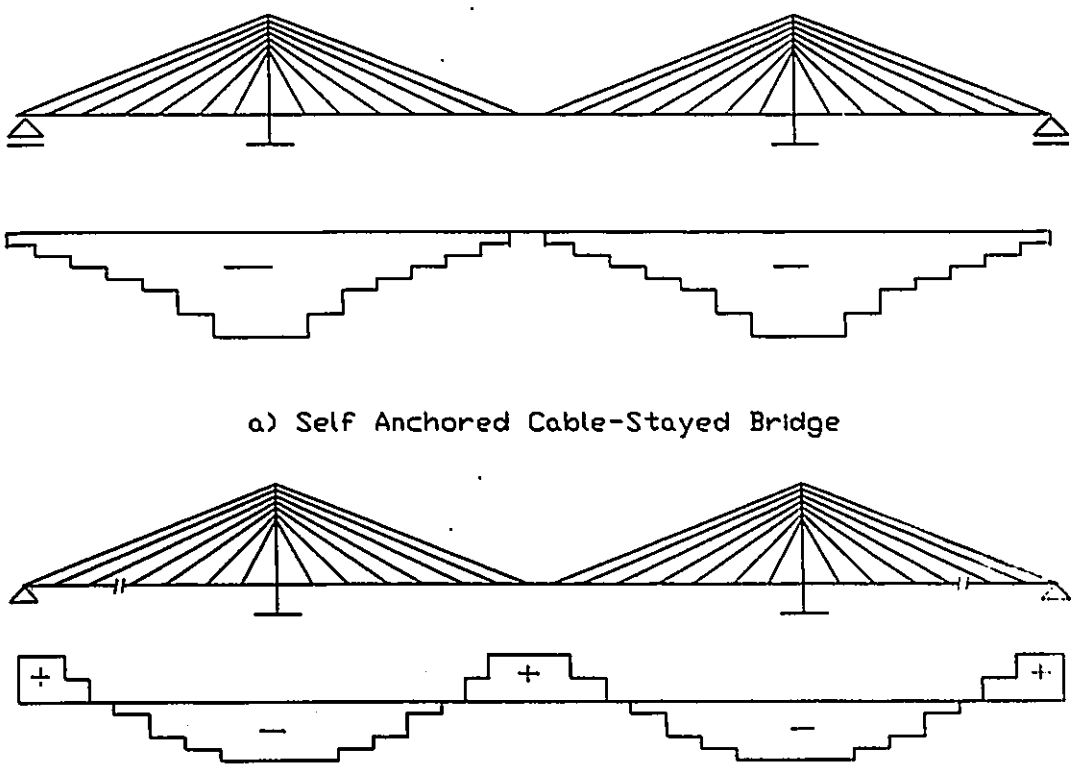

Figure 3.23 Effect of Degree of Anchorage of Cable-Stayed Bridge Deck on the Static Axial Force Distribution (Ohtsuka and Sonoda, 1987).

CHAPTER 4

METHODS OF SEISMIC ANALYSIS

4.1 INTRODUCTION

Finite element models were used in Chapter 3 to study the modal characteristics of cable-stayed bridges. Modal analysis of a structure may employ different families of vector bases but the most employed vector basis is the exact eigenvectors of the structural system under study. Previous studies, Wilson et al (1982), conducted on large 3-D structures such as off-shore towers and platforms, showed that using eigenvectors in analyzing this kind of structure has the following short comings:

- The number of eigenvectors required to obtain an accurate dynamic solution is not known until after the eigenvalue problem is solved.
- It has not been proven that the use of the exact eigenvectors in a mode superposition analysis is better, in achieving response convergence, than the use of any other set of orthogonal vectors.
- Solution of the exact eigenvalue problem of large 3-D structures requires considerable computer storage and takes multiples of the solution time consumed by other vector bases.

So, it is the objective of this chapter of the research work to investigate the suitability of two vector bases, eigenvectors and load dependent Ritz vectors, for modal

analysis of cable-stayed bridges and to propose a frequency cut-off criteria suitable for both vector bases. In order to meet these objectives, this chapter contains a review of time history analysis by direct integration of the full equations of the structural system and by superposition of eigenvectors and load dependent Ritz vectors. A comparison between the use of eigenvectors and load dependent Ritz vectors is given to examine: their ability to represent the dynamic characteristics of cable-stayed bridges, their ability to simulate the seismic response of cable-stayed bridges, and the ease of implementing the proposed frequency cut-off criteria in a computer code using either vector basis. A 2-D finite element model was employed in this study. It was subjected to 3 different synthetic time history records (each having 2 components, longitudinal and vertical). Each time history record represents a category of earthquake frequency content as expressed by the A/V ratio.

4.2 TIME HISTORY ANALYSIS OF LARGE 3-D STRUCTURES

The dynamic equilibrium of a structure modeled using a finite number of nodes may be expressed by the matrix equation:

$$[M]\{\ddot{u}\} + [C]\{\dot{u}\} + [K]\{u\} = \{F(x,t)\} \qquad (4.1)$$

where,

[M] = NxN mass matrix of the structure, and N is the total number of degrees of freedom (dof) in the model.

[C] = NxN damping matrix of the structure.

[K] = NxN stiffness matrix of the structure.

{u} = Nx1 relative displacement vector, $\{u\} \equiv \{u(t)\}$.

{F(x,t)} = Nx1 load vector that takes the form $-[M]\{r\}\ddot{u}_g(t)$ in seismic applications where,

{r} = influence coefficient vector.

$\ddot{u}_g(t)$ = ground acceleration.

Dots denote derivatives with respect to time.

The response of the structure {u(t)} to the dynamic load {F(x,t)} may be obtained by either of two well-established approaches, direct integration or modal analysis.

4.2.1 Time History Analysis by Direct Integration

Many numerical integration schemes are available to find the response of the dynamic system expressed by equation 4.1 such as the Wilson-θ (Bathe and Wilson, 1976) and Newmark-β (Newmark, 1962) methods . When the integration time step used in the integration process is small enough, as will be shown later in this section, then the solution using direct integration schemes gives response equivalent to using all modes in a modal time history analysis. In this research work the Wilson-θ method was used to calculate a reference response of the bridge model to different earthquake input motions. In the Wilson-θ numerical integration scheme a linear variation in the acceleration ($\ddot{u}$) from time (t) to time ($t+\theta\Delta t$) is assumed as shown in Figure 4.1a.

Accuracy of the solution was studied by Wilson et al, (1973) and Bathe and Wilson (1976), and they recommended to use $\theta \geq 1.37$ (preferably 1.4) and $\Delta t/T \leq 0.1$ (Δt is integration time step and 1/T is the highest load frequency required to be included in the integration). Figure 4.1b shows the relation between $\Delta t/T$ and the percentage amplitude decay (%AD), which is used as a measure of accuracy, for $\theta = 1.4, 2.0$. It is evident that for $\Delta t/T \leq 0.1$, %AD is less than 10% which is sufficiently accurate for engineering purposes. In this research work "Δt" was taken as 0.02 sec and this means that frequencies up to 5 Hz are integrated with high accuracy.

Although time history analysis by direct integration is a well established procedure, it does have several draw backs when applied to large 3-D structures. Among these draw backs are the following:

1- it is time consuming (the 1200 dof Quincy Bridge 3-D model required $\approx$ 2.5 hours on a SUN work station. The input ground motion record was 20 seconds long).

2- considerable storage capacity is required (the same model requires 12 Mb of disk storage).

3- physically useful quantities such as frequencies and mode shapes are not computed.

4.2.2 Time History Analysis by Mode Superposition

Mode superposition analysis transforms geometric displacement coordinates to normal coordinates. For most analyses in civil structural dynamics and earthquake

engineering this approach enables reduction in problem size, saves on solution time, reduces storage requirements, and produces physically meaningful quantities (modal frequencies and mode shapes).

In equation 4.1 the transformation of the displacement vector **{u}** may be expressed as:

$$\{u(x,t)\} = [X(x)]\{Y(t)\} \tag{4.2}$$

[X(x)] is a matrix containing the linearly independent basis vectors (the modal matrix) and is of order Nxn, n $\ll$ N.

{Y(t)} is a vector of n generalized coordinates obtained by solving a reduced system of (n) equation having the form:

$$[M]^*\{\ddot{Y}\} + [C]^*\{\dot{Y}\} + [K]^*\{Y\} = \{F(x,t)\}^* \tag{4.3}$$

where,

$$[M]^* = [X]^T[M][X]$$

$$[C]^* = [X]^T[C][X]$$

$$[K]^* = [X]^T[K][X]$$

$$\{F(x,t)\}^* = [X]^T\{F(x,t)\}$$

The solution for the reduced system of equations (4.3) may be performed by any one of the direct integration schemes.

The transformation basis vectors [X(x)], must satisfy the following conditions, as stated by Leger and Wilson (1987):

- vectors should be linearly independent and completely span the space of the solution to fully characterize the dynamic response.
- they should satisfy the geometric boundary conditions.
- they should produce acceptable deformation shapes to characterize the dynamic response.
- they should be simple and computationally inexpensive to generate.
- there should be simplicity in an automatic selection of their number to obtain convergence of typical response quantities.

The traditional transformation vector basis consists of the eigenvectors obtained by the solution of the generalized eigenvalue problem associated with the mass and the stiffness matrices of the full system of equations (equation 4.1).

Recently, the use of a family of load dependent Ritz vectors has been proposed for coordinate transformation in the modal analysis of large 3-D structures (Wilson et al, 1982; Nour-Omid and Clough, 1984; Arnold et al, 1985; Wilson and Bayo, 1987; Chen and Taylor, 1990; and Xia and Humar, 1992). A detailed treatment of eigenvectors and Ritz vectors as applied to cable-stayed bridges is given in section 4.4.

4.3 VECTOR BASES FOR MODAL TIME HISTORY ANALYSIS

This section illustrates the mathematical procedures used in generating eigenvectors and Ritz vectors. It summarizes the similarities and the differences between them, and shows the advantages of each.

4.3.1 Modal Analysis by Superposition of Eigenvectors

The most commonly employed transformation vector basis in structural dynamics is the eigenvectors associated with the stiffness and mass matrices. The eigenvalue problem is formulated as:

$$|[K] - \omega^2[M]| \{X\} = \{0\} \tag{4.4}$$

where,

ω = a circular frequency of the dynamic system.

There are N possible eigenvectors for a N-dof system, however, usually the lowest "n" are sufficient to express with accuracy the dynamic structural response. Applying the coordinate transformation of equation 4.2, the dynamic equilibrium equations 4.1 can be written in the form:

$$[M][X]\{\ddot{Y}\} + [C][X]\{\dot{Y}\} + [K][X]\{Y\} = \{F(x,t)\} \tag{4.5}$$

The eigenvectors are mass and stiffness orthogonal. If the damping matrix is expressed so that the eigenvectors are orthogonal to it also, then equation 4.5 can be reduced to the uncoupled form:

$$\ddot{Y}_r + 2\zeta_r\omega_r\dot{Y}_r + \omega^2{}_rY_r = \psi_r(t) \qquad (4.6)$$

$$(r = 1,\ldots n)$$

where,

ζ_r = Modal damping (in mode r) as a percentage of critical damping.

Ψ_r (t) = Modal force for mode r.

For a simple structural model such as a 2-D frame the lowest 2 or 3 eigenvectors may be sufficient to obtain a good estimate of dynamic response. For a cable-stayed bridge finite element model which contains three interacting dynamic sub-systems (deck, towers, and cables), the finite element model size is usually large (it may contain over a thousand dof) and the number of eigenvectors required to include all of the important modes may be very large. This fact has been demonstrated by the study of the dynamic characteristics of cable-stayed bridges, presented in Chapter 3. It has been shown in Chapter 3 that the first local tower mode of the Quincy Bayview Bridge appears as the forty-second eigenvector and the second local tower mode appears as the sixty-first eigenvector. Furthermore, for the Quincy Bayview Bridge there are more than 60 eigenvector modes with frequencies less than 5 Hz (Table 3.1), well within the range of predominant earthquake ground motion frequencies. This number of eigenvectors is relatively large and consequently considerable computer storage capacity and long processing times are required. This makes the use of eigenvectors as the modal transformation basis a computationally intensive process. It is also obvious that eigenvectors are independent of the dynamic load and for this reason, for some dynamic

loads, not all the modes in their sequence of generation are excited by the dynamic load. However, since the superposition process uses the eigenvectors strictly in their order of generation, many eigenvectors are required to get reasonable response predictions of a cable-stayed bridge, even though only a relatively small number may contribute to the total response.

4.3.2 Modal Analysis by Superposition of Load Dependent Ritz Vectors

Research work by Wilson et al (1982), introduced a load dependent vector basis for the coordinate transformation of mass and stiffness matrices. This new vector basis has the sequence of vectors, (Xia and Humar, 1992) (r, Dr, D^2r, D^3r,.....D^mr) where, r is arbitrary and [$D = K^{-1}M$]. Wilson et al (1982) and Leger and Wilson (1987) suggested the following procedure for generating the required Ritz vectors:

1- Ritz vectors are generated using the recurrence relationship

$$[K]\{x^*_i\} = [M]\{x_{i-1}\} \tag{4.7}$$

The first Ritz vector $\{x^*_1\}$ is obtained from the equation

$$[K]\{x_1^*\} = \{f\} \tag{4.8}$$

where, $\{f\}$ is the spatial distribution of the load vector $\{F(x,t)\}$.

The vectors are orthogonalized and normalized at each step by:

$$\{x_i\} = \{x^*_i\} - \sum_{j=1}^{i-1} c_j\{x_j\} \qquad (4.9)$$

where,

$$c_j = \{x_j\}^T[M]\{x^*_i\}$$

In this form, the first Ritz vector represents a static response to the load vector $\{f\}$. This sequence of steps will terminate when the next generated vector is orthogonal to all previous vectors. This numeric procedure is fast, easy and less costly than the procedure used in generating eigenvectors because it involves a series of static load solutions.

2- A reduced system of equations, as given by equation 4.5, is formed. Contrary to eigenvectors, the reduced system of equations will remain coupled, second order, first degree differential equations. In order to decouple the reduced system of equations, the exact eigenvectors of the reduced system may be evaluated through:

$$|[K^*]-\omega^2_i[M^*]|\ \{z_i\} = \{0\} \qquad (4.10)$$

K^*, M^* are defined in equation 4.3.

ω_i is an exact eigenvalue of the reduced system and an approximate frequency of the complete system. This eigenvalue problem is very small compared to the exact eigenvalue problem associated with the full system and this results in a further saving in time and cost.

3- The $\{z_i\}$ vectors are orthogonalized and normalized too. The final Ritz vectors are given by:

$$[^{*}X] = [x][z] \tag{4.11}$$

where, [x], [z] are matrices containing column vectors $\{x_i\}$ and $\{z_i\}$

The procedure to generate Ritz vectors is obviously load dependent (i.e. equation 4.8), which means that the vectors must be generated for each dynamic load case. However, for earthquake engineering applications, the load vector $\{F(x,t)\}$ is given by:

$$\{F(x,t)\} = -[M]\{r\}\ddot{u}_g(t) \tag{4.12}$$

which means that the vector $\{f\}$ used in calculating $\{x_1\}$ is given by:

$$\{f\} = -[M]\{r\} \tag{4.13}$$

In such a case, the vector $\{f\}$ does not depend on the earthquake characteristics but only on the spatial mass distribution within the structure. This means that, similar to eigenvectors, Ritz vectors can be generated once, saved, and used for any further seismic analysis of the structure.

In general, Ritz vectors have the following advantages over eigenvectors:

1- They take into account the important aspect of the spatial load distribution.

2- It is easier and less costly to generate these vectors because their generation involves a series of static load solutions.

3- Only a very small eigenvalue problem is solved as one of the stages of the generation process.

A detailed algorithm was provided by Wilson et al (1982) that illustrates the steps of generating the mass and stiffness orthogonal load dependent Ritz vectors.

Subsequent application of this procedure to example structures such as space frames and off-shore towers demonstrated the efficiency of the new vector basis in accelerating the convergence of response quantities and in reducing the storage requirements (Nour-Omid and Clough, 1984; Arnold et al, 1985; Leger and Wilson, 1987; and Xia and Humar, 1992). Also reported was a significant reduction in the cost of the analysis, and that fewer Ritz vectors were required to give the same level of accuracy as the eigenvector calculations. Section 4.3.3 provides four simple examples to demonstrate the characteristics of Ritz vectors.

4.3.3 Examples of Ritz Vectors Applied to Beams

The following four simple examples are provided to demonstrate the efficiency of using load dependent Ritz vectors as a basis for the required coordinate transformation for mode superposition analysis. The examples are:

a 1-span beam, a 2-span symmetric beam, a 3-span symmetric beam and a cantilever

beam. These example structures were chosen as simple representations of two of the sub-systems (deck, towers) in cable-stayed bridges. All beams have uniform mass distribution of "m", uniform bending rigidity "EI" and a main span of "l". Program SAP 90 by Habibullah and Wilson (1989), was used for the eigenvector and Ritz vector analysis of each structure. The vector shapes and normalized frequency values (λ^2_i), are defined in equation 4.14, for the lowest four vectors of each basis are given in Figures 4.2-4.5.

$$\lambda^2{}_i = \frac{2\pi l^2 f_i}{\sqrt{EI/m}} \tag{4.14}$$

Studying Figures 4.2-4.5, it may be concluded that:

1- When a few number of Ritz vectors is generated for symmetric beams, the size of the eigenvalue problem solved during the generation process of the Ritz vectors becomes small and this leads to the generation of only symmetric vectors as shown in Figures 4.2 and 4.3. This is the reason Ritz vectors span a wider frequency range than the same number of eigenvectors.

2- To generate the anti-symmetric modes using Ritz vectors, a large number of vectors must be requested to enlarge the size of the eigenvalue problem that is solved in step "2" (section 4.3.2) of their generation procedure. This behaviour accelerates the convergence of the response calculations with fewer Ritz vectors than eigenvectors.

3- Ritz vectors for the cantilever beam are identical to the eigenvectors as shown in Figure 4.5. The reason is that the vectors are not anti-symmetric and

consequently the generated load dependent Ritz vectors are not affected by the size of the eigenvalue problem that is solved during their generation process.

4- A cable-stayed bridge consists of the two basic systems (continuous beam as the deck, and cantilever beam as the towers) and hence, the Ritz vectors of a cable-stayed bridge are expected to have a combination of the observed behaviours of the two simple dynamic systems. It is expected that the interaction between the two dynamic sub-systems will change the observed behaviour of the separate sub-systems when Ritz vectors are used. It can be expected that tower response (deflections and forces) will converge faster to the correct response when Ritz vectors are used as the mode superposition basis. It is also expected that response quantities of the bridge deck will need the same number of vectors. Section 4.4 examines the dynamic behaviour of cable-stayed bridges using Ritz vectors.

4.4 COMPARATIVE APPLICATION OF EIGENVECTORS AND RITZ VECTORS TO CABLE-STAYED BRIDGES

A 2-D finite element model of the Quincy Bridge was used to compare eigenvectors and Ritz vectors as bases for mode superposition seismic analysis of cable-stayed bridges. It was decided to use 2-D model and to focus on the vertical plane of Quincy Bridge because the bridge's response in this plane is not coupled with the T/T response and it is characterized by the dynamic interaction of both the deck and tower systems. This approach helps to demonstrate the advantages and disadvantages of each vector basis in the modal analysis of cable-stayed bridges. The 2-D model has the deck

pin-connected at the abutments and free to move longitudinally at the towers. Thirty Ritz vectors and thirty eigenvectors were generated for the 2-D model, and each vector basis was subjected to three different synthetic time history records. Each record has two components, longitudinal and vertical. The synthetic time history records were constructed with standard techniques to be compatible with target acceleration response spectra representative of earthquakes of three different frequency contents (high frequency A/V $>$ 1.2, intermediate frequency $0.8 < A/V < 1.2$ and low frequency $A/V < 0.8$, where A is the maximum ground acceleration in (g), V is the maximum ground velocity in m/sec)[1]. This approach of using A/V to categorize earthquake ground motions is used in the seismic zoning in the National Building Code of Canada (NBCC 1990). Each of the three target acceleration spectra were obtained by averaging the response spectra of 15 actual ground motion records having the required A/V ratio (Tso et al 1992). Figure 4.6 shows the mean response spectra for the three A/V categories, scaled to a peak horizontal ground acceleration of 1 g. The vertical component is scaled to a peak ground acceleration of 0.6 g. Figures 4.7-4.9 show the three synthetic time history records. The different frequency content and durations of strong motion are clearly evident in these figures. The properties of the seed records used in generating these time histories are summarized in Table 4.1. The response of the 2-D model to the three input motions was studied using the two vector bases and is discussed in the following sections. As suggested by the title of this section, the discussions will

[1]Units of A/V are g/m/sec., but in this thesis A/V ratios are reported without units, as is conventional practice.

emphasize comparisons of Ritz vector and eigenvector analyses. Additional detailed discussions of seismic response are the topic of Chapter 5.

4.4.1 Frequencies and Mode Shapes

It is known that accuracy of the eigenvalues (frequencies) and eigenvectors (mode shapes) of the model does not depend on the number of eigenvectors requested (generated) in the eigenanalysis. On the contrary, load dependent Ritz vectors and their associated frequencies do depend on the number of vectors generated in the solution. The reason for this is that the size of the eigenvalue problem which is used to calculate Ritz vectors changes with the number of requested vectors, Wilson et al (1982). In order to demonstrate this behaviour the shapes of the first, third and sixth vectors were compared in four cases:

1- eigenvectors are used in the analysis

2- 6 Ritz vectors are requested

3- 10 Ritz vectors are requested

4- 30 Ritz vectors are requested

Figure 4.10 shows three vector shapes when eigenvectors are used. Figures 4.11-4.13 show the shapes of the same 3 vectors when 6,10,30 Ritz vectors are requested, respectively. Examining Figures 4.10-4.13, it is noticeable that the first and third vectors are not affected by the change in the number of Ritz vectors requested in the solution. It is also obvious that the sixth vector is greatly affected by the number of requested vectors. When six Ritz vectors are requested (Figure 4.11), the sixth vector appears as

the first local tower mode. Increasing the number of requested Ritz vectors, the sixth vector becomes a vertical bending deck mode (the sixth deck mode). It can be concluded that the last requested Ritz vector is an early estimate of a higher frequency mode. The effect of such a mode on the effective modal mass will be discussed in section 4.4.2.

Table 4.2 contains numerical results of a frequency monitoring study performed for different numbers of requested Ritz vectors. A classification of the lowest 30 eigenvectors is given as a reference. Figure 4.14 gives a graphical representation of the frequency values when 6,10,15,20,25 Ritz vectors are requested. It is observed that:

- Load dependent Ritz vectors span a wider frequency range than the same number of eigenvectors.
- The last few Ritz vectors in a requested sequence are distorted and have frequency estimates that are shifted from the true frequencies. The number of distorted Ritz vectors increases with an increase in number of requested vectors.
- The appearance of the first local tower mode was traced with the increase in the number of requested Ritz vectors. This appears for the first time when 6 vectors are requested as the sixth vector with a frequency of 2.18 Hz. When 15 Ritz vectors are requested it appears as vector number 13 with frequency of 2.29 Hz. When 20 Ritz vectors are requested it appears as the thirteenth vector with a frequency of 2.33 Hz. When comparing these results with the eigenvectors and eigenvalues, it appears that this same vector also has the thirteenth place with the same frequency of 2.33 Hz. The deflected shape of the towers differ slightly near the top with the increase in number of requested vectors. On the other hand the

deck deflection changes very much with the increase in the number of requested Ritz vectors. When many Ritz vectors are requested the maximum ordinate in deck deflection is small compared to the tower and many half cycles constitutes the vertical deck deflection as shown in Figure 4.15. Figure 4.16 gives the different calculated frequencies of this vector. The frequency estimation of the first local tower mode is less than the exact value (calculated using eigenanalysis) when 6 Ritz vectors are requested. It jumps to very close value when 10 or more Ritz vectors are generated.

- The distortion in Ritz vector shapes changes their effective modal mass and thus affects the contribution of these vectors toward the dynamic response of the complete bridge. To avoid inaccuracy in response calculations that will occur due to distortion in the last few Ritz vectors, a large enough number of modes must be requested so that the last contributing vector is covered by 3 or 4 more vectors. This should ensure that the last required vector is neither distorted in shape nor has a shifted frequency. It is also noticeable that the anti-symmetric deck modes such as the second mode of Figure 3.2 appear in Ritz vectors, contrary to the beam case. This happens because most anti-symmetric deck modes are coupled with the contributing tower modes. This shows that the mathematical procedure of generating Ritz vectors omits only the modes that are not contributing to any part of the structure.

4.4.2 Effective Modal Masses

The relationship between the effective modal masses and the number of requested vectors in the vertical and longitudinal directions was studied using Ritz vectors and eigenvectors. Figure 4.17a shows the trend of behaviour of effective modal mass in the longitudinal direction. The following observations are drawn from Figure 4.17a:

1- Ritz vectors always have more effective modal mass than the same number of eigenvectors because, as shown earlier, the last few Ritz vectors are early estimates of the high frequency, high participating vectors.

2- The first high vertical jump in the value of effective modal mass in the longitudinal direction (%EM_x) on the different curves in Figure 4.17a occurs because of inclusion of the first local tower mode. While the order of this mode is constant regardless of the number of requested eigenvectors, the order of the same vector changes with changing the number of requested Ritz vectors. The order of this vector is stable as mode number 13 when 15 Ritz vectors or more are requested. The number of vectors at which the order of the first local tower mode stabilizes depends on the model size, the deck mass and stiffness properties, and the tower mass and stiffness properties.

3- Slight changes occur in the shape of the first local tower mode (mostly at the top) depending upon its order of appearance in the sequence of generated Ritz vectors, as shown in Figure 4.15. Different values of effective modal mass are associated with changes in number of generated Ritz vectors.

4- Requesting more than fifteen Ritz vectors leads to the generation of higher local

tower modes, which give the observed small jumps near the end of each curve on Figure 4.17a.

Figure 4.17b shows the behaviour of effective modal mass in the vertical direction with an increase in the number of requested modes. It is observed that:

1- The important contributions come from low frequency deck modes which results in all curves being coincident for the lowest 5 vectors.

2- Distortion of the highest few requested Ritz vectors gives the observed jumps at the end of each curve.

3- When 20 or more Ritz vectors are requested for Quincy Bayview Bridge, the last two modes are unrealistic, high frequency, axial vibration tower modes that causes higher jumps at the end of the $\%EM_z$ lines (models of other bridges may need a different number of modes).

4- Similar to the case of $\%EM_x$; Ritz vectors used in the vertical direction represent a greater effective modal mass than the same number of eigenvectors.

Comparisons of seismic response deflections and forces that are studied in the following sections will determine the effect of input motion's frequency content on the seismic response obtained with Ritz and eigenvectors, the effect of the distorted Ritz vectors on the seismic response, and the number of vectors required in each basis to give a seismic response that is within 10% of the response computed by direct integration.

4.4.3 Deflections

Tower and deck deflections were computed for different A/V ratio input motions scaled to 1.0g peak acceleration, and the effect on the observed deflections of the bridge with increasing numbers of requested modes was studied. Longitudinal deflection of the tower tip and vertical and longitudinal deflections at quarter-main span and at mid-side span were computed. Results are summarized in Figures 4.18 and 4.19. The curves on these response figures are identified by three letters: the first letter gives the frequency content ("H" for high A/V, "I" for intermediate A/V and "L" for low A/V), the second letter is always "S" which means that the input motion is a synthetic time history, and the third letter denotes the vector basis ("R" for Ritz and "E" for eigenvectors).

4.4.3.1 Tower Tip Deflections

Figure 4.18a shows the values of tower tip deflections with different A/V ratio input motions and with an increasing number of Ritz vectors and eigenvectors included in the solution. It is noticeable from the figure that this response quantity, which depends on the first local tower mode, needs at least 15 eigenvectors to be estimated with reasonable accuracy. It is observed that the response predicted by Ritz vectors fluctuates between 60%-120% of the exact solution (by direct integration) as shown in Figure 4.18b when less than 15 modes are requested because of the distortion in computation of the first local tower mode. However, the error in the tower tip deflection by Ritz vectors, as compared to the direct integration response, is less than the error calculated for eigenvectors response as shown in Figure 4.18b. Figure 4.18b shows that the error in

deflection calculation by Ritz vector analysis is usually less than the error calculated for eigenvector analysis. For 15 modes the percentage error using Ritz vectors drops to $< 10\%$ for all A/V inputs. The situation is the same for eigenvectors except for high A/V where 20 modes are required. Low A/V input causes the largest tower tip deflection as shown in Figure 4.18a, high A/V causes the lowest tower tip deflection. The tower drift is 0.6% for low A/V input and 0.18% for high A/V input. These values are very small considering the high value of ground acceleration used in the analysis (1 g). The lowest value of tower deflection is caused by high A/V input. The effect of the first local tower mode appears clearly in the jump observed for the eigenvector curves.

4.4.3.2 Deck Deflections

The vertical deflection of the deck depends on only a few of the lowest vertical deck modes. This is the reason that the vertical deflection values calculated using Ritz and eigenvectors, as shown in Figure 4.19a, are identical when 6 or more vectors are requested. The vertical deflection of the two examined locations, mid point of side span and quarter point of main span, demonstrated slightly different behaviour when the requested number of vectors is less than 6. The peak that appears in the response curve of the mid point of side span calculated using Ritz vectors may be explained with the following: The first, third, and fifth vectors contribute most toward the vertical response of the bridge deck. However, when only 3 Ritz vectors are generated, the third is distorted from its actual shape. When four vectors are requested, the fourth will have the same problem. The distortion in the last vector affects side span deflection more than the

main span deflection because of the vector shape.

Low A/V input motions cause the largest vertical deck deflections. A ratio of 2.5 is observed for vertical deflection of mid-side span caused by low A/V input (Figure 4.19a) when compared to the same location's deflection caused by intermediate A/V input. This ratio remains almost the same when comparing intermediate A/V to high A/V deflections. Almost the same ratios are also observed at the quarter-main span (Figure 4.19b). For any input motion, the numeric values of the vertical deflection at both location are almost the same.

The longitudinal deflection of the two points is shown in Figure 4.19c,d. Only the response to high A/V ratio input motion is given because the response curves for other A/V ratio input motions are almost identical. It is observed that this response quantity is dependent on the inclusion of high frequency modes. Although these high frequency modes appear early when Ritz vectors are used, they are distorted and additional modes are required to obtain more accurate response estimation. This leads to the result that almost the same number of vectors (approximately 25) are required when either Ritz or eigenvectors are used to compute longitudinal deflections of the deck.

4.4.4 Internal Forces

The internal forces of interest are normal force, shear force and bending moment. These quantities were monitored at the bridge abutment, quarter-point of main span, mid-points of the deck's main and side spans, and at the base of the tower. Figures 4.20-4.23 show the internal forces at the different locations with an increase in the number of

requested modes and with the changes in input motion frequency content. The same legend (i.e. HSR, ISR, LSR) that was used for the deflection curves is used to identify different curves of internal forces.

4.4.4.1 Deck Internal Forces

Deck Normal Force

Normal force in the deck demonstrated different behaviour at different locations as shown in Figure 4.20. It is observed that:

1- Normal force at abutments, mid-point of side span, and quarter-point of main span, is affected by higher frequency (2.5 Hz-4.5 Hz) axial deck modes which are coupled with local tower modes. This appears in the two jumps in the eigenvector response curves of Figure 4.20a,b,c. The normal force at mid-main span (Figure 4.20d), though small compared to forces at other locations because the deck is considered hinged at the abutments, is affected by low frequency modes alone because the high frequency modes do not cause a significant relative axial motion near the deck centre.

2- The fluctuation in the Ritz vectors response at all locations, except for deck centre, is caused by the distortion in the higher frequency modes when only a few vectors are requested. The response estimations became more stable with an increase in the number of requested modes (more than 12 vectors) because their distortion in the higher frequency vectors is reduced.

3- The shapes of jumps in the region of response fluctuation (between vectors 5 and 15) are affected by the A/V ratio of the input motion as shown in Figure 4.20a,b,c. The

magnitude of the normal forces depends upon both the A/V ratio and the location on the deck. The largest normal forces may be caused by either the low or intermediate A/V inputs. A more detailed discussion on the effect of A/V ratio on the response values will be presented in Chapter 5.

4- In general, 20 Ritz vectors are required for reliable normal force estimates; 25 eigenvectors are required for the same level of accuracy.

5- The effect of A/V ratio on normal force is shown most clearly when considering normal force at mid-main span. A ratio of 2 is observed between normal forces caused by low and intermediate A/V inputs and a ratio of 3 is observed between normal forces caused by intermediate and high A/V inputs. However, at mid-main span the force is relatively small, and at other locations the ratio between largest and smallest normal force is about 1.5.

6- Examining Figure 4.20a,b,c,d it is noticeable that the normal force decreases as the distance increases from the abutment, and this is valid for all three input motions.

Deck Shear Force

Shear force at the same deck locations are shown in Figure 4.21. Studying this figure, the following observations were made:

1- Shear forces require more vectors than any other response quantity to predict their values because they are functions of the highest deflection derivatives. This explains the reason for requiring 25 eigenvectors or Ritz vectors to predict their values at some deck locations and for some A/V input motions (Figure 4.21c,d). It also

explains the reason for having a long region of response fluctuations when Ritz vectors are employed in the analysis, as the case of Figure 4.21b,c,d.

2- Maximum shear force occurs at the abutment. The shear forces at quarter-main span and mid-main span are approximately 30% of the shear force at the abutment (for low A/V input). The shear force is almost constant at different deck locations for each of the intermediate and high A/V inputs as shown in Figure 4.21.

3- Low A/V input generally causes the highest shear force (twice as high as caused by intermediate A/V input and 3-4 times as high as caused by high A/V input as shown in Figure 4.21a,b). An exception appears to be at the quarter main span where the forces caused by the intermediate A/V are essentially the same as those caused by the low A/V motions.

4- The effect of frequency content of input motion reduces at quarter-main span as shown in Figure 4.21c.

5- The shear force increases gradually when eigenvectors are used in the analysis, indicating that many modes contribute to the total force in the deck. This is in contrast to the behaviour of the normal force where only a few modes contribute and the plots are characterized by rapid jumps in the force.

Deck Bending Moment

Bending moments at mid-side span, quarter-main span and mid-main span are shown in Figure 4.22. It is observed that:

1- Bending moment at the mid-points of both side and main spans, Figure 4.22a,c, are

expressed with good accuracy for almost all cases by using only 5 eigenvectors because the bending moments are affected by only a few low frequency vertical deck modes.

2- Bending moment at the quarter-point of the main span, Figure 4.22b, requires approximately 15 eigenvectors to predict its value for any input motion because the deflection at this location is affected by higher modes associated with tower deflections.

3- In all cases Ritz vector analysis required more vectors than eigenvector analysis to achieve a similar accuracy.

4- This observed behaviour may be attributed to the fact that if the lowest 5 eigenvectors are required (such as the case of bending moment at mid-points of side and main spans as shown in Figure 4.22a,c), then more Ritz vectors are required to obtain good accuracy in the mode shapes. This is different from the case when only the fifteenth and twentieth modes are required (the case of tower tip deflection, Figure 4.18a). In the latter case less Ritz vectors than eigenvectors are required because these modes, though distorted, appear early in the Ritz vector generation process.

5- Low A/V input motion causes the highest bending moment. At all deck locations, the ratio of bending moment caused by different A/V inputs differs by the location. The highest ratios are observed at mid-side span (a ratio of 2 for low/intermediate and 6 for low/high). These ratios reduce to 1.3 and 3 at quarter-main span and 1.3 and 4 at mid-main span.

6- The largest bending moment at mid-side span is almost equal to the largest bending

moment at mid-main span (this occurs for low A/V input). Bending moments at the three locations are approximately the same for each of the intermediate and high A/V inputs.

4.4.4.2 Tower Base Internal Forces

Figure 4.23 shows the behaviour of the tower base reactions with an increasing number of requested modes. The following observations were made:

1- Normal force requires ≈ 15 eigenvectors for accurate response predictions, while approximately 10 Ritz vectors will give the same level of accuracy, as shown in Figure 4.23a.

2- The local tower modes provide almost all of the contributions toward the shear force and bending moment at the tower base. This is observed on Figures 4.23b,c by the jumps in response between 10 and 15, and then between 20 and 25 requested vectors.

3- There is rather long range (15 modes) in the Ritz vector response in which fluctuations occur in the shear force and bending moment predictions.

4- Fewer Ritz vectors than eigenvectors are required to obtain reasonable predictions of shear force and bending moment.

5- The reason for observations 3 and 4 is that local tower modes contribute to most of the response and they appear early in the generation of Ritz vectors but with distorted shapes and shifted frequencies so that they cause the observed response fluctuations in the shear force and bending moment curves.

4.5 FREQUENCY CUT-OFF CRITERIA

The study of 3-D eigenvectors of the Quincy Bayview Bridge in Chapter 3 and the comparative application of Ritz vectors and eigenvectors to cable-stayed bridges in this chapter showed that:

1- The decoupled dynamic behaviour of vertical response from those involving torsional and transverse motions means that response quantities in each category (Vertical or T/T) are affected by different mode shapes.

2- Cable-stayed bridges have many closely-spaced frequencies. For the Quincy Bayview Bridge, 65 modes cover the frequency range between 0.371 Hz and 4.5 Hz. This is similar to the trend for other cable-stayed bridges as shown in Table 4.3.

3- The response comparisons of section 4.5 show that as many as 25 2-D modes for the Quincy Bayview Bridge are required to obtain accurate estimates of the bridge seismic response. This ensures that the second local tower mode (twenty second mode) is included. The third local tower mode will have a frequency outside the range of significant seismic ground motion frequencies. This sets the frequency of the second local tower mode as one limit on the upper frequency that needs to be included in the analysis. When 3-D analysis is used the number of modes will increase to more than sixty in order to contain the second local tower mode.

4- The above-mentioned points show that an arbitrary choice of the number of modes to be included in a dynamic modal analysis of the bridge may lead to a substantial underestimation of the bridge's seismic response. This may occur if too few modes are used. The degree of underestimation depends upon several specific factors as

illustrated by the analyses presented in section 4.4 and is difficult to predict a priori.

The analyses and discussions so far show that it is desirable to establish criteria for an upper limit on modal frequencies to be included in the analyses in order to ensure an acceptable level of accuracy in the seismic response calculations of cable-stayed bridges. In this thesis this will be referred to as frequency cut-off criteria. The required criteria should be applicable to any cable-stayed bridge, and be neither model nor load dependent. They also should be easy to implement in existing computer codes to check the accuracy of response calculations.

A systematic approach to establishing a frequency cut-off for seismic analysis is preferable to using an arbitrary limit selected by reference only to the spectral content of the ground motion. A ground motion spectrum will provide an indication of an upper limit on the frequency content of the input, however this upper limit will typically be of the order of approximately 10 Hz for horizontal ground motions. This criterion alone will result in the use of a very large number of modes in the analysis, many of which are likely to contribute only a negligible amount to the response. Therefore, it is more desirable to establish criteria for an upper frequency limit based on the actual modal behaviour of the structure, as suggested in the following paragraphs.

The seismic response of a bridge is a function of its mode shapes and frequencies. It is therefore appropriate to define the required criteria in terms of parameters related to these two quantities. Although modal participation factors are used successfully to determine the required number of modes for framed structures because of the obvious decay trend with higher modes, it has been pointed out in section 3.2.2 that modal

participation factors may not be the most suitable basis for the required criteria for cable-stayed bridges. Based on that discussion, it is suggested to use both the frequency of local tower modes and the effective modal mass (%EM_j, j=X,Y,Z) to be the bases for the proposed criteria. These two parameters are proposed because:

- The frequencies of local tower modes provide an estimate of an upper frequency limit for inclusion of a considerable amount of the effective modal mass (the first longitudinal local tower mode contributes 45% toward the effective modal mass in the longitudinal direction in the case of Quincy Bridge. The second local tower mode contributes 10%).
- The effective modal mass is a function of the mode shape and it provides a measure of the amount of mass that is participating in the seismic response of the structure. It has a ceiling value of 100% for each global direction and it may be calculated from readily available mass and modal parameters.
- The use of the effective modal mass and the frequency range ensures the inclusion of all important modes in the mode superposition process by covering the frequency range that contains the high frequency tower modes, and by checking the amount of mass that is expected to respond within the defined frequency range.

The frequency range is defined using the analytic models developed in Chapter 2. The models can be used to calculate the frequencies of the tower structure in the two horizontal directions. It is recommended to calculate the lowest two frequencies in each horizontal direction because the lowest two modes for a cantilever-like structure contain more than 80% of the effective modal mass of the cantilever (this is about 40% of the

mass of the complete bridge). The frequency range then, must include all frequencies up to these calculated tower frequencies.

The frequency cut-off criteria proposes that the effective modal masses for the whole structure in the three spatial directions should have the following minimum values:

$\%EM_x = 70\%$ (longitudinal)

$\%EM_y = 70\%$ (transverse)

$\%EM_z = 50\%$ (vertical)

These values of $\%EM_x$ and $\%EM_y$ are chosen because the mass of the full structure is divided almost equally between the deck and the towers. Many modes from the deck are excited in the low frequency range, and hence almost 90% of the mass of the deck is included in these modes. Only two local modes of the tower would tend to be excited by seismic frequencies and these would contribute about 70% of the tower mass to the overall response of the bridge. Thus, almost 70% of the total bridge mass is expected to contribute to the response in each of these two directions. The value of $\%EM_z$ was chosen as 50% because the tower, which has almost half the total mass of the bridge, is very stiff in the vertical direction and all bridge modes within the frequency range of interest for seismic applications do not include any axial tower modes. Thus the 50% represents the effective modal mass of the deck.

The validity of the criteria may be established by studying the responses in Figures 4.18-4.23. It is observed that the last large increase in the $\%EM_i$ (as shown in Figure 4.17) occurs in the twentieth to twenty-fifth mode range. This mode range contains the second longitudinal tower mode. The effective modal mass of this number

of eigenvector modes (Figure 4.17a and b) is 70% (longitudinal) and 50% (vertical). However, a better check for the validity of the criteria is the value of the error (based on the difference between the modal analysis and the direct integration) calculated for the different response quantities. Figure 4.24 shows the percentage error calculated for the bending moment and shear force at the tower base and quarter point of the main span. In the cases shown, less than 10% error occurs when 25 modes are used. The proposed values for effective modal masses are valid for any 3-span uniform cable-stayed bridge because of the similarity in mode shapes and the nearly equal distribution of mass between the tower and the deck for this class of cable-stayed bridge.

The above arguments are valid whether eigenvectors or Ritz vectors are used in the analysis. However, Ritz vector shapes and associated frequencies and effective modal masses are dependent on the requested number of vectors. It has been pointed out in section 4.4 that if 10 vectors contribute toward a response quantity then perhaps 15 Ritz vectors should be generated. This means that a higher percentage of effective modal mass is expected. For the required 25 vectors, Figure 4.17 shows that $\%EM_x = 90\%$ and $\%EM_z = 70\%$. Although the conducted study on Ritz vectors was limited to 2-D analysis, it may be deduced (based on the dynamic characteristics studied in Chapter 3) that $\%EM_y$ should also be taken $\geq 90\%$. The reason for this choice is that there is a combination of low frequency transverse deck modes and higher frequency transverse tower modes that are expected to participate in the response in this direction.

4.6 SUMMARY AND CONCLUSIONS

A review of the mathematical basis for time history analysis by direct integration and by modal analysis was presented. The use of eigenvectors and Ritz vectors as the modal transformation basis was explained. Both vector bases were applied to a 2-D finite element model of the Quincy Bayview Bridge to determine their effectiveness in seismic response calculations.

Table 4.4 contains a summary of the required minimum number of vectors for estimation of each response quantity. Based on the highest number of required vectors for any response quantity, 25 vectors, it is obvious from Figure 4.17 that these vectors have the following values of effective modal masses:

EM_x%	70% (eigenvectors)	90% (Ritz vectors)
EM_z%	50% (eigenvectors)	70% (Ritz vectors)

Based on the study of the seismic response of cable-stayed bridges presented in this chapter, and the dynamic characteristic study in Chapter 3, frequency cut-off criteria were suggested to check the accuracy of seismic analysis by the modal superposition method.

It can be concluded from the study that:

1- Time history analysis by direct integration of the full equations of motion of cable-stayed bridges requires a small integration time step ($\leq$ 0.02 sec.) which leads to a time consuming analysis and large storage requirements because of the large number of degrees of freedom in the model.

2- Modal analysis of cable-stayed bridges provides a suitable means to reduce the time

and cost of the dynamic analysis. It is also important because it provides relevant information about the structure deflection mechanisms and frequencies.

3- The process of generating load dependent Ritz vectors involves the solution of an eigenvalue problem. The size of this eigenvalue problem depends on the number of requested vectors which in turn, affects the shapes of the generated vectors. For a simple dynamic system such as a simple beam, requesting a few modes leads to the generation of symmetric modes only and accelerates the response convergence. For a complicated dynamic system such as a cable-stayed bridge, requesting a few number of modes will lead to generating some low frequency modes and some high frequency modes. This behaviour may lead to excluding important modes in between the generated low and high frequency modes, consequently affecting the full structure's response.

4- Frequencies calculated for Ritz vectors are very close to the eigenvalues except for the frequencies of the last few generated Ritz vectors. The number of inaccurate Ritz vectors is dependent on the total number of generated vectors. The result of this behaviour is that there is no real reduction in the number of vectors required to estimate the bridge response.

5- Another result of the behaviour noted in 4 above is the observed fluctuations in Ritz-calculated responses compared to eigenvector responses when only a few Ritz vectors are generated. High response errors (up to 100%) may occur if the response quantity, such as shear force in the deck, is a function of many modes.

6- In order to efficiently utilize either of the vector bases, the proposed frequency cut-

off criteria should be applied to the finite element model under study. When eigenvectors are used, the frequency cut-off criteria are defined as:

A frequency range is defined by calculating an estimate of the lowest deck frequency and frequency of the second local tower mode. Then this frequency range should contain modes that have effective modal mass more than the following values:

$\%EM_x \geq 70\%$, $\%EM_y \geq 70\%$, $\%EM_z \geq 50\%$.

For Ritz vectors a change in the value of the specified effective modal mass is suggested, as follows, to adapt the criteria to the characteristics of these vectors:

$\%EM_x \geq 90\%$, $\%EM_y \geq 90\%$, $\%EM_z \geq 70\%$.

Table 4.1 Ground Motion Parameters of Seed Records and Synthetic Time History Records.

Record	Seed Parameters				Synthetic Record Parameters			
	Event	Site	horizontal A/V	vertical A/V	A_{max} (horizontal)	A_{max} (vertical)	horizontal A/V	vertical A/V
LS low (A/V)	San Fernando Feb., 9, 1971.	800 West 1st., L.A. California.	0.50	0.71	1 g	0.6 g	0.52	0.55
IS int (A/V)	Imperial Valley May, 18, 1940.	El Centro	1.04	1.94	1 g	0.6 g	0.93	1.28
HS high (A/V)	Parkfield, June,27,1966.	Cholame	1.70	1.64	1 g	0.6 g	2.33	2.95

Table 4.2 Effect of Number of Requested Vectors on Frequency Values (Hz) of Ritz Vectors in 2-D Model.

Mode No.	Number of Requested Ritz Vectors									Eigen	Mode Classification
	1	3	6	10	15	20	25	30	35		
1	0.38	0.37	0.37	0.37	0.37	0.37	0.37	0.37	0.37	0.371	VT
2		0.49	0.49	0.49	0.49	0.49	0.49	0.49	0.49	0.499	VT
3		0.82	0.77	0.77	0.77	0.77	0.77	0.77	0.77	0.770	VL
4			0.95	0.85	0.85	0.85	0.85	0.85	0.85	0.854	VL
5			1.08	1.02	1.02	1.02	1.02	1.02	1.02	1.023	VL
6			2.2*	1.32	1.28	1.28	1.28	1.28	1.28	1.279	VL
7				1.44	1.35	1.35	1.35	1.35	1.35	1.345	VL
8				1.67	1.38	1.38	1.38	1.38	1.38	1.383	VL
9				2.08	1.67	1.67	1.67	1.67	1.67	1.665	VL
10				2.3*	1.99	1.99	1.99	1.99	1.99	1.988	VT
11					2.16	2.14	2.14	2.14	2.14	2.141	VT
12					2.22	2.26	2.26	2.26	2.22	2.261	VT
13					2.3*	2.3*	2.3*	2.3*	2.3*	2.33*	TL
14					3.98	2.42	2.42	2.42	2.42	2.419	VT
15					4.27	2.64	2.64	2.64	2.64	2.641	VT
16						3.33	3.11	3.08	3.08	3.082	VL
17						4.37	3.55	3.30	3.30	3.297	VL
18						5.2**	3.70	3.42	3.42	3.425	VL
19						6.75	3.98	3.68	3.68	3.684	VT
20						9.71	4.22	3.84	3.84	3.838	VL
21							4.8**	4.36	4.36	4.355	VT
22							5.57	4.4**	4.4**	4.4**	TL
23							6.90	4.74	4.53	4.527	TL
24							10.2	4.82	4.63	4.624	VL
25							14.7	5.10	4.82	4.779	VL
26								8.40	5.79	5.200	VL
27								9.70	6.39	5.735	VL
28								12.4	7.50	6.045	VL
29								17.7	9.00	6.228	VL
30								19.7	9.68	6.621	VL

* denotes first local tower mode

** denotes second local tower mode

Table 4.3 Eigen Frequencies of Selected Cable-Stayed Bridges

Name	Main Span (ft)	Fundamental Frequency (Hz)	10th Frequency (Hz)	20th Frequency (Hz)	30th Frequency (Hz)
Abdel-Ghaffar (Bridge I*)	1100	0.3109	0.804	1.189	1.787
Abdel-Ghaffar (Bridge II*)	2200	0.1924	0.474	0.714	0.9915
Quincy Bayview	900	0.3708	1.023	1.383	1.747
Houston Baytown**	1270	0.178	0.537	0.687	0.877
Sunshine Skyway**	1220	0.287	0.767	N/A	N/A
Talmadge Memorial**	1117	0.171	0.645	1.027	N/A
Vancouver Skytrain***	1133	0.15	0.61	N/A	N/A

* Abdel-Ghaffar and Nazmy, (1987)

** Stroh, (1987)

*** Khalil and Bush, (1987)

N/A Not Available

Table 4.4 Minimum Number of Vectors Required for Calculation of Seismic Forces and Moments.

Location	Normal Force	Shear Force	Bending Moment
Abutment	16 Ritz 25 Eigen	20 Ritz 15 Eigen	N/A N/A
Mid-Side Span	15 Ritz 25 Eigen	25 Ritz 25 Eigen	12 Ritz 5 Eigen
Quarter-Main Span	20 Ritz 25 Eigen	25 Ritz 25 Eigen	20 Ritz 15 Eigen
Mid-Main Span	5 Ritz 5 Eigen	25 Ritz 20 Eigen	20 Ritz 15 Eigen
Tower	10 Ritz 15 Eigen	15 Ritz 25 Eigen	15 Ritz 25 Eigen

N/A: Not Applicable

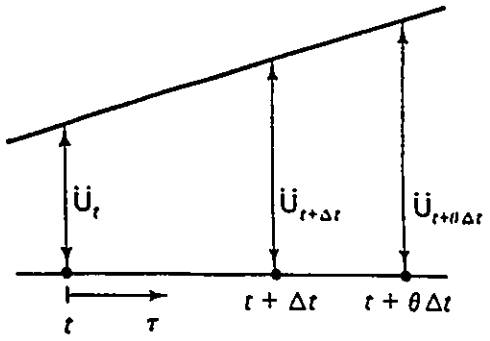

a) Illustration of the Different Parameters (Bathe and Wilson, 1976)

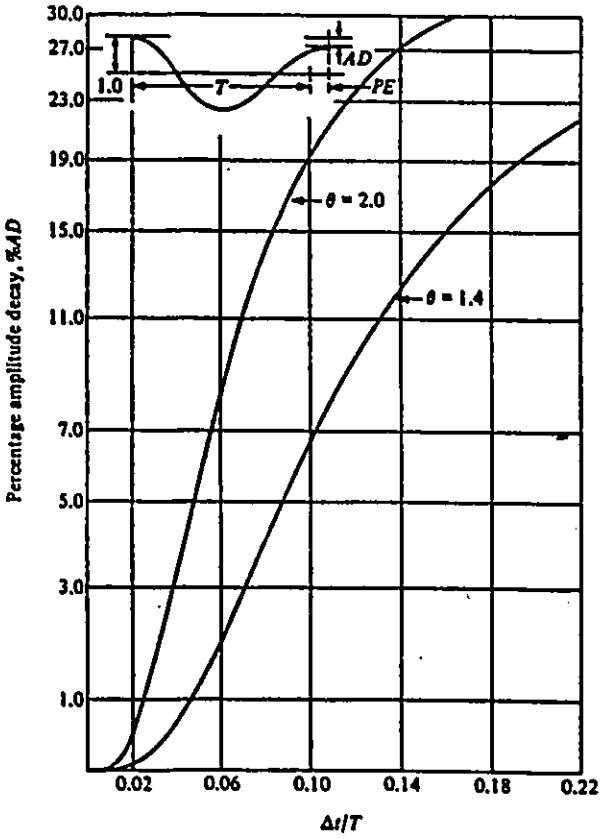

b) Effect of Value of θ and Δt on the Amplitude Decay (Wilson et al, 1973)

Figure 4.1 Parameters of Wilson-θ Numerical Integration Scheme.

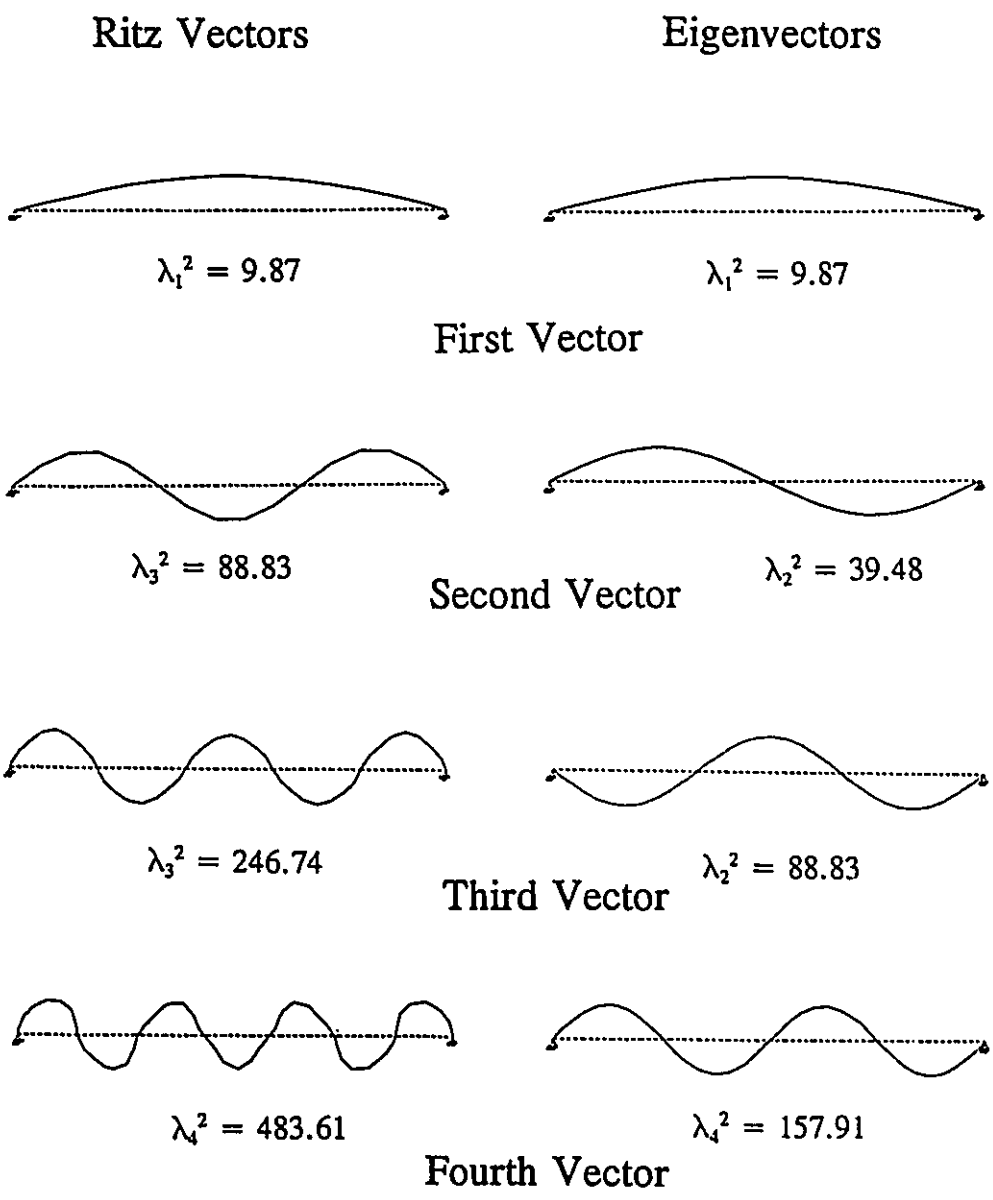

Figure 4.2 Ritz Vectors, Eigenvectors and Normalized Frequencies (λ_i^2) of a Simple Beam.

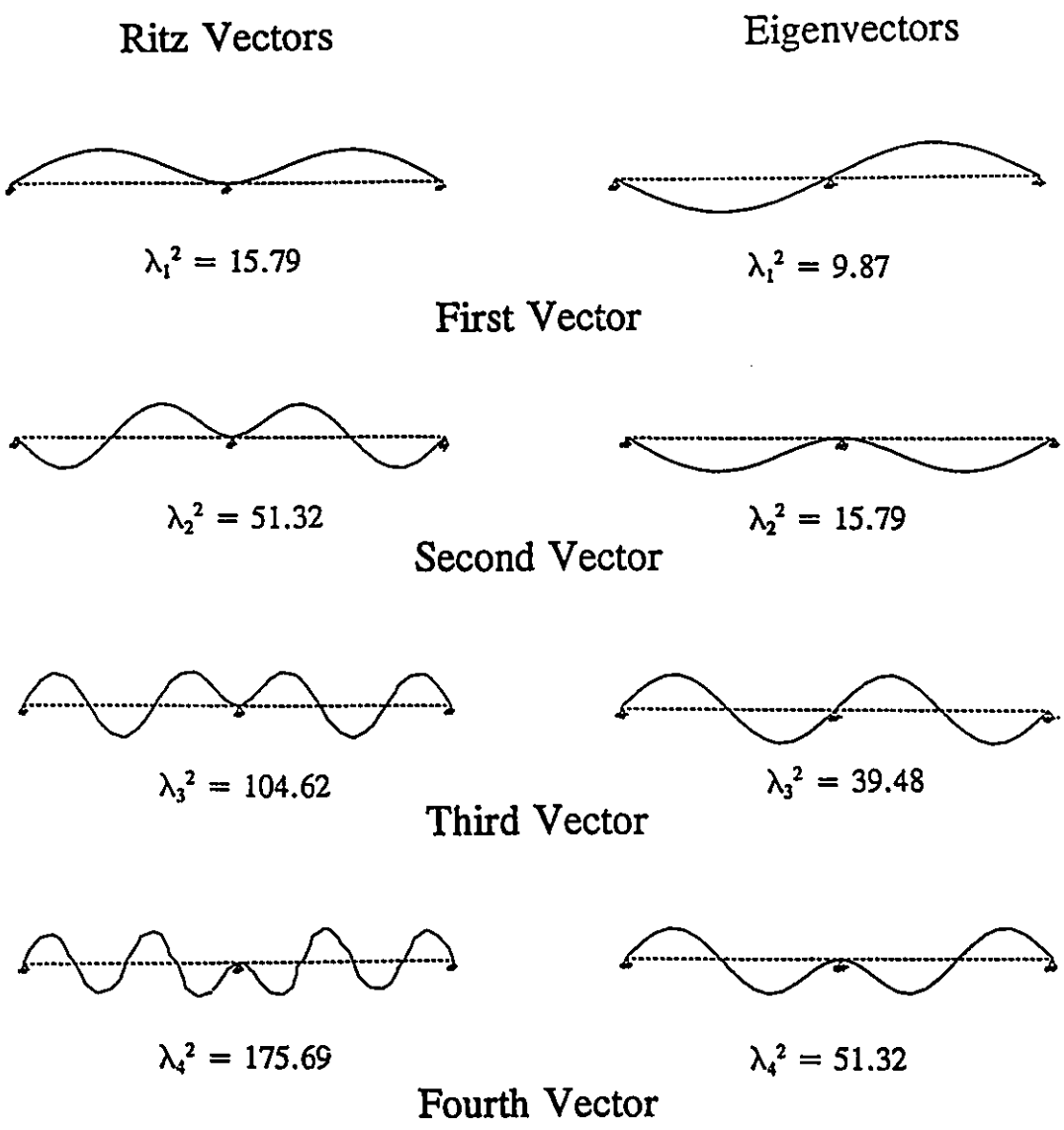

Figure 4.3 Ritz Vectors, Eigenvectors and Normalized Frequencies (λ_i^2) of a 2-Span Symmetric Beam.

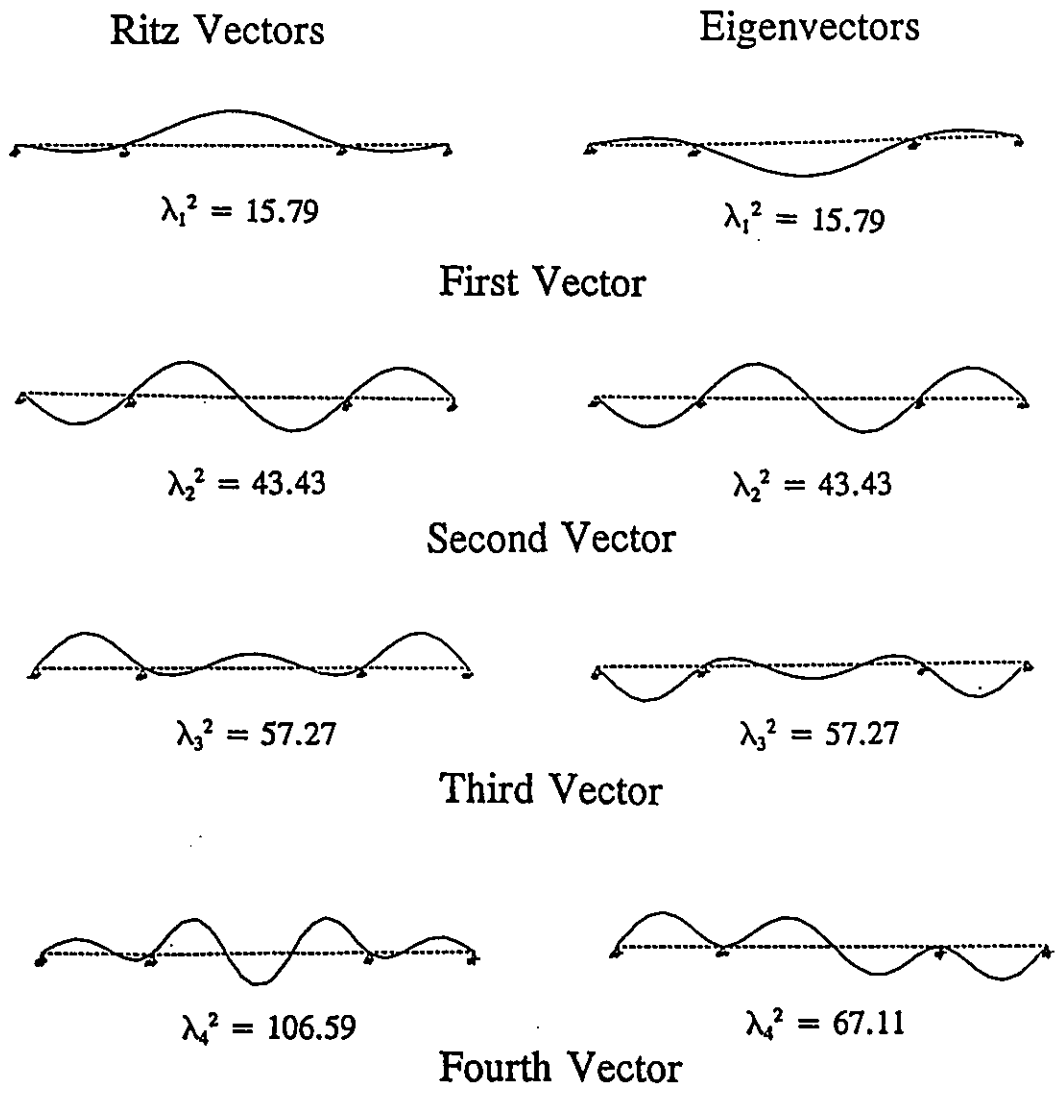

Figure 4.4 Ritz Vectors, Eigenvectors and Normalized Frequencies (λ_i^2) of a 3 Span Symmetric Beam.

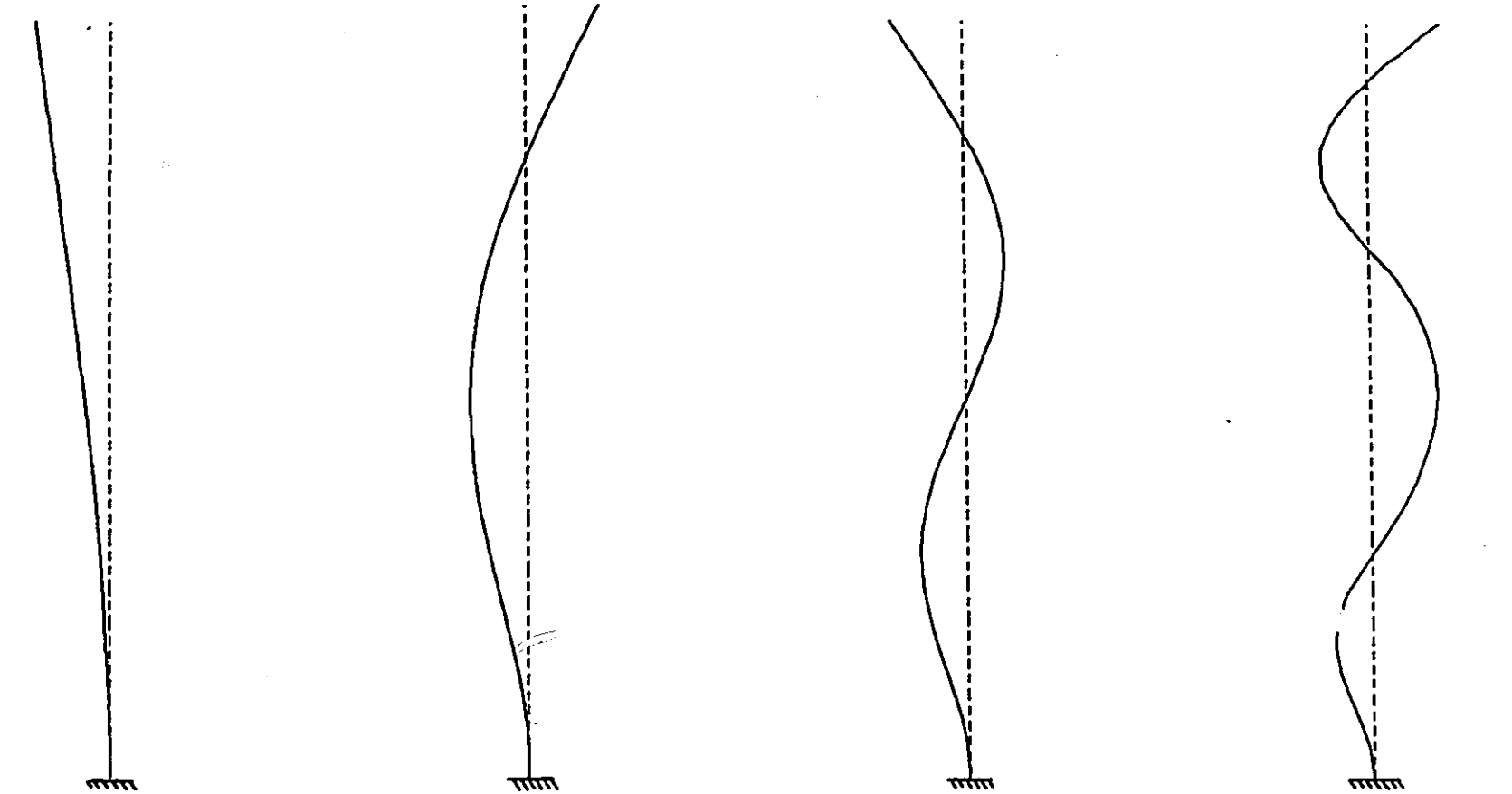

Figure 4.5 Ritz Vectors, Eigenvectors and Normalized Frequencies (λ_i^2) of a Cantilever Beam.

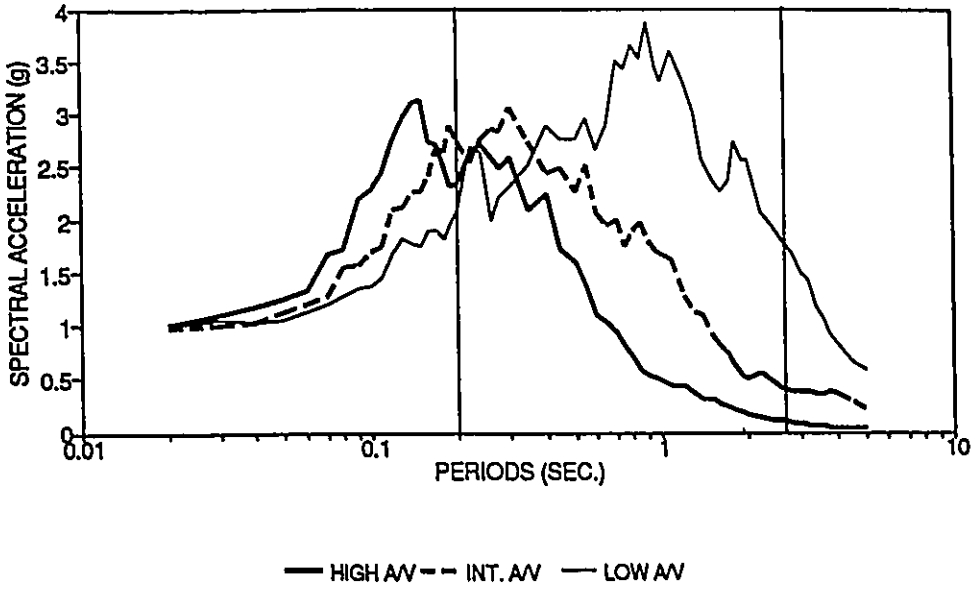

a) Horizontal Component

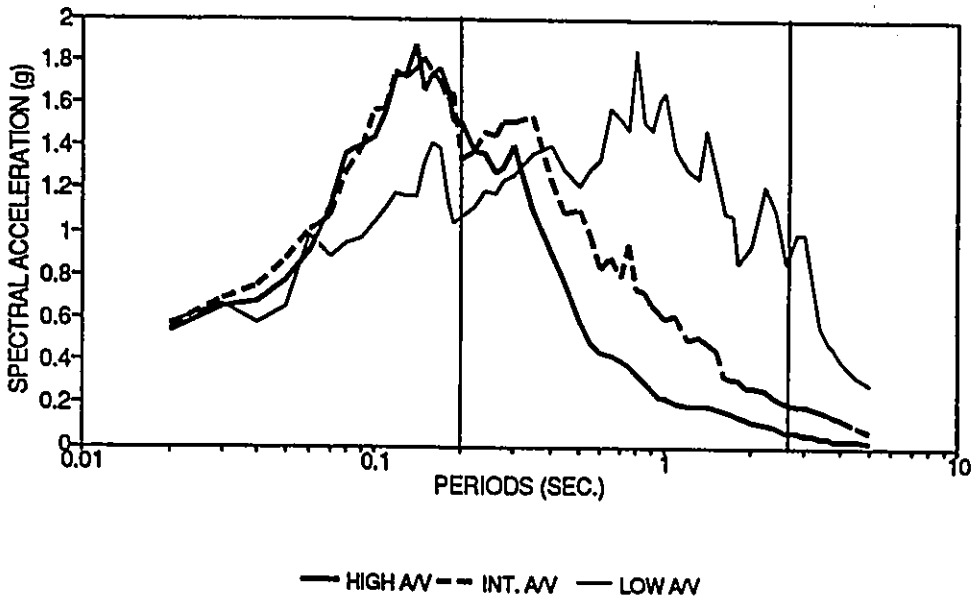

b) Vertical Component

Figure 4.6 Mean Response Spectra for the Three A/V Categories.

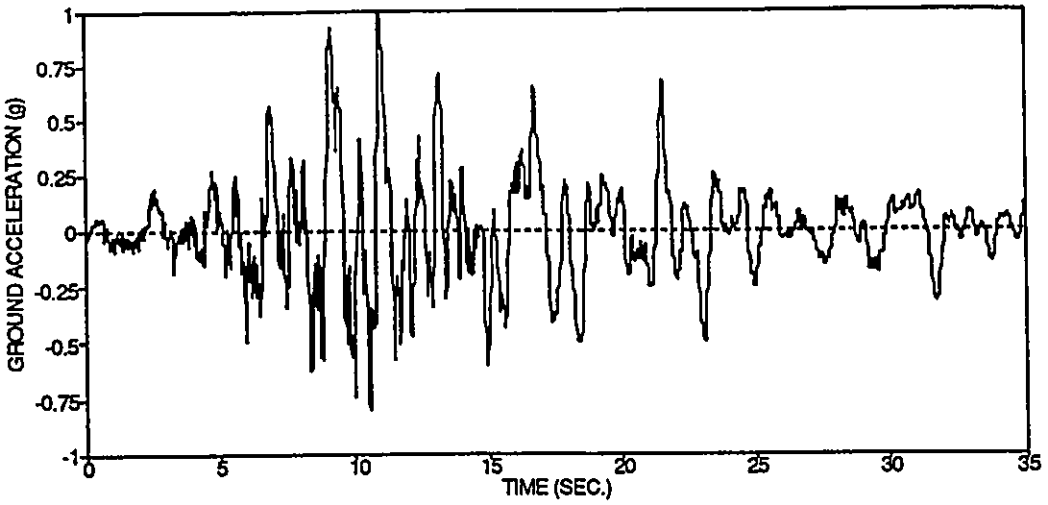

a) Horizontal Component

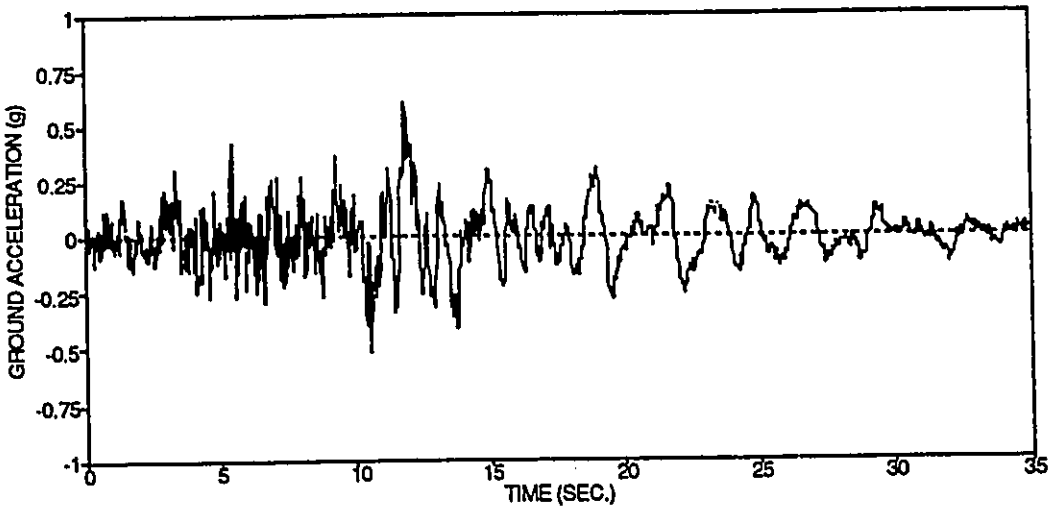

b) Vertical Component

Figure 4.7 Low A/V Synthetic Time History (LS).

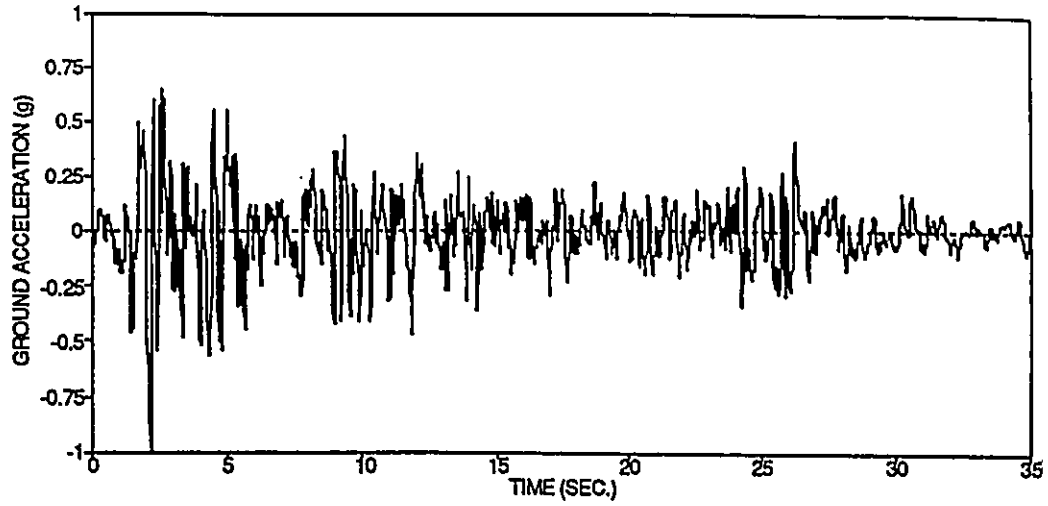

a) Horizontal Component

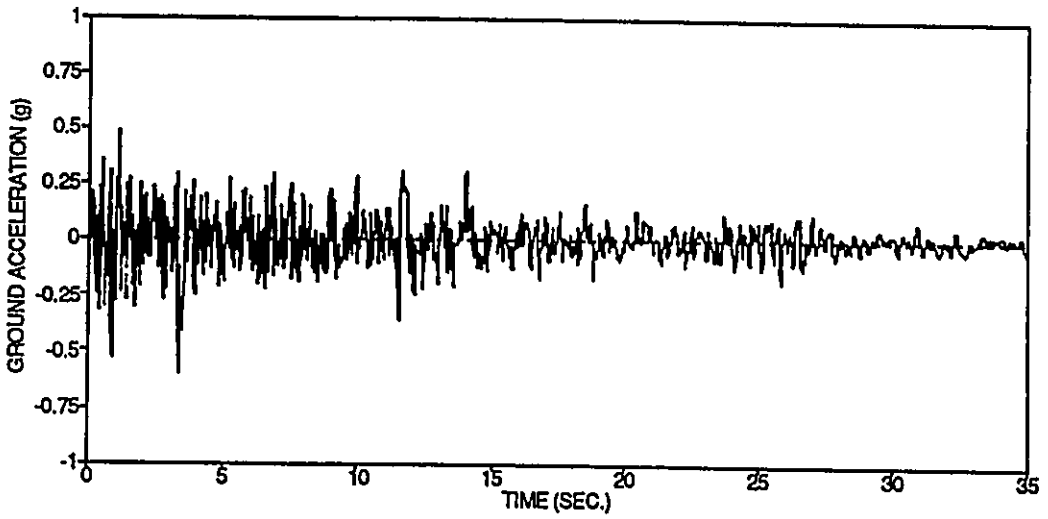

b) Vertical Component

Figure 4.8 Intermediate A/V Synthetic Time History (IS).

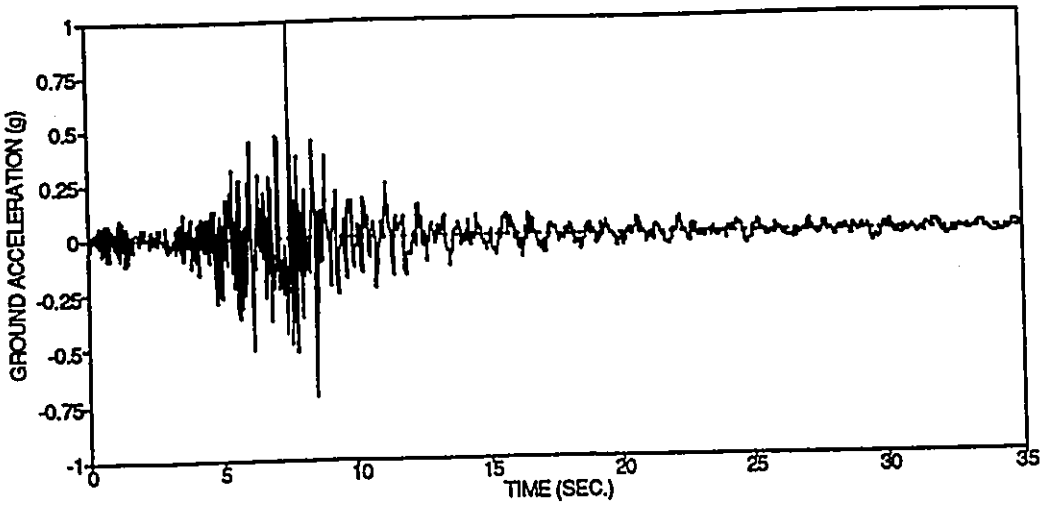

a) Horizontal Component

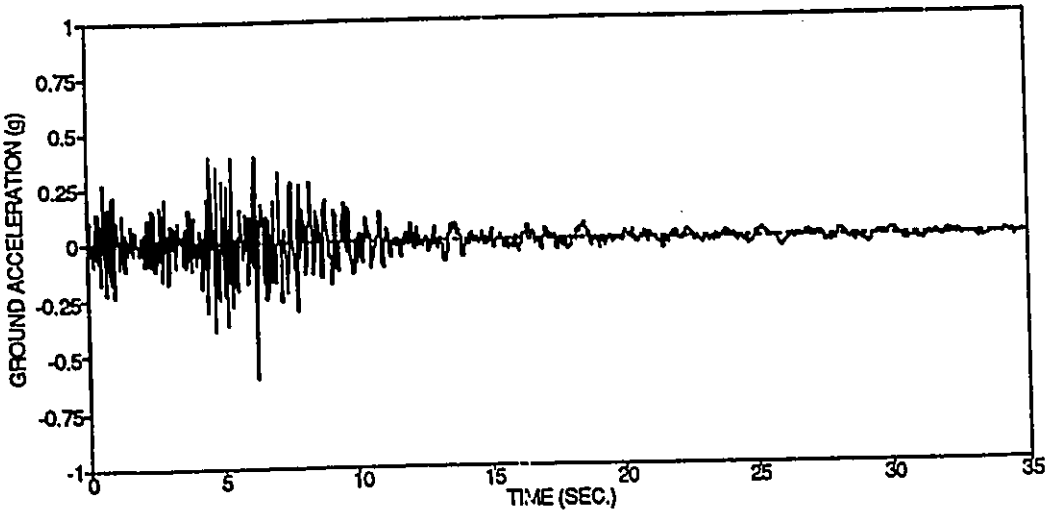

b) Vertical Component

Figure 4.9 High A/V Synthetic Time History (HS).

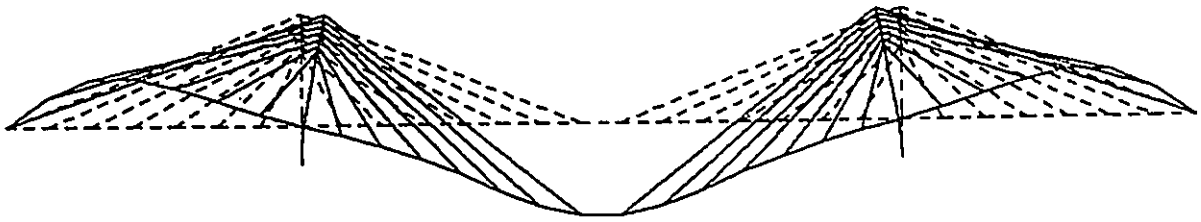

First Bridge Mode (f=0.371 Hz)

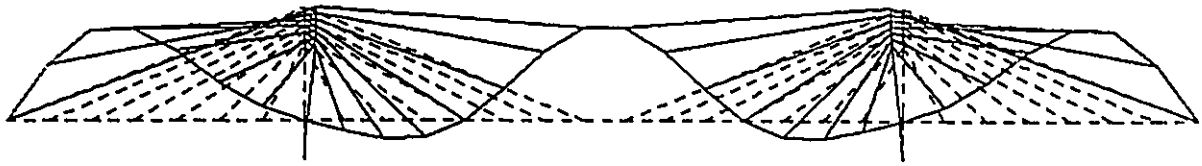

Third Bridge Mode (f=0.770 Hz)

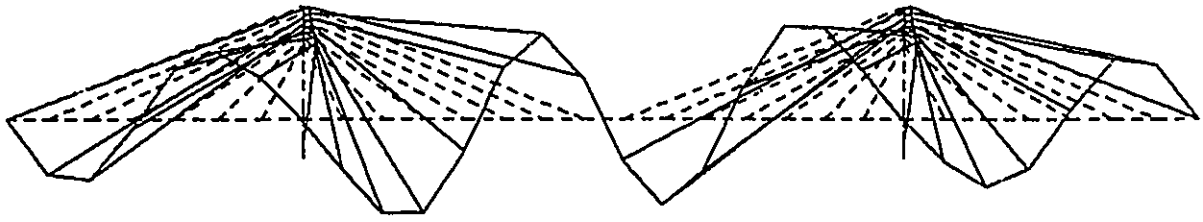

Sixth Bridge Mode (f=1.277 Hz)

Figure 4.10 Shapes of Selected Eigenvectors of the Quincy Bayview Bridge 2-D Model.

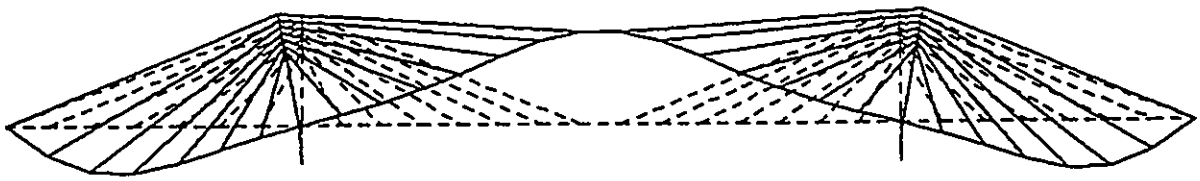

First Ritz Vector (f=0.370 Hz)

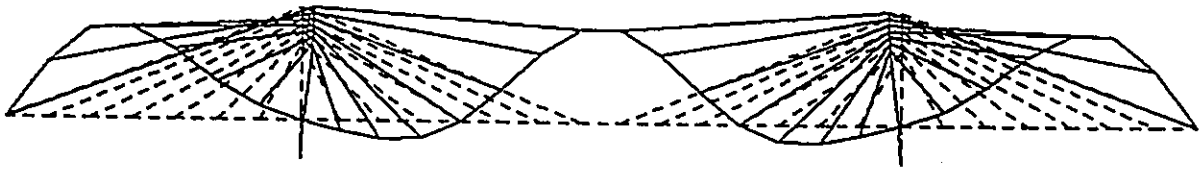

Third Ritz Vector (f=0.770 Hz)

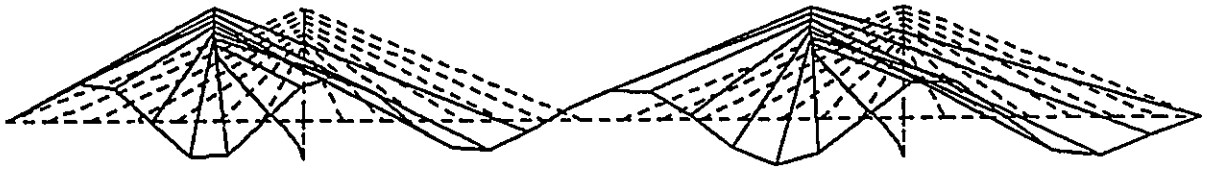

Sixth Ritz Vector (f=2.200 Hz)

Figure 4.11 Shapes of Selected Ritz Vectors When 6 Vectors are Requested.

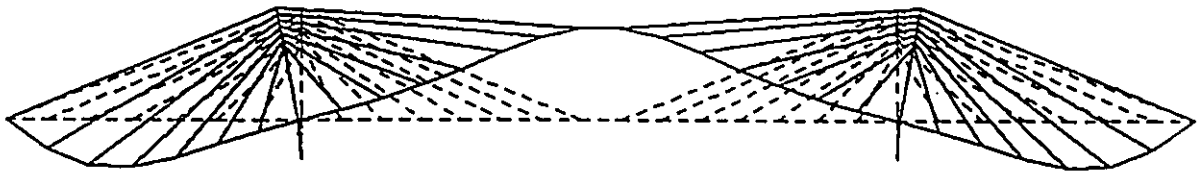

First Ritz Vector (f=0.370 Hz)

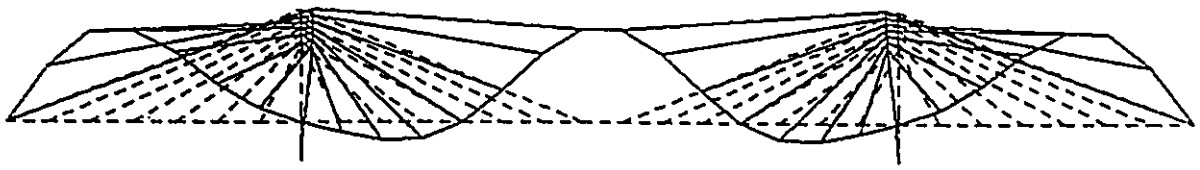

Third Ritz Vector (f=0.770 Hz)

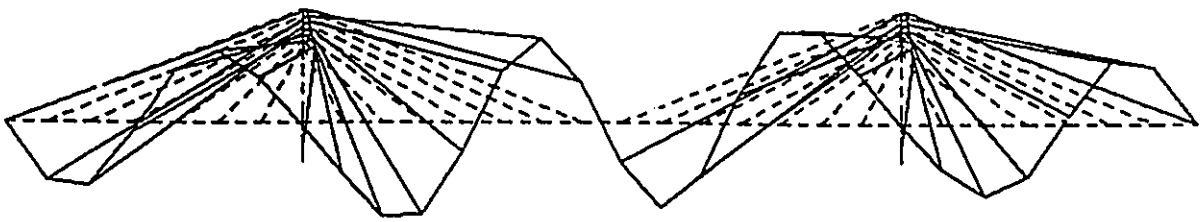

Sixth Ritz Vector (f=1.320 Hz)

Figure 4.12 Shapes of Selected Ritz Vectors When 10 Vectors are Requested.

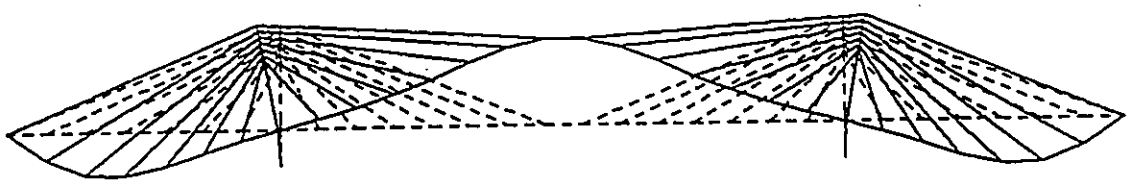

First Ritz Vector (f=0.370 Hz)

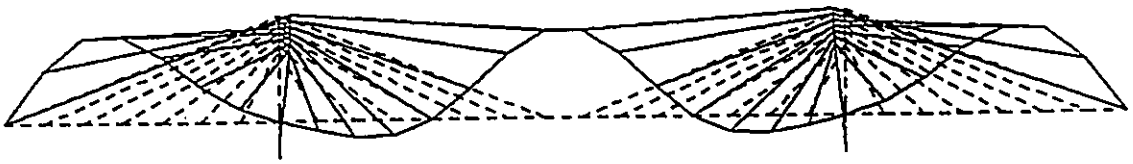

Third Ritz Vector (f=0.770 Hz)

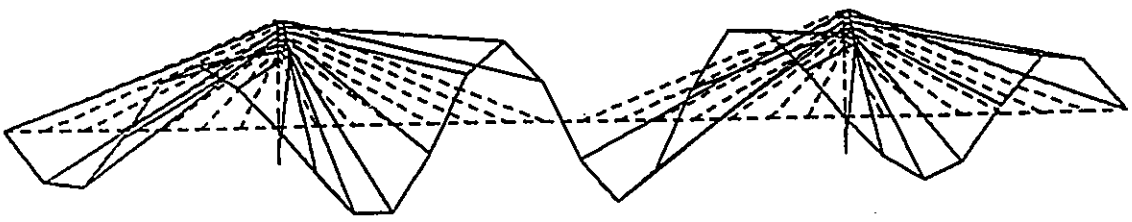

Sixth Ritz Vector (f=1.280 Hz)

Figure 4.13 Shapes of Selected Ritz Vectors When 30 Vectors are Requested.

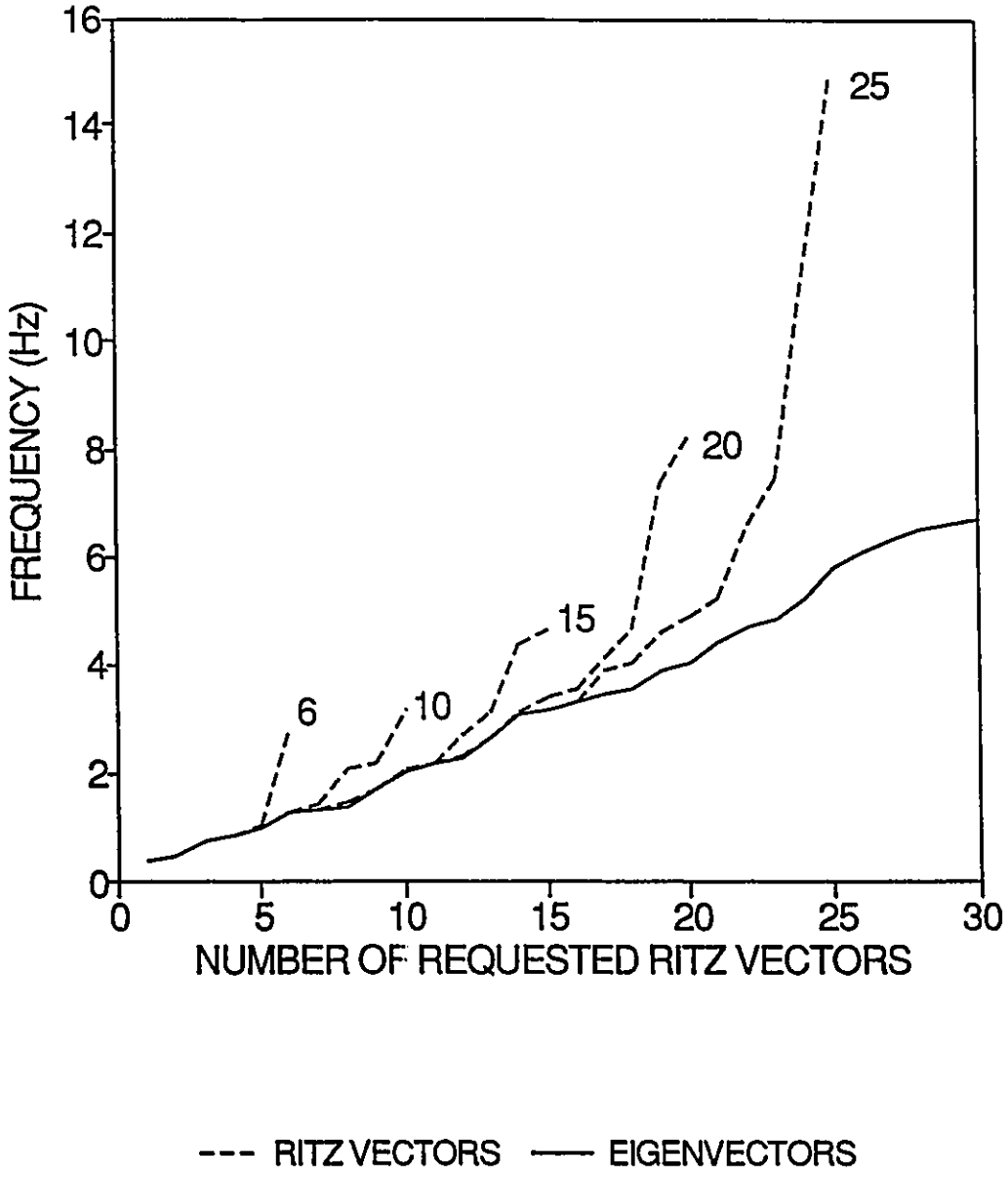

Figure 4.14 Effect of Number of Requested Ritz Vectors on the Calculated Frequencies of Quincy Bayview Bridge.

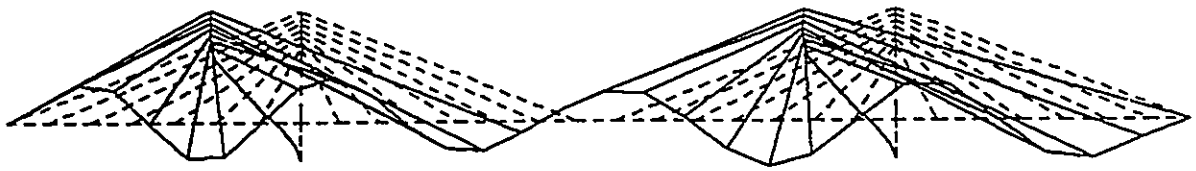

6 Requested Ritz Vectors (f=2.2 Hz)

10 Requested Ritz Vectors (f=2.3 Hz)

15 Requested Ritz Vectors (f=2.3 Hz)

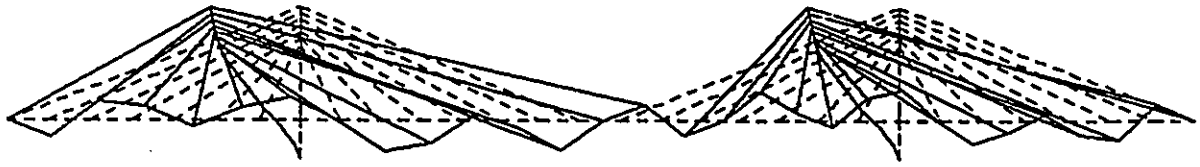

20 Requested Ritz Vectors (f=2.3 Hz)

Figure 4.15 Shapes and Frequencies of the First Local Tower Mode with Different Numbers of Requested Ritz Vectors.

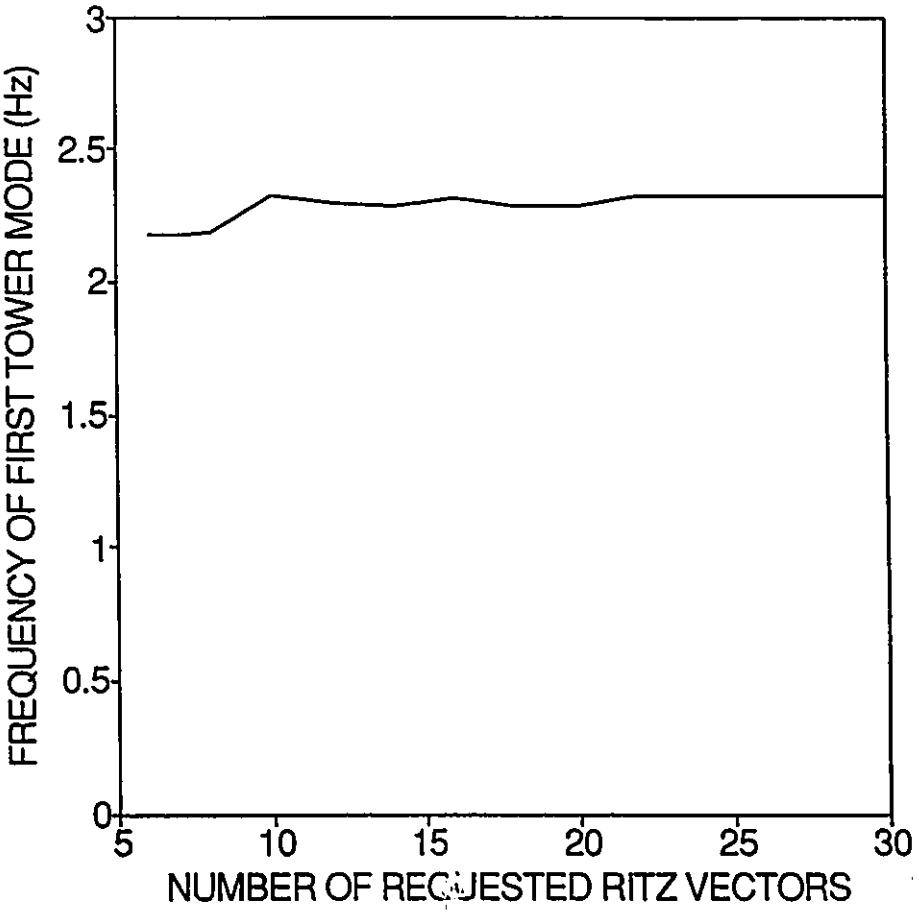

Figure 4.16 Effect of Number of Requested Ritz Vectors on the Frequency of the First Local Tower Mode.

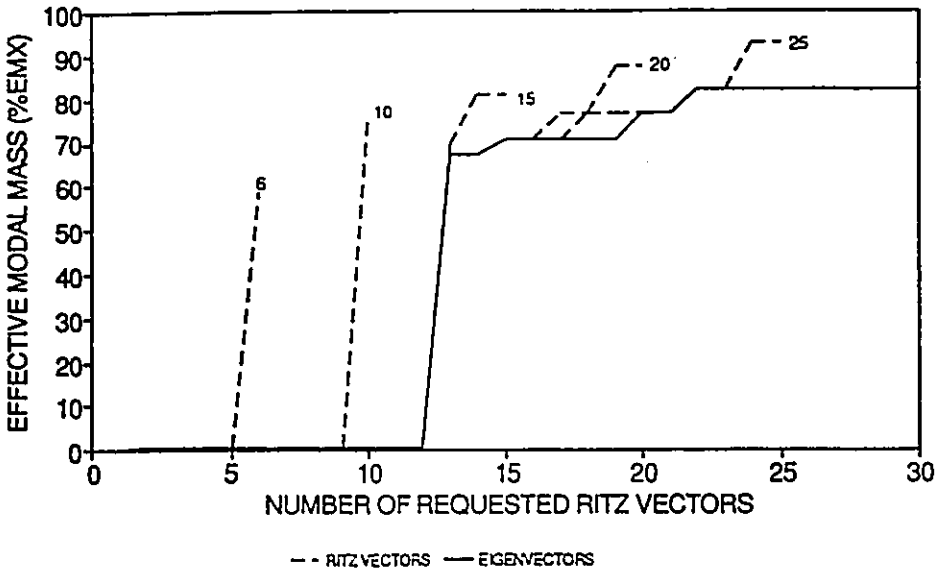

a) Effective Modal Mass in the Longitudinal Direction

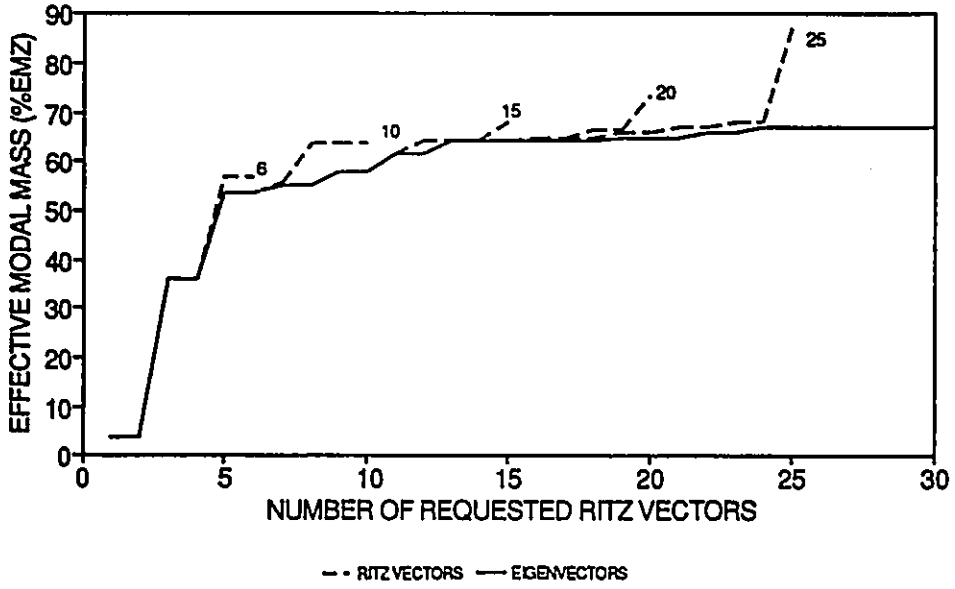

b) Effective Modal Mass in the Vertical Direction

Figure 4.17 Effect of Number of Requested Ritz Vectors on the Effective Modal Mass.

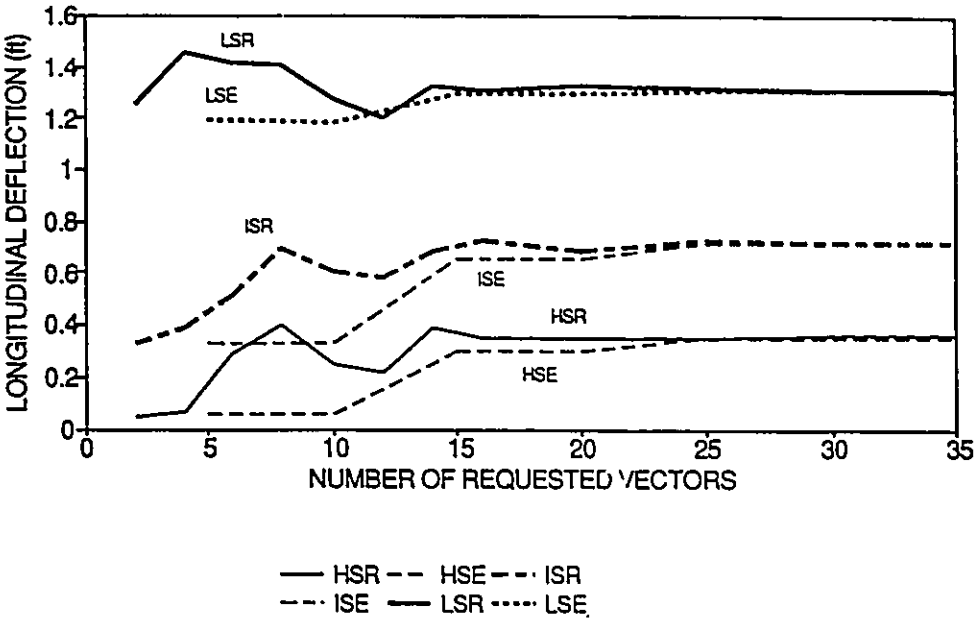

a) Effect of Number of Requested Vectors on the Tower Tip Longitudinal Deflection

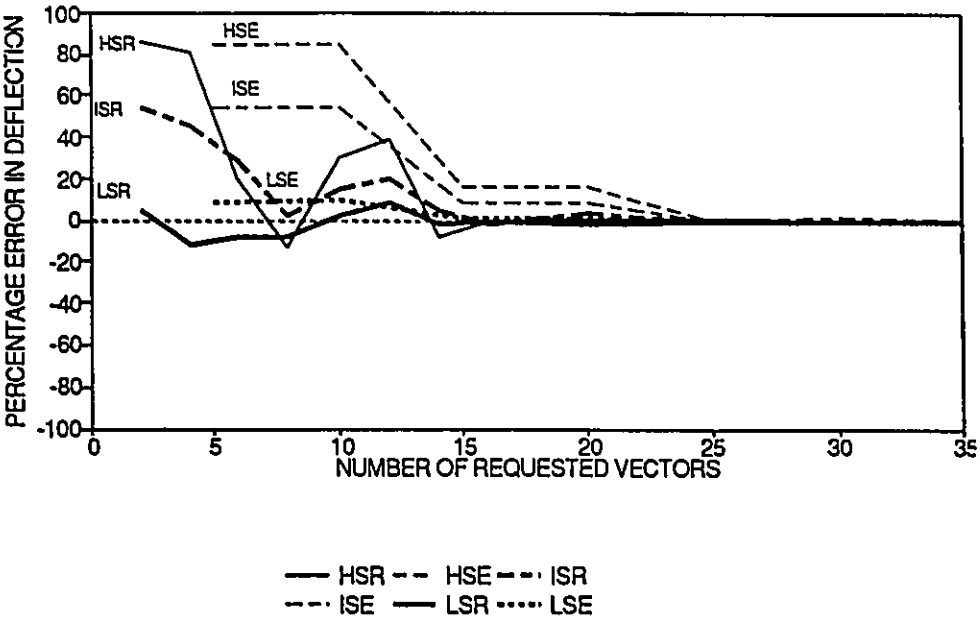

b) Effect of Number of Requested Modes on the Error in Calculating Tower Tip Longitudinal Deflection.

Figure 4.18 Tower Tip Deflection as Affected by the Number of Eigen and Ritz Vectors.

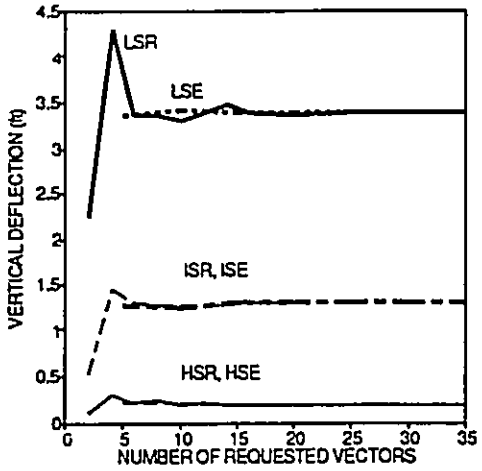

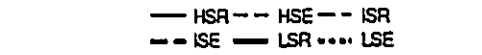

a) Vertical Deflection of Mid Point of Side Span

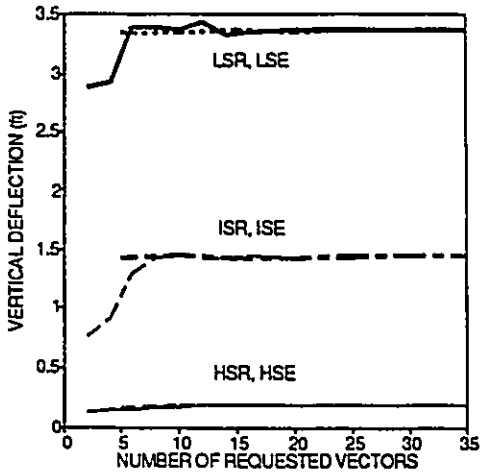

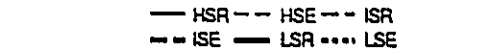

b) Vertical Deflection of Quarter Point of Main Span

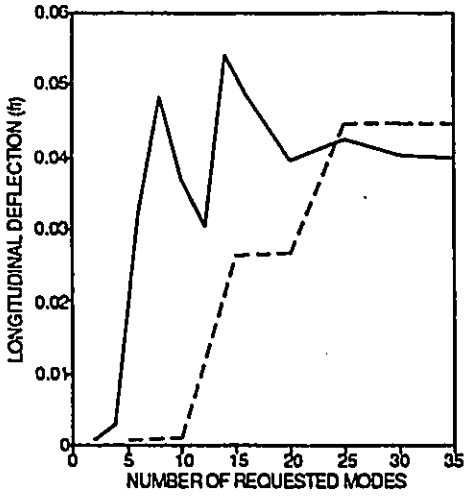

c) Longitudinal Deflection of Mid Point of Side Span

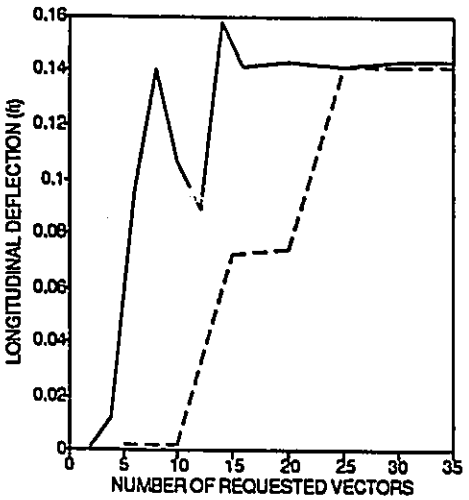

d) Longitudinal Deflection of Quarter Point of Main Span

Figure 4.19 Effect of Number of Requested Vectors on the Bridge Deck Deflection.

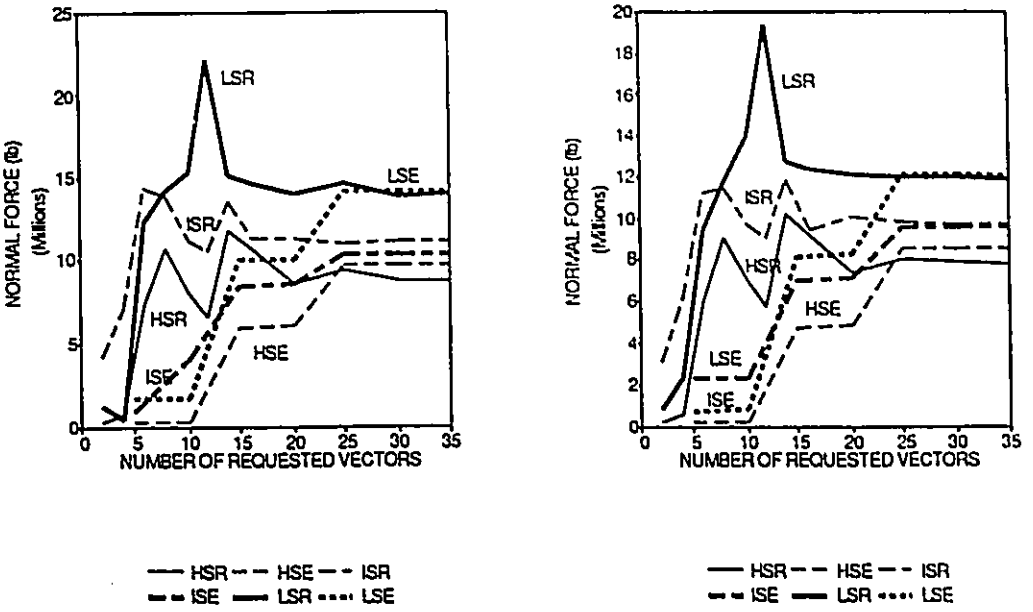

a) Abutment

b) Mid Point of Side Span

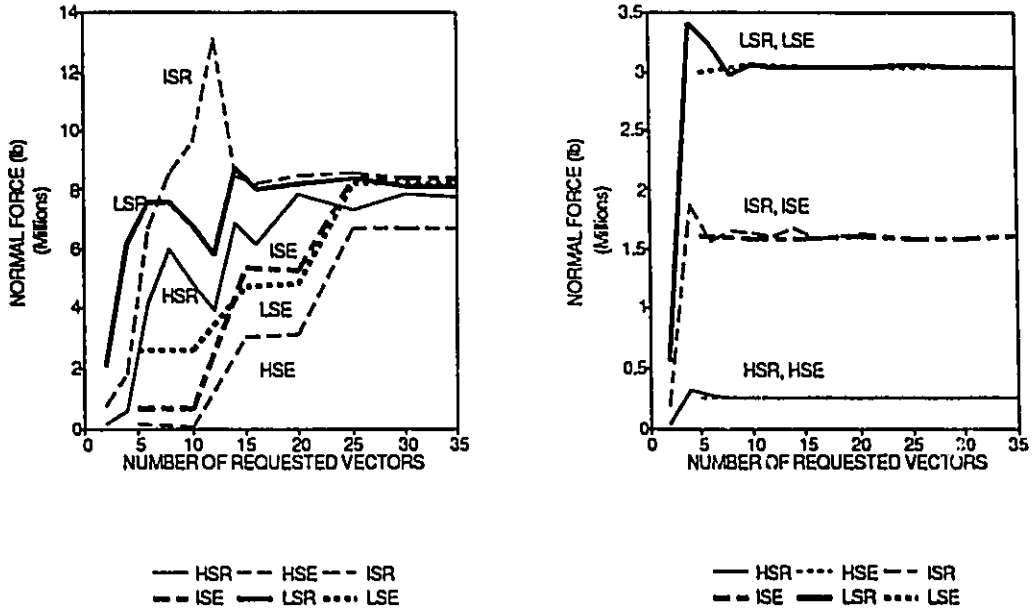

c) Quarter Point of Main Span

d) Mid-Point of Main Span

Figure 4.20 Effect of Number of Requested Vectors on the Normal Force at Different Locations on the Deck.

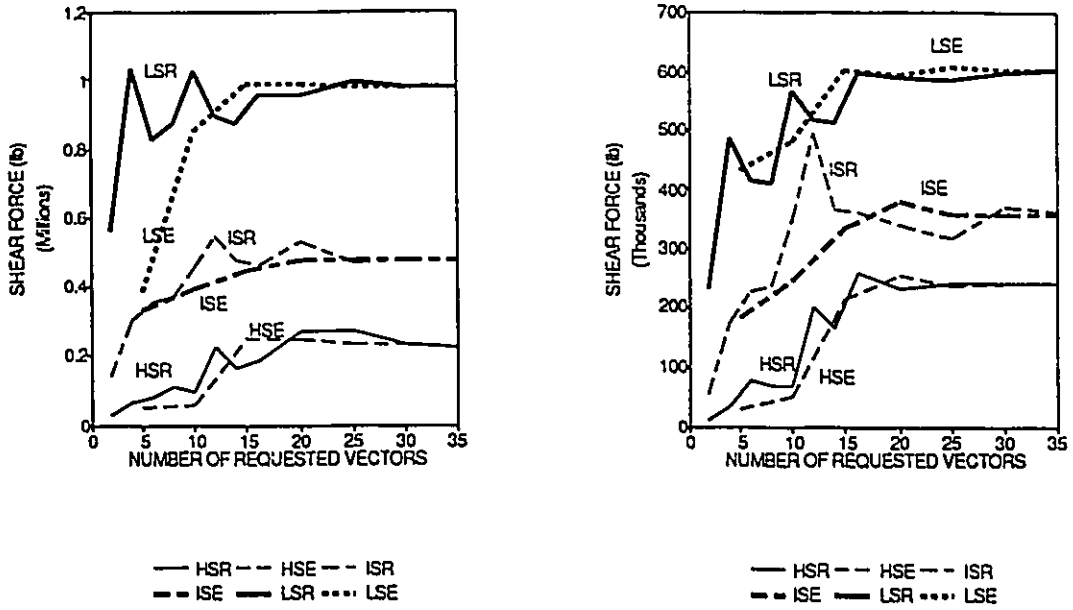

a) Abutment

b) Mid Point of Side Span

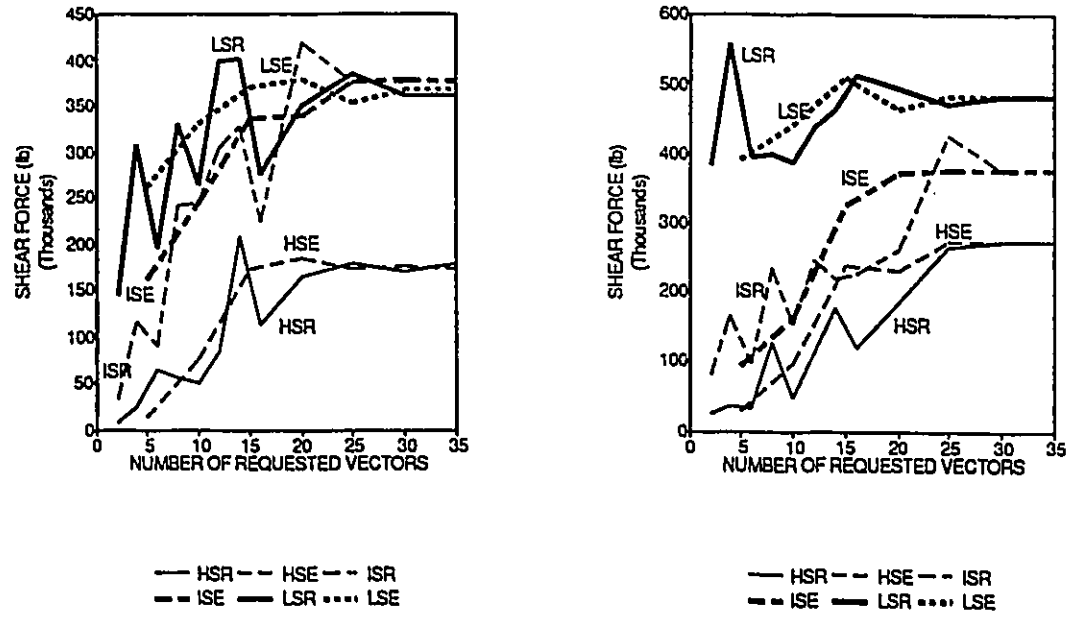

c) Quarter Point of Main Span

d) Mid Point of Main Span

Figure 4.21 Effect of Number of Requested Vectors on the Shear Force at Different Locations on the Deck.

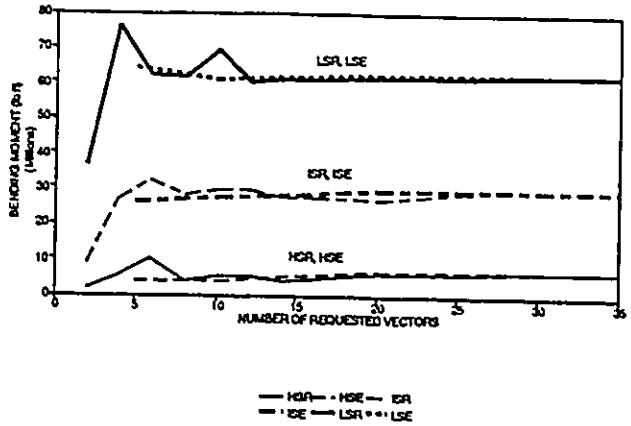

a) Mid Point of Side Span

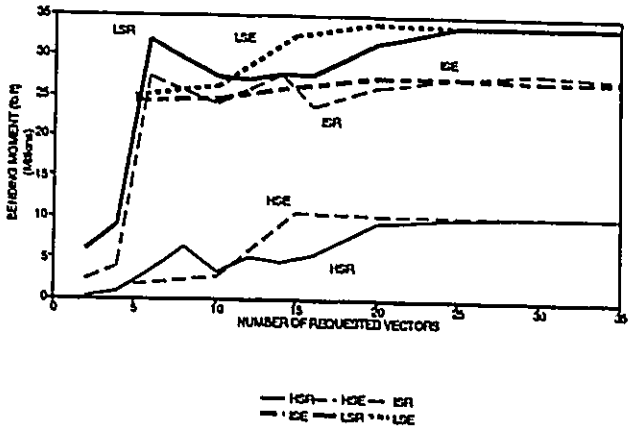

b) Quarter Point of Main Span

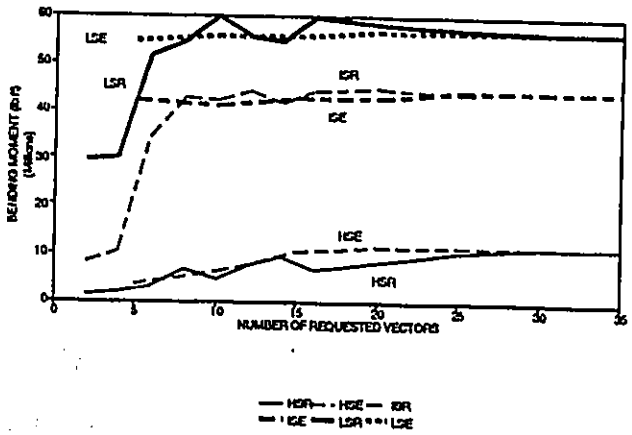

c) Mid Point of Main Span

Figure 4.22 Effect of Number of Requested Vectors on the Bending Moment at Different Locations on the Deck.

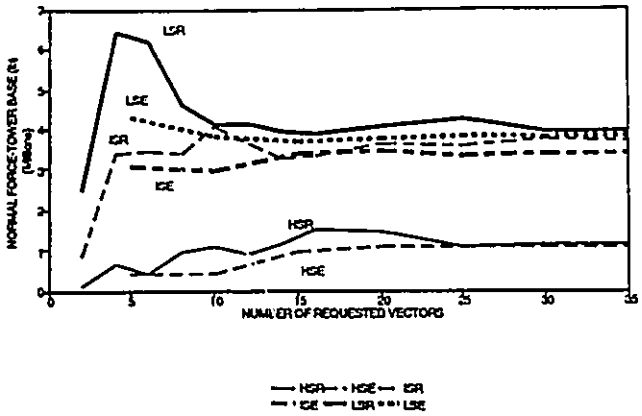

a) Normal Force at Tower Base

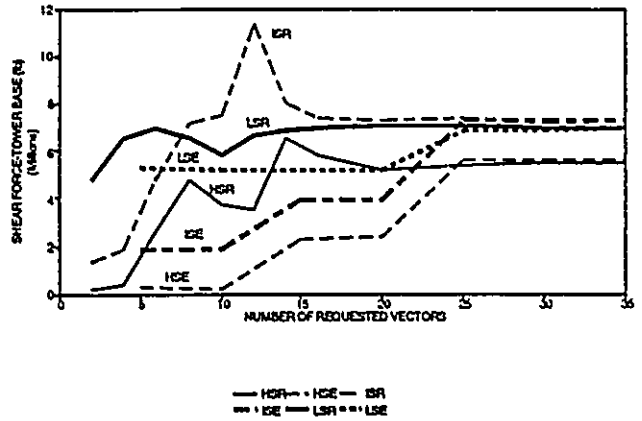

b) Shear Force at Tower Base

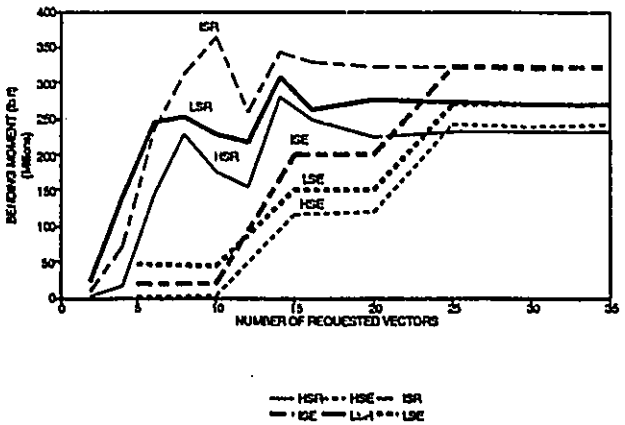

c) Bending Moment at Tower Base

Figure 4.23 Tower's Base Internal Forces.

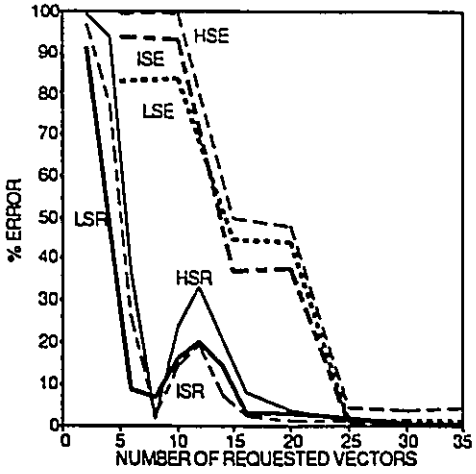

a) Bending Moment at Tower's Base

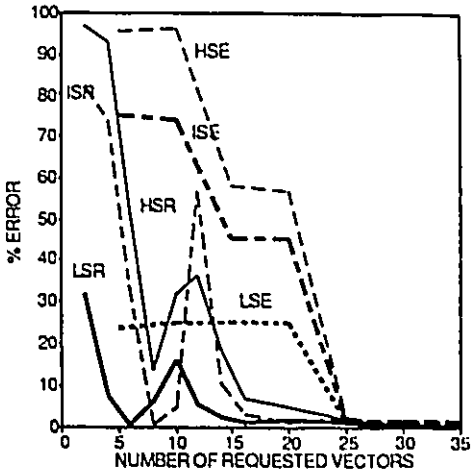

b) Shear Force at Tower's Base

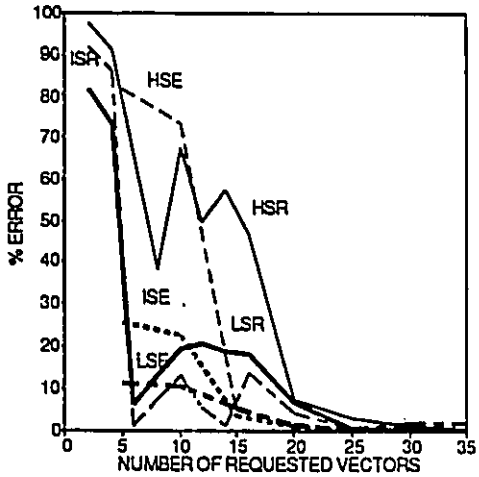

c) Bending Moment at Quarter Point of Main Span

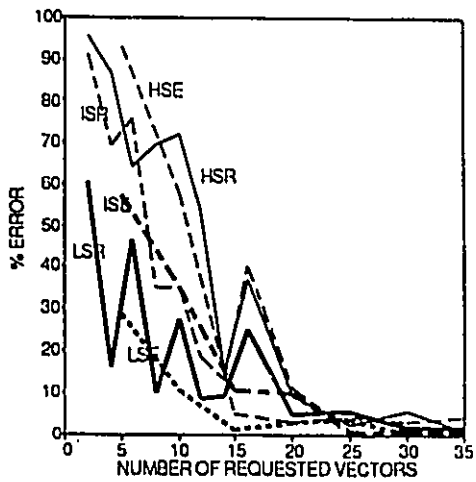

d) Shear Force at Quarter Point of Main Span

Figure 4.24 Effect of Number of Requested Vectors on the Error in Some Response Quantities.

CHAPTER 5

CHARACTERISTICS OF SEISMIC RESPONSE

5.1 INTRODUCTION

The previous chapters discussed the modelling of cable-stayed bridges for dynamic analysis, their dynamic characteristics, and different methods of dynamic modal analysis. Frequency cut-off criteria were proposed to ensure the inclusion of all important modes in analysis. The principal objectives of this chapter are to:

- Investigate the effect of frequency content of earthquake ground motion on the bridge's seismic behaviour to determine which frequency content will produce the largest seismic forces in the bridge's different locations.
- Investigate the effect of bridge deck support condition on the bridge's seismic behaviour. The bridge deck can be pinned to abutments and/or towers (Quincy Bridge deck is pinned to the abutments and free to move longitudinally at the towers) or it can be free to move in the longitudinal direction (such as the Higashi-Kobe Bridge, Japan). This part of the study aims at determining which support condition would result in the least seismic forces and for which frequency content.
- Determine locations on the bridge that are most vulnerable to seismic forces. This part of the study will determine the focus of seismic design for future bridge design.

In order to meet these objectives, knowledge about the dynamic and modal characteristics of cable-stayed bridges is used as developed in previous chapters to study the seismic response characteristics of cable-stayed bridges. Sixty-five modes are used in the modal analysis in order to include two local tower modes in each direction as required by the frequency cut-off criteria.

To prepare the ensemble of input ground motions, thirty four actual ground motion records divided into 3 frequency content categories were analyzed. The mean acceleration response spectra of each category were calculated and scaled to a common peak acceleration of (0.1 g) and used to generate an ensemble of nine synthetic time history records, three for each category of frequency content.

The 3-D model of the Quincy Bridge was subjected to the synthetic time history records for three cases: (1) deck pin-connected to the abutments and free at the towers (FMMF case), (2) deck free to move longitudinally at the abutments and pin-connected to the towers (MFFM case), and (3) deck is free to move longitudinally (MMMM case). The following sections describe the used procedure, discuss the analysis results, and compare the seismically induced forces to dead, live and wind induced forces.

5.2 GROUND MOTION

This section discusses the categorization of actual ground motion records, the scaling procedure used in the study, and the process of generating the synthetic time history records used as input motions in this part of the research program.

5.2.1 Ground Motion Categorization

Earthquake ground motion records may be characterized by parameters such as peak ground acceleration in g (A), peak ground velocity in m/sec (V), frequency content, strong motion duration, spectrum intensity, earthquake magnitude, and earthquake epicentral distance. A simple characterization used in previous studies (Zhu, 1989; Tso et al, 1992) and used in the National Building Code of Canada (NBCC, 1990) is the A/V ratio. The A/V ratio has been found to provide useful information on frequency content and duration of strong shaking for ground motions resulting from different seismic environments (Tso et al, 1992). High A/V ground motion records are associated with small or moderate earthquakes at short epicentral distances. Low A/V ground motion records are associated with moderate or large earthquakes occurring at large epicentral distances.

The NBCC 1990 uses relative values of the acceleration-related and velocity-related zones, Z_a, and Z_v, respectively, to characterize the ground motion at a particular geographical location. This is illustrated by the following examples:

Low A/V

$Z_a/Z_v < 1$ (e.g., Prince Rupert, B.C. $Z_a = 3$ $Z_v = 5$ $A/V = 0.5$)

Intermediate A/V

$Z_a/Z_v = 1$ (e.g., Vancouver, B.C. $Z_a = 4$ $Z_v = 4$ $A/V \simeq 1.0$)

High A/V

$Z_a/Z_v > 1$ (e.g., Ottawa, Ontario $Z_a = 4$ $Z_v = 2$ $A/V \geq 2.0$)

The Ontario Highway Bridge Design Code (OHBDC, 1991) and American Association

of State Highway and Transportation Official's code (AASHTO, 1983) use similar seismic zoning.

A set of real ground motion records was analyzed and used to generate a set of synthetic ground motion records having prescribed spectral characteristics. A total of thirty-four ground motion records (each one has three components) were selected from the McMaster University Seismic Executive data base (MUSE) to represent the three A/V categories (H, I, L). The records are listed in Tables 5.1-5.3. Tables 5.4-5.6 present acceleration data for the records. A_1 is the peak ground acceleration of the first horizontal component, A_2 is the peak ground acceleration of the second horizontal component, and A_3 is the peak ground acceleration in the vertical direction. The A/V categorization in these tables is based on the A/V value of the first horizontal component in each record. For a single event, individual A/V ratios may vary considerably in the different spatial directions such as for El Centro earthquake (record no. 1, Table 5.2). However, the mean values of A/V for the three components in each category of earthquake records are reasonably close to each other as shown in the last row of Tables 5.1-5.3. This is important because input motions for the three A/V categories will be characterized by mean spectral properties, and not by A/V ratios of individual records.

The ratio of A_2/A_1 varies between 0.61 and 2.07 as shown in Tables 5.4-5.6. The average value of A_2/A_1 is 1.0 for high A/V records, 0.93 for intermediate A/V records, and 1.08 for low A/V records, as provided in Table 5.7. Although the averages in the three categories are very close, the least dispersion in the A/V values is observed for the intermediate A/V category and the largest dispersion is observed for the high A/V

category as shown by the coefficient of variation in Table 5.7. The ratio of A_3/A_1 varies between 0.27 and 1.37. The average value of A_3/A_1 is 0.67 for high A/V records, 0.60 for intermediate A/V records, and 0.61 for low A/V records. Although the averages are very close in the three categories, the least dispersion in the values of A_3/A_1 is observed for the low A/V category while the largest dispersion is observed for the high A/V. This is important because the mean values of peak ground accelerations in the three spatial directions for the different A/V categories are used in scaling the synthetic ground motion records in section 5.2.3.

5.2.2 Scaling of Ground Motion Records

Two normalization schemes are common. The first is to scale records to a common peak velocity, the second is to scale records to a common peak acceleration. Previous studies conducted by Tso et al (1992), Zhu (1989), and Naumoski et al (1987), on different ground motion records showed that scaling to a common peak ground velocity would result in acceleration spectra that are different for short periods up to 0.5 sec. (as shown in Figure 5.1a, Tso et al, 1992) but are almost identical for periods longer than 0.5 sec. They also reported that the coefficient of variation (COV) of the mean acceleration response spectra when records are scaled to a common peak velocity demonstrates a uniform distribution that varies in the range of 20-40% along the whole period range.

Scaling the records to a common peak acceleration will lead to almost identical acceleration spectral shapes for periods up to 0.2 sec. but significant differences were

reported by Naumoski et al (1988) and Zhu (1989) in the acceleration spectral values of the A/V spectra for periods $\geq$ 0.2 sec. In this case, similar to the case of scaling to peak velocity, the COV of the mean response spectra varies in the range of 20-40%. Figure 5.1b shows three spectra of horizontal earthquake components scaled to a common peak acceleration (Tso et al, 1992).

Scaling records to a common peak velocity will lead to different input energy over the short period range. On the other hand, scaling records to a common peak acceleration will lead to a different input energy over the moderate to long period range. Scaling records to a common peak acceleration will also give consistency in the response comparison because the effective force is given by $-[M]\{r\}\ddot{u}_g(t)$, as shown in equation 4.1. For these reasons, scaling records to a common velocity is desirable for studies of frame structures (with short to moderate periods). However, it is preferred to scale the records to a common peak acceleration when studying the seismic response of cable-stayed bridges (which have moderate to long periods). Using input motions scaled to a common peak acceleration in the analysis of cable-stayed bridges is equivalent to analyzing the bridges for different velocity zones that have the same expected peak ground acceleration.

5.2.3 Synthetic Ground Motion Records

For the purposes of this study it was desirable to obtain uniformity in the input ground motion records in the three directions and then spectrum-compatible synthetic ground motion records were used as the input motions.

A data ensemble consisting of nine synthetic records were generated such that there were three synthetic records in each of the three A/V categories. To generate a synthetic time history, a target acceleration spectrum and a seed time history record were required. The target spectra used in the generation process were the mean acceleration response spectra (scaled to common peak acceleration) of the data set in the MUSE database (Naumoski et al, 1988) calculated for 2% damping, as shown previously in Figure 4.6.

Because of the similarity between the spectral shapes in the two horizontal directions, it was appropriate to consider one spectral shape for both horizontal directions for each category of A/V ratio, as shown in Figure 4.6a. The maximum acceleration for the second horizontal direction of all generated synthetic records was taken as 0.9 A_1. This closely corresponds to the 0.93 average value of A_2/A_1 for intermediate A/V categories as shown in Table 5.7. The spectral shapes for the vertical components are different than those of the horizontal direction and so the mean vertical acceleration response spectra were calculated for the A/V categories as shown in Figure 4.6b. It was shown in Table 5.7 that the mean value of $A_3/A_1 \approx 0.6$, so it was appropriate to scale the vertical components of the synthetic records to a common peak acceleration of $0.6A_1$.

The seed records and ground motion parameters of the synthetic records are shown in Table 5.8. The nine seeds were selected to represent earthquakes with different A/V ratios, magnitudes and epicentral distances. The three SL records were generated using the low A/V target spectrum in Figure 4.6; SI records used the intermediate A/V target spectrum; SH records used the high A/V target spectrum. The synthetic records

were scaled to maximum accelerations A_1=0.1g, A_2=0.09g, A_3=0.06g. This is referred to as a 0.1g reference input. (Since the Quincy Bayview Bridge is constructed in an area with expected maximum ground acceleration in the range of 0.05-0.1g, the 0.1g scaling was expected to result in reasonably realistic seismic forces, without further scaling being necessary).

Figures 5.2-5.10 show the nine synthetic time history records. Although each category (H, I, L) of the synthetic records was compatible with a specified spectrum, the generated acceleration time histories had different frequency contents, different durations of strong shaking, different numbers of peaks, and different start times of strong shaking. These differences were expected to result in variations in the seismic response of the bridge within the same A/V category.

Modal time history analyses of the 3-D finite element model of Quincy Bayview Bridge were performed using 65 modes, and using the nine synthetic time history records as the input motions. Sections 5.3 and 5.4 present results for the case when the deck is pin-connected to the abutments and free in the longitudinal direction at the towers (FMMF case). Section 5.5 examines two other cases when the deck is free to move longitudinally (MMMM case) and when the deck is pin-connected to the towers but free to move longitudinally at the abutments (MFFM case). The results are presented in the form of absolute maxima extracted from the time-history analyses.

5.3 SEISMIC RESPONSE OF DECK

The seismic response of the deck to the nine synthetic time history records (scaled to 0.1g peak acceleration) was studied in the form of seismic deflections and internal forces.

5.3.1 Deflections

The vertical, transverse and longitudinal displacements along the bridge deck were studied. A Discussion to the analyses results is provided in what follows:

Vertical Displacement

Figure 5.11 shows the vertical (Z) seismic deflection profiles computed for the Quincy Bayview Bridge deck. The towers are located at the 445 and 1335 ft marks. The figure shows that the vertical deck deflection has contributions from more than one mode because the deflection lines are not smooth. The effect of higher deck modes appears most clearly for the deflections caused by the high A/V ratio input motions (Figure 5.11c). There are distinct differences in the amplitude of deflections caused by the different categories of A/V input motions. There is a ratio of 3 to 4 between the deflections caused by low and intermediate frequency input motions, and a ratio of approximately 3 between the deflections of the intermediate and high synthetic records categories. These high ratios are observed because deck modes have low, closely-spaced frequencies, and the target acceleration response spectra of the three A/V categories have well separated ordinates in the low frequency range (up to 1.0 Hz). The vertical

deflection profiles shown in Figure 5.11 are not symmetric because both longitudinal and vertical ground motion components contribute toward the deck vertical deflection. This is a result of the spatial coupling in the vertical plane between the vertical motion of the deck and longitudinal motion of the tower (the fundamental bridge mode is a coupled deck-tower mode at a frequency of 0.3708 Hz as shown in Figure 3.1). Figure 5.12 compares the maximum calculated vertical deflection on the main span and side span due to the different input motions. With the exception of LS2 and IS1, the main span and side span deflections are within about 20% of each other, and in many cases are almost the same. The limited number of records used in each A/V category makes it difficult to identify more detailed trends of response behaviour.

The maximum main span deflection/main span length ratios are 1/1800, 1/6000, 1/16000 for L, I, H synthetic records categories, respectively. The maximum side span deflection/side span length ratios are 1/880, 1/3700, 1/8000 for L, I, H, respectively. Although most codes do not specify maximum acceptable ratios for seismic deflections, the computed values are very small compared to the maximum live load deflection/span length permitted by most highway bridges design codes (e.g., 1/550 for traffic induced deflection as specified by OHBDC 1991 for a bridge with fundamental frequency of 0.3 Hz that does not carry pedestrians).

These results clearly indicate that vertical displacements of both the main span and side spans are most sensitive to low frequency seismic input motions. The amplitude of response of all spans decreases with increasing A/V ratio of the input motion. There may

be differences in maximum amplitudes caused by low and high A/V input motions as large as ten times.

Transverse Displacement

Figure 5.13 shows the transverse (Y) deflection profiles computed for the Quincy Bayview Bridge deck. This is primarily a single mode response and produces the smooth deflection shapes shown in Figure 5.13 a,b. A small participation of higher transverse modes appears with the high frequency input motion, producing the slightly less smooth Y-deflection curve in Figure 5.13c. This behaviour is attributed to the fact that the transverse deck modes have well separated frequencies (the first mode has a frequency of 1.23 Hz and the second mode has a frequency of 2.2 Hz).

It may also be observed from Figures 5.13 and 5.14 that the ratio of maximum main span deflection/maximum side span deflection changes from approximately 6 when the frequency content of the input motion is low to approximately 1.5 when it is high. This is in marked contrast to the vertical deflection where the maximum main span and side span displacements are approximately equal for all input motions (Figure 5.12). This is attributed to the fact that the higher frequency deck modes excited by high frequency input motions have more contribution toward deflection of the side spans than to deflection of the main span. This observation is consistent with the shapes of modes of 3-span beams that have a half-cycle of deflection in the side spans and increasing numbers of half-cycles in the main spans for the first 3 modes, similar to the vertical deck modes shown in Figures 3.1-3.10. This is also supported by the study conducted

by Ayre and Jacobsen (1950) on frequencies and mode shapes of multiple span beams. This observation is quite different from the case of vertical deflections where main span deflections are approximately equal to side span deflections because vertical deck modes have low, closely-spaced frequencies.

Figure 5.14 shows that the maximum deflections for each input category are distinct from the values of other input categories. For main span deflection there is a ratio of $\simeq$ 3.5 between the maximum deflection due to low A/V input motions and maximum deflection due to intermediate A/V input motions, and a ratio of $\simeq$ 3 between the maximum deflection due to intermediate A/V input motions and the maximum deflection due to high A/V input motions. These ratios are similar to those observed for vertical deflections. For side span deflection these ratios become about two for each case. The maximum main span deflections for each of the three cases L, I, H are about the same for the vertical and transverse response.

The maximum deflection/span ratio for the main span has values of 1/1700, 1/6000, 1/16000 for low, intermediate, and high A/V synthetic records, respectively. The maximum deflection/span ratio for the side span has values of 1/3500, 1/7400, 1/11000 for low, intermediate, and high A/V synthetic records respectively. Similar to the vertical deflection case, the calculated transverse deflection values are very small compared to the guidelines of most codes.

Longitudinal Displacement

The calculated longitudinal deck displacements are very small compared to the vertical and transverse displacements because of the high axial rigidity of the bridge deck cross-section and the pinned-end conditions. These small displacement values are of little consequence to the bridge and are not discussed further here.

5.3.2 Deck Internal Forces

This section provides a discussion on the calculated values of internal normal forces (F_x), shear forces (Q_y, Q_z), and torsional (M_x) and bending moments (M_y, M_z) in the deck for the 0.1g reference input motion. Figure 5.15 shows the spatial directions of the internal forces. The internal forces shown in Figures 5.16-5.21 are absolute maxima extracted from modal time history analyses. the plots of F_x, Q_z and M_y show asymmetries from the contribution of longitudinal response of the bridge. Additional discussions and comparisons of seismic forces arising from other load conditions are given in section 5.6.

Normal Force (F_x)

Figure 5.16 shows the maximum absolute normal seismic force in each of the two main girders for the case of FMMF. The maximum normal force occurs at the abutments and decreases toward the middle of the deck. This behaviour is caused by the reduction in the relative axial (longitudinal) displacements between adjacent deck points with increasing distance from the abutments. The reduction in the relative longitudinal deck displacements toward the middle of the bridge is caused by the opposite motion of the

two towers in the contributing deck-tower or local tower modes as shown in Figure 4.15 and in Figure 4.20d. The local tower modes contribute the most to deck internal forces at abutment, mid-side span and quarter-main span as shown in Figure 4.20a,b,c, and discussed in 4.4.4.1.

The highest F_x is caused by low A/V input motions. The highest value is 1.1×10^6 lb, caused by LS2. The lowest F_x is caused by high A/V input motions. The lowest value is 0.48×10^6 lb, caused by HS3.

There is a ratio of $\simeq$ 1.2 between max. F_x due to low A/V input motions and max. F_x due to intermediate A/V input motions, and a ratio of $\simeq$ 1.1 between max. F_x due to intermediate A/V input motions and max. F_x due to high A/V input motions. This means that the normal force in the deck, which depends on both low frequency deck-tower modes and high frequency local tower modes as shown in Figure 4.20a,b,c, is not as sensitive to changes in the A/V ratio as are the vertical or transverse deck deflections.

Dispersion of response values of F_x within the category of intermediate A/V input motions is very small. Greater dispersion is observed for response in the low A/V and high A/V categories as shown in Figure 5.16a.

Transverse Shear Force (Q_y)

This response quantity is usually assumed to be carried by the web of the bridge's cross-section (i.e. the concrete slab), so the values shown in Figure 5.17 are the computed values for the 3-D model and are not divided by two as the case of F_x.

The most critical location of the bridge deck with respect to Q_y is at the towers where the highest Q_y values are observed. The next critical locations are the abutments. The transverse shear decreases to zero at the mid span because the deck is symmetric about the mid point of the deck and the uniform transverse seismic excitation is symmetric with respect to the same point.

As observed before, the dispersion in most response values within each A/V category is generally small (although the high A/V responses show some higher dispersions) and distinct levels of response are recognized for each category of A/V input motion. This is reflected in the maximum response ratio calculated for different categories of input motions. The observed ratios are $\approx$ 1.7 for low/intermediate and $\approx$ 1.2 for intermediate/high.

Vertical Shear Force (Q_z)

Figure 5.18 shows the absolute maximum vertical shear force along one of the main girders of the bridge deck. The maximum Q_z may occur in either the main span or side span. In the main span, the maximum Q_z occurs within the middle third region of the deck. In the side span, the maximum Q_z occurs at or near the abutment. This is different from the case of Q_y because the symmetric deck is affected by vertical ground excitation (symmetric) and longitudinal ground excitation (anti-symmetric). The longitudinal component of excitation causes non-zero vertical shear to occur in the middle part of the bridge deck. There is a ratio of 1.6 for maximum Q_z caused by low A/V input with respect to maximum Q_z caused by intermediate A/V. This ratio is reduced to 1.2

when comparing maximum Q_z caused by intermediate A/V to maximum Q_z caused by high A/V inputs.

For each A/V category, Q_y is approximately ten times greater than Q_z. This is caused by the higher stiffness of the deck in the transverse direction compared to the vertical direction ($I_z/I_y \simeq 60$). There is a larger dispersion in the Q_z values than for the Q_y values is observed for different records within each A/V input category. The observed dispersion is linked to the variation in the A/V ratio of both the longitudinal and vertical components within the same frequency content category (the values of A/V are given in Table 5.8).

It is noteworthy to mention that more than 90% of Q_z at mid-main span is caused by the longitudinal ground motion component (with peak ground acceleration of 0.1g). The longitudinal ground motion component contributes approximately 30% to Q_z at other deck locations.

Torsional Moment (M_x)

Figure 5.19 shows the torsional moment (M_x) profile along the bridge deck. Similar to the case of Q_y, the torsional moment is zero at mid main span. The maximum main span M_x occurs just outside the middle portion of the deck (at the fourteenth cable anchorage).

The dispersion of the M_x values within A/V category is generally small (with some greater dispersion occurring for the high frequency content). There is also obvious distinction between the amplitude of response in the different categories of input motions.

The ratios of the maximum response in the different categories take the values low/intermediate ≈ 2.4 and intermediate/high ≈ 3.3. These differences are attributed to the low torsional rigidity of the deck and consequently the low frequency torsional deck modes (the highest torsional deck mode in the 3-D finite element model has a frequency of 2.57 Hz as in Table 3.1).

Vertical Bending Moment (M_y)

Figure 5.20 shows the vertical bending moment (M_y) along one of the bridge deck's main girders (the total vertical deck moments are, therefore, twice the values shown in Figure 5.20). The asymmetry of the curves is caused by the response to the longitudinal ground motion component. Intermediate and high frequency inputs excite higher modes and cause the moment diagrams to be less smooth than for low A/V inputs. This behaviour was demonstrated in Figure 4.22 which shows that for some deck locations such as quarter-main span higher modes are excited by high frequency inputs.

There are distinct ranges for the values of M_y in the bridge deck for the A/V three categories. The response ratios between the categories are low/intermediate $\simeq 2.0$ and intermediate/high $\simeq 1.5$. Within each category the maximum amplitudes on the main span and on the side spans are essentially the same. The maximum moment in the side span occurs near the anchorages of the second and third cables from the end of the deck because these locations have the lowest vertical stiffness component from the cables. The maximum M_y of the main span occurs in the middle third of the span for the same reason. The most noticeable dispersion within a single A/V category is for the HS

category. For this case, the M_y response to HS2 record is $=$ 1.6 of HS1 and HS3 in the side spans. The reason for this is the relatively low A/V ratio for the vertical component of this record, as shown in Table 5.8.

Transverse Bending Moment (M_z)

Figure 5.21 shows the total absolute maximum transverse bending moment (M_z) along the bridge deck. The effect of frequency content appears clearly in the change of the moment diagrams. Higher frequency inputs excite higher transverse deck modes, and this is the reason that the M_z diagrams for intermediate and high A/V inputs are less smooth than for low A/V. However, in terms of magnitude of the moments, the maximum M_z values for low A/V inputs are much higher than for intermediate and high inputs (ratios are low/intermediate $\simeq$2.5, and intermediate/high $\simeq$1.5). There is observed a ratio of approximately 10 between M_z and total M_y that is carried by the deck (i.e. $2M_y$/ girder). This high ratio is a result of the higher deck stiffness in the transverse direction.

The critical locations on the deck with respect to M_z are near the towers and at mid main span. This occurs because the cables provide no lateral support to the deck and in this case the deck behaves similar to 3-span beam with no cable support, where maximum moments occur at the intermediate supports and at the mid spans.

5.4 SEISMIC RESPONSE OF TOWERS

This section discusses the seismic response of the bridge towers for different A/V synthetic input motions. The deflections will be treated first and then the internal forces.

5.4.1 Tower Deflections

The seismic deflections along the tower height for the 0.1g reference input are depicted in Figure 5.22 and 5.23. Figure 5.24 compares the two components of the tower deflection. Study of these figures indicates that longitudinal tower deflection is affected by both low frequency coupled deck-tower modes and higher frequency local tower modes. The local tower modes (at frequencies of 2.33 Hz and 4.4 Hz) are excited by intermediate and high A/V inputs. This was also shown earlier in Figure 4.18a. The effect of these higher modes appears as a reduction in the slope of the deflection line for intermediate and high A/V inputs. It is noticeable that low A/V inputs give higher deflections in both directions than other A/V input motions. The reason is that most response comes from modes in the long period range where the low A/V inputs have much higher spectral accelerations. A ratio of about 3.0 is observed for tower tip deflections caused by low A/V when compared to deflections caused by intermediate A/V inputs; a ratio of about 2.0 is observed between deflections of intermediate and high A/V inputs. The change in slope of deflection lines in Figure 5.23 a,b occurs at the top strut location (Figure 2.3) where there is a change in the tower stiffness.

Figure 5.24 shows that transverse tower tip deflection is usually larger than longitudinal tower tip deflection. The reason for this is the action of the cables stiffens

the tower in the longitudinal direction. This is evident by the frequencies of the local tower modes in the transverse (1.23 Hz for the first mode and 2.2 Hz for the second) and longitudinal directions (2.3 Hz for the first mode and 4.4 Hz for the second) shown in Table 3.1). The ratio between the transverse and longitudinal tower tip deflections is $\simeq 1.5$ for low A/V inputs, $\simeq 3$ for intermediate A/V inputs, and $\simeq 1.1$ for high A/V inputs. Below the deck level, longitudinal deflections of the tower are almost 1.5 times the transverse deflections. This occurs because there is a transverse stiffening web between the tower legs. The web is intended to provide protection to the tower in the event of ship collision. This feature of the Quincy Bayview Bridge is not always part of cable-stayed bridges in this class.

5.4.2 Tower Internal Forces

This subsection presents discussions of seismically induced internal forces in each of the tower legs. Figure 5.25 shows the directions of the internal forces acting on one of the tower's legs.

Normal Force (F_x)

Figure 5.26 shows the profile of F_x along the height of one of the tower legs. About 20% of the total normal force at base of the tower is a result of the forces from the cables. Ratios of F_x at the base of the tower caused by different input motions are: 1.6 between low and intermediate A/V, and 3.0 between intermediate and high A/V. The dispersion between responses for the low A/V inputs is the largest of the three categories.

The responses within intermediate and high A/V response categories are generally very close, as shown in Figure 5.26b,c. Comparing the values of A_3/V_3 shown in Table 5.8 for the different input motions, it is realized that LS3 that produces the highest F_x has the lowest A_3/V_3 and that IS1 which produces the highest F_x for intermediate A/V category has the highest A_3/V_3 within intermediate A/V category. For high A/V inputs the change in A_3/V_3 does not cause any dispersion in the response. The big jump in the F_x value is located at the top strut location. The finite element model represents the part between the 15 ft mark and 91 ft mark on the tower by a single beam element and this is the reason that this part of the tower height has a constant F_x value that represents 80% of the total F_x carried by the tower.

Transverse Shear Force (Q_y)

The profile of Q_y along the height of one of the tower legs is shown in Figure 5.27. The transverse local tower modes (the first has a frequency of 1.23 Hz and the second has a frequency of 2.2 Hz as shown in Table 3.1) contribute most to this response quantity. Q_y does not receive any contribution from the cable forces because it is orthogonal to the cable planes. This appears in the uniform build up in the value of Q_y. The web-stiffened part of the tower below the deck (below level "0") extracts about 40-50% of the total developed Q_y because of its high stiffness. The dispersion in response within each A/V category is very small. There is a ratio of $\approx$ 2 between Q_y caused by low A/V input motions and Q_y caused by intermediate A/V input motions. The ratio is $\approx$ 2.5 when comparing responses to IS inputs with responses to HS inputs.

Longitudinal Shear Force (Q_z)

The distribution of this response quantity along the height of one of the tower legs is given in Figure 5.28. The effect of longitudinal tower modes on this response quantity was discussed in section 4.4.4.2 and is supported by the jumps shown in the response Figure 4.23b. The first two local longitudinal tower modes have frequencies of 2.33 Hz and 4.43 Hz which means that intermediate and high A/V inputs are more likely to excite these modes. However, in magnitude Q_z caused by low A/V inputs is higher than Q_z caused by other A/V input motions. Q_z caused by low A/V inputs are affected by low frequency coupled deck-tower modes. The coupled motion causes forces to be transmitted from the cables to the towers and This is the reason for the high shear forces observed at the top of the tower in Figure 5.28. Although Q_z caused by intermediate and high A/V inputs are affected by high frequency local tower modes, these modes do not cause as much force in the cables as the coupled deck-tower modes and consequently a lower Q_z is observed near the tower top. Values of Q_z at the tower base are spread over the range of 275-450x10^3 lb. This relatively narrow range indicates that Q_z at the base is somewhat less sensitive than other response quantities to changes in A/V of the input motions.

Comparing longitudinal (Q_z) and transverse (Q_y) shear forces, a ratio of ≈ 2.5 is observed for Q_y/Q_z caused by low A/V inputs. This ratio decreases to ≈ 1.8 for intermediate A/V inputs and to ≤ 1 for high A/V inputs. The lower tower frequencies in the transverse direction cause Q_y to be higher with low A/V input motions. Intermediate and high A/V input motions affect high frequency modes and thus cause the ratio of Q_y/Q_z to decrease.

Torsional Moment (M_x)

The distribution of absolute maximum M_x along the height of one of the tower legs is given in Figure 5.29. Within each response category the values are very close. There are distinct ranges for the response in each category as shown in Figure 5.29. The lowest frequency coupled torsional deck-tower mode (mode 14 of Table 3.1 with frequency 1.25 Hz) that gives most of the response in the low A/V category causes the two tower struts (at elevations 91 and -15 ft) to bend in phase and thus they absorb some of the torsion developed in the tower legs as shown in Figure 5.29a,b. Higher tower torsional modes (excited by high A/V inputs) cause the two tower struts to bend out of phase and thus the lower strut will contribute to the torsion developed in the tower below its position as shown in Figure 5.29c. Above the top strut, each tower leg is working separately and their torsional rigidities are very small and thus the developed torsional moments are negligible as shown in Figure 5.29.

Longitudinal Bending Moment (M_y)

The distribution of this response quantity along the tower height is shown in Figure 5.30. There are two critical locations on the tower with respect to this response quantity namely, the top strut location and the tower base where the maximum M_y is observed. The ratios of M_y at top strut/M_y at tower base takes the values of 1.5, 1.8, and 1.9 for low, intermediate and high A/V inputs, respectively. As observed before, the responses within each category of input motions lie in a relatively narrow range and over most of the tower height responses to different categories of input motions have distinct

ranges. The ratios of maximum M_y in the different input categories take the ratios of 1.5 (for low/intermediate) and 1.1 (for intermediate/high). The excitation of higher modes caused a reduction in the response ratio in the high A/V category. These values show that M_y in the tower is less sensitive to changes in A/V of input motion than Q_y and M_x.

Transverse Bending Moment (M_z)

Figure 5.31 is provided to show the distribution of M_z along the height of one of the tower legs. There are two critical locations for M_z (these are the same two critical locations as M_y, i.e. at the locations of the top strut and the tower base). The ratios of base M_y/top strut M_y are 2.4, 2.33, and 2.33 for low, intermediate and high A/V input motions, respectively. There are distinct ranges for the responses of different input motion categories but the responses for different records within the same A/V category of input motions are very close. There is a ratio of about 2-2.5 between M_z/M_y in any input motion category.

5.5 RESPONSE OF A DECK WITH MOVABLE ENDS

Two additional cases were studied in this section to recognize that cable-stayed bridges may have deck support conditions in the longitudinal direction that are different from the Quincy Bayview Bridge prototype. The first case is for a deck that is free to translate longitudinally at the ends and at the towers (roller supports at these locations). This is referred to as case MMMM where M denotes movable. The second case is for a deck that is free to translate longitudinally on rollers at the ends and pin-connected to

the towers. This is referred to as case MFFM where F denotes fixed in translation. Figure 3.17d shows the three different deck support conditions, including the original FMMF case. Figures 5.33-5.38 show calculated response quantities for three 0.1g synthetic input motions (LS1, IS1, HS1). Only one synthetic input motion record was chosen from each category because the different input motion records within the same A/V category caused very close responses for the FMMF case of Figure 3.17d.

Figure 5.32 compares the fundamental modes of the MMMM, MFFM, and the fundamental mode of the original Quincy Bridge (FMMF). In each case it is a vertical plane mode (Figure 5.32e). The MFFM and FMMF cases have identical coupled symmetric vertical deck-longitudinal tower modes as shown in Figure 5.32. The first mode of the MMMM case has coupled longitudinal deck-tower motion with vertical anti-symmetric deck motion as shown in Figures 5.32a,b,e. The second mode of MMMM is identical to the first mode of MFFM and FMMF cases, and subsequent modes are identical in all cases. The MFFM case was found to have a slightly higher fundamental frequency of 0.39 Hz than the FMMF case (0.37 Hz). MMMM has the lowest fundamental frequency of 0.23 Hz. Thus, the most significant difference in mode shapes caused by changing the support conditions on the deck is that a new antisymmetric mode is introduced for the MMMM case at a frequency lower than the fundamental frequency of the other models.

5.5.1 Deck Deflections

The deck longitudinal deflection was found to be significantly affected by change in the deck supporting condition. Figure 5.33 shows deck deflections for MMMM and MFFM cases. A rigid body motion of the deck exists for the MMMM case with values of 1.1, 0.3, and 0.07 ft for LS1, IS1, and HS1 input motions, respectively, as shown by the solid lines in Figure 5.33a. The longitudinal deck deflection for the case of MFFM is very low compared to the longitudinal deflections in the MMMM case. The longitudinal deflection for the MMMM case with LS1 input motion is the highest value of longitudinal deflection for the bridge. For input motions larger than 0.1g it is possible that a special bearing design at the abutments and towers may be required to accommodate this size of deflection. The high ratios of 4.0 between deflections caused by LS1 and IS1, and 16.0 between the deflections caused by LS1 and HS1 show that this deflection is caused by the fundamental coupled longitudinal deck-tower mode at a frequency of 0.23 Hz.

Comparing Figures 5.13 and 5.33b, it is observed that the transverse deflections along the deck are the same for all deck support cases. This is expected because the bridge deck transverse mode shape is not affected by the deck's longitudinal supporting conditions.

Comparing Figures 5.11 and 5.33c, it is seen that the vertical deck deflection in the case of MMMM has increased to approximately double its value in the case of MFFM, and the vertical deflection of MFFM is almost 1.3 times the vertical deflection

of FMMF. The coupling between the longitudinal tower motion and the deck vertical motion (though anti-symmetric) in the new fundamental bridge mode for the MMMM case will cause the longitudinal earthquake component to contribute a significant amount toward the vertical deflection of the deck. The shift to higher frequencies in higher subsequent modes leads to higher contributions from these modes under low frequency inputs.

. The ratio of vertical deflection caused by different inputs takes the values of 6 for low/intermediate A/V, and 3.5 for intermediate/high inputs in MMMM case. These ratios decrease to 3 and 2 for the MFFM case which shows the effect of the first mode in MMMM case and its sensitivity to the A/V ratio of input motion.

5.5.2 Tower Deflections

. The longitudinal deflection of the tower is also affected by the deck support conditions. For the MMMM case the tower tip deflections are 1.1, 0.2, 0.07 ft for LS1, IS1, and HS1 input motions, respectively as shown in Figure 5.34a. Comparing these values with deck deflection values, in Figure 5.33a, it may be concluded that the rigid body longitudinal deflection of the MMMM deck is about equal to the deflection at the tower tip. When comparing Figure 5.22a to Figure 5.34a, it appears that there is a ratio of about 7 between deflections of MMMM and deflections of FMMF, for low A/V input. This shows the pronounced contribution of the longitudinal fundamental mode to the tower deflection in the MMMM case and its relation to low A/V inputs. The calculated deflection values give deflection/tower height ratios of 1/200, 1/1000, 1/3000 for low,

intermediate and high A/V inputs, respectively. The value 1/200 is considerably higher than previously calculated drift ratios. This produces tip deflection of approximately 1ft per 0.1g input acceleration. In this case recommendations might possible be made to reduce this value through different design of the tower or a P-Δ analysis might be advisable for strong ground motion inputs.

Comparing Figures 5.22 and 5.34a, it appears that MFFM case results in longitudinal tower deflections about 1.3 times larger than FMMF case for all A/V categories. From Figure 5.34a the effect of A/V is to cause a reduction in amplitude from the case of MMMM to the case of MFFM. The ratio of tower tip deflection caused by low A/V input motion to the same quantity caused by intermediate A/V input motion reduces from 6 to 3.

Figures 5.23 and 5.34b show that the transverse deflection of the tower tip is not affected by the deck support conditions.

5.5.3 Deck Internal Forces

A noticeable change in the normal force (F_x) distribution between the FMMF and the cases of MMMM and MFFM is observed by comparing Figures 5.16 and 5.35a. The bridge with a movable deck (MMMM) is of the self-anchored type which causes the horizontal component of cable forces to be carried completely by the deck. In both cases of MMMM and MFFM the maximum value of F_x is moved from the deck end (its location for FMMF) to another location in the side span as shown in Figure 5.35a, and the lowest value of F_x generally occurs at the ends. In the case of MFFM the maximum

F_x is always at the towers, consistent with the fixed conditions at these locations. A ratio of 2 between maximum F_x caused by LS1 in the case of FMMF and MMMM. This ratio reduces to 1.6 when considering FMMF and MFFM. Although F_x reduces by a factor of 6 for MMMM when comparing IS1 to LS1, the ratio is only 2 for MFFM and about 1.2 for FMMF. This shows that the fundamental mode of MMMM case contributes most of the response when excited by low A/V input.

Maximum Q_z for the case of FMMF is always at the abutments or middle third of main span while it is at mid-main span for the cases of MMMM and MFFM as shown in Figures 5.18 and 5.35c. Low A/V causes the highest Q_z in all examined bridge deck cases, and for this frequency content Q_z for the MMMM case is as twice as Q_z for the case of FMMF. For other input motions Q_z for MFFM case is slightly higher than Q_z for the FMMF and MMMM cases.

Low A/V input causes the maximum M_y and for this frequency content M_y for the MMMM and MFFM cases is approximately 2.5 times higher than M_y for the case of FMMF. The case of MFFM gives the highest M_y in response to high and intermediate input motions. These observations are drawn from the comparison of Figures 5.20 and 5.35e.

The change in shapes and frequencies of some of the lowest vertical and coupled vertical-longitudinal modes caused this large increase in Q_z and M_y.

The distribution and magnitudes of transverse shear force, and torsional and transverse bending moments for MMMM and MFFM remained the same as for the FMMF case.

5.5.4 Tower Internal Forces

Figure 5.36 contains the tower's seismic response of the cases MMMM and MFFM. When comparing Figures 5.28 to Figure 5.36c it appears that highest value of Q_z is always at the base. Low A/V input causes the highest Q_z in all studied bridge cases and for this input motion Q_z of the MMMM case is twice Q_z for the MFFM and FMMF cases near the tower top. For intermediate and high A/V inputs, MFFM case has the highest Q_z above the deck level (zero level). Below the deck level the case of MFFM has the highest Q_z for any input motion.

Comparing Figure 5.29 to Figure 5.36d it can be deduced that low A/V causes the highest M_x and for this frequency content the MMMM case has slightly higher M_x than the other two cases. Below the deck the case of MFFM has the highest M_x for intermediate and high frequency inputs.

In the case of M_y low A/V input motion causes the highest response. The case of MMMM has the highest response for low A/V input motion. The case of MFFM has the highest M_y for intermediate and high A/V as shown in Figures 5.30 and 5.36e.

F_x, Q_y, and M_z are not affected by the deck support conditions.

5.5.5 Seismic Response Comparisons

The three cases of bridge deck supports affect the dynamics of the full structure. For low A/V input motions, the FMMF case has the lowest responses in the deck and towers except for the normal force at the abutments, and the MMMM case gives much higher responses than FMMF and MFFM cases. For intermediate and high A/V input

motions, the seismic response of FMMF and MMMM cases are very close and less than the seismic response of the MFFM case, generally by a factor of approximately 1.5. This shows that the deck support conditions can significantly influence the distribution of seismic forces in the bridge. The magnitude and distribution of the forces will also be affected by the ground motion characteristics.

5.6 DISCUSSION OF SEISMIC ANALYSIS RESULTS

This section presents comparisons between the acceleration response spectra used in this study with other common seismic design spectra, quantitative and qualitative comparisons are also made between the seismic-induced forces and the design dead, live and wind forces in the Quincy Bayview Bridge. The dead, live, and wind loads were obtained from structural drawings of the bridge (Modjeski and Masters, 1983).

5.6.1 Design Spectra

This research used three acceleration response spectra calculated for 2% damping to represent three categories of input motion frequency content (low, intermediate, and high). Similar concepts are adopted in Ontario Highway Bridge Design Code (OHBDC91) which provides 5% damped acceleration response spectra for different values of expected peak ground velocity (V). American Association of State Highway and Transportation Officials Code (AASHTO83) gives 5% damped acceleration response spectra for different expected peak accelerations (A). Figure 5.37 compares the three horizontal acceleration response spectra from this study, recomputed for 5% damping,

to OHBDC91 and AASHTO83 spectra. Two spectra were selected from OHBDC91 to represent high and low velocities. The AASHTO83 spectrum is scaled to a peak ground acceleration of 0.1g.

The AASHTO83 and OHBDC91 spectra appear to provide an adequate representation of the ground motions for high and intermediate A/V events, but are inadequate for low A/V events for periods exceeding about 0.5 seconds. As was shown in the previous sections of this chapter, the seismic response of cable-stayed bridges is particularly sensitive to low-frequency ground motions and therefore a design response spectrum for cable-stayed bridges must realistically represent the long-period ground motions expected at the bridge site. The importance associated with cable-stayed bridge structures means that it will not be generally sufficient to use a standard "building code" type of design spectrum. Development of a site specific spectrum that pays due attention to representing long-period motions is an essential part of the seismic analysis procedure.

5.6.2 Bridge Deck

Figure 5.38 compares the spatial distribution along the pinned bridge deck of F_x, Q_z, and M_y induced by LS1, IS1 and HS1 input motions, to the same design quantities induced by dead load (D.L.) and live load (L.L.). The absolute values of seismic induced forces per girder are presented on Figure 5.38 because they are reversible in their algebraic signs. The D.L. and L.L. were applied to the original design of the bridge which has a tie rod connecting the deck end to the abutment. The original Quincy Bayview Bridge has roller supports at both deck ends and this is the reason the

distribution of design D.L. and L.L. F_x has the symmetric pyramid distribution shown in Figure 5.38a. At the ends of the bridge deck the seismically induced forces are approximately the same as the D.L. F_x ($\simeq 0.7 \times 10^6$ lb). At towers, the D.L. F_x is more than 7 times the values of F_x due to other loads.

The seismic induced shear force (Q_z) along the deck is (10-30%) of the D.L. Q_z, and (20-40%) of the L.L. Q_z, depending on the frequency content of the input motion. The locations of maximum combined D.L., L.L. and seismic Q_z are the ends of the bridge deck and the mid main span.

D.L. M_y is almost constant along the deck (2×10^6 lb.ft). L.L. M_y has two peaks, one in the side span (5.6×10^6 lb.ft)and another one in the middle section of the main span (4×10^6 lb.ft). The peak seismic M_y occurs at the same locations and is 65-100% of L.L. M_y in the case of LS1, and 30-50% of L.L. M_y for IS1 and HS1.

The above discussion shows that for 0.1g input the seismic bending moment can be large enough that it is a significant percentage of the dead and live loads. Other response quantities, Q_z and F_x, are dominated by D.L. and L.L. and the seismic component is a much smaller fraction of the total force. However, for ground motions larger than 0.1g, the seismic component will become an even larger percentage of the total force in the deck.

A longitudinally movable deck (MMMM from section 5.5) has a distribution of seismically induced F_x, described in section 5.5.3 and shown in Figure 5.39. In this case the seismic F_x is $\leq$10% of D.L. F_x for the cases of IS1 and HS1, and $\approx$ 50% of D.L. F_x at the deck ends and 10% of D.L. F_x at the tower locations for LS1. Q_z due to LS1

increased at the deck ends and at mid main span to be 80% of D.L. Q_z and 100% L.L. Q_z respectively. Q_z induced by IS1 and HS1 input motions kept the same ratios to D.L. and L.L. Q_z along the deck. M_y induced by the LS1 input motion increases over the previous case to be up to 50% higher than L.L. M_y at most locations.

In summary, the longitudinally moving deck decreases the seismic F_x along the deck, does not substantially affect seismic Q_z and M_y due to intermediate and high A/V input motions, and significantly increases Q_z and M_y for low A/V input motions.

5.6.3 Bridge Tower

In addition to dead and live loads, wind and earthquake loads must also be considered in the design of the towers. Because either wind or earthquakes are considered in the design, and because wind load is a governing design loading for bridge towers, it is appropriate to compare their corresponding values. Wind loads in two perpendicular directions are considered in the analysis and design, wind load along the transverse axis of the bridge deck (W0), or wind load perpendicular to the transverse axis of the bridge deck (W90). Absolute maximum seismic induced tower's leg internal forces are compared to D.L., L.L. and the critical of either W0 or W90 loads in Figures 5.40 and 5.41. The following observations were made on the forces calculated for the FMMF case: D.L. F_x is 3-4 times higher than seismic F_x as shown in Figure 5.40a. L.L. and W0 F_x are negligible. W90 Q_z is approximately equal to LS1 Q_z at the tower base. L.L. Q_z is almost 1/3 their value. Q_z due to IS1 and HS1 are less than Q_z due to LS1 input motion but 2-3 times higher than L.L. Q_z. D.L. Q_z at the tower base is negligible.

Transverse shear forces (Q_y) induced by the different seismic loads are (1-3 times) higher than wind induced Q_y in the region above the deck as shown in Figure 5.40b. In the region below the deck W0 $Q_y \simeq 0.8$ LS1 Q_y, $\simeq 1.3$ IS1 Q_y, $\simeq 4.0$ HS1 Q_y. These results show that low A/V inputs do affect the combinations of design loads.

Seismic induced M_x is higher than any other component of M_x along the tower height (between zero level and 91 ft level) as shown in Figure 5.40d. Below the deck level W90 and L.L. cause torsional moments nearly equal to M_x caused by HS1 and IS1 input motions. LS1 M_x is almost as twice as M_x caused by other seismic, wind, or L.L. input.

Figure 5.40e shows the distribution of absolute maximum M_y along the tower height due to different seismic inputs. It also shows the design M_y components due to wind (although they may be positive or negative in sign they were plotted in negative sign to facilitate the visualisation on the graph) and live load. Seismic M_y caused by IS1 and HS1 inputs are close in values and distribution to M_y caused by W0, W90 and L.L. M_y caused by LS1 input is higher than M_y caused by other inputs by a ratio of 2-3 at the tower base and a ratio of 3-6 at the top strut. These calculated values indicate the importance of considering seismic forces even for geographical locations where maximum A is as low as 0.1g. The low frequency earthquakes has more pronounced effects on the bridge than intermediate or high A/V earthquakes.

It is evident that Transverse bending moment (M_z), shown in Figure 5.40f, is caused mainly by seismic loads because seismic $M_z \geq 10$ times other values.

The case of the longitudinally movable deck is considered in Figure 5.41. The

effect of deck support condition is limited to the M_y and Q_z as shown in section 5.5.4 The increase in M_y and Q_z will make the tower sections more vulnerable to seismic loads.

The case of bridge deck with roller ends and pinned to the towers gave higher seismic responses than the original Quincy Bridge because of the frequency shift in its modes, as explained before, which makes it a less favourable alternative for seismic forces.

The seismic analyses were conducted for a maximum ground acceleration of 0.1g. The results show that some locations on the bridge are affected by the seismic induced forces especially when A/V of the input motion is low. When the bridge is subjected to higher peak ground accelerations, the seismic response will increase by the ratio of the peak ground acceleration to the 0.1g value used in these analyses. This means that in a seismic zone with intermediate or high A/V characteristics and expected peak ground acceleration of 0.3g would make the design of the deck, tower top, and tower base governed by earthquake forces (it was not earthquake governed for 0.1g). The case of low A/V (at 0.1g) had high seismic forces at tower bases and deck abutments and mid-main span.

5.7 SUMMARY AND CONCLUSIONS

This chapter presents a study of seismic response characteristics of cable-stayed bridges. The study examined the effect of ground motion frequency content, as expressed by the A/V ratio, on the seismic response of cable-stayed bridges with fixed (pinned) or

longitudinally movable decks. A set of nine synthetic time history records representing 3 different ground motion frequency content categories was used in the study. Comparisons of the seismic induced forces to dead, live and wind induced forces were made for all regions of the deck and towers.

It may be concluded that:

1- The seismic response of cable-stayed bridges depends on the frequency content of the input ground motion. This has been quantified in this research by use of the A/V ratio. Some response quantities (such as deck shear force, deck bending moment and deflections of both deck and tower) are sensitive to frequency content of the input motion. Other response quantities such as tower base shear force and tower longitudinal bending moment are less sensitive to the A/V ratio of input motions. In general, low A/V inputs cause higher bridge responses because the bridge has many deck and deck-tower modes with low frequencies.

2- Critical seismically induced internal forces (compared to D.L., L.L. and wind) are: deck shear forces and bending moments, and tower shear forces and bending moments because they exceed (especially for low A/V inputs) the corresponding values of live load internal forces (seismic forces replace L.L. in load combinations). In some extreme cases examined here the exceedance was found to be as large as 700%, such as the case of Q_z near the tower top.

3- Critical locations which have high seismic forces compared to D.L., L.L., and wind are deck ends, deck sections near towers, cable anchorage region on the towers, and the bases of the towers.

4- The deck support condition has a significant effect on the seismic forces developed in the bridge because the dynamics of the full structure is altered as shown in section 5.5. A deck that is completely movable in the longitudinal direction (case MMMM) will introduce a low frequency longitudinal deck-tower mode which will contribute significantly to the vertical plane response of the deck and the towers. In this situation there will be a reduction in the deck normal force (F_x) that is induced by any A/V input motion, however the vertical and longitudinal deck deflections, the vertical shear force (Q_z), and vertical bending moment (M_y) will all increase significantly under low A/V input motions. The tower longitudinal deflection, longitudinal bending moment and longitudinal shear forces are also increased as a result of the change in the deck support condition. On the other hand, having a deck fixed to the towers with a pin connection and free to move longitudinally at the ends (the case of MFFM) will stiffen the deck in vertical bending and this will raise the frequencies of deck and tower in the vertical plane and will result in the response to intermediate and high A/V earthquakes to be higher than either the MMMM or FMMF cases.

5- Input ground motions, especially with low A/V, with peak ground acceleration as low as 0.1 g were found to induce shear forces and bending moments in the deck and towers of Quincy Bayview Bridge prototype model that were high enough to affect the governing load combinations.

Table 5.1 Ground Motion Parameters of High A/V Records (A/V ≥ 1.2)

Record No.	Earthquake	Date	Site	1st Horizontal A/V	2nd Horizontal A/V	Vertical A/V	Magnitude	Epic. Dist. (km)	Soil Cond.
1	Parkfield, California	June,27, 1966	Temblor	1.86	1.54	3.30	5.6	7	Rock
2	Parkfield, California	June,27, 1966	Cholame,Shandon, No. 5	1.70	1.53	1.64	5.6	5	Rock
3	San Francisco, California	March,22 ,1957	San Francisco, Golden Gate Park	2.27	1.70	3.17	5.25	11	Rock
4	San Francisco, California	March,22 ,1957	San Francisco, State Bldg.	1.69	1.36	1.84	5.25	17	Stiff Soil
5	Helena, Montana	Oct.,31, 1935	Helena, Montana, Carroll College	2.03	1.09	0.93	6.0	8	Rock
6	Lytle Creek	Sept.,12, 1970	6074 Park Dr., Wrightwood, Cal.	2.06	1.60	1.70	5.4	15	Rock
7	Oroville, California	Aug., 1, 1975	Seismogr. Station, Oroville Dam	1.90	2.68	2.35	5.7	13	Rock
8	San Fernando, California	Feb.,9, 1971	Pacoima Dam	1.88	1.03	1.22	6.4	4	Rock
9	San Fernando, California	Feb.,9, 1971	Lake Hughes, Station 4	1.72	2.99	2.17	6.4	26	Rock
10	Nahanni, N.W.T. Canada	Dec.,23, 1985	Site 1, Iverson	2.38	N/A	N/A	6.9	7.5	Rock
11	Monte Negro, Yugoslavia	April,9, 1979	Albatros Hotel, Ulcinj	2.63	2.31	N/A	5.4	12.5	Rock
			Average	2.01	1.78	2.04			

Table 5.2 Ground Motion Parameters of Intermediate A/V Records ($0.8 \leq A/V < 1.2$)

Record No.	Earthquake	Date	Site	1st Horizontal A/V	2nd Horizontal A/V	Vertical A/V	Magnitude	Epic. Dist. (km)	Soil Cond.
1	Imperial Valley, California	May,18 ,1940	El Centro	1.04	0.58	1.94	6.6	8	Stiff Soil
2	Kern County, California	July,21, 1952	Taft Lincoln School Tunnel	1.01	0.99	1.56	7.6	56	Rock
3	Borrego Mtn., California	April,8, 1968	San Onofre, SCE Power Plant	1.11	1.11	1.79	6.5	122	Stiff Soil
4	San Fernando, California	Feb.,9, 1971	3838 Lankershim Blvd., L.A.	1.01	1.36	1.43	6.4	24	Rock
5	San Fernando, California	Feb.,9, 1971	Hollywood Storage, P.E. Lot, L.A.	1.00	1.03	1.61	6.4	35	Stiff Soil
6	San Fernando, California	Feb.,9, 1971	3407 6th St., L.A.	1.00	0.88	0.64	6.4	39	Stiff Soil
7	San Fernando, California	Feb.,9, 1971	Griffith Park Observatory, L.A.	0.88	1.18	1.68	6.4	31	Rock
8	San Fernando, California	Feb.,9, 1971	234 Figueroa St., L.A.	1.19	1.04	0.88	6.4	41	Stiff Soil
9	Monte Negro, Yugoslavia	April, 15,1979	Albatros Hotel, Ulcinj	0.88	0.80	1.93	7.0	17	Rock
10	Mexico	Sept., 19,1985	El Suchil, Guerrero Array	0.91	1.31	0.85	8.1	230	Rock
11	Mexico	Sept., 19,1985	La Villita, Guerrero Array	1.17	0.77	1.24	8.1	44	Rock
			Average	0.93	1.00	1.41			

Table 5.3 Ground Motion Parameters of Low A/V Records (A/V ≤ 0.5)

Record No.	Earthquake	Date	Site	1st Horizontal A/V	2nd Horizontal A/V	Vertical A/V	Magn.	Epic. Dist. (km)	Soil Cond.
1	San Fernando	Feb.,9, 1971	800 W.,1st., L.A., Cal.	0.50	0.73	0.71	6.4	41	Rock
2	Mexico	Sept.,19, 1985	Siamex Puebla, Mexico City	0.42	0.50	0.40	8.1	469	Rock
3	San Fernando	Feb.,9, 1971	4680 Wilshire Blvd, L.A., Cal.	0.40	0.54	0.96	6.4	38	Stiff Soil
4	San Fernando	Feb.,9, 1971	2500 Wilshire Blvd., L.A., Cal.	0.52	0.66	0.56	6.4	40	Stiff Soil
5	Long Beach	March, 10,1933	L.A. Subway Terminal	0.41	0.37	0.72	6.3	59	Rock
6	Tang Shan	July,28, 1976	Hongshan, Hebei	0.50	0.83	0.54	7.8	373	Sandy Rock
7	Tang Shan After Shock	July,28, 1976	Beijing Diplomat's Apartments, Point 1, Basement	0.58	0.81	0.88	7.1	170	Sandy Clay
8	Tang Shan After Shock	Nov.,15,1976	Beijing Hotel	0.58	0.78	N/A	6.9	122	Sandy Clay
9	Mexico	Sept.,19,1985	U.N.A.M Mexico City	0.36	0.28	0.27	8.1	379	Rock
10	Mexico	Sept.,19,1985	Mesa Vibradora C.V., Mexico City	0.41	0.36	0.24	8.1	379	Rock
11	Mexico	Sept.,19,1985	Siamex Puebla, Mexico City	0.50	0.42	0.40	8.1	469	Hard Soil
12	Mexico	Sept.,19,1985	Tacubaya D.F.	0.35	0.25	0.24	8.1	380	Hard Soil
			Average	0.43	0.46	0.50			

Table 5.4 Ratios of Acceleration Components for High A/V Records

Record No.	Earthquake	Site	1st Horizontal Acceleration (A_1) cm/sec^2	2nd Horizontal Acceleration (A_2) cm/sec^2	Vertical Acceleration (A_3) cm/sec^2	A_2/A_1	A_3/A_1
1	Parkfield	Temblor	264.35	340.81	129.75	1.29	0.50
2	Parkfield	Cholame, Shandon	425.68	347.82	116.90	0.82	0.28
3	San Francisco	San Francisco, Golden Gate Park	102.81	81.80	36.72	0.80	0.36
4	San Francisco	San Francisco, State Blvd.	83.81	55.12	43.01	0.66	0.51
5	Helena, Montana	Helena Montana, Carroll College	143.71	142.50	87.62	0.61	0.99
6	Lytle Creek	6074 Park Dr., Wrightwood, Cal.	194.40	139.04	53.05	0.72	0.27
7	Oroville,	Oroville Dam	82.50	90.60	112.83	1.10	1.37
8	San Fernando	Pacoima Dam	1054.95	1148.06	695.97	1.10	0.66
9	San Fernando	Lake Hughes	143.51	168.11	150.83	1.17	1.05
10	Nahanni	Site I Iverson	1080.08	N/A	N/A	N/A	N/A
11	Monte Negro	Albatros Hotel	41.20	72.594	N/A	1.76	N/A

Table 5.5 Ratios of Acceleration Components for Intermediate A/V Records

Record No.	Earthquake	Site	1st Horizontal Acceleration (A_1) cm/sec^2	2nd Horizontal Acceleration (A_2) cm/sec^2	Vertical Acceleration (A_3) cm/sec^2	A_2/A_1	A_3/A_1
1	Imperial Valley	El Centro	347.05	210.14	206.33	0.62	0.60
2	Kern County	Taft Lincoln	175.94	152.71	102.84	0.87	0.59
3	Borrego Mtn.	San Onofre	45.54	40.03	54.07	0.88	1.19
4	San Fernando	3838 Lankershim Blvd., Basement, L.A., Cal.	147.63	164.25	69.82	1.11	0.47
5	San Fernando	Hollywood Storage	206.99	167.26	87.40	0.88	0.42
6	San Fernando	3407 6th St., L.A. Cal.	161.95	158.18	55.49	0.98	0.34
7	San Fernando	Griffith Park, L.A., Cal.	176.90	167.44	120.25	0.95	0.68
8	San Fernando	234 Figueroa St., L.A., Cal.	195.65	188.19	67.55	0.96	0.35
9	Monte Negro	Albatros Hotel	167.75	218.05	159.85	1.30	0.95
10	Mexico	El Suchil	103.12	81.45	49.62	0.79	0.48
11	Mexico	La Villita	120.87	120.99	57.51	1.00	0.48

Table 5.6 Ratios of Acceleration Components for Low A/V Records

Record No.	Earthquake	Site	1st Horizontal Acceleration (A_1) cm/sec^2	2nd Horizontal Acceleration (A_2) cm/sec^2	Vertical Acceleration (A_3) cm/sec^2	A_2/A_1	A_3/A_1
1	San Fernando	800 W.,1st., L.A., Cal.	86.92	137.81	60.85	1.59	0.70
2	Mexico	Siamex Puebla Mexico City	29.55	32.60	15.85	1.10	0.54
3	San Fernando	4680 Wilshire Blvd, L.A., Cal.	82.24	114.98	64.75	1.40	0.79
4	San Fernando	2500 Wilshire Blvd., L.A., Cal.	98.75	96.57	42.48	0.98	0.43
5	Long Beach	L.A. Subway Terminal	95.63	62.33	63.61	0.65	0.67
6	Tang Shan	Hongshan, Hebei	7.24	15.00	4.71	2.07	0.65
7	Tang Shan After Shock	Beijing Diplomat's Apartments, Point 1, Basement	24.02	26.61	15.31	1.11	0.64
8	Tang Shan After Shock	Beijing Hotel	25.09	31.66	N/A	1.26	N/A
9	Mexico	U.N.A.M Mexico City	33.45	28.10	21.57	0.84	0.65
10	Mexico	Mesa Vibradora C.V. Mexico City	37.36	38.83	20.14	1.04	0.54
11	Mexico	Siamex Puebla Mexico City	32.60	29.55	15.85	0.91	0.49
12	Mexico	Tacubaya D.F.	33.32	34.40	19.16	1.04	0.58

Table 5.7 Statistical Characteristics of Ground Motions

A/V	A_2/A_1			A_3/A_1		
	Ave.	STD	COV	Ave.	STD	COV
High	1.00	0.34	34.0	0.67	0.37	55.2
Intermediate	0.93	0.17	18.3	0.60	0.25	41.7
Low	1.08	0.25	23.1	0.61	0.10	16.4

Ave. Average ratio

STD Standard Deviation

COV Coefficient of variation (%)

Table 5.8 Properties of Synthetic Time History Records

Record No.	Seed	A_1 (g)	V_1 m/sec.	A_2 (g)	V_2 m/sec.	A_3 (g)	V_3 m/sec.	A_1/V_1	A_2/V_2	A_3/V_3
LS1	San Fernando, 800 W. 1st., 1st floor	0.10	0.20	0.09	0.21	0.06	0.11	0.52	0.43	0.55
LS2	San Fernando, 4680 Wilshire Blvd.	0.10	0.31	0.09	0.23	0.06	0.08	0.33	0.39	0.73
LS3	Mexico, (U.N.A.M.), Mexico City	0.10	0.23	0.09	0.18	0.06	0.12	0.45	0.51	0.51
IS1	Imperial Valley, California (El Centro)	0.10	0.11	0.09	0.11	0.06	0.05	0.93	0.83	1.28
IS2	San Fernando, 3407 6th St., L.A., California	0.10	0.10	0.09	0.08	0.06	0.03	1.03	1.18	1.71
IS3	Mexico, El Suchil	0.10	0.10	0.09	0.09	0.06	0.04	0.89	0.93	1.36
HS1	Parkfield, Cholame, Shandon No. 5, California	0.10	0.04	0.09	0.03	0.06	0.02	2.33	2.60	2.95
HS2	San Fernando, California, Pacoima Dam	0.10	0.04	0.09	0.03	0.06	0.02	2.83	2.71	2.31
HS3	Monte Negro, Yugoslavia, Albatros Hotel	0.10	0.05	0.09	0.05	0.06	0.02	2.09	1.62	2.78

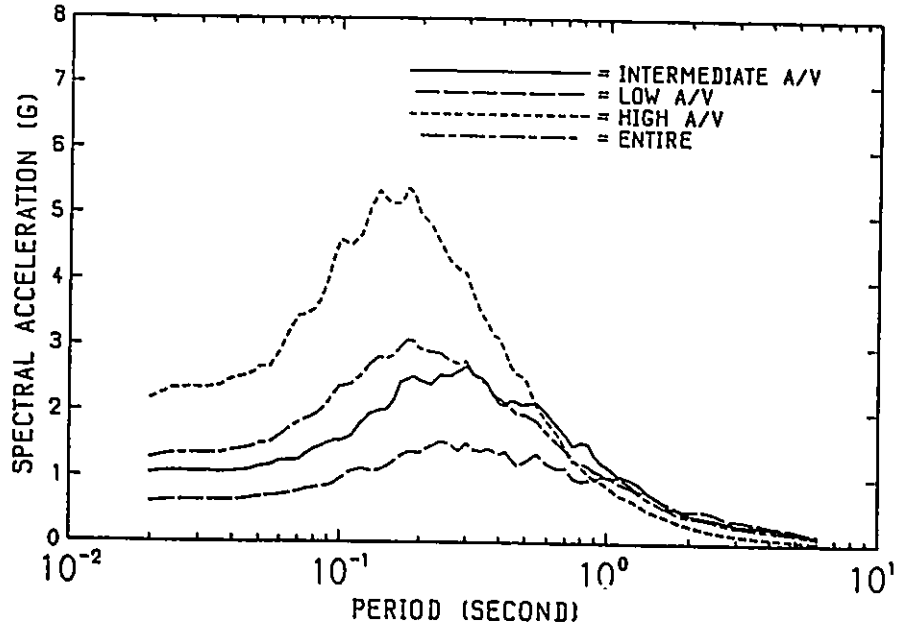

a) Acceleration Spectra Scaled to a Common Peak Ground Velocity of 1 m/sec.

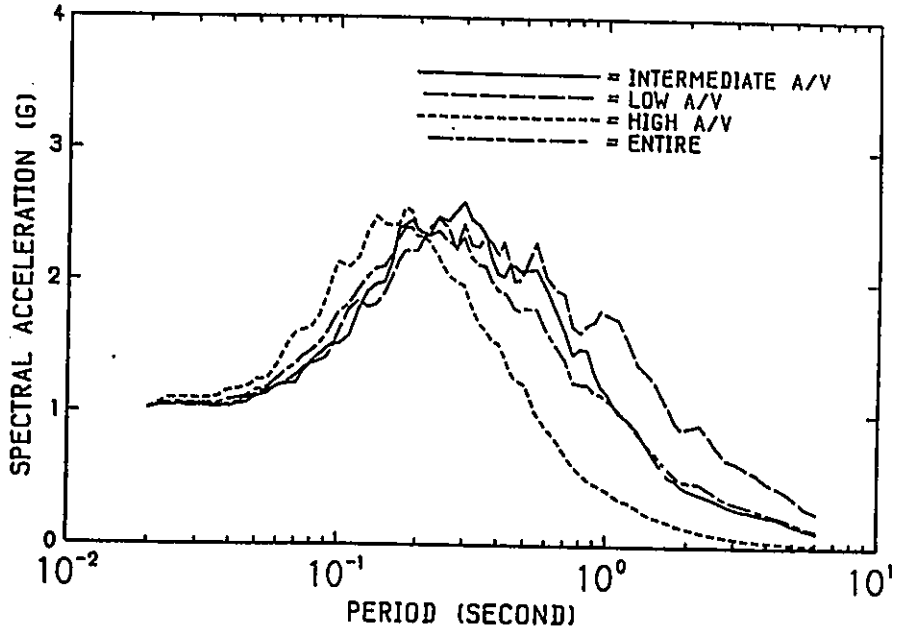

b) Acceleration Spectra Scaled to a Common Peak Ground Acceleration of 1 g.

Figure 5.1 Effect of Scaling on Acceleration Response Spectra (Tso et al 1992).

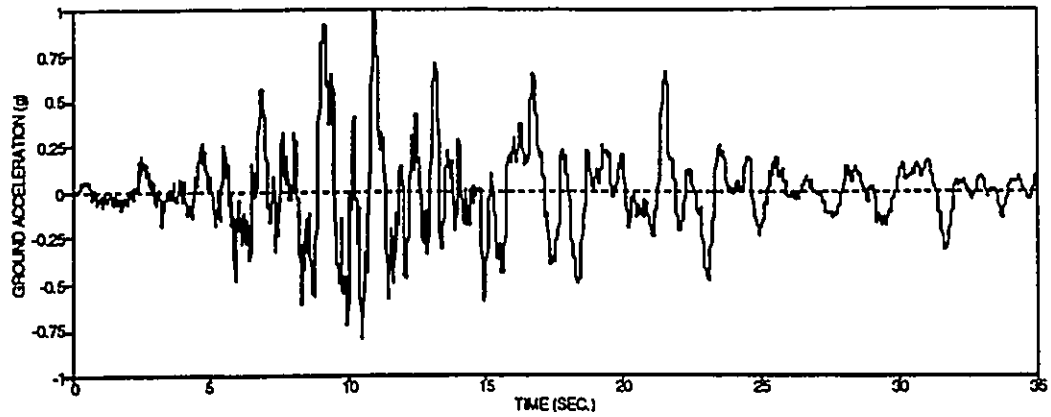

a) Longitudinal Component

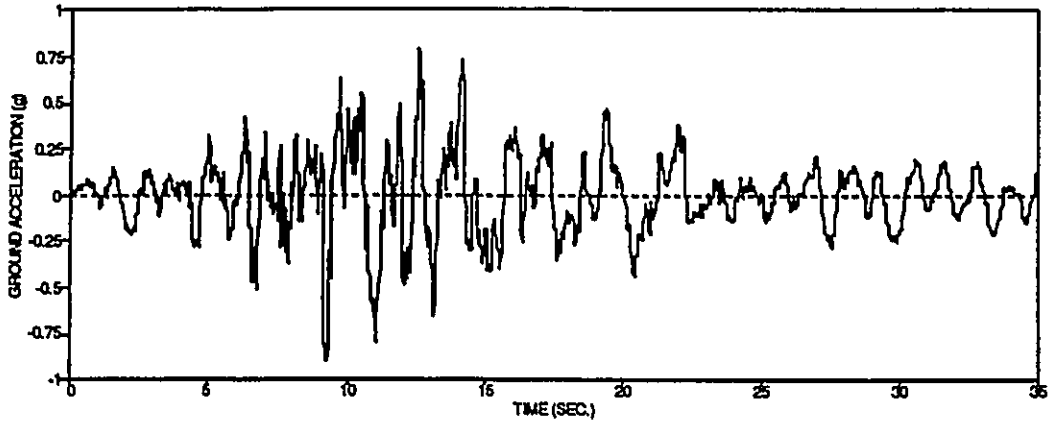

b) Transverse Component

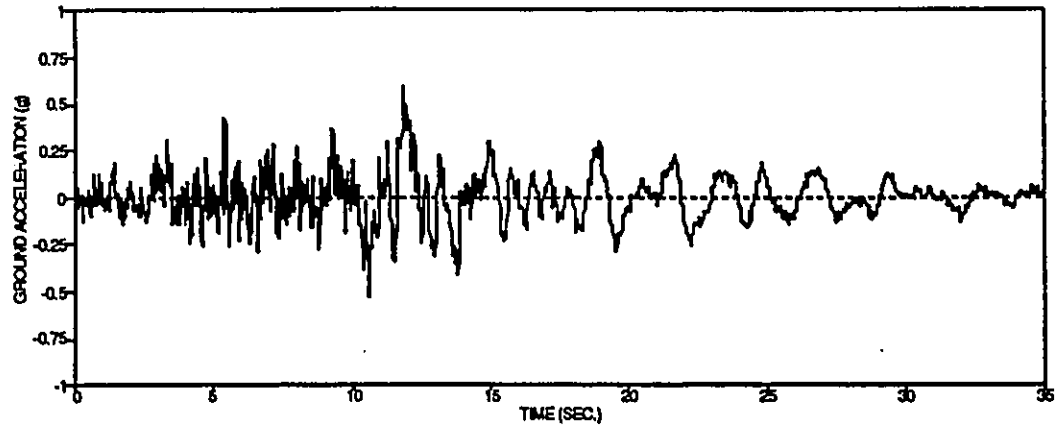

c) Vertical Component

Figure 5.2 Acceleration Time History Components of the LS1 Record

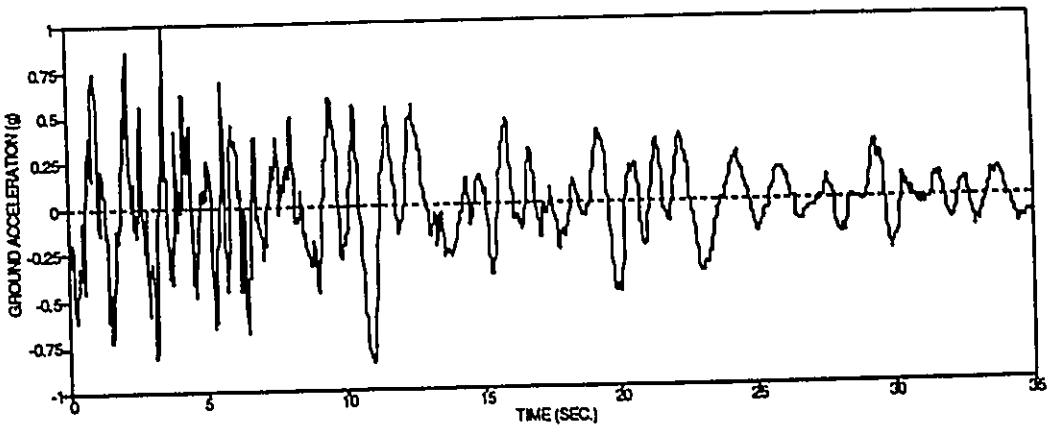

a) Longitudinal Component

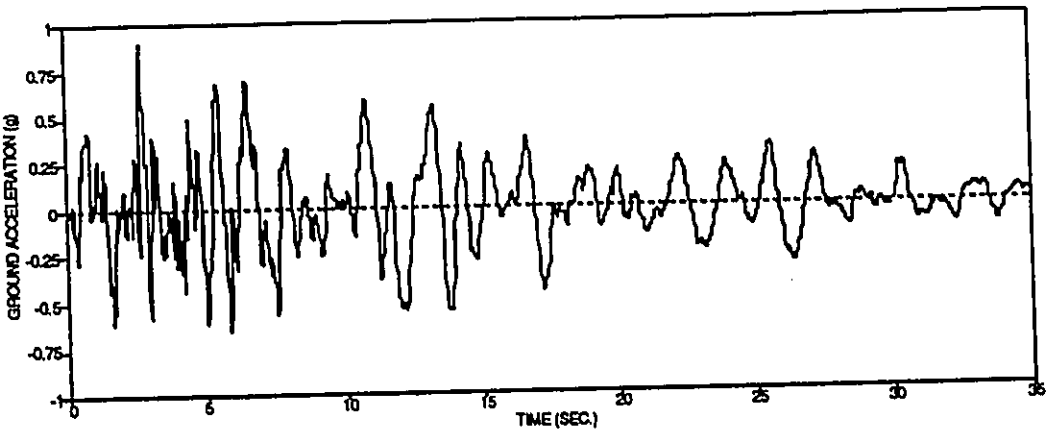

b) Transverse Component

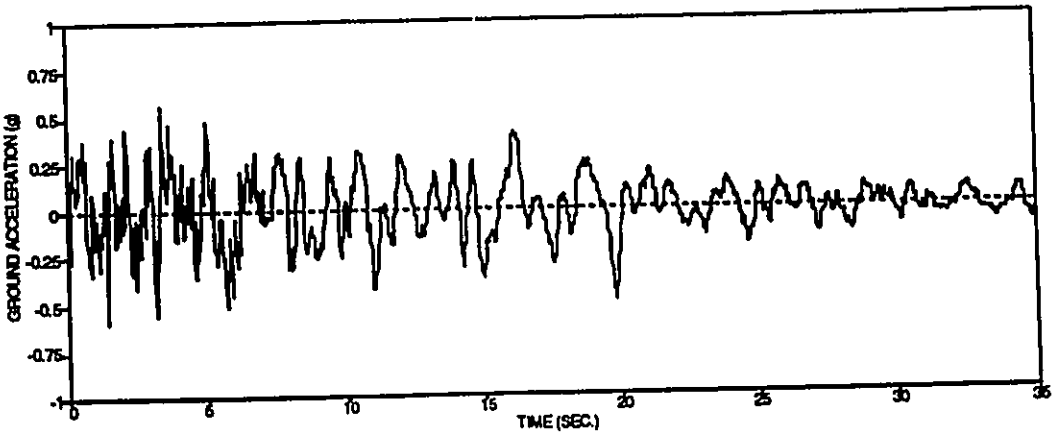

c) Vertical Component

Figure 5.3 Acceleration Time History Components of the LS2 Record

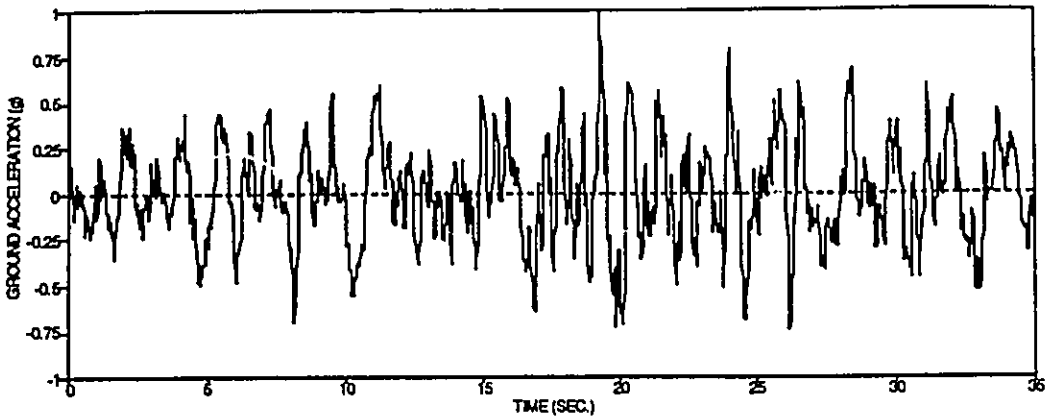

a) Longitudinal Component

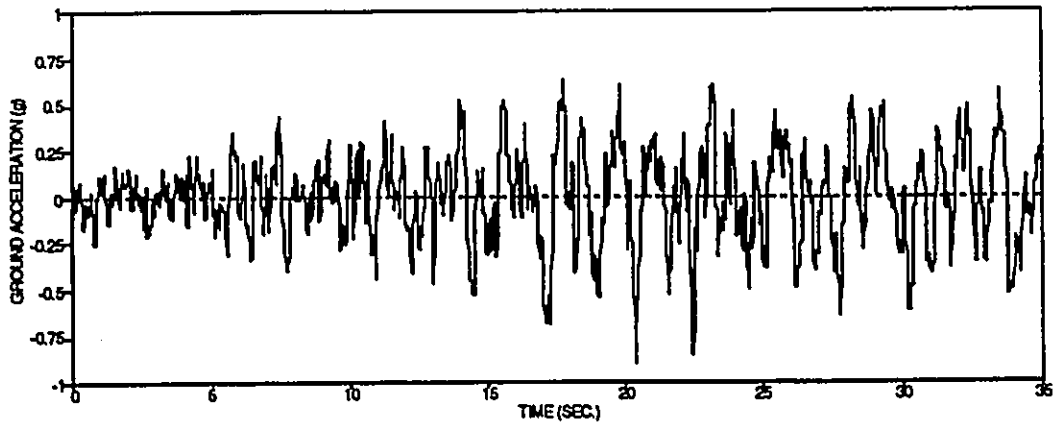

b) Transverse Component

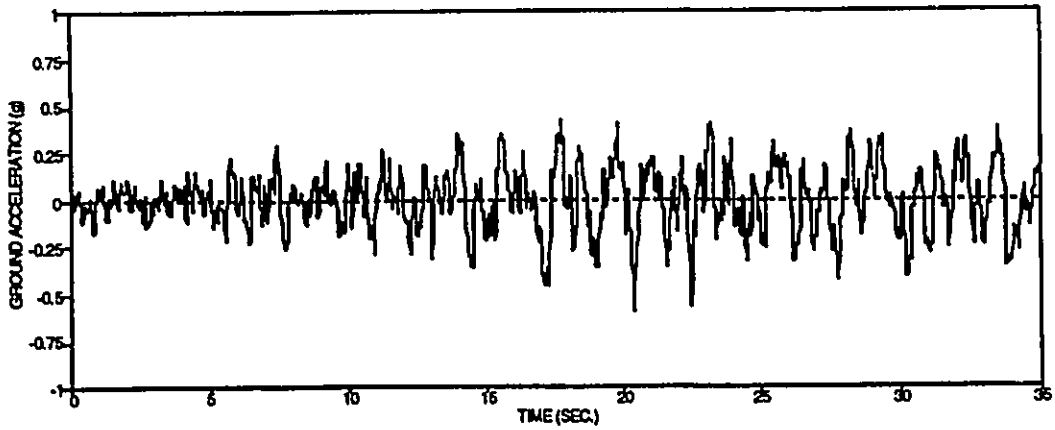

c) Vertical Component

Figure 5.4 Acceleration Time History Components of the LS3 Record

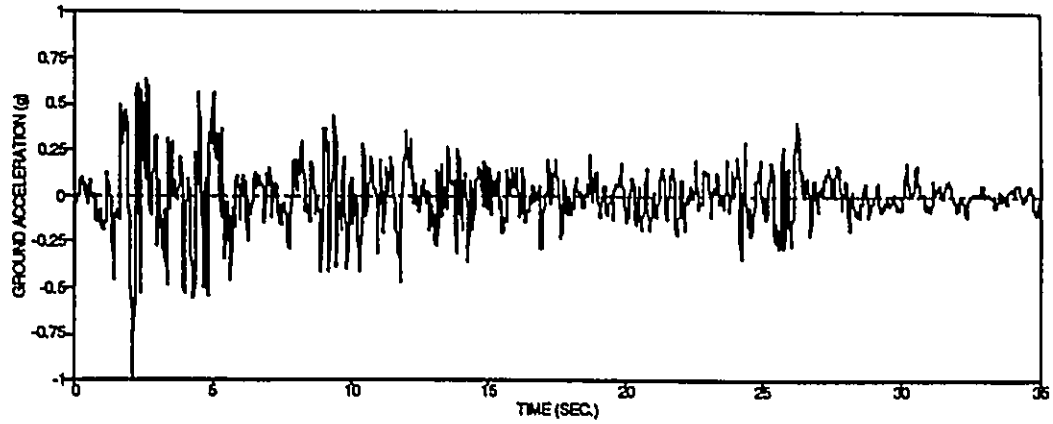

a) Longitudinal Component

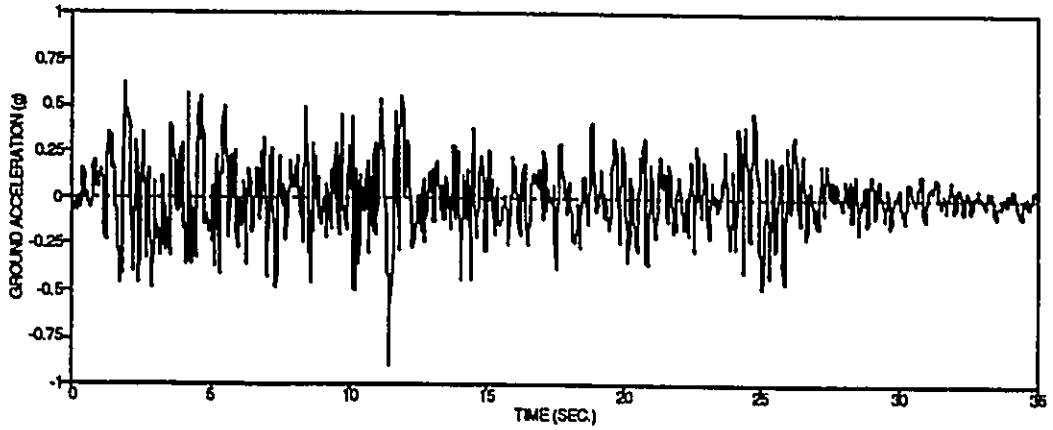

b) Transverse Component

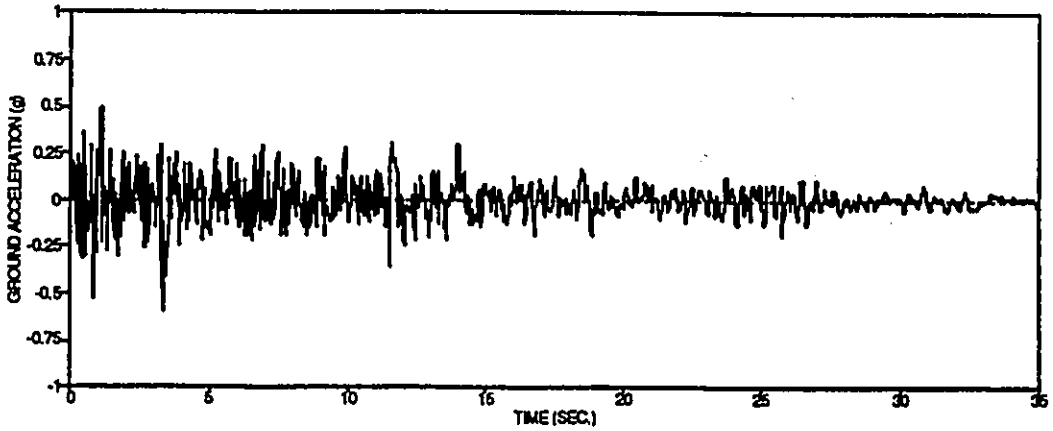

c) Vertical Component

Figure 5.5 Acceleration Time History Components of the IS1 Record

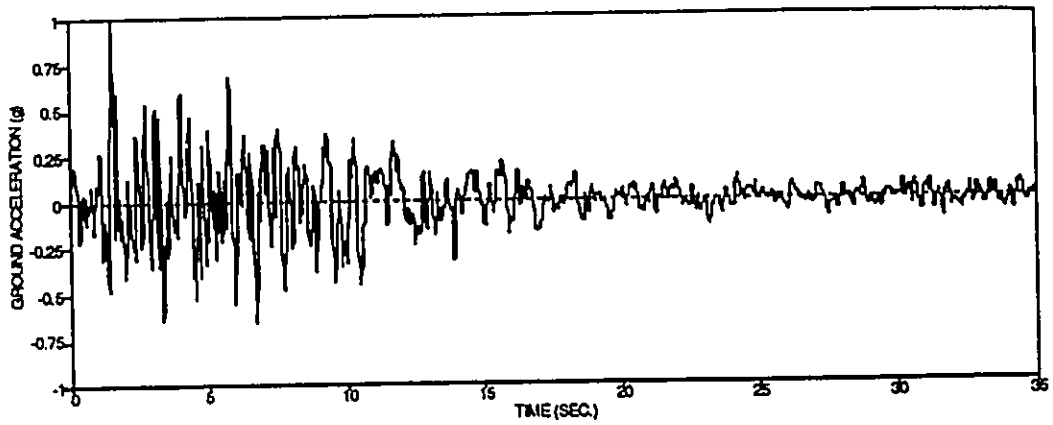

a) Longitudinal Component

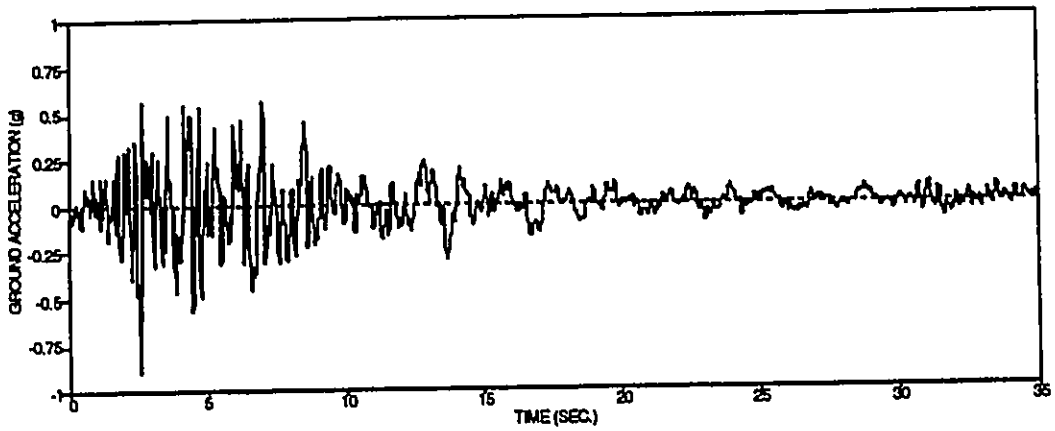

b) Transverse Component

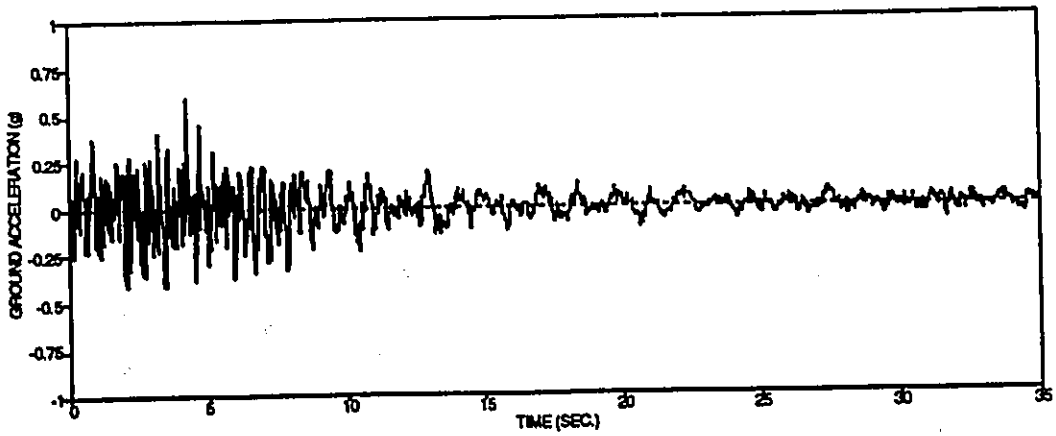

c) Vertical Component

Figure 5.6 Acceleration Time History Components of the IS2 Record

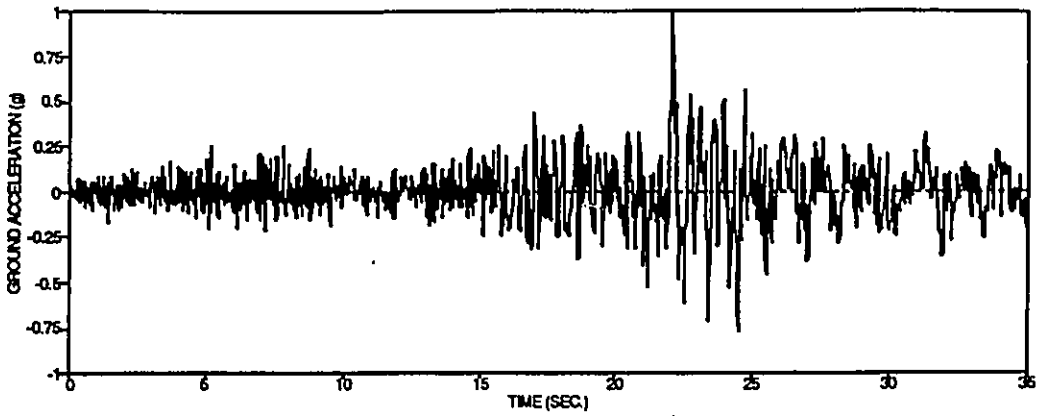

a) Longitudinal Component

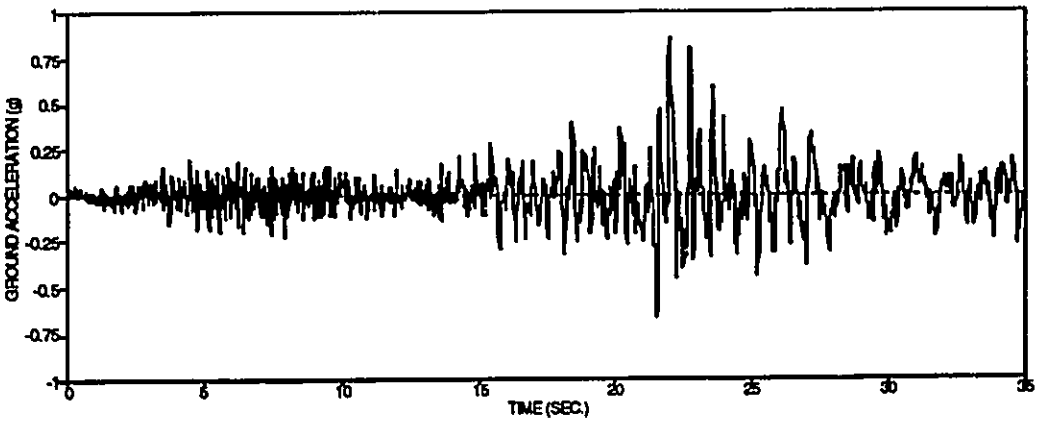

b) Transverse Component

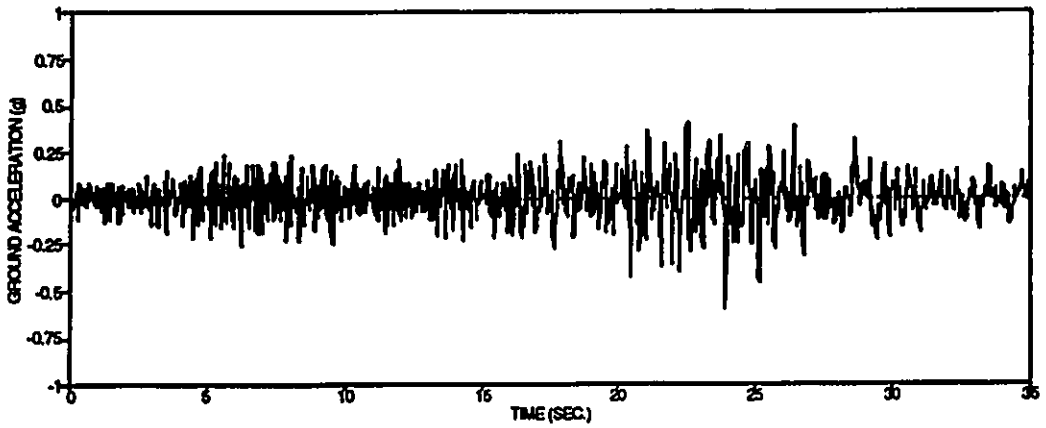

c) Vertical Component

Figure 5.7 Acceleration Time History Components of the IS3 Record

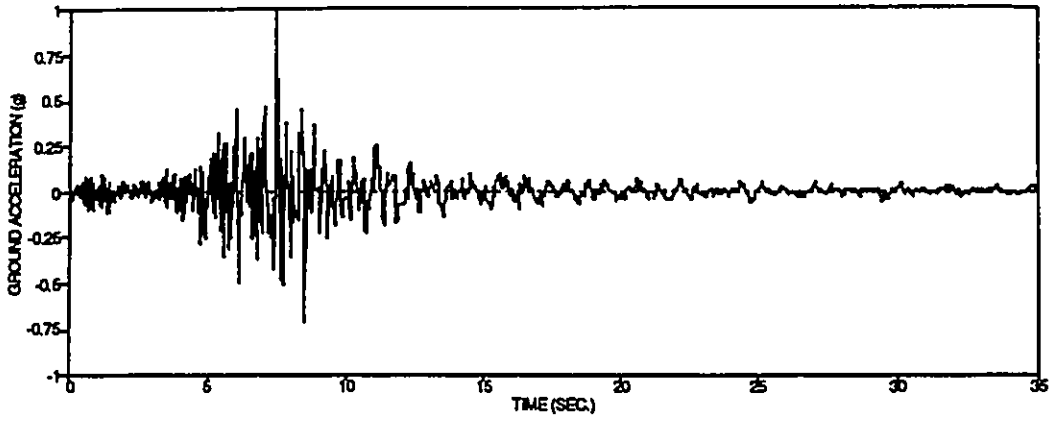

a) Longitudinal Component

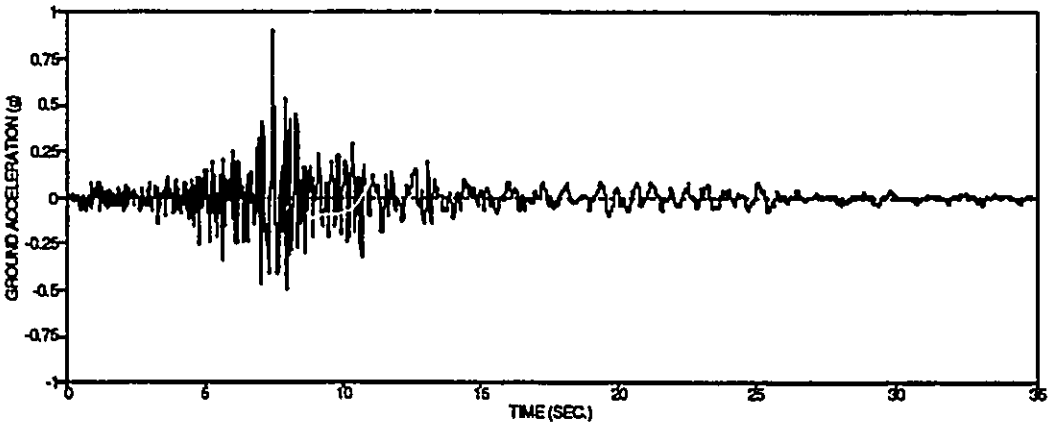

b) Transverse Component

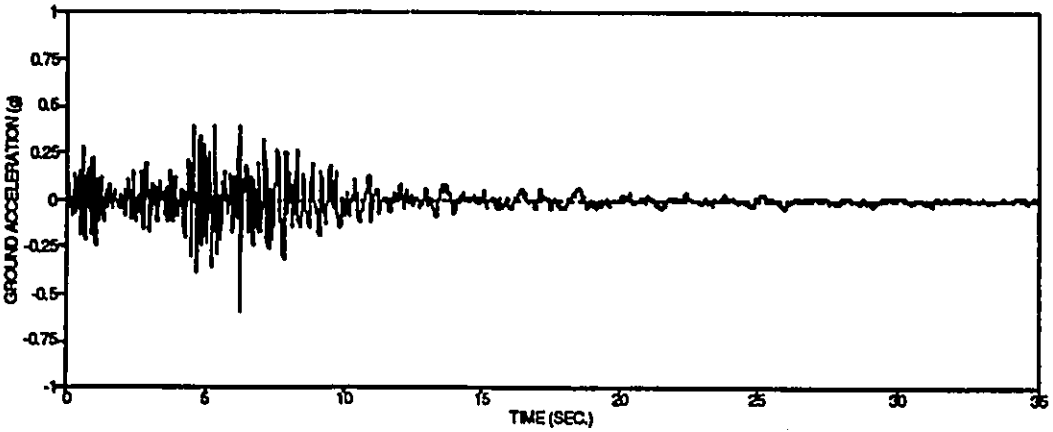

c) Vertical Component

Figure 5.8 Acceleration Time History Components of the HS1 Record

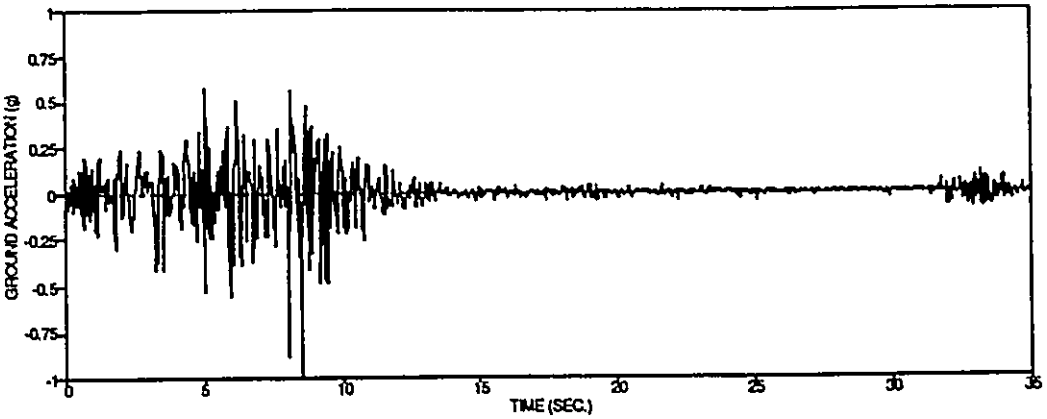

a) Longitudinal Component

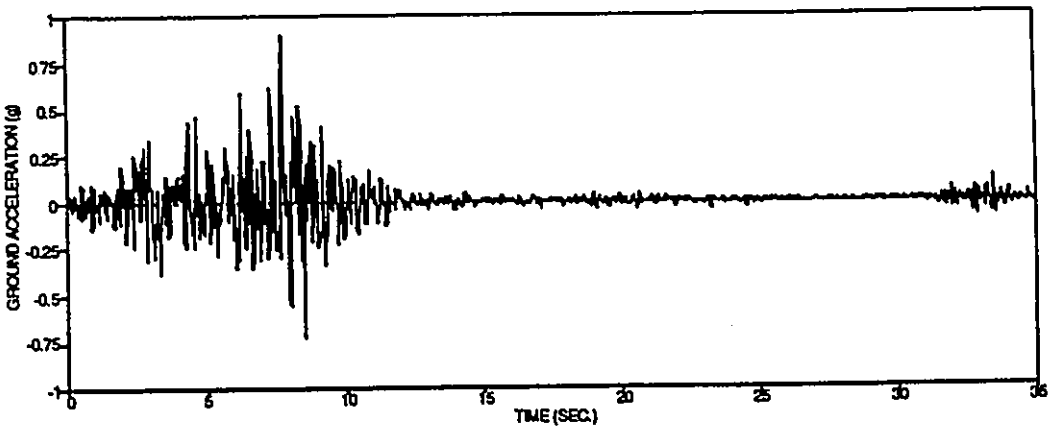

b) Transverse Component

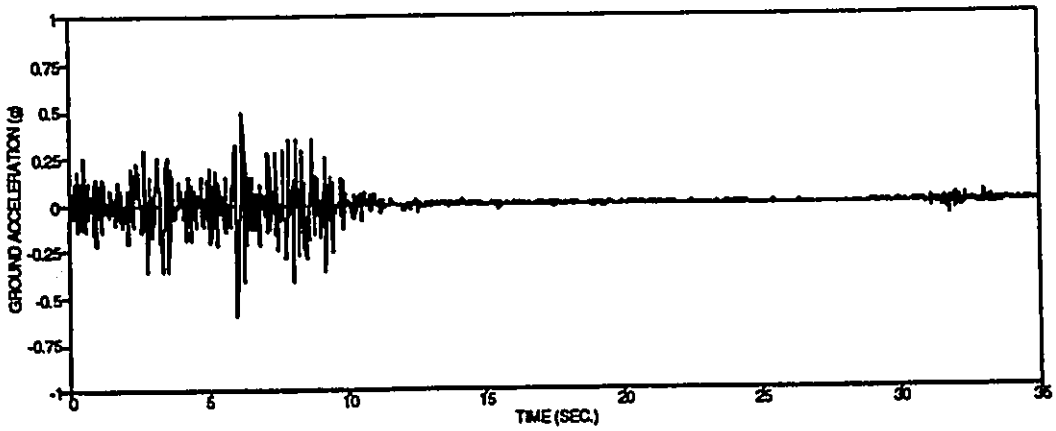

c) Vertical Component

Figure 5.9 Acceleration Time History Components of the HS2 Record

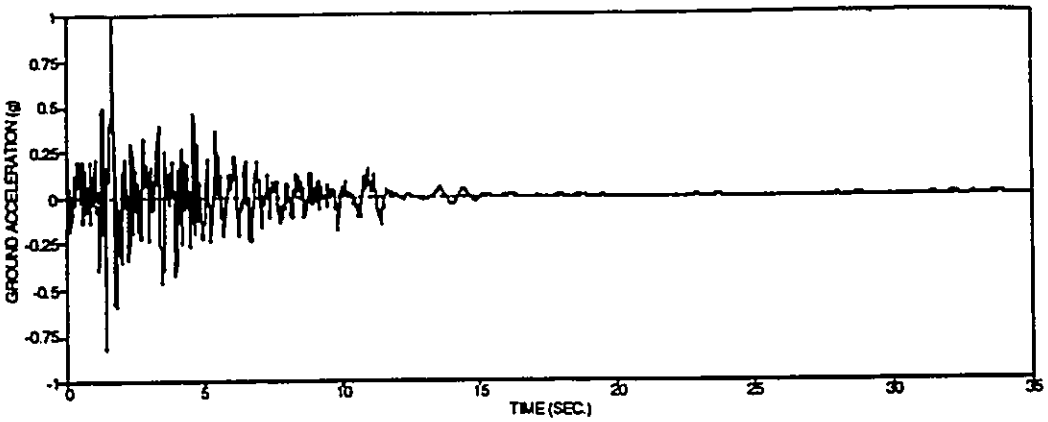

a) Longitudinal Component

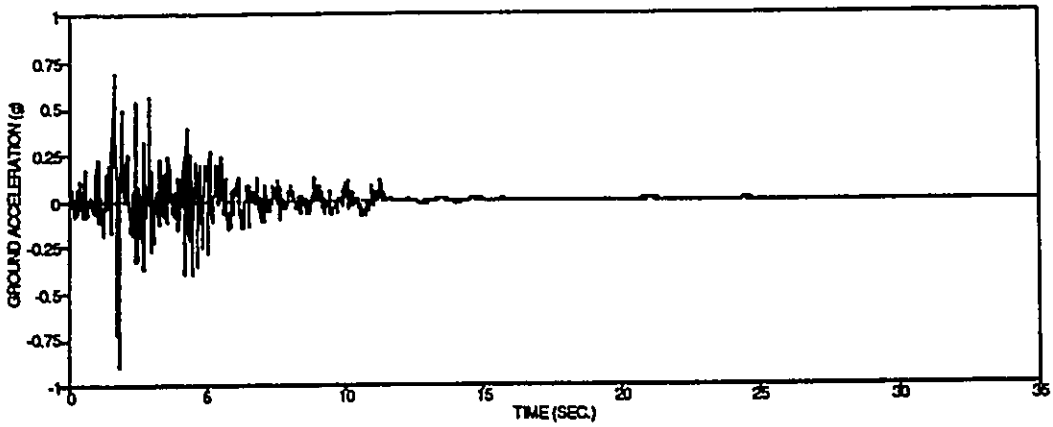

b) Transverse Component

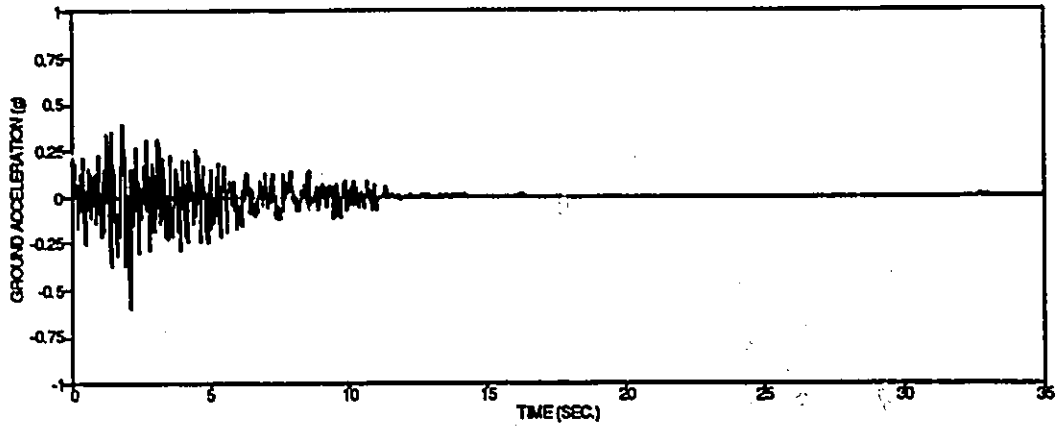

c) Vertical Component

Figure 5.10 Acceleration Time History Components of the HS3 Record

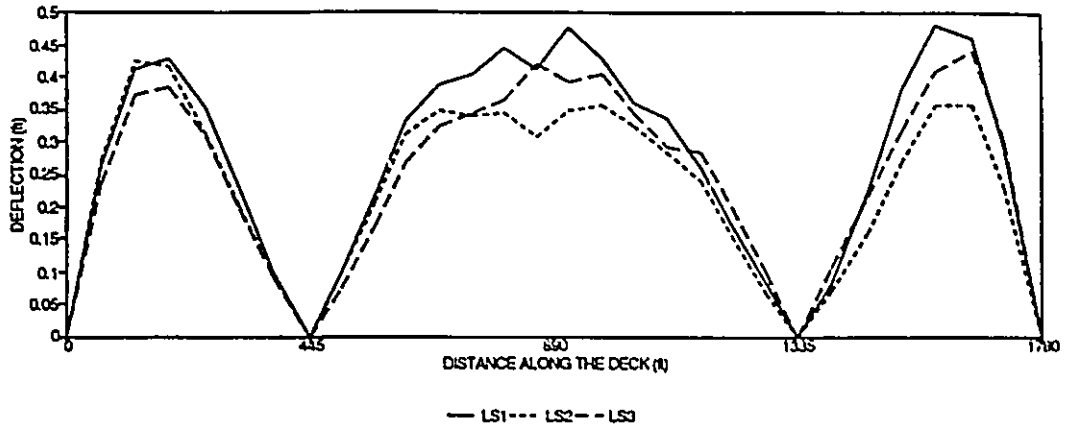

a) Low Frequency Content

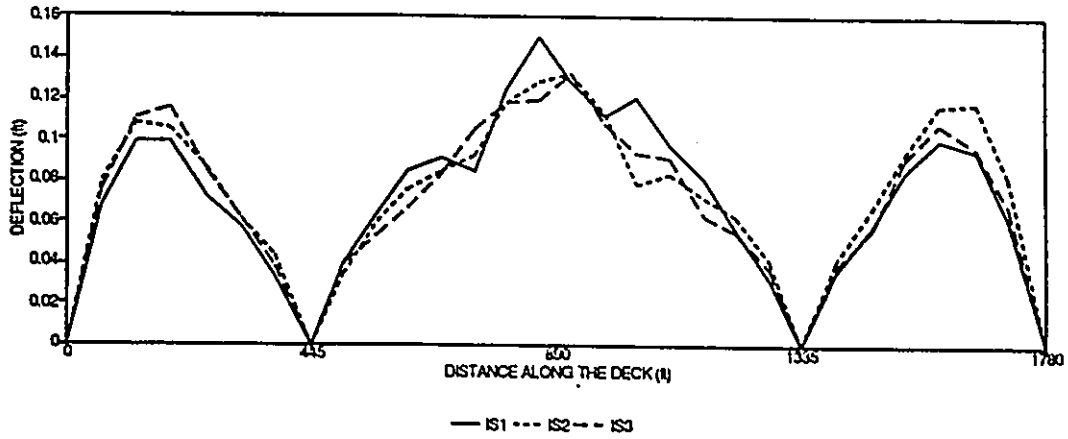

b) Intermediate Frequency Content

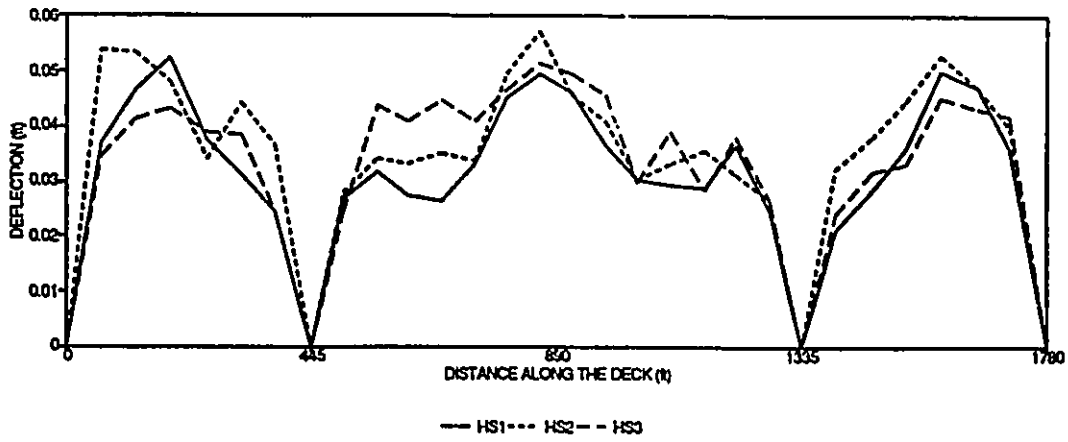

c) High Frequency Content

Figure 5.11 Effect of Input Motion Frequency Content on the Quincy Bayview Bridge Deck Vertical Deflection

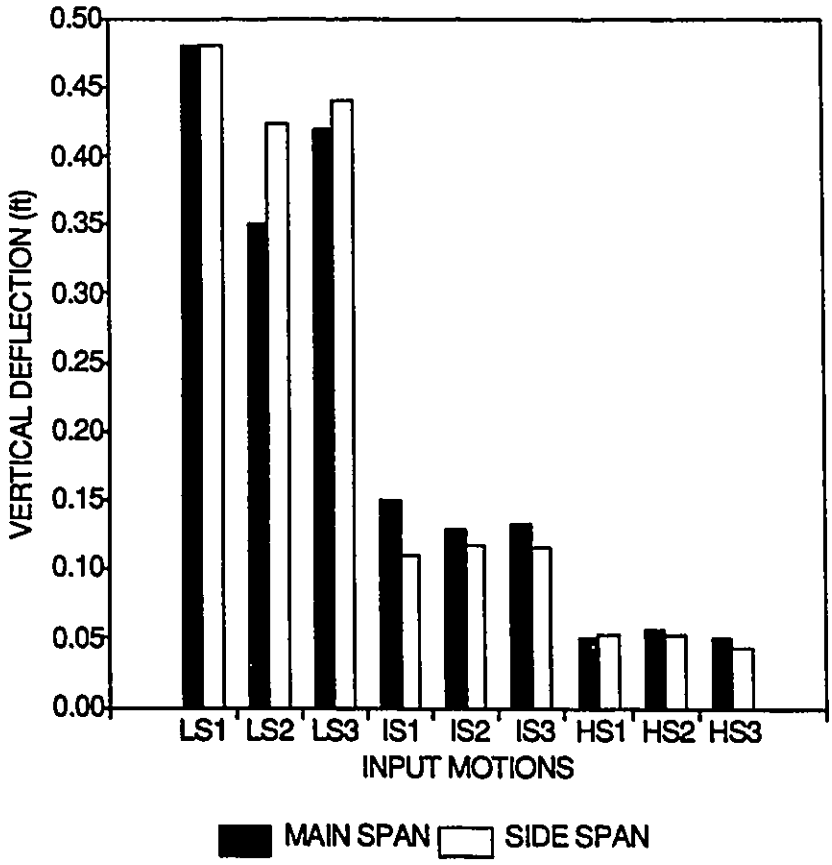

Figure 5.12 Maximum Vertical Deflection in the Main Span and Side Span of the Quincy Bayview Bridge Deck Under Different Frequency Content Input Motions

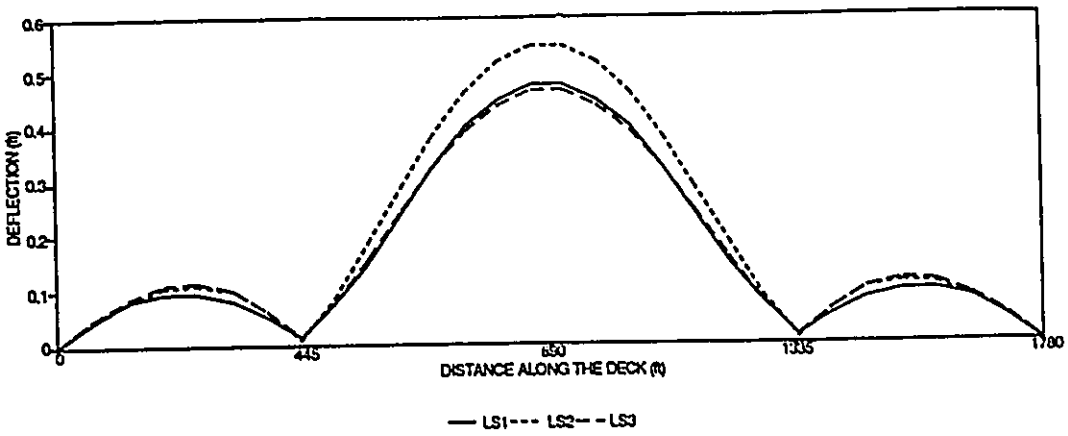

a) Low Frequency Content

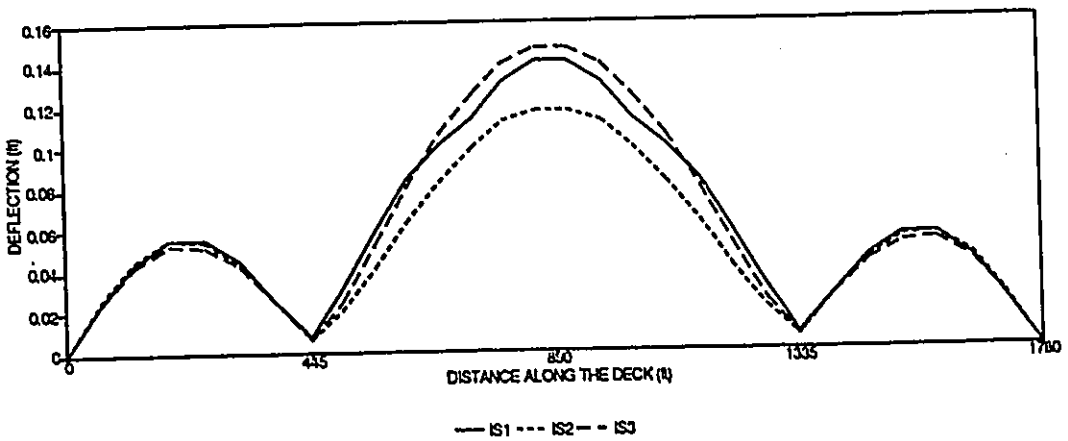

b) Intermediate Frequency Content

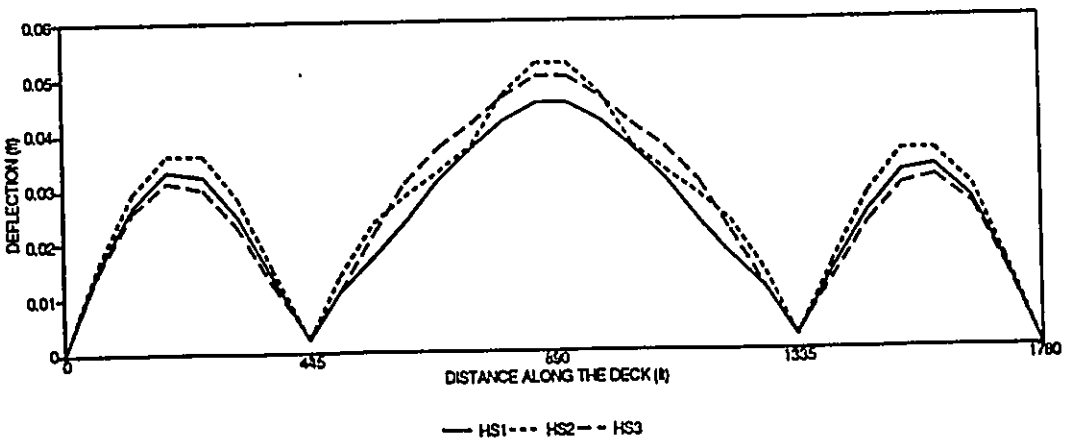

c) High Frequency Content

Figure 5.13 Effect of Input Motion Frequency Content on the Quincy Bayview Bridge Deck Transverse Deflection

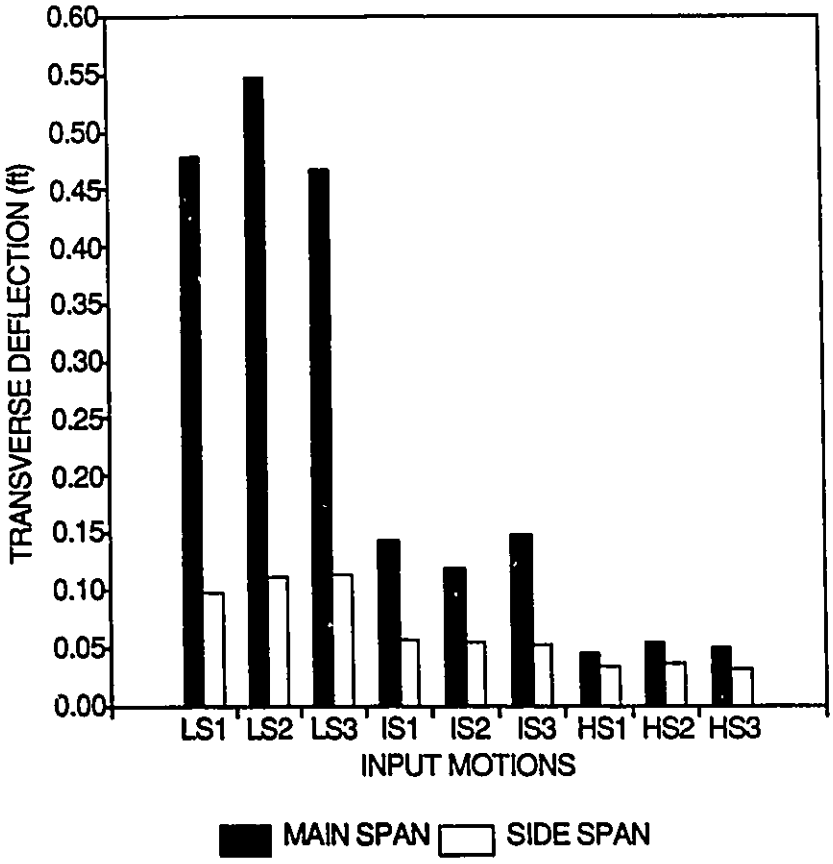

Figure 5.14 Maximum Transverse Deflection in the Main Span and Side Span of the Quincy Bayview Bridge Deck Under Different Frequency Content Input Motions

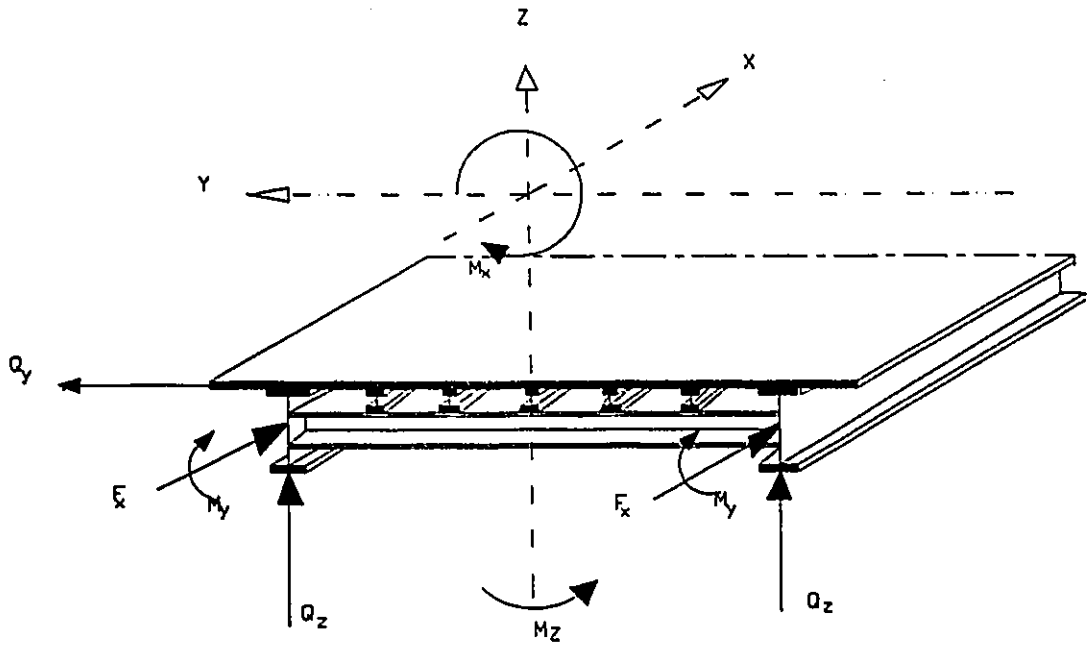

Figure 5.15 Directions of the Different Internal Forces of the Bridge Deck Cross-Section

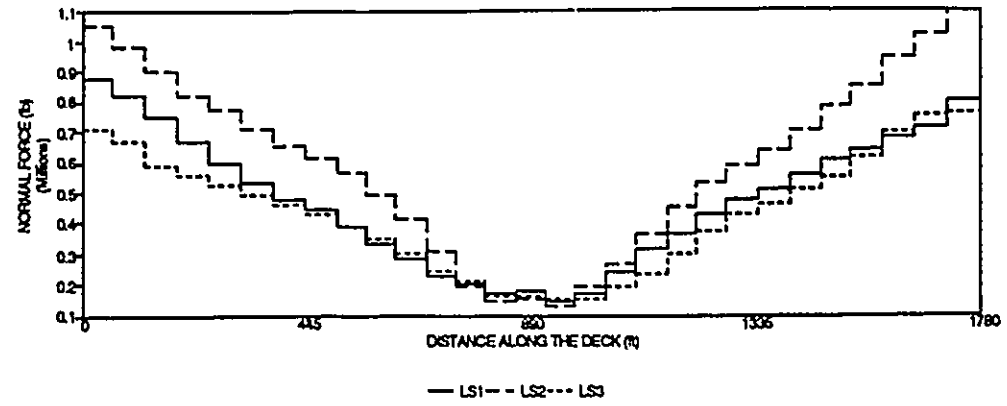

a) Low Frequency Content

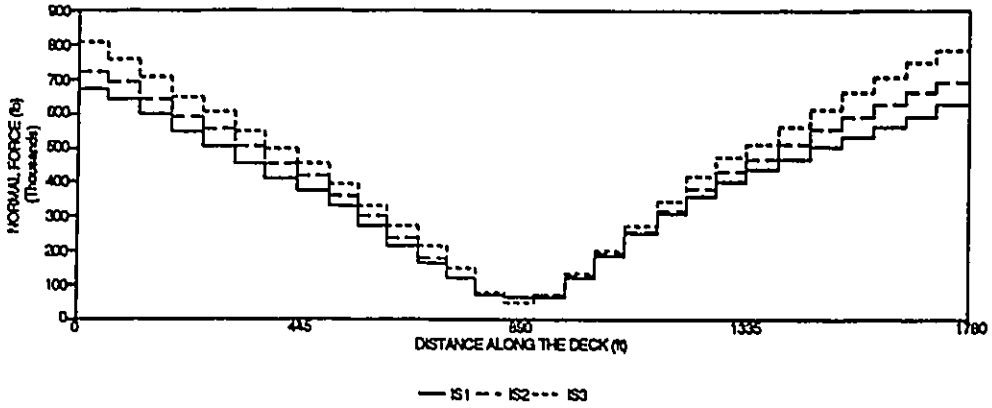

b) Intermediate Frequency Content

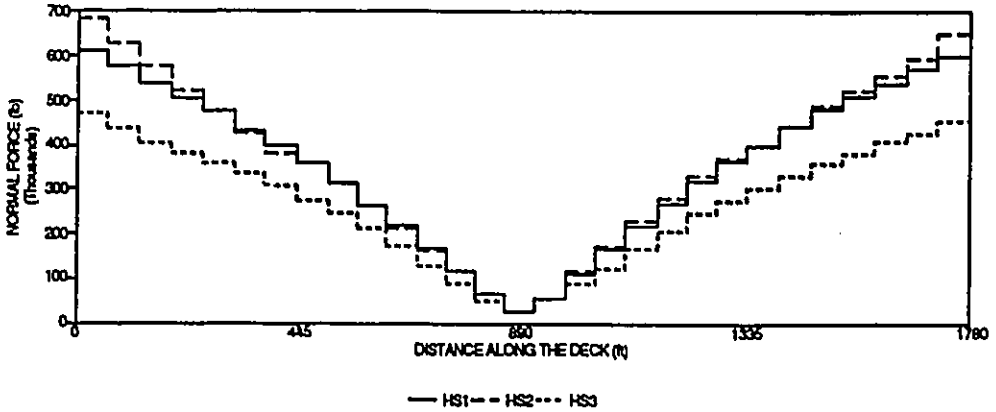

c) High Frequency Content

Figure 5.16 Effect of Input Motion Frequency Content on the Quincy Bayview Bridge Deck Normal Force (F_x)

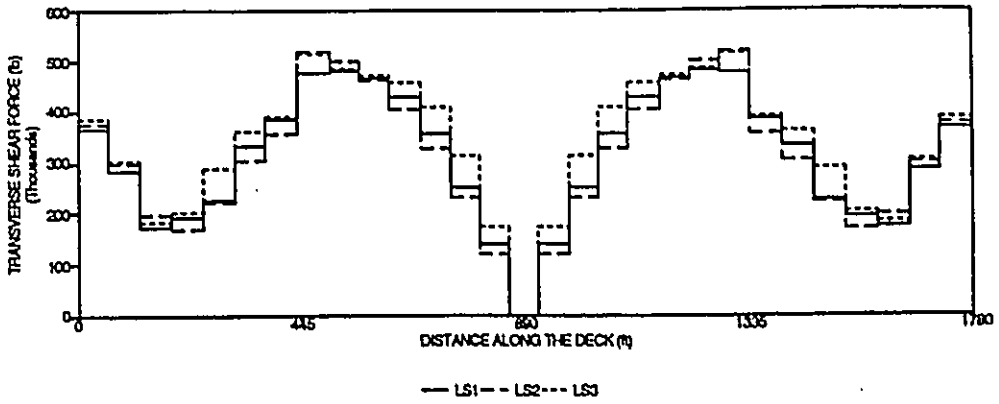

a) Low Frequency Content

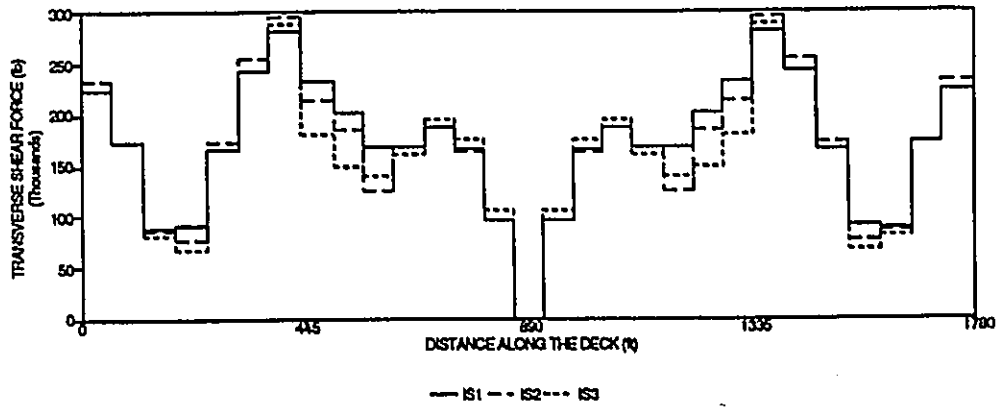

b) Intermediate Frequency Content

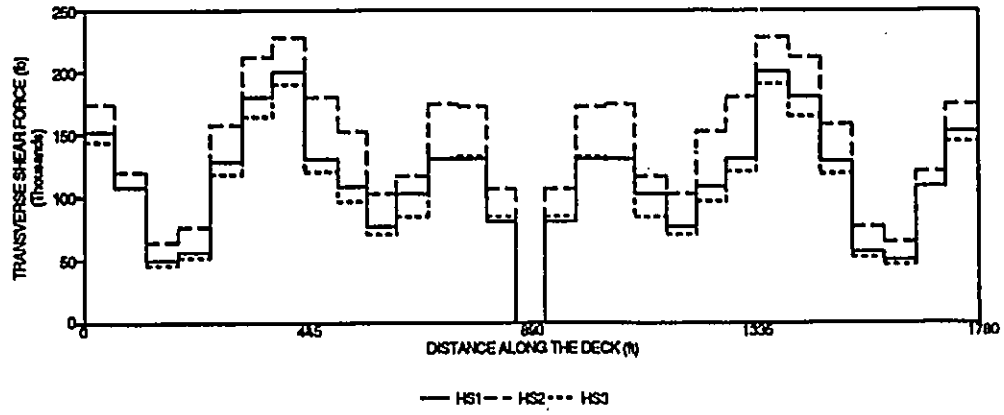

c) High Frequency Content

Figure 5.17 Effect of Input Motion Frequency Content on the Quincy Bayview Bridge Deck Transverse Shear Force (Q_y)

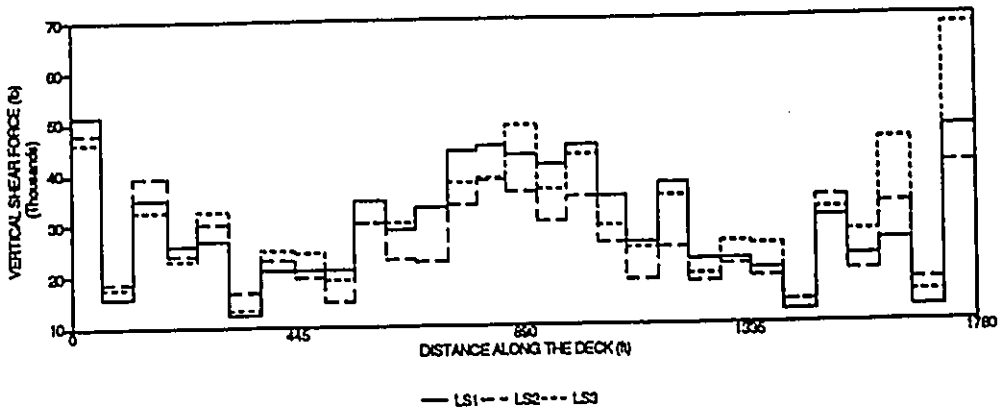

a) Low Frequency Content

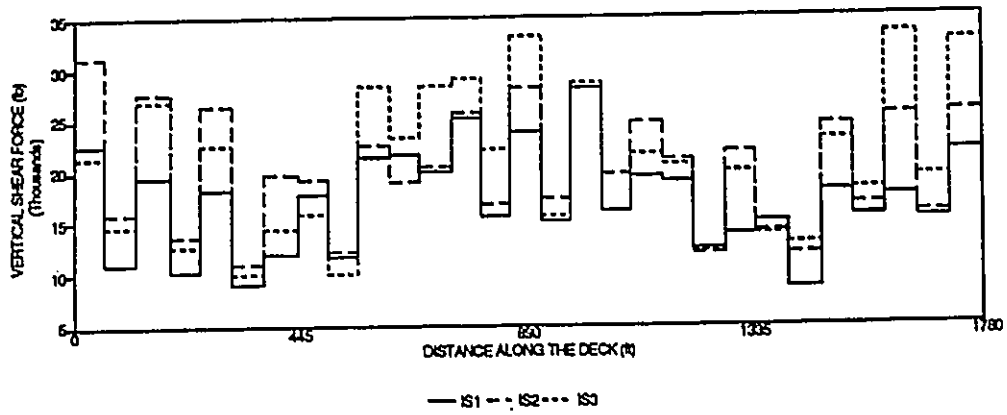

b) Intermediate Frequency Content

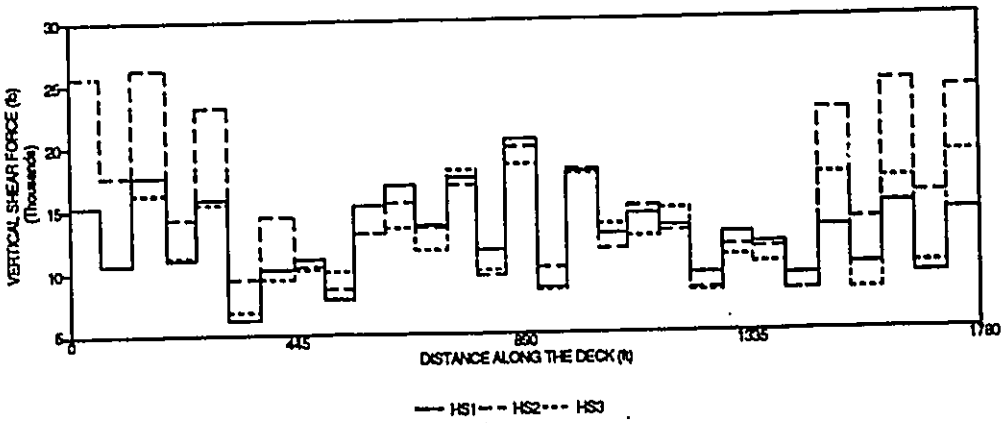

c) High Frequency Content

Figure 5.18 Effect of Input Motion Frequency Content on the Quincy Bayview Bridge Deck Vertical Shear Force (Q_z)

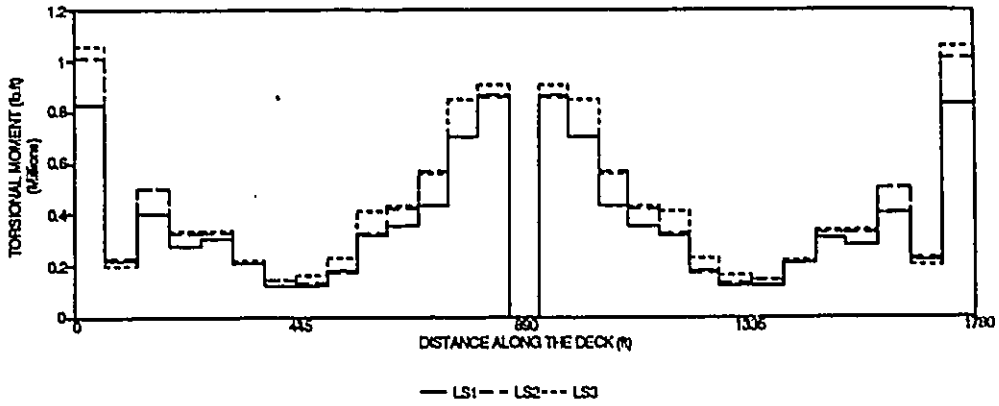

a) Low Frequency Content

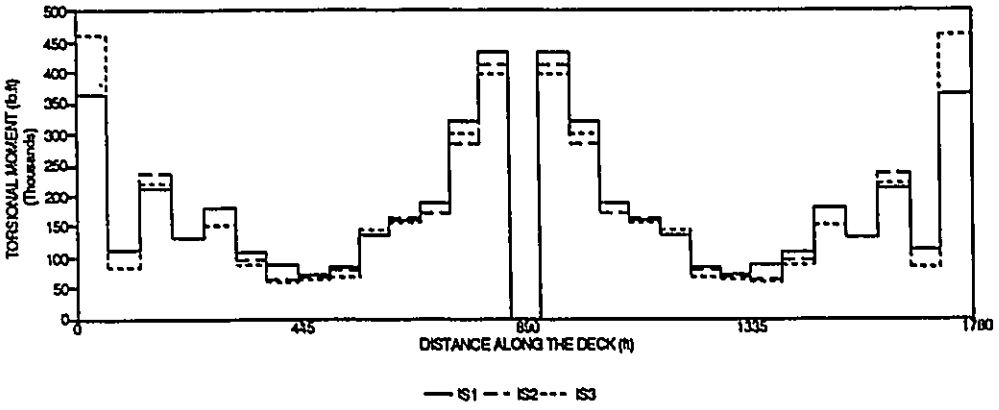

b) Intermediate Frequency Content

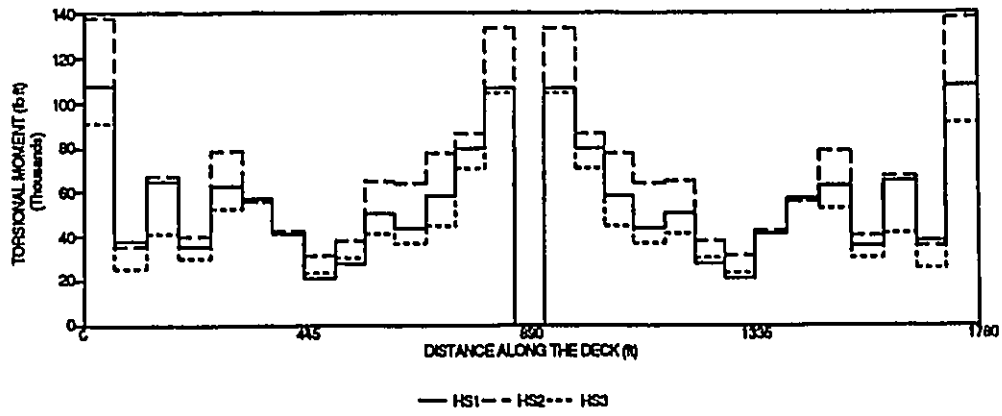

c) High Frequency Content

Figure 5.19 Effect of Input Motion Frequency Content on the Quincy Bayview Bridge Deck Torsional Moment (M_x)

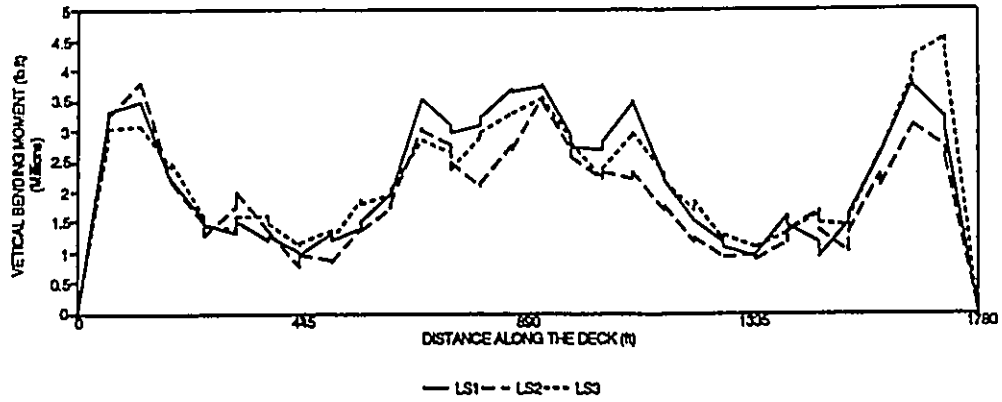

a) Low Frequency Content

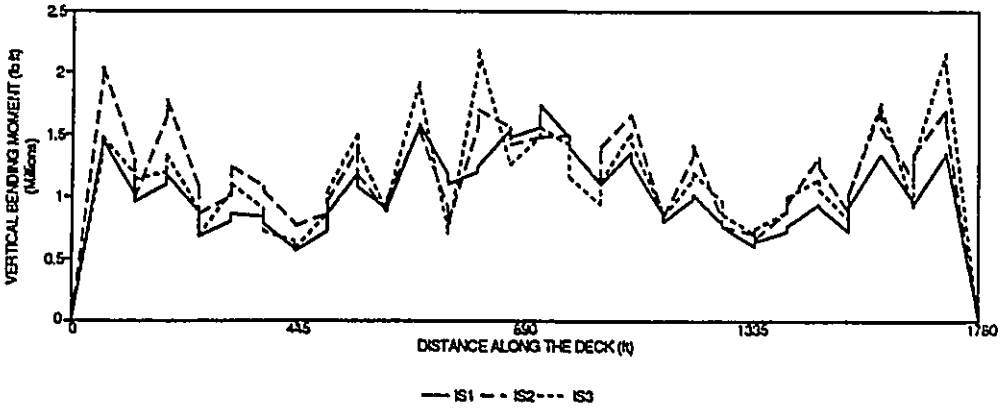

b) Intermediate Frequency Content

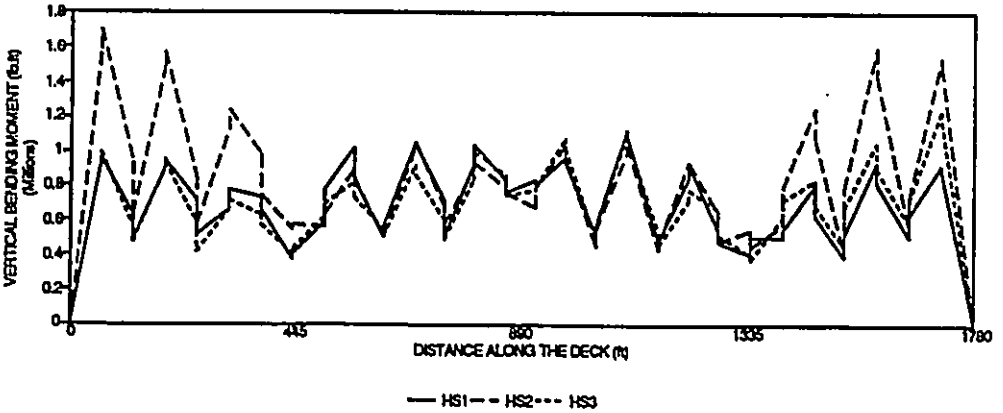

c) High Frequency Content

Figure 5.20 Effect of Input Motion Frequency Content on the Quincy Bayview Bridge Deck Vertical Bending Moment (M_y)

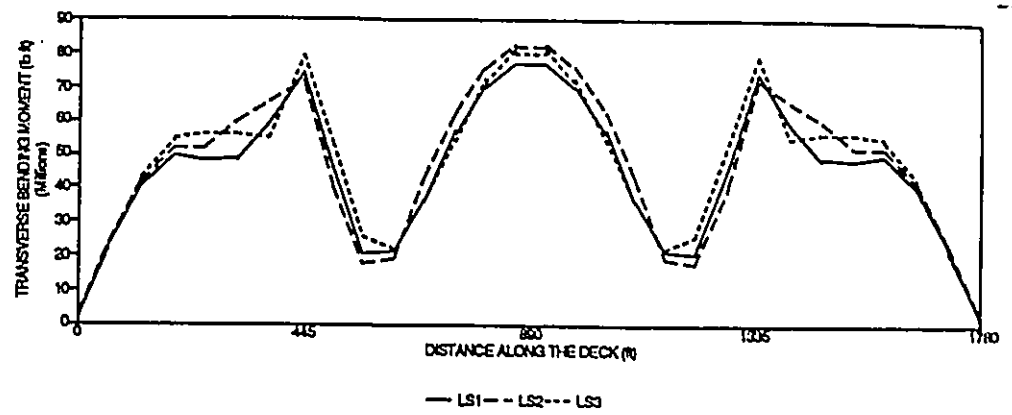

a) Low Frequency Content

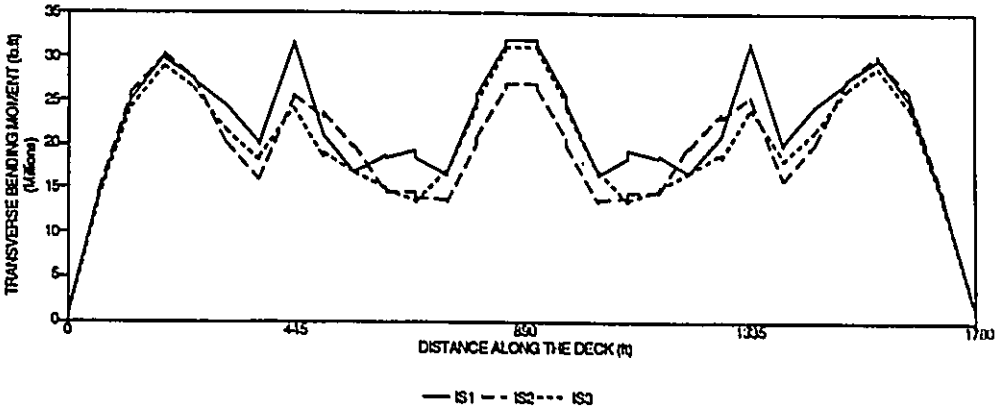

b) Intermediate Frequency Content

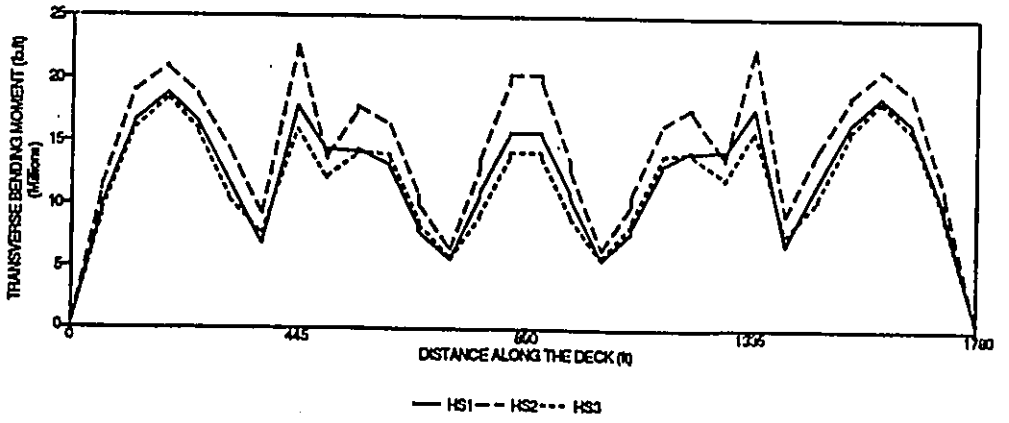

c) High Frequency Content

Figure 5.21 Effect of Input Motion Frequency Content on the Quincy Bayview Bridge Deck Transverse Bending Moment (M_z)

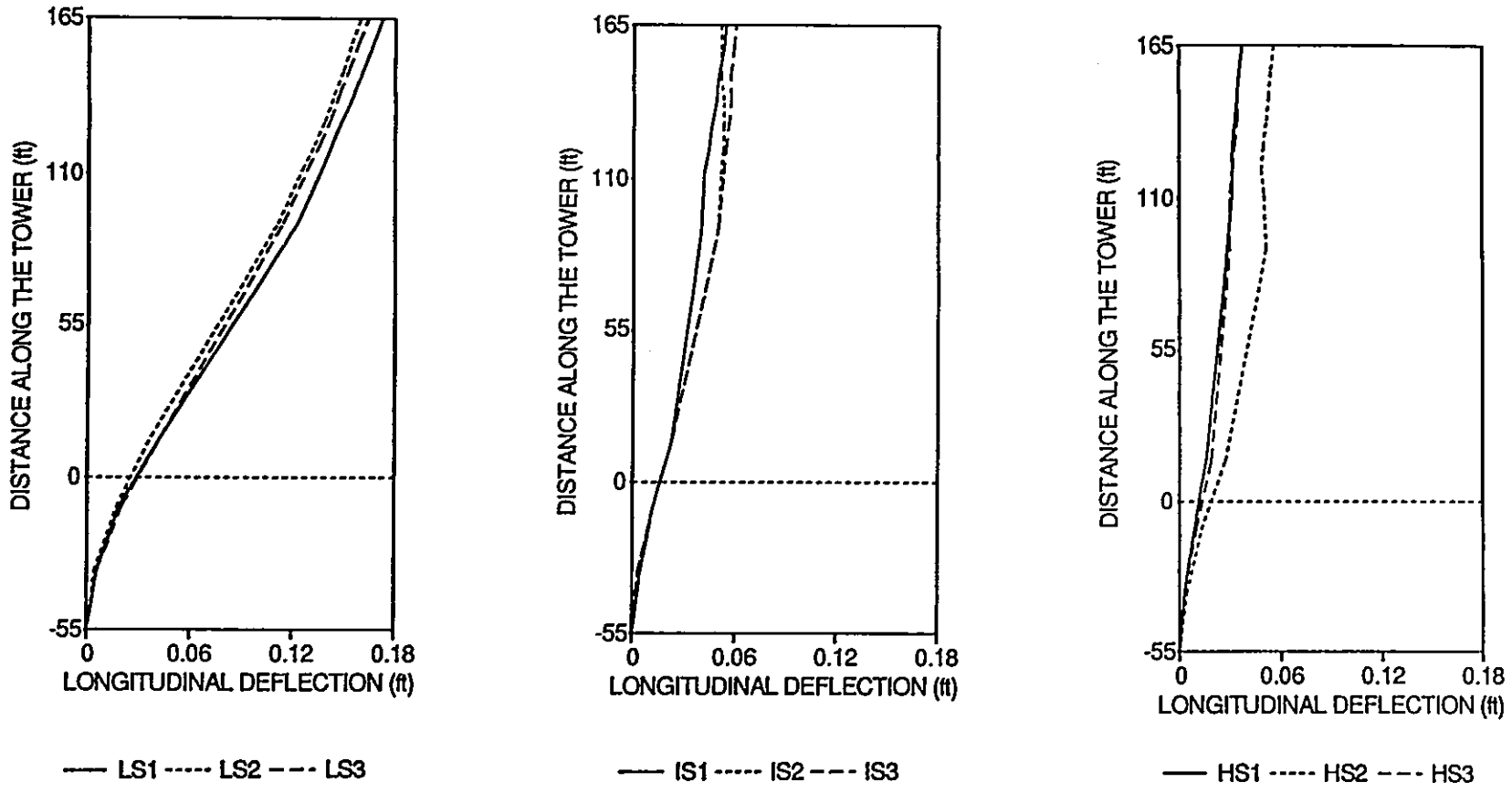

a) Low Frequency Content

b) Intermediate Frequency Content

c) High Frequency Content

Figure 5.22 Effect of Input Motion Frequency Content on the Quincy Bayview Bridge Tower Longitudinal Deflection

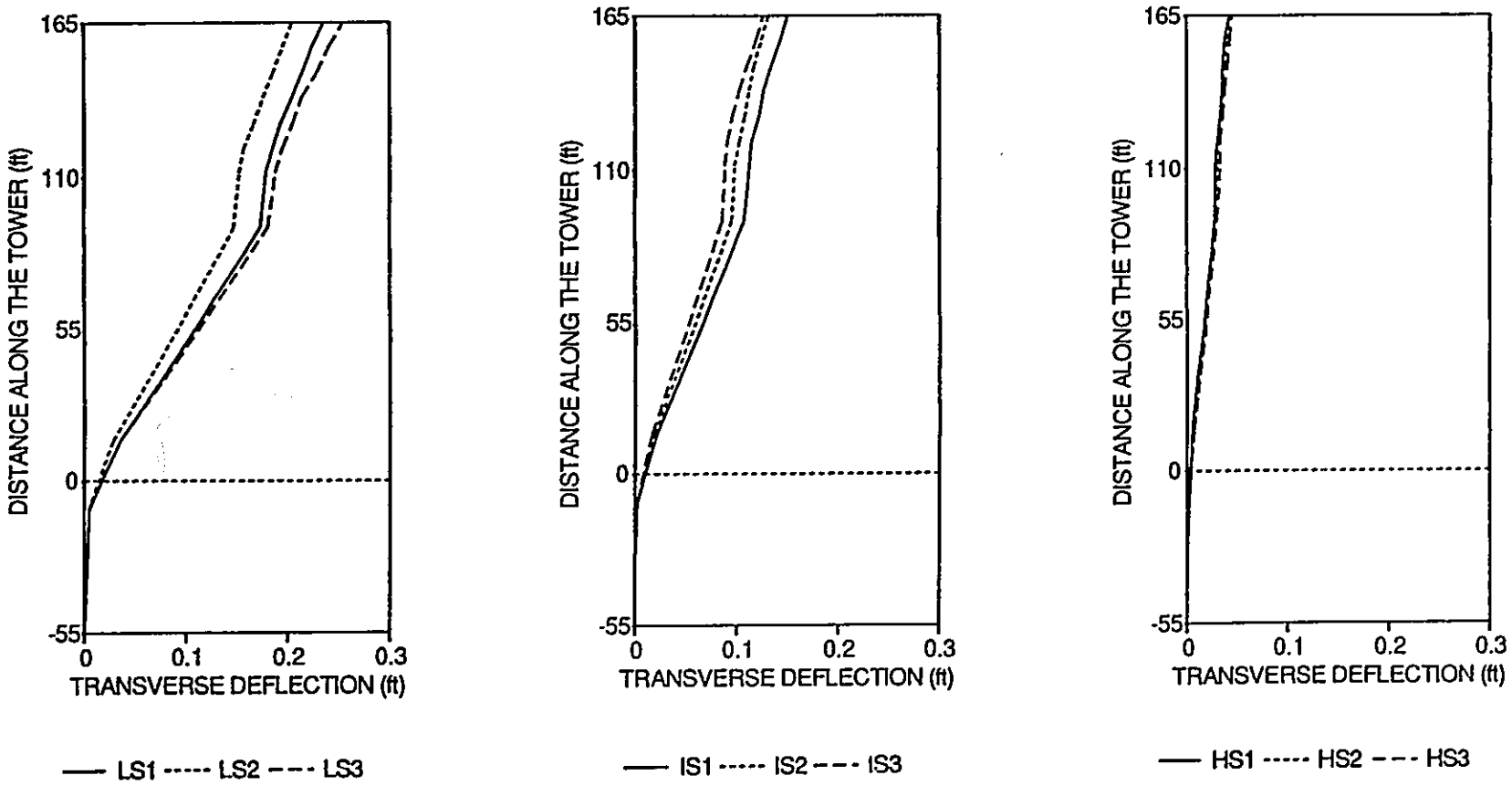

a) Low Frequency Content

b) Intermediate Frequency Content

c) High Frequency Content

Figure 5.23 Effect of Input Motion Frequency Content on the Quincy Bayview Bridge Tower Transverse Deflection

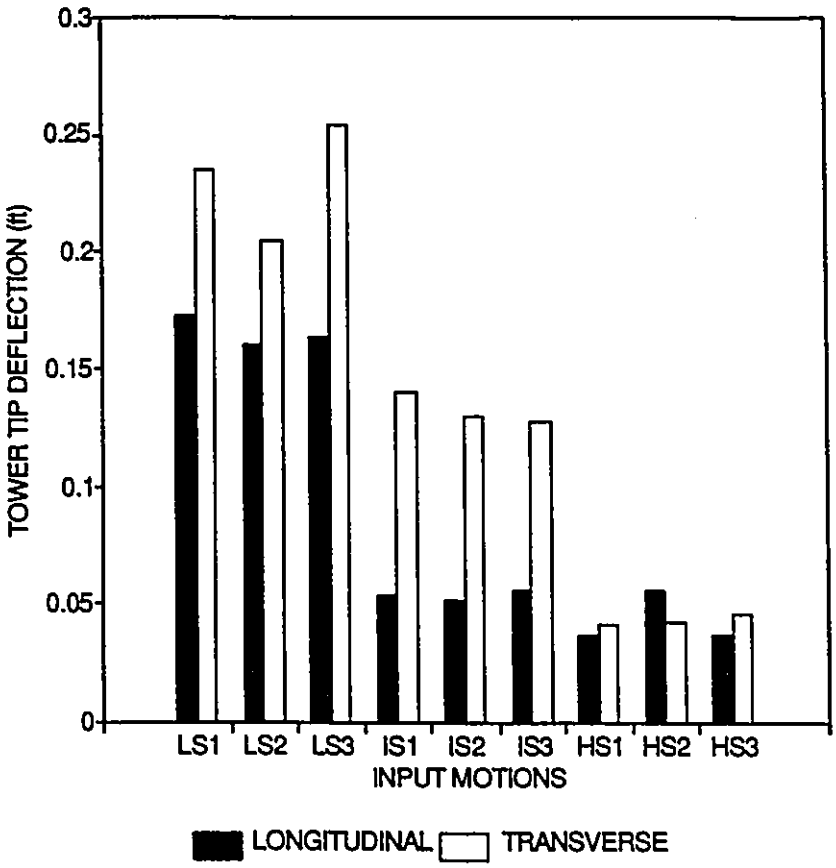

Figure 5.24 Maximum Longitudinal and Transverse Tower Tip Deflection of the Quincy Bayview Bridge Under Different Frequency Content Input Motions

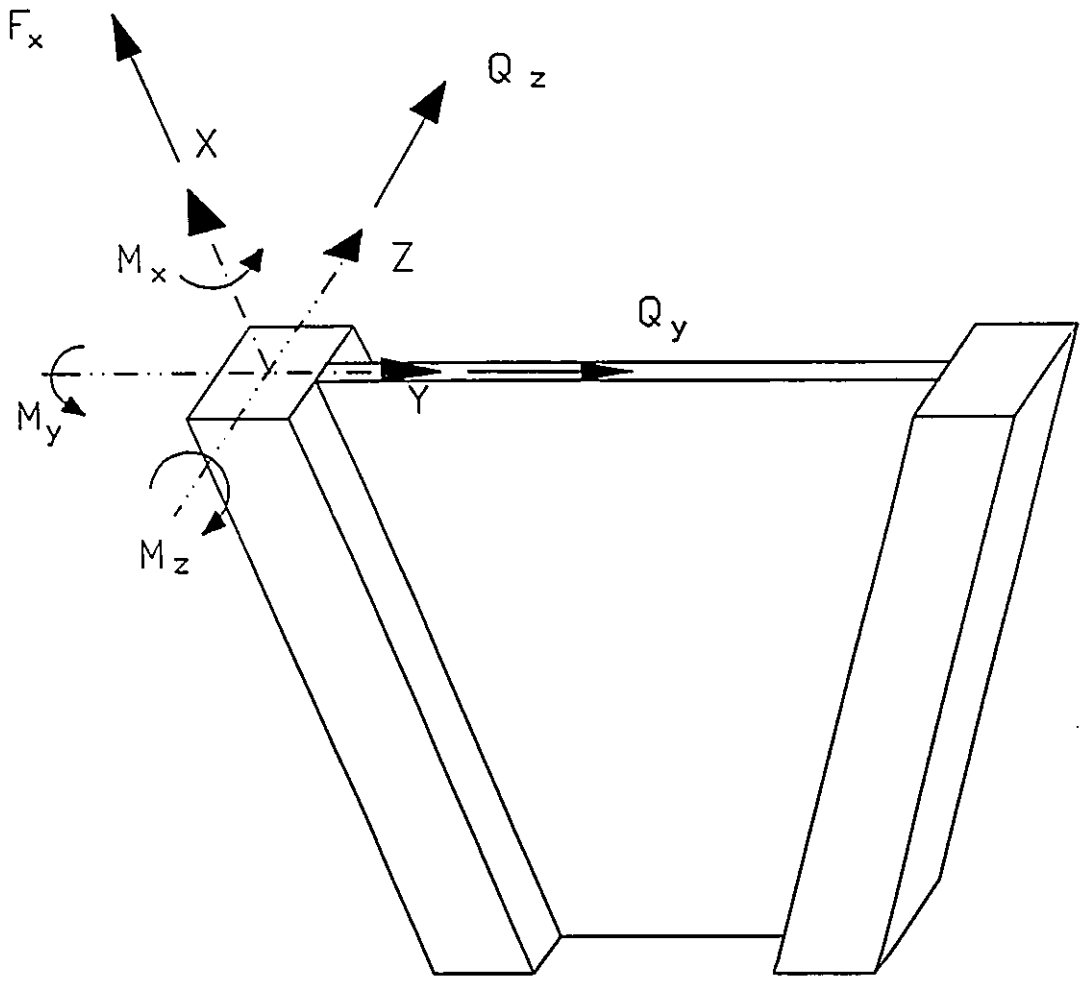

Figure 5.25 Directions of the Different Internal Forces

on the Quincy Bayview Bridge Tower Cross-Section

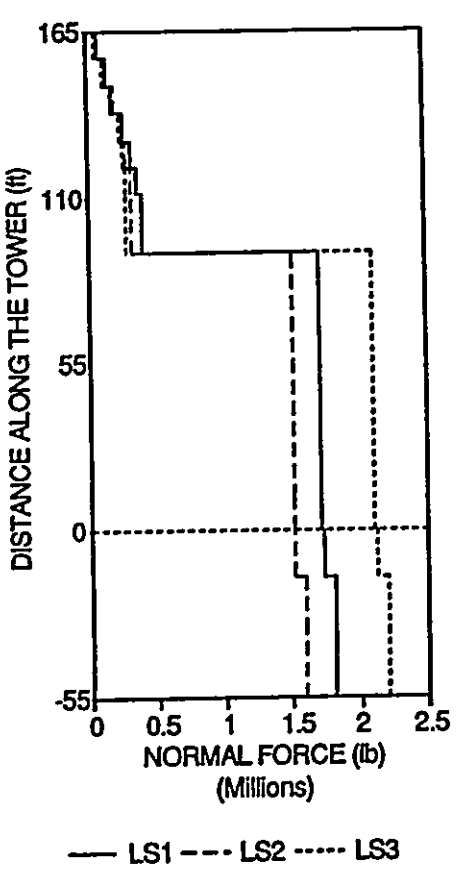

a) Low Frequency Content

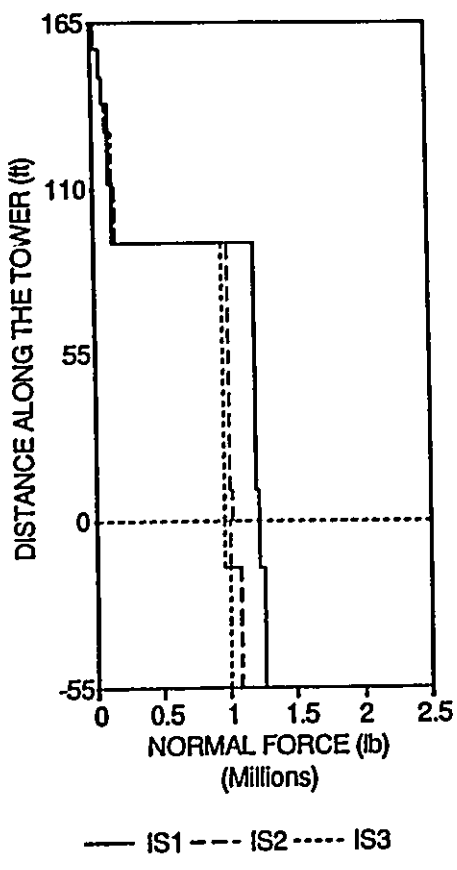

b) Intermediate Frequency Content

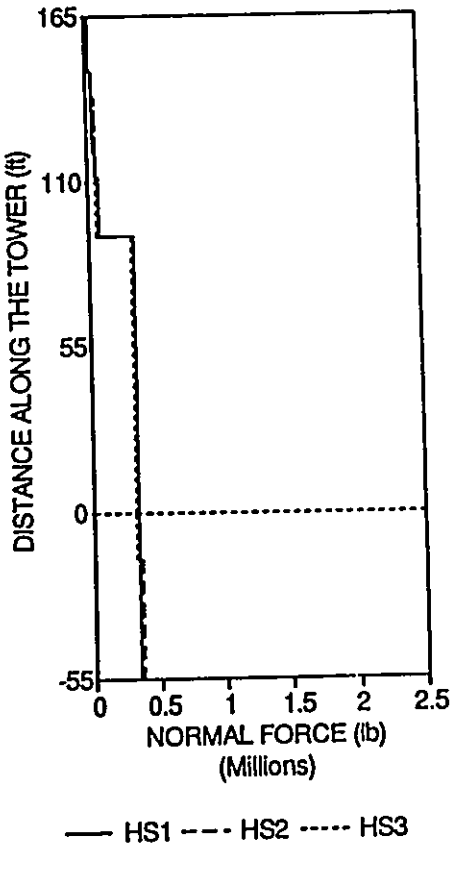

c) High Frequency Content

Figure 5.26 Effect of Input Motion Frequency Content on the Quincy Bayview Bridge Tower Normal Force (F_x)

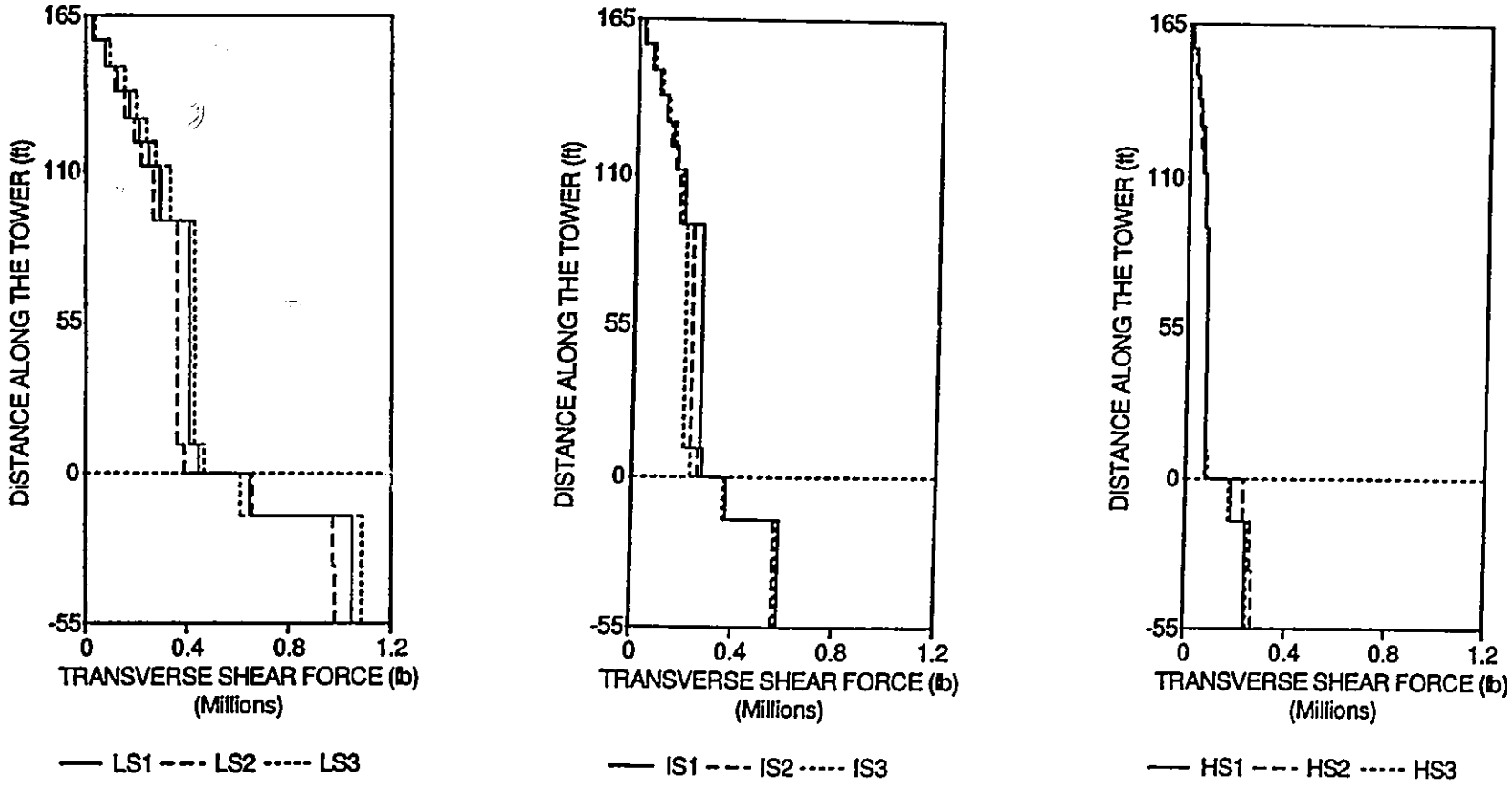

a) Low Frequency Content

b) Intermediate Frequency Content

c) High Frequency Content

Figure 5.27 Effect of Input Motion Frequency Content on the Quincy Bayview Bridge Tower Transverse Shear Force (Q_y)

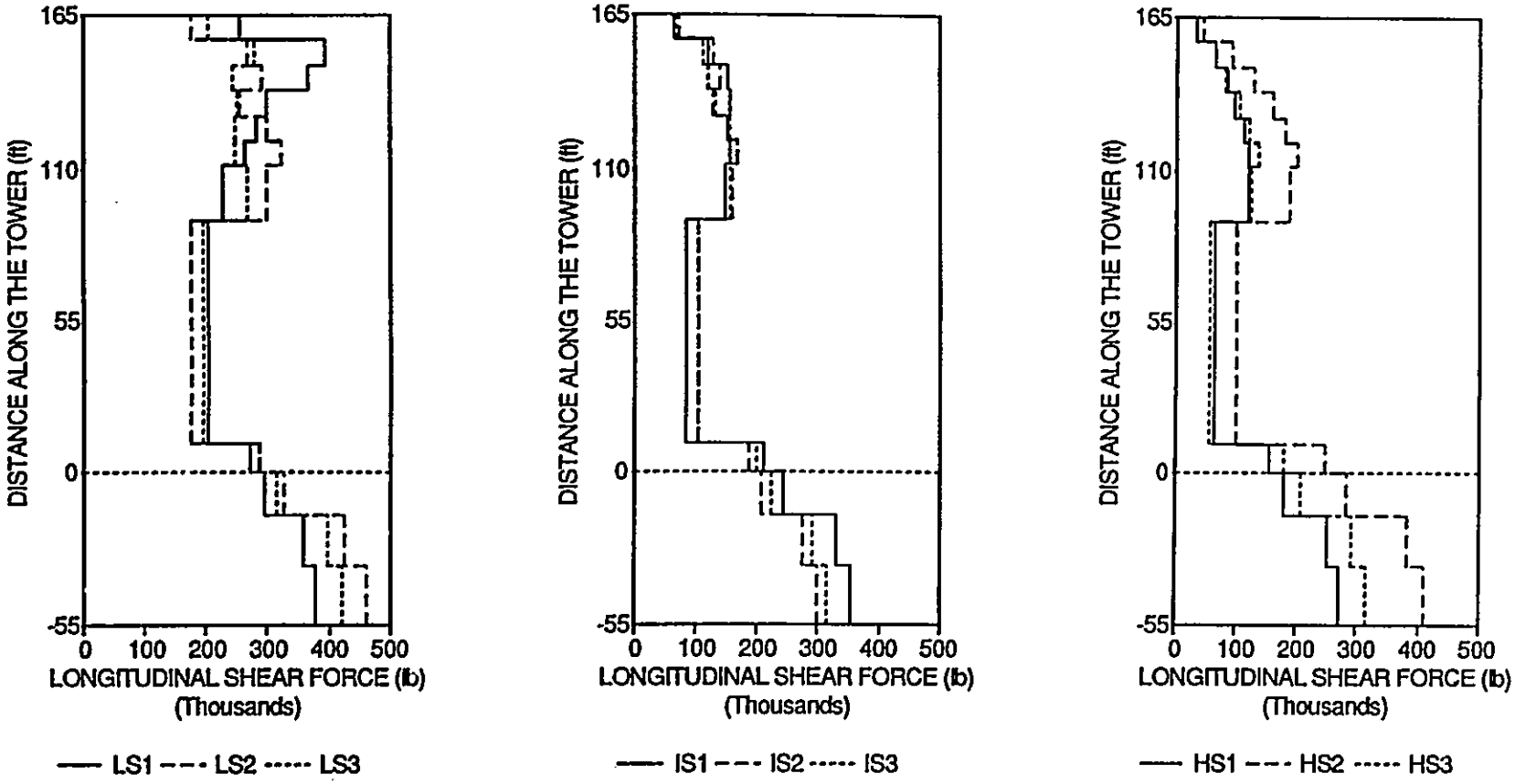

a) Low Frequency Content

b) Intermediate Frequency Content

c) High Frequency Content

Figure 5.28 Effect of Input Motion Frequency Content on the Quincy Bayview Bridge Tower Longitudinal Shear Force (Q_z)

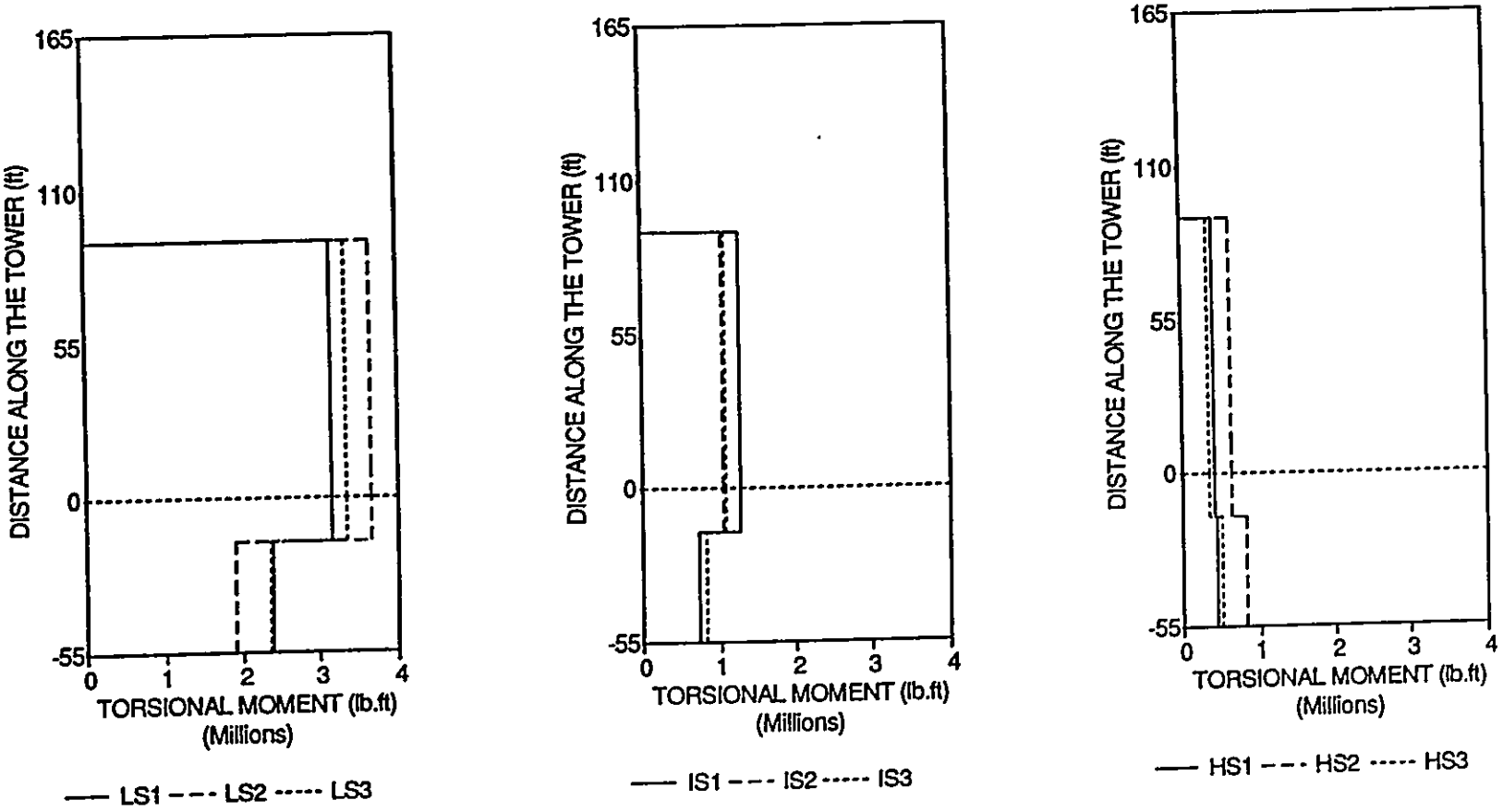

a) Low Frequency Content

b) Intermediate Frequency Content

c) High Frequency Content

Figure 5.29 Effect of Input Motion Frequency Content on the Quincy Bayview Bridge Tower Torsional Moment (M_t)

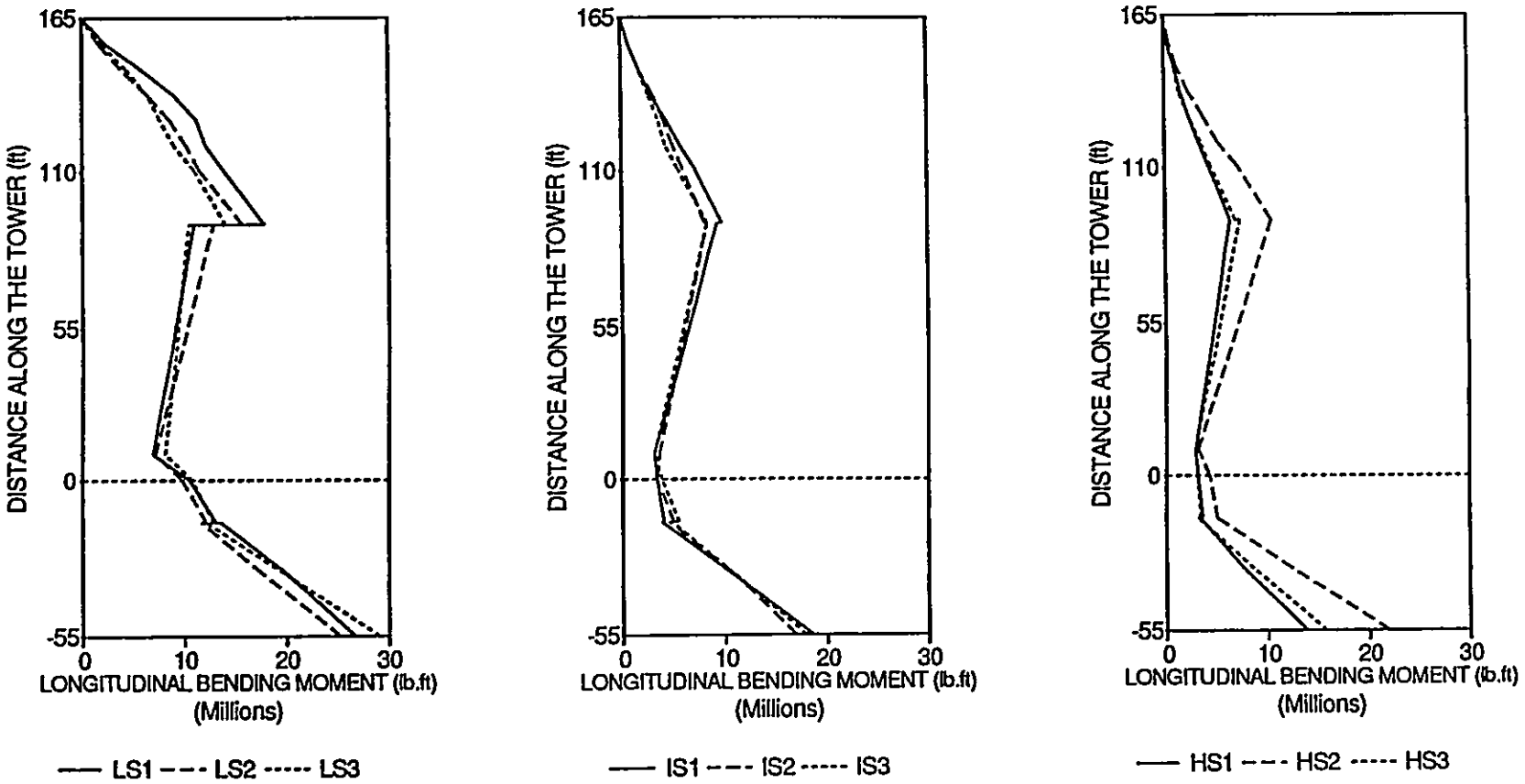

a) Low Frequency Content

b) Intermediate Frequency Content

c) High Frequency Content

Figure 5.30 Effect of Input Motion Frequency Content on the

Quincy Bayview Bridge Tower Longitudinal Bending Moment (M_y)

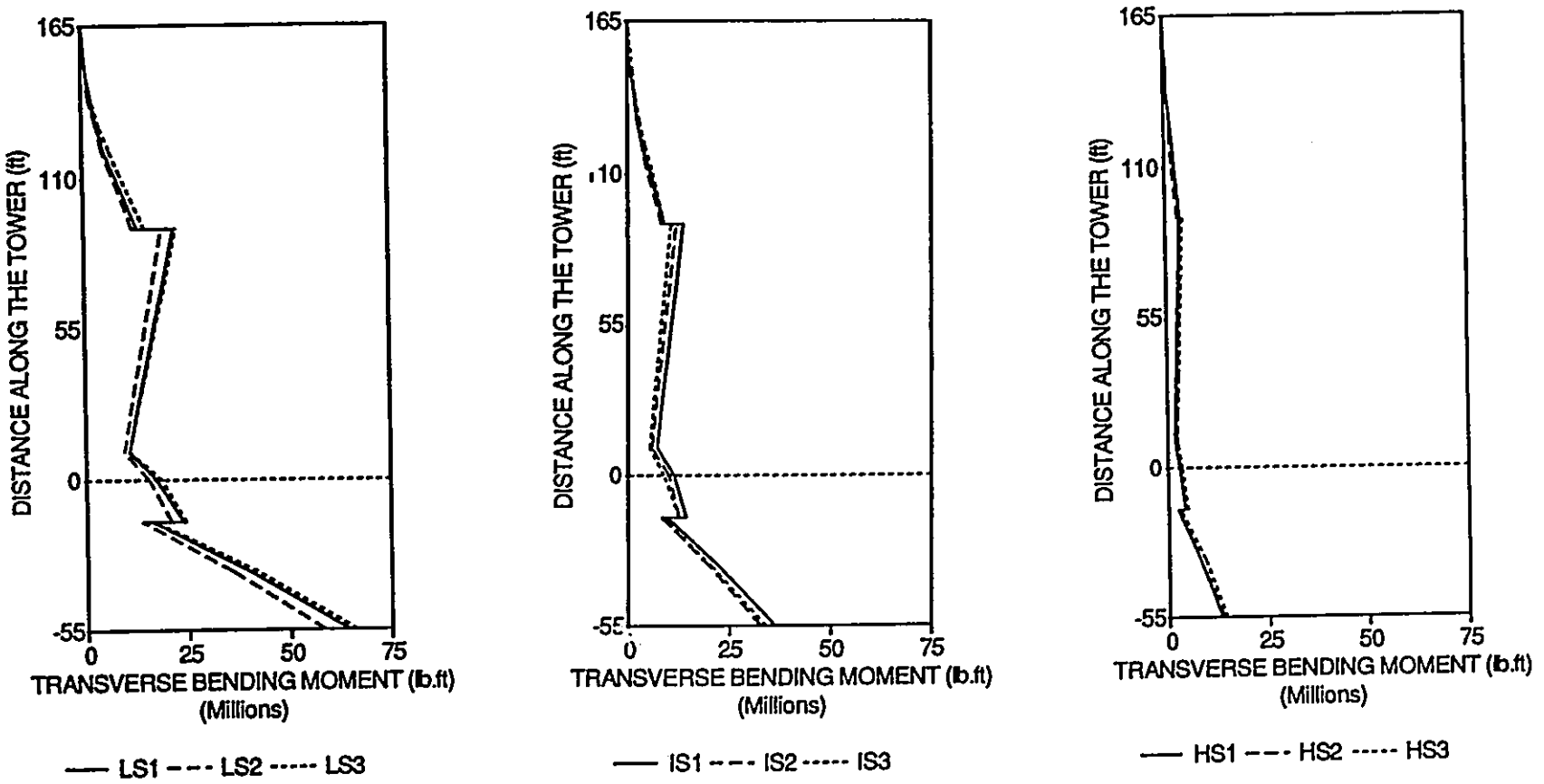

a) Low Frequency Content

b) Intermediate Frequency Content

c) High Frequency Content

Figure 5.31 Effect of Input Motion Frequency Content on the Quincy Bayview Bridge Tower Transverse Bending Moment (M_z)

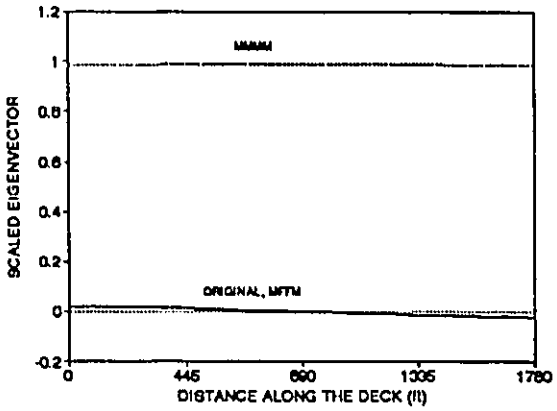

(a) Ordinates of Mode Shapes in the Longitudinal Direction

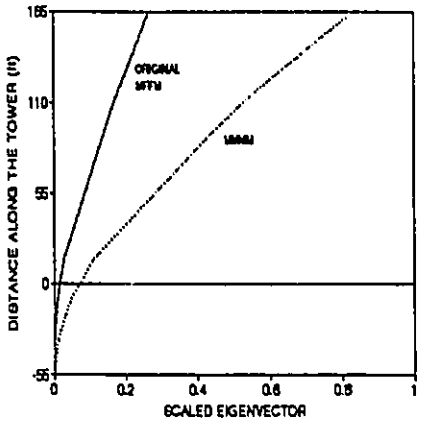

(b) Side Elevation: X-Z Plane

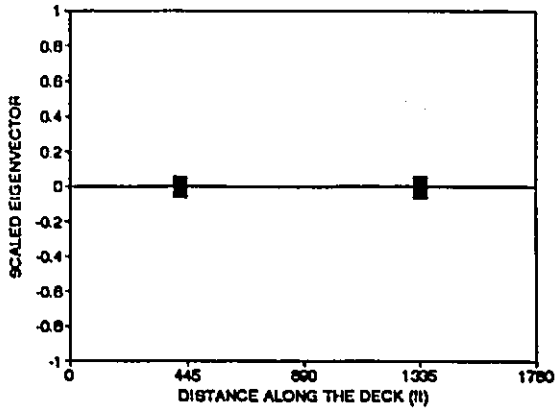

(c) Plan: X-Y Plane

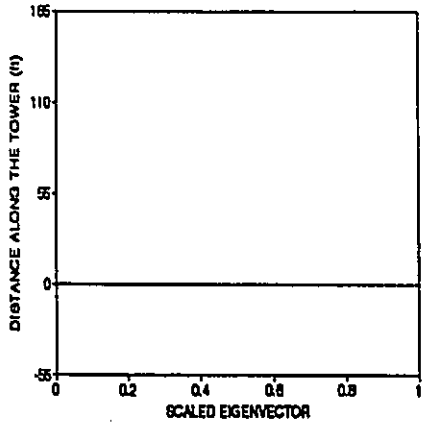

(d) Elevation: Y-Z Plane

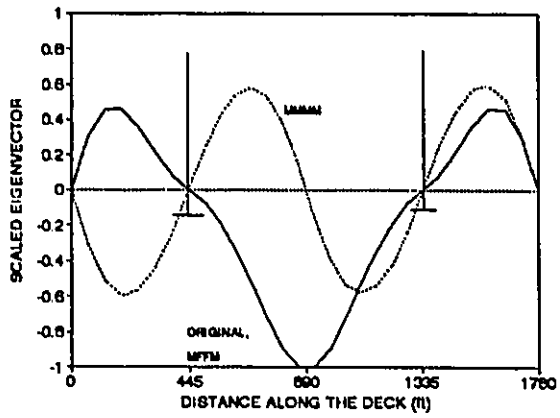

(e) Elevation: X-Z Plane

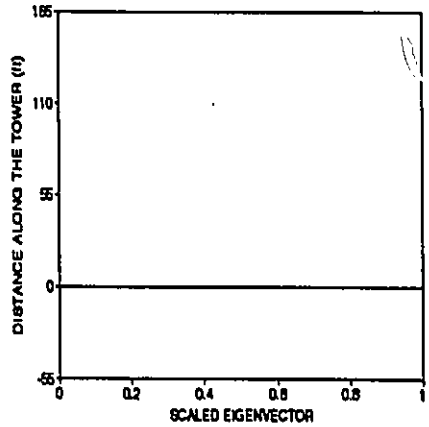

(f) Side Elevation: X-Z Plane

Figure 5.32 Fundamental Mode Shape of Quincy Bridge with Different Deck Supports.

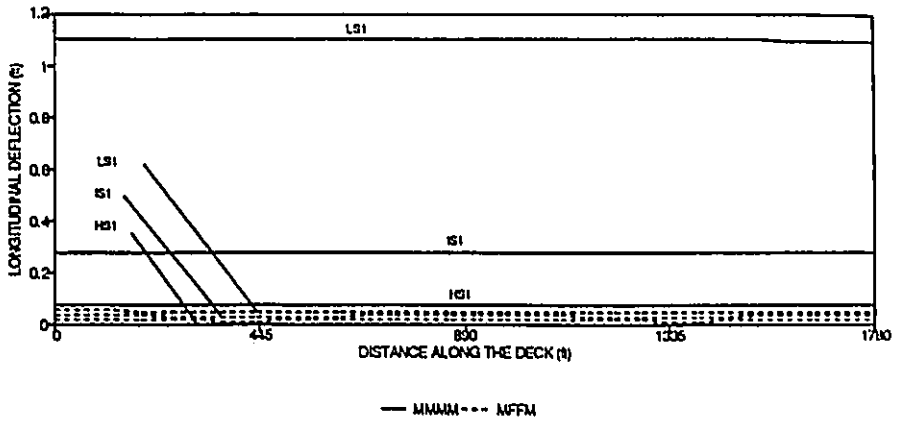

a) Longitudinal Deflection

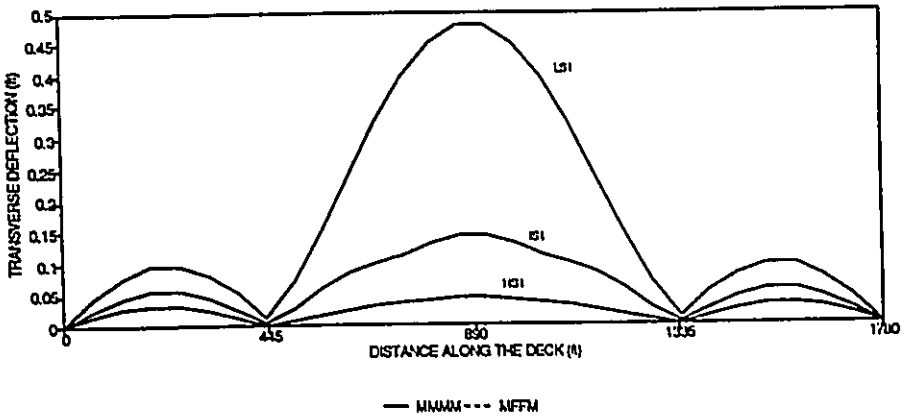

b) Transverse Deflection

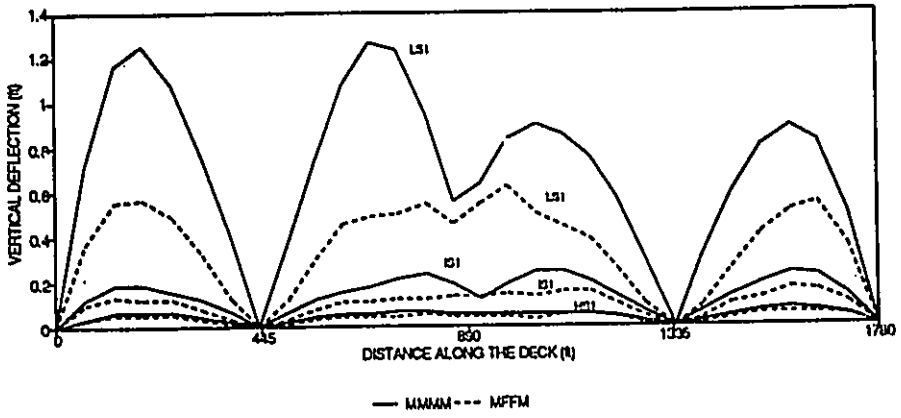

c) Vertical Deflection

Figure 5.33 Deck Deflections of the Quincy Bayview Bridge

with Longitudinally Movable Deck Ends

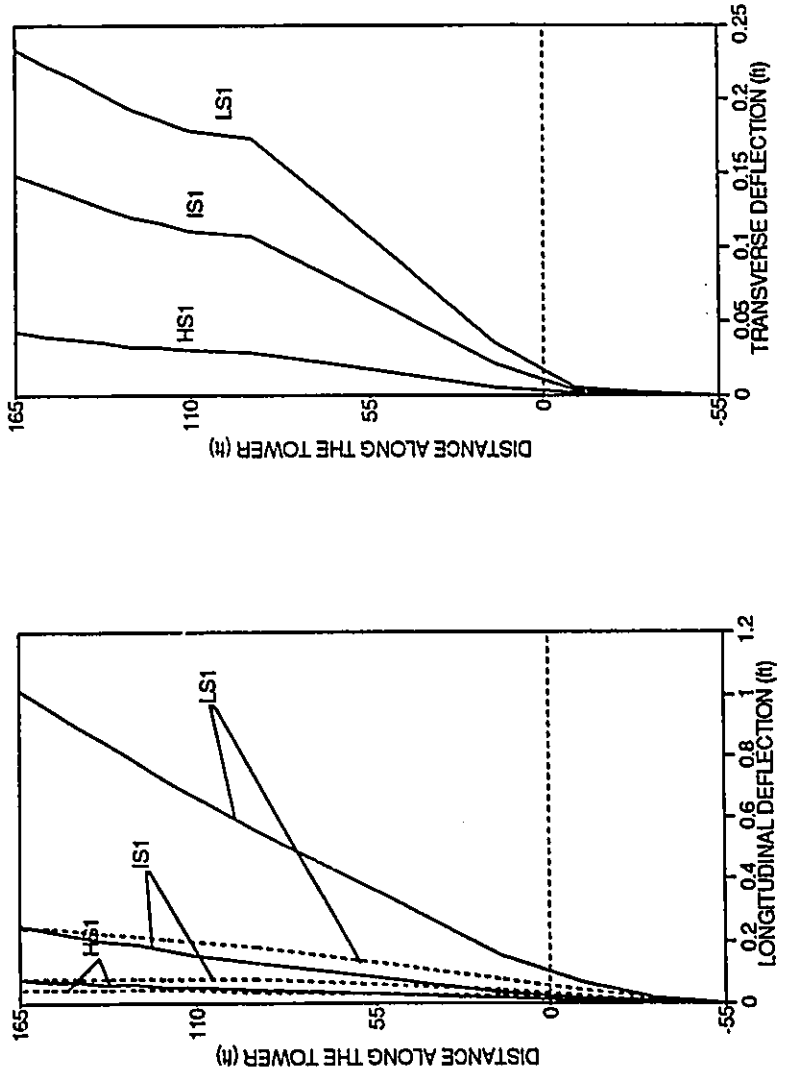

a) Longitudinal Deflection b) Transverse Deflection

Figure 5.34 Tower Deflections of the Quincy Bayview Bridge with Longitudinally Movable Deck Ends

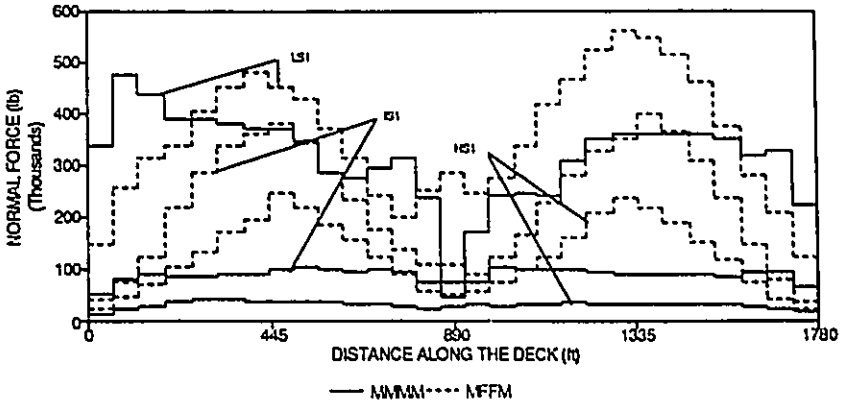

a) Normal Force (F_x)

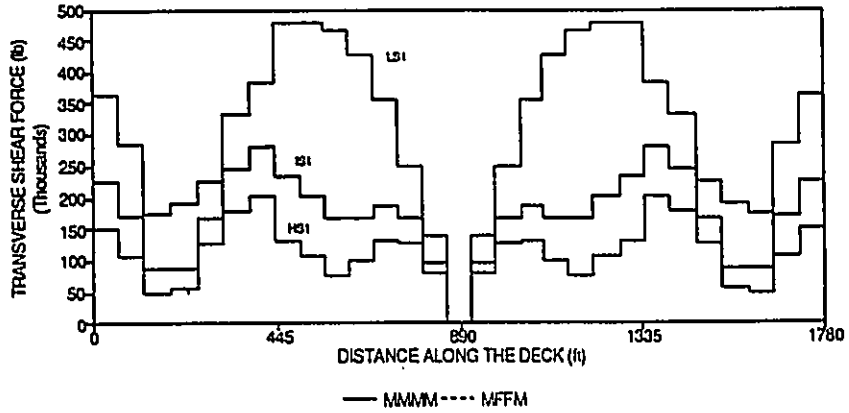

b) Transverse Shear Force (Q_y)

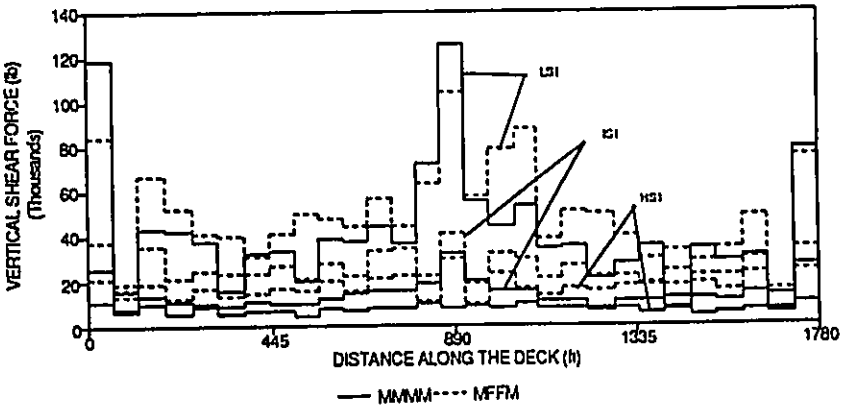

c) Vertical Shear Force (Q_z)

Figure 5.35 Deck Internal Forces of the Quincy Bayview Bridge with Longitudinally Movable Deck Ends

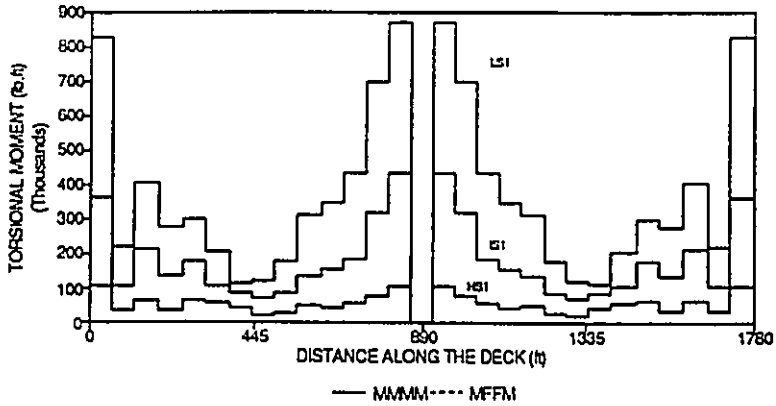

d) Torsional Moment (M_x)

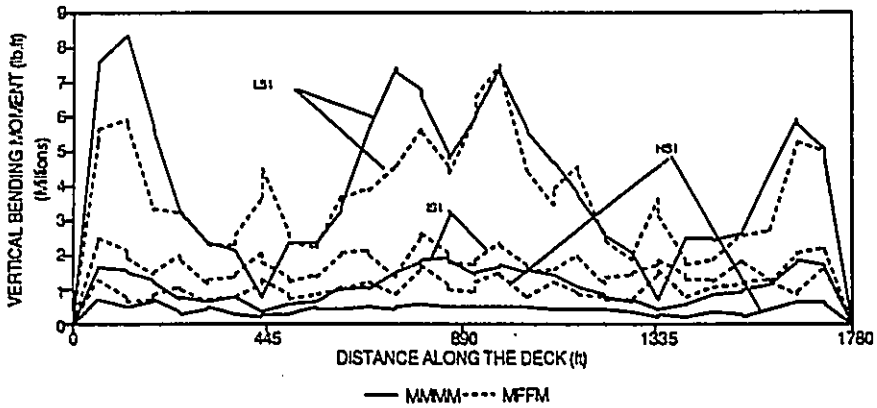

e) Vertical Bending Moment (M_y)

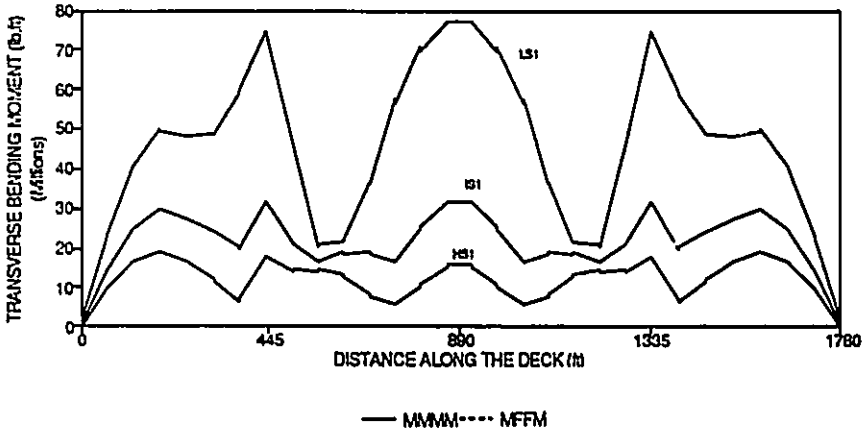

f) Transverse Bending Moment (M_z)

Figure 5.35 Cont'd

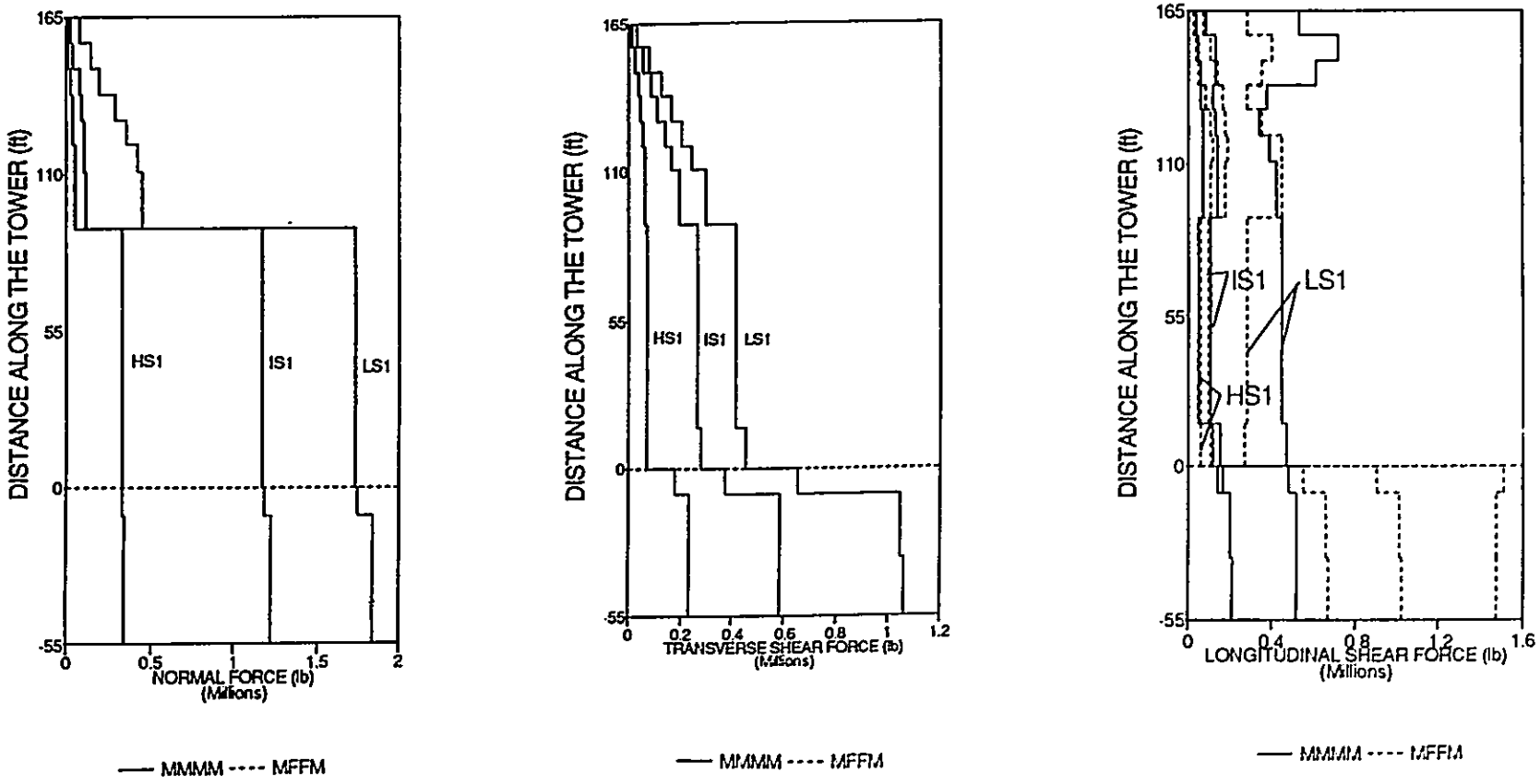

a) Normal Force (F_x) b) Transverse Shear Force (Q_y) c) Longitudinal Shear Force (Q_z)

Figure 5.36 Tower Internal Forces of the Quincy Bayview Bridge

with Longitudinally Movable Deck Ends

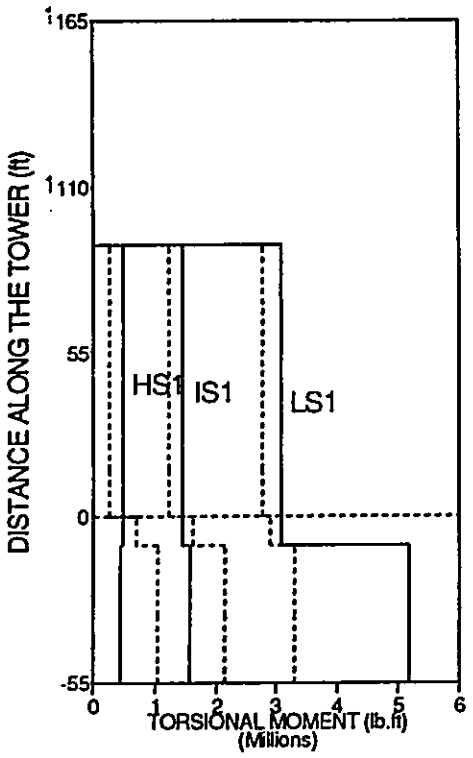

d) Torsional Moment (M_z)

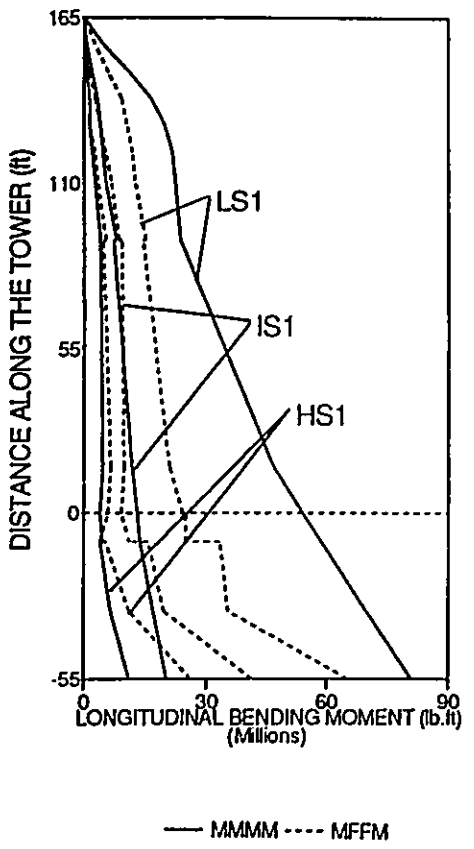

e) Longitudinal Bending Moment (M_y)

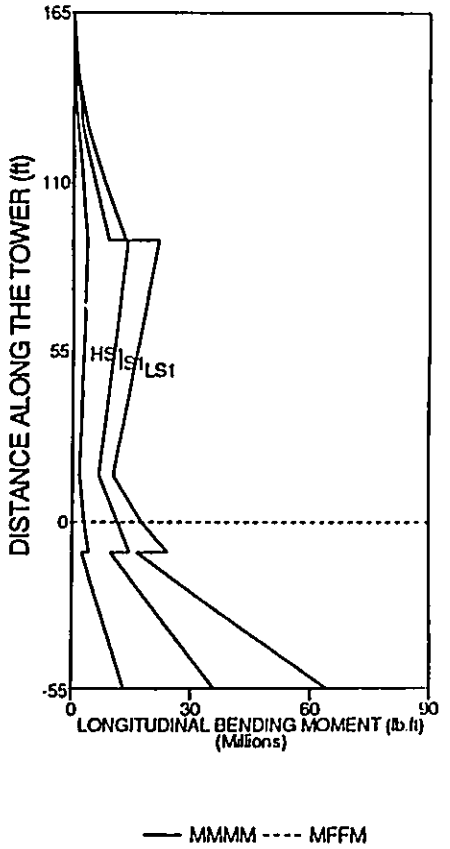

f) Transverse Bending Moment (M_x)

Figure 5.36 Cont'd

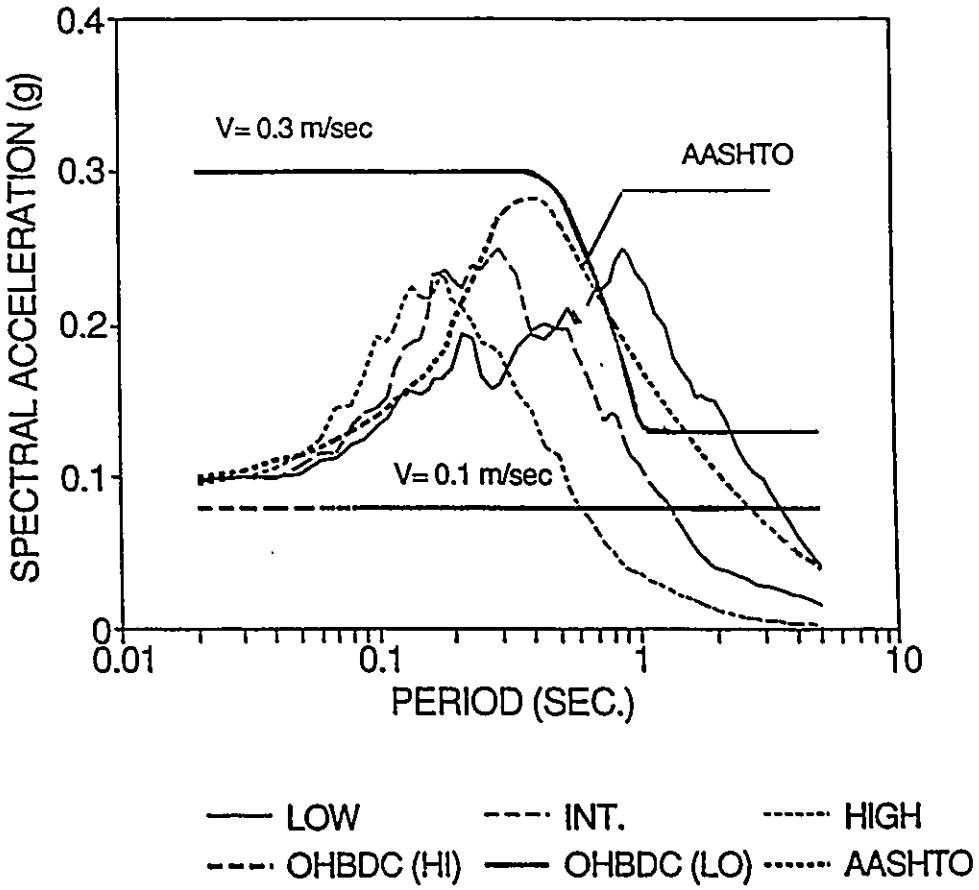

Figure 5.37 Comparison of Acceleration Response Spectra

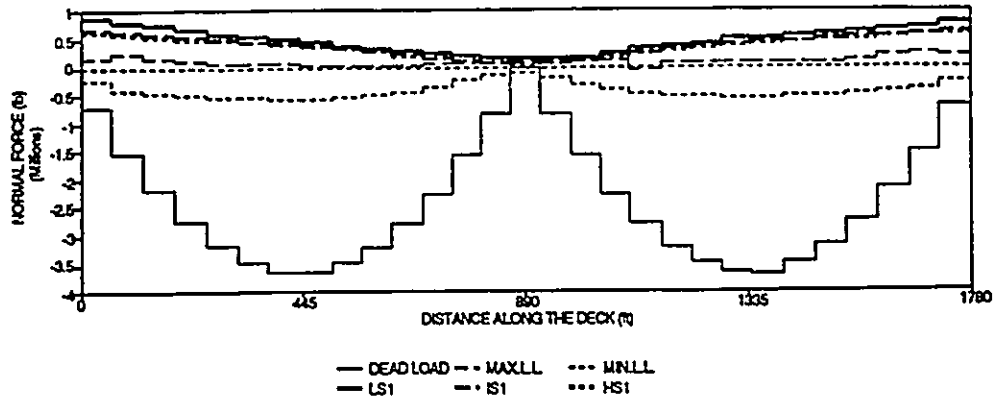

a) Normal Force (F_z)

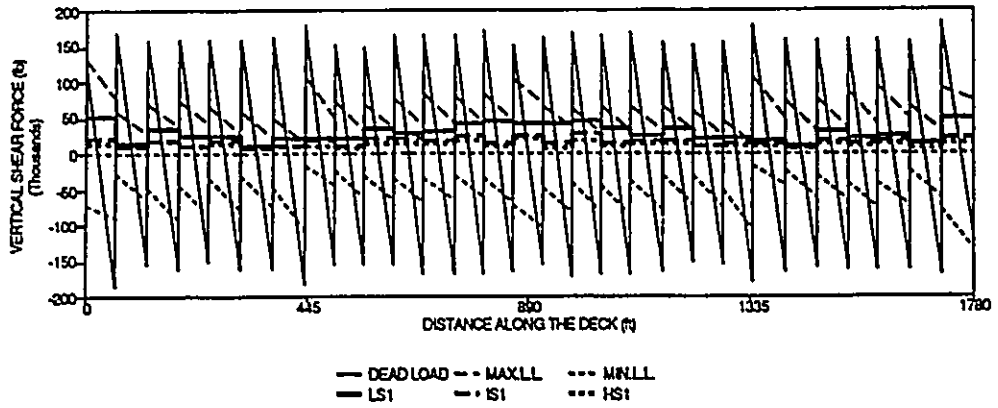

b) Vertical Shear Force (Q_z)

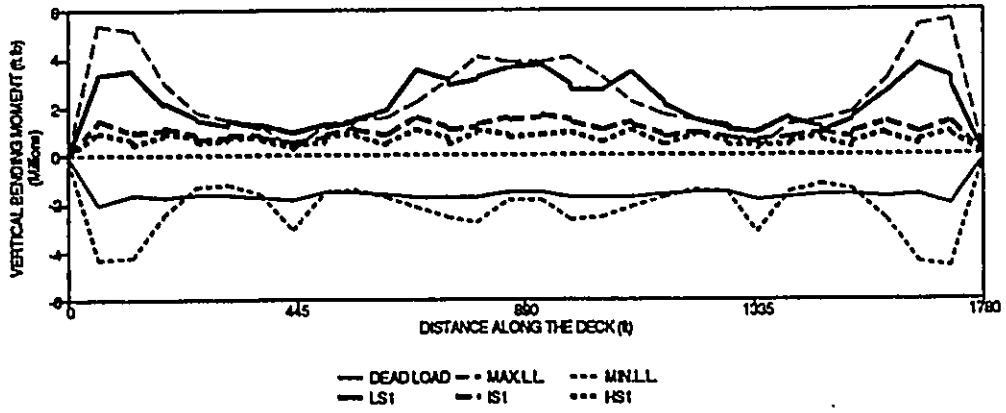

c) Vertical Bending Moment (M_y)

Figure 5.38 Deck Internal Forces of the Quincy Bayview Bridge

Induced by Different Loads

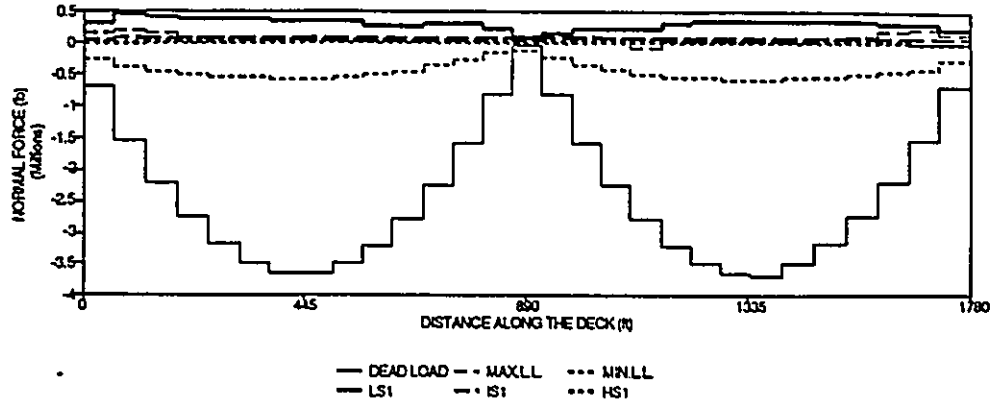

a) Normal Force (F_x)

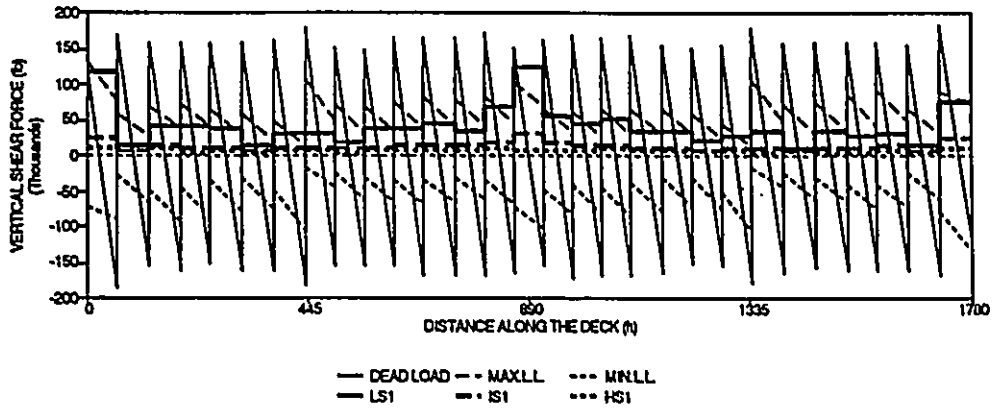

b) Vertical Shear Force (Q_z)

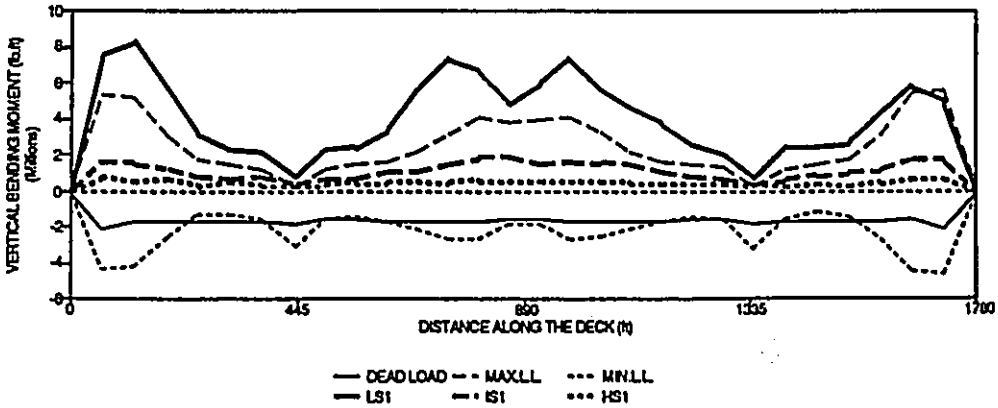

c) Vertical Bending Moment (M_y)

Figure 5.39 Deck Internal Forces of the Quincy Bayview Bridge,

with Longitudinally Movable Deck Ends, Induced by Different Loads

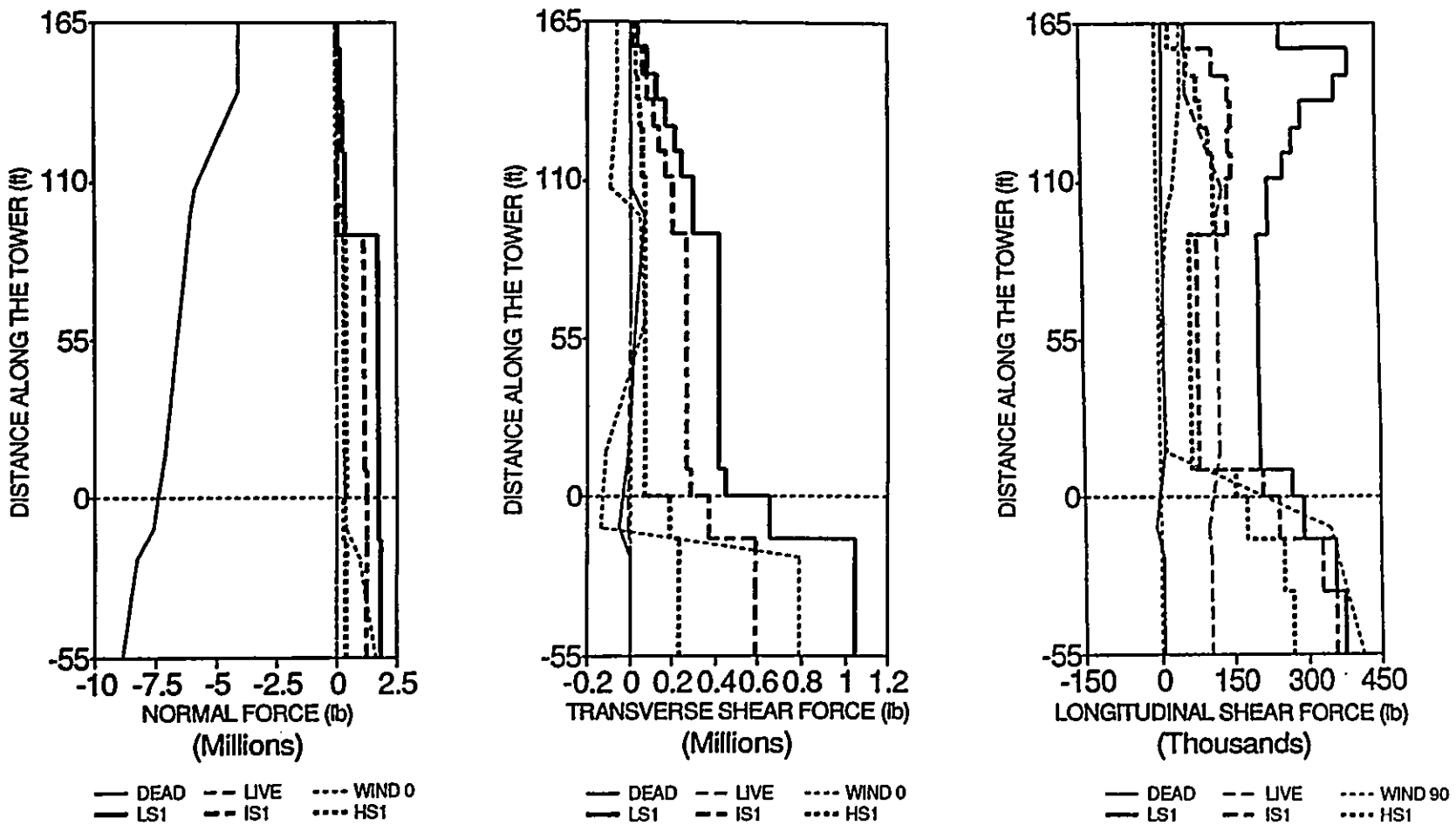

a) Normal Force (F_z)

b) Transverse Shear Force (Q_y)

c) Longitudinal Shear Force (Q_x)

Figure 5.40 Comparison of the Seismic Tower Internal Forces of the Quincy Bayview Bridge to Tower Internal Forces Induced by Dead, Live and Wind Loads

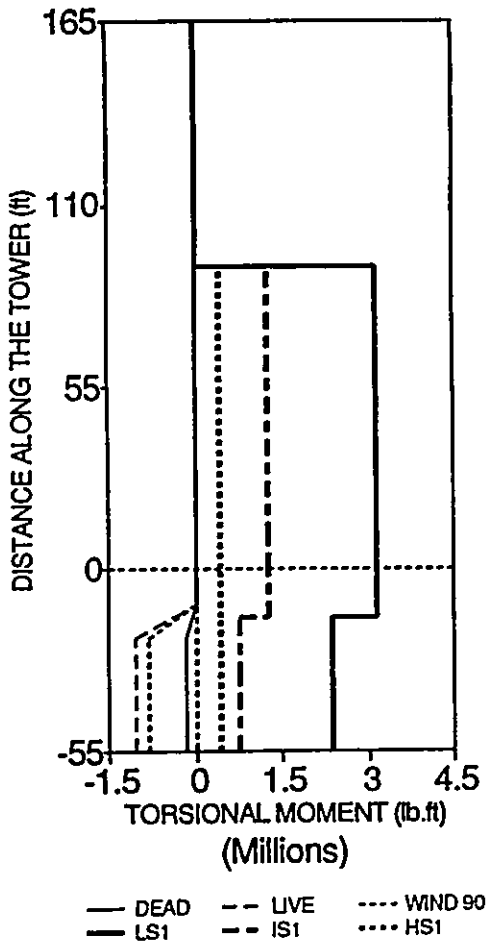

d) Torsional Moment (M_x)

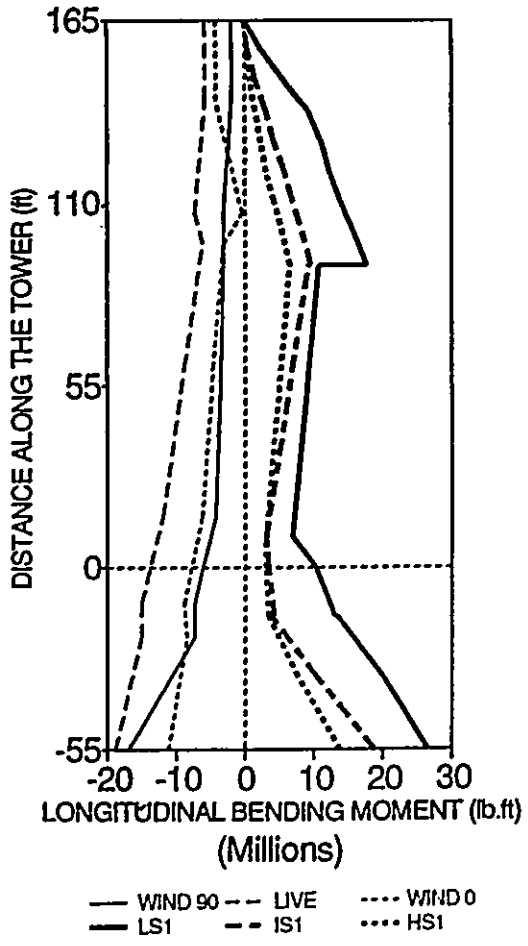

e) Longitudinal Bending Moment (M_y)

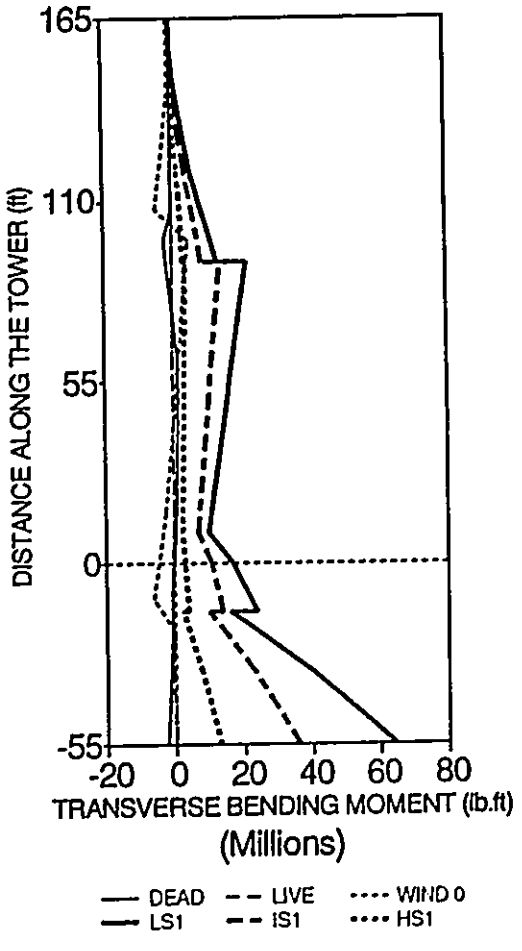

f) Transverse Bending Moment (M_z)

Figure 5.40 Cont'd

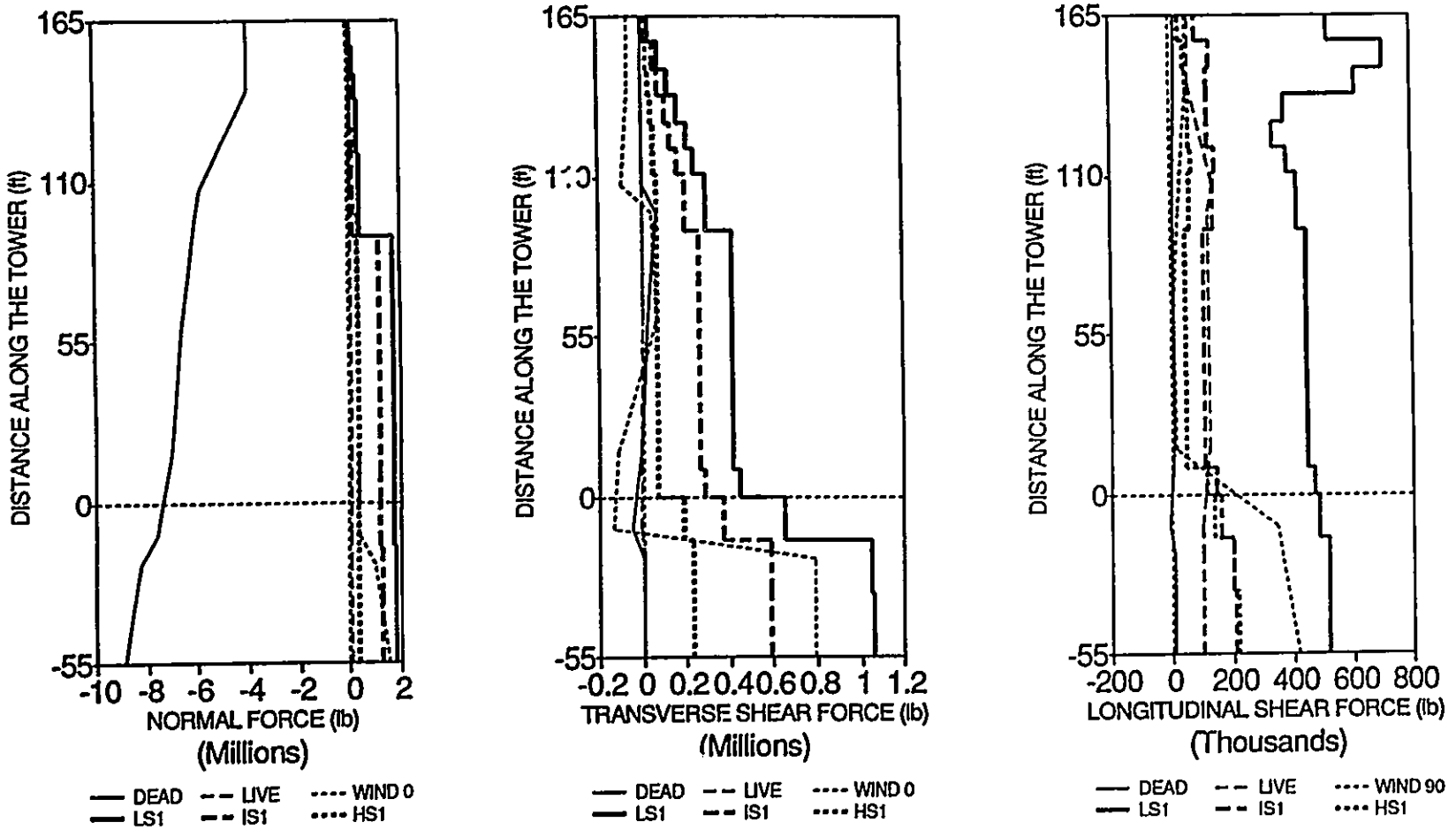

a) Normal Force (F_x)

b) Transverse Shear Force (Q_y)

c) Longitudinal Shear Force (Q_z)

Figure 5.41 Comparison of the Seismic Tower Internal Forces of the Quincy Bayview Bridge with Longitudinally Movable Deck to Tower Internal Forces Induced by Dead, Live and Wind Loads

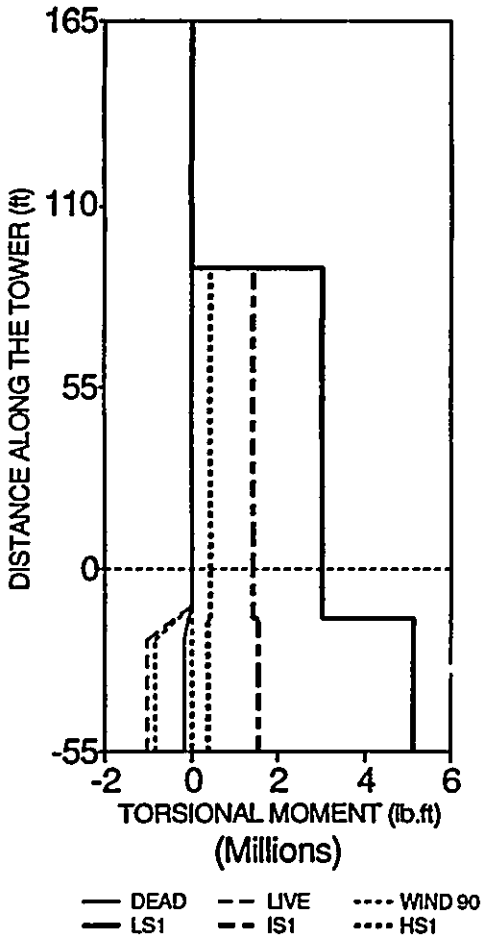

d) Torsional Moment (M_x)

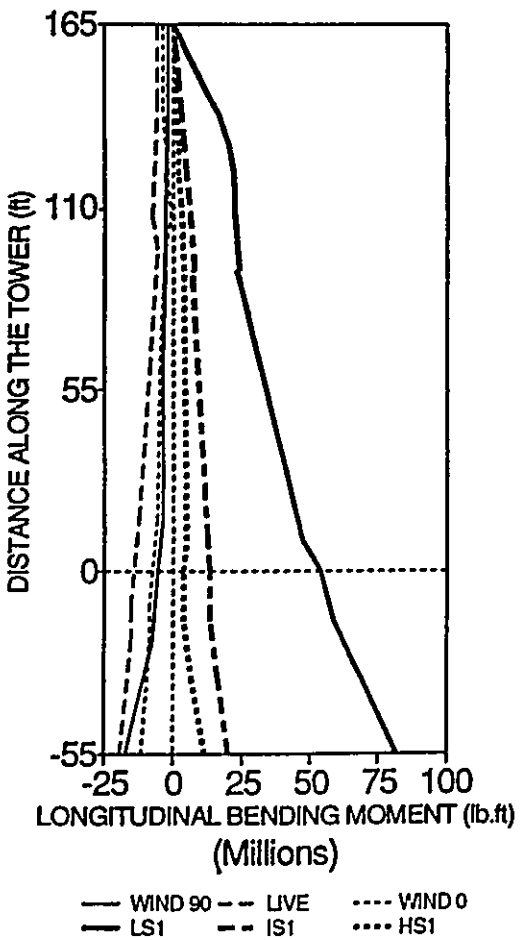

e) Longitudinal Bending Moment (M_y)

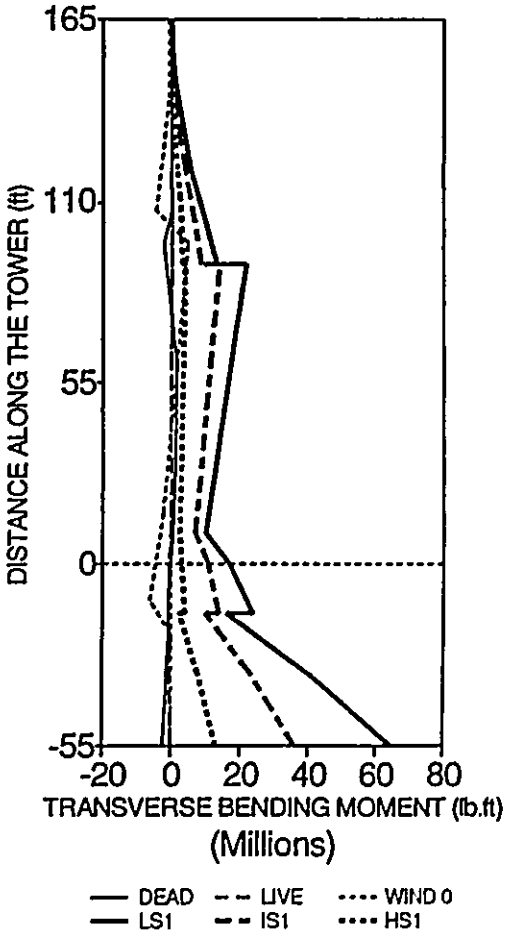

f) Transverse Bending Moment (M_z)

Figure 5.41 Cont'd

CHAPTER 6

SUMMARY AND CONCLUSIONS

6.1 SUMMARY

Cable-stayed bridges are an effective and aesthetic type of bridge construction to span medium and long crossings. The construction of longer spans, the susceptibility of these bridges to adverse effects due to wind loads, and location of these bridges in seismic regions, have created a need to more fully understand their dynamic behaviour. The research presented in this thesis has addressed this problem by examining the dynamic and seismic characteristics of cable-stayed bridges. The research program was divided into four stages:

1) Analytic models were developed for estimating frequencies of the deck and towers, two of the main structural systems of cable-stayed bridges. Vibration of the cables was not addressed in this thesis.
2) A 3-D finite element model of the Quincy Bayview Bridge was used to study modal characteristics of cable-stayed bridges. The study investigated the spatial coupling of modes and proposed a mode classification system to help simplify understanding of the apparent complex dynamic behaviour of these bridges. Modal participation factors and effective modal masses were examined to judge which parameter is a better measure for assessing the number of modes required for dynamic analysis by modal

superposition. The sensitivity of the modal characteristics to major structural changes in geometry was also investigated.

3) Eigenvectors and load dependent Ritz vectors were examined to compare their appropriateness as bases for modal transformation. Seismic response studies of the Quincy Bayview Bridge prototype were conducted in each vector basis to judge which is more suitable for seismic analysis. Based on these studies criteria suitable for both vector bases were proposed that would ensure the inclusion of all important modes in modal superposition analysis of cable-stayed bridges. These criteria were termed "frequency cut-off criteria".

4) The proposed criteria were applied in a seismic response study that used an ensemble of synthetic time history records representing different frequency contents of earthquake ground motions. The study examined seismically induced forces in the bridge, the relationship of these forces to the frequency content of the input ground motions, and compared the seismic forces to other internal forces imposed by dead, live and wind loads.

The thesis provides original contributions to the engineering of cable-stayed bridges by:

- introducing simple analytic models for frequency estimates of deck and towers;
- providing simplified descriptions of the rather complex dynamics of cable-stayed bridges;
- proposing criteria that can be used to ensure the inclusion of all important modes in a modal superposition analysis of cable-stayed bridges;

- presenting a detailed study of the seismic response characteristics of cable-stayed bridges and the effect of ground motion frequency content.

The present study was carried out using structural property data from the Quincy Bayview Bridge. This is representative of three-span, double-plane cable-stayed bridges with main span lengths up to approximately 1000 ft. Other cable-stayed bridge configurations such as two-span, skew or curved bridges are also possible, however this study does not examine their dynamic and seismic response characteristics. The linear analysis approach used in this thesis is suitable for bridges with main spans up to 1500 ft as many researchers such as Nazmy and Abdel-Ghaffar (1987) have suggested. A longer main span may require consideration of geometric nonlinearities, as discussed by Nazmy and Abdel-Ghaffar (1987). This thesis assumed very stiff soil conditions with the implication that there was synchronous seismic input motion at all supports. It did not consider the case of differing soil conditions at the bridge supports which could give rise to non-synchronous seismic excitations. Future work is required to investigate the effect of various bridge configurations and soil conditions on the dynamic and seismic characteristics of cable-stayed bridges.

6.2 CONCLUSIONS

The following conclusions are drawn from the research work on the dynamic characteristics and seismic response of cable-stayed bridges:

1- The spatial coupling within each mode shape of a cable-stayed bridge involves principally two directions (torsional/transverse motion, or vertical/longitudinal

motion). This means that the complex modal behaviour can be simplified by considering two main mode categories: vertical plane, and torsional/transverse. Within each category, mode classes are related to simple deformation mechanisms. The simple mode classes (e.g. vertical bending, longitudinal bending, torsion,...) have been modeled analytically to provide tools for preliminary design calculations. These simple mode classes facilitate interpretation of trends of frequency, modal participation factors, and effective modal masses as a function of mode number.

2- The research program proposed frequency cut-off criteria to determine a sufficient number of modes to be included in a modal superposition analysis of cable-stayed bridges. The criteria are based on calculating an upper limit frequency using the simple analytic models, generating modal vectors that have frequencies up to the set limit, and then checking that the effective modal mass associated with the modal vectors meets a pre-set percentage of the total mass.

3- The two modal transformation bases, eigenvectors and load dependent Ritz vectors, require approximately the same number of vectors to meet the proposed frequency cut-off criteria. This is unlike the case for simpler structures such as 2-D frames, where fewer Ritz vectors than eigenvectors are required. Load dependent Ritz vectors, however, provide ease of numerical handling, and require less computer storage and run time than eigenvectors.

4- Only a few modes are effective in contributing to each structural response quantity, but these are spread over a wide frequency range because of the interaction of the two main dynamic sub-systems, deck and towers. To achieve a reliable dynamic

analysis a relatively large number of modes is required to cover this broad frequency band of response.

5- The frequency content of earthquake ground motion has a pronounced effect on the response of cable-stayed bridges. Low frequency content input motions (as characterized by a low A/V ratio) produce higher responses than intermediate or high frequency content input motions. The response of the bridge deck was found to be more sensitive to the frequency content of the input motion than the tower. However, there are some response quantities such as shear force and bending moment at the tower base, that are less sensitive to the frequency content of input motion. These quantities are usually affected by both low frequency coupled deck-tower modes and higher frequency local tower modes.

6- Although permitting the bridge to move longitudinally will lower the fundamental frequency of the whole structure (and thus reduce the seismic response in the fundamental mode), it may also lead to an increase in the seismic forces at the tower bases and in the bridge deck for low A/V input motions. A longitudinally movable deck will also result in large longitudinal seismic displacements.

7- The seismic induced shear forces and bending moments in the prototype structure were high enough, even for input motions with peak ground acceleration of 0.1 g, to affect the design forces at the deck ends, mid main span, tower top, and tower base.

REFERENCES

AASHTO 1983, "Standard Specifications For Highway Bridges", The American Association of State Highway and Transportation Officials, Washington, D.C.

Abdel-Ghaffar, A.M., and Nazmy, A.S., 1987, "Effects of Three-Dimensionality and Non-linearity on the Dynamic and Seismic Behaviour of Cable-Stayed Bridges", Bridges and Transmission Line Structures, ed. Lambert Tall, pp.389-404.

Abdel-Ghaffar, A.M., 1991, "Cable-Stayed Bridges Under Seismic Action", Cable-Stayed Bridges, Recent Developments and Their Future, ed. Ito, M., et al, pp. 171-192, Elsevier Science Publications, New York.

Abdel-Ghaffar, A.M., and Khalifa, M.A., 1991, "Importance of Cable-Vibration in Dynamics of Cable-Stayed Bridges", Proc. ASCE, Journal of Structural Engineering, v.117, No.11, pp.2571-2589.

Abdel-Ghaffar, A.M., and Nazmy, A.S., 1991, "Non-Linear Seismic Behaviour of Cable-Stayed Bridges", Proc. ASCE, Journal of Structural Engineering, v.117, No.11, pp.356-3476.

Arnold, R.R., Citerley, R.L., Chargin, M., and Galant, D., 1985, "Application of Ritz Vectors for Dynamic Analysis of Large Structures", Computers and Structures, v.21, No.5, pp.901-907.

Ayre, R.S., and Jacobsen, L.S., 1950, "Natural Frequencies of Continuous Beams of Uniform Span Length", Proc. ASCE, Journal of Applied Mechanics, v.17, pp.391-395.

Bathe, K.J., Wilson, E.L., and Peterson, F.E., 1973, "SAP IV: A structural Analysis Program for Static and Dynamic Response of Linear Systems", Report No. EERC 73-11, University of California, Berkeley.

Bathe, K.J., and Wilson, E.L., 1976, "Numerical Methods in Finite Element Analysis" Prentice-Hall, Englewood Cliffs, N.J.

Blevins, R.D., 1984, "Formulas for Natural Frequencies and Mode Shapes", Robert E. Krieger Publishing Co., Florida.

Bruno, D., and Leonardi, A., 1986, "Non-Linear Analysis of Cable-Stayed Bridges

Eccentrically Loaded", IABSE Proceedings pp.103-86.

Chen, H.C., and Taylor, R.L., 1990, "Solution of Viscously Damped Linear Systems Using a Set of Load-Dependent Vectors", International Journal of Earthquake Engineering and Structural Dynamics, v.19, pp.653-665.

Clough, R.W., and Penzien, J., 1975, "Dynamics of Structures", McGraw-Hill Inc., New York.

Fleming, J.F., and Egeseli, E.A., 1980, "Dynamic Behaviour of a Cable-Stayed Bridge", International Journal of Earthquake Engineering and Structural Dynamics, v.8, pp.1-16.

Garevski, M.A., Brownjohn, J.M.W., Blakeborough, A., and Severn, R.T., 1991, "Resonance-Search Tests on a Small Scale Model of a Cable-Stayed Bridge", Engineering Structures, v.13, pp.59-66.

Garevski, M.A., and Severn, R.T., 1992, "Dynamic Analysis of Cable-Stayed Bridges by Means of 3-D Analytical and Physical Modelling", Proceedings of the Tenth World Conference on Earthquake Engineering, Madrid, pp.4809-4814.

Gilsanz, R.E., and Biggs, J.M., 1983, "Cable-Stayed Bridges: Degrees of Anchoring", Journal of Structural Engineering, v.109, No.1, pp.200-220.

Gimsing, N.J., 1983, "Cable Supported Structures", John Wiley and Sons Ltd., New York.

Goschy, B., 1961, "Dynamics of Cable-Stayed Pipe Bridges", Acier, Stahl, Steel, No.6, pp.277-282.

Gravelle, W., 1990, "Dynamic Modelling and Seismic Response of a Cable-Stayed Bridge", M.Eng. Thesis, McMaster University, Hamilton, Ontario, Canada.

Habibullah, A., and Wilson, E.L., 1989, "SAP 90, A Series of Computer Programs for the Finite Element Analysis of Structures", Computers and Structures Incorporation, Berkeley, California.

Jones, N.P., and Thompson, J.M., 1992, "Ambient Vibration Survey and Preliminary Dynamic Analysis: Sunshine Skyway Cable-Stayed Bridge", A Report Submitted to the Florida Department of Transportation, Johns Hopkins University, Baltimore, Maryland.

Kawashima, K., Unjoh, S., and Azuta, Y., 1988, "Damping Characteristics of Cable-Stayed Bridges", Proceedings of the Ninth World Conference on Earthquake

Engineering, Tokyo.

Kawashima, K., Unjoh, S., 1989, "Damping Characteristics of Cable-Stayed Bridges Associated with Energy Dissipation at Movable Supports", Proceedings of Japanese Society of Civil Engineers, No.404/I-11, pp.145-152.

Kawashima, K., Unjoh, S., and Azuta, Y., 1990, "Analysis of Damping Characteristics of a Cable-Stayed Bridge Based on Strong Motion Records", Proceedings of Japanese Society of Civil Engineers, No.416/I-13, pp.181-190.

Kawashima, K., and Unjoh, S., 1992, "Damping Characteristics of Cable-Stayed Bridges", Proceedings of the Tenth World conference on Earthquake Engineering, Madrid, pp.4803-4808.

Kawashima, K., Unjoh, S., and Tunomoto, M., 1993, "Estimation of Damping Ratio of Cable-Stayed Bridges for Seismic Design", Proc. ASCE, Journal of Structural Engineering, v.119, No.4, pp.1015-1031.

Khalil, M.S., and Bush, L.H., 1987a, "Vancouver's Skytrain Cable-Stayed Bridge-Dynamic Behaviour", Bridges and Transmission Line Structures, ASCE, Lambert Tall, ed., pp.357-372.

Khalil, M.S., and Bush, L.H., 1987b, "Seismic Analysis and Design of the Skytrain Cable-Stayed Bridge", Proceedings of the 5th Canadian Conference on Earthquake Engineering, Ottawa, pp.355-364.

Kitazawa, M., Nishimori, K., Noguchi, J., and Shimoda, I., 1992, "Earthquake Resistant Design of a Long-Period cable-Stayed Bridge", Proceedings of the Tenth World Conference on Earthquake Engineering, Madrid, pp.4797-4802.

Kosko, E., 1968, "The Frequency Spectrum of a Structural Member in Coupled Flexural-Torsional Vibration", Journal of Sound and Vibration, v.7, No.2, pp. 143-155.

Leger, P., and Wilson, E.L., 1987, "Load Dependent Vector Bases for Earthquake Response Analysis", Proceedings of the 5th Canadian Conference on Earthquake Engineering, Ottawa, pp.115-124.

Leonhardt, F., and Zellner, W., 1980, "Cable-Stayed Bridges", IABSE Surveys 13/80, pp.21-48.

Liu,T., 1989, "Full-Scale Ambient Vibration Measurements on a Cable-Stayed Bridge" M.Eng. Thesis, McMaster University, Hamilton, Ontario.

Masaki, Y., Sano, S., and Sakai, F., 1987, "Analysis and Design of Wind- and Earthquake-Resistance of an S-Curved Cable-Stayed Bridge", Bridges and Transmission Line Structures, ASCE, Lambert Tall, ed., pp.341-356.

Modjeski and Masters, 1983, "Structural Drawing of the Quincy Bayview Cable-Stayed Bridge", Modjeski and Masters Consulting Engineers, Harrisburg, Pennsylvania, U.S.A.

Muria-Villa, D., Gomez, R., and King, C., 1991, "Dynamic Structural Properties of Cable-Stayed Tampico Bridge", Proc. ASCE, Journal of Structural Engineering, v.117, No.11, pp.3396-3416.

Naumoski, N., Tso, W.K., and Heidebrecht, A.C., 1988, "A Selection of Representative Strong Motion Earthquake Records Having Different A/V Ratios", Earthquake Engineering Research Group, EERG Report 88-01, McMaster University.

Nazmy, A.S., and Abdel-Ghaffar, A.M., 1987, "Seismic Response Analysis of Cable-Stayed Bridges Subjected to Uniform and Multiple-Support Excitations" Report No.87-SM-1, Princeton University.

Nazmy, A.S., and Abdel-Ghaffar, A.M., 1990a, "Non-Linear Earthquake Response Analysis of Long Span Cable-Stayed Bridges: Theory", International Journal of Earthquake Engineering and Structural Dynamics, v.19, pp.45-62.

Nazmy, A.S., and Abdel-Ghaffar, A.M., 1990b, "Non-Linear Earthquake Response Analysis of Long Span Cable-Stayed Bridges: Application", International Journal of Earthquake Engineering and Structural Dynamics, v.19, pp.63-76.

Nazmy, A.S., and Abdel-Ghaffar, A.M., 1992, "Effects of Ground Motion Spatial Variability on the Response of Cable-Stayed Bridges", International Journal of Earthquake Engineering and Structural Dynamics, v.21, pp.1-20.

NBCC 1990, "National Building Code of Canada", Associate Committee on the National Building Code, National Research Council of Canada, Ottawa.

NBCC 1990, "Supplement to the National Building Code of Canada 1990", National Research Council of Canada, Ottawa.

Newmark, N.M., 1962, "A Method of Computation for Structural Dynamics", Transactions, ASCE, v.127, pp.1406-1435.

Newmark, N.M., and Hall, W.J., 1982, "Earthquake Spectra and Design", Earthquake Research Institute, El Cerrito, California.

Nour-Omid, B., and Clough, R.W., 1984, "Dynamic Analysis of Structures Using Lanczos Co-Ordinates", International Journal of Earthquake Engineering and Structural Dynamics, v.12, pp.565-577.

OHBDC 1991, "Ontario Highway Bridge Design Code", Ministry of Transportation of Ontario, Quality and Standards Division, Toronto, Ont.

Ohtsuka, H., Ohta, T., and Imai, F., 1984, "Optimum Anchoring for Long Span Cable-Stayed Bridges", Proceedings of Japanese Society of Civil Engineers, v.1, No.2, pp.87-95.

Ohtsuka, H., and Sonoda, Y., 1987, "Non-Linear Behaviour of Long Span Cable-Stayed Bridges with Full, Self and Partial Anchorages", Memoires of the Faculty of Engineering, Kyushu University, v.47, No.2, pp.145-155.

Parvez, S.M., and Wieland, M., 1988, "Earthquake Behaviour of Continuous Multi-Span Cable-Stayed Bridge" Proceedings of the Ninth World Conference on Earthquake Engineering, Tokyo, v.6, pp.477-482.

Podolny, W., and Scalzi, J.B., 1986, "Construction and Design of Cable-Stayed Bridges", John Wiley and Sons Inc., New York.

Rajaraman, A., Loganathan, K., and Raman, N.V., 1980, "Non-linear Analysis of Cable-Stayed Bridges", IABSE Proceedings P-37/80, pp.205-216.

Scanlan, R.H., 1987, "Aspects of Wind and Earthquake Dynamics of Cable-Stayed Bridges", Bridges and Transmission Line Structures, ASCE, L. Tall ed., pp.329-340.

Scanlan, R.H., and Jones, N.P., 1990, "Aeroelastic Analysis of Cable-Stayed Bridges", Proc. ASCE, Journal of Structural Engineering, v.116, pp.279-297.

Smith, B.S., 1967, "The Single Plane Cable-Stayed Girder Bridge: A Method of Analysis Suitable for Computer Use", Proceedings of the Institute of Civil Engineers, v.37, pp.183-194.

Stiemer, S.F., Taylor, P., and Vincent, D.H.C., 1988, "Full Scale Dynamic Testing of the Annacis Bridge", IABSE Proceedings P-122/88, pp.1-16.

Stroh, S.L., 1987, "Dynamic Behavior of Three U.S. Cable Stayed Bridges", Bridges and Transmission Line Structures, ed. Lambert Tall, pp.373-388.

Taylor, P.R., van Selst, A.M., Hodge, W.E., and Sexsmith, R.G., 1985, "Annacis Cable-Stayed Bridge-Design for Earthquake", Canadian Journal of Civil

Cable-Stayed Bridge-Design for Earthquake", Canadian Journal of Civil Engineering, v.12, pp.472-481.

Troitsky, M.S., 1988, "Cable-Stayed Bridges-An Approach to Modern Bridge Design", Van Nostrand Reinhold Co., New York.

Tso, W.K., Zhu, T.J., and Heidebrecht, A.C., 1992, "Engineering Implication of Ground Motion A/V Ratio", Soil Dynamics and Earthquake Engineering, v. 11, pp.133-144.

Vaz, C.T., Rito, A., and Duarte, R.T., 1988, "Seismic Studies of the Arade River Cable-Stayed Bridge" Proceedings of the Ninth World Conference on Earthquake Engineering, Tokyo, v.6, pp.507-512.

Wilson, E.L., Farhoomand, I., and Bathe, K.J., 1973, "Non-linear Dynamic Analysis of Complex Structures", International Journal of Earthquake Engineering and Structural Dynamics, v.1, pp.241-252.

Wilson, E.L., Yuan, M-W., and Dickens, J.M., 1982, "Dynamic Analysis by Direct Superposition of Ritz Vectors", International Journal of Earthquake Engineering and Structural Dynamics, v.10, pp.813-821.

Wilson, E.L., and Bayo, E.P., 1987, "Use of Special Ritz Vectors in Dynamic Substructure Analysis", Proc., ASCE, Journal of Structural Engineering, v.112, No. 8, pp.1944-1954.

Wilson, J.C., and Gravelle, W., 1991, "Modelling of a Cable-Stayed Bridge for Dynamic Analysis", International Journal of Earthquake Engineering and Structural Dynamics, v.20, pp.707-721.

Wilson, J.C., and Liu, T., 1991, "Ambient Vibration Measurements on a Cable-Stayed Bridge", International Journal of Earthquake Engineering and Structural Dynamics, v.20, pp.723-747.

Xia, H., and Humar, J.L., 1992, "Frequency Dependent Ritz Vectors", International Journal of Earthquake Engineering and Structural Dynamics, v.21, pp.215-231.

Yamada, N., Shiraishi, N., Toki, K., Matsumoto, M., Matsuhashi, K., Kitazawa, M., and Ishizaki, H., 1991, "Earthquake-Resistant and Wind-Resistant Design of the Higashi-Kobe Bridge", Cable-Stayed Bridges, Recent Developments and Their Future, ed. Ito, M. et al, pp 171-192, Elsevier Science Publications, New York.

Yokoyama, M., Tanaka, S., and Iwano, M., 1988, "Analytical Study on Seismic Behaviour of Cable-Stayed Concrete Bridge" Proceedings of the Ninth World

Conference on Earthquake Engineering, Tokyo, v.6, pp.489-494.

Zhu, T.J., 1989, "Inelastic Response of Reinforced Concrete Frames to Seismic Ground Motions Having Different Characteristics", Ph.D. Thesis, McMaster University, Hamilton, Ontario.